Structure-Stability Relationships of Water-based Polyurethane Dispersions

Inaugural – Dissertation

zur

Erlangung des Doktorgrades

der Mathematisch-Naturwissenschaftlichen Fakultät

der Universität zu Köln

vorgelegt von

Christoph Grau

angenommen im Jahr 2026

Kurzzusammenfassung

Wasserbasierte Polyurethandispersionen (PUDs) gewinnen als umweltfreundliche Alternative zu lösungsmittelbasierten Systemen zunehmend an Bedeutung. Die Einflussfaktoren der kolloidalen Stabilität sind bislang allerdings nur unzureichend untersucht. Obwohl elektrostatische Abstoßung einen zentralen Beitrag zur Stabilisierung leistet, mehren sich Hinweise darauf, dass weitere, strukturell bedingte Wechselwirkungen maßgeblich zur Dispersionsstabilität beitragen. Die vorliegende Arbeit untersucht systematisch den Zusammenhang zwischen Struktur und Dispersionsstabilität in elektrostatistisch stabilisierten, wasserbasierten Polyurethandispersionen.

Hierzu werden diverse PUDs nach dem Acetonverfahren synthetisiert, um drei wesentliche Strukturparameter zu analysieren: die Polyolkomponente (Polycarbonat-, Polyester- und PolyTHF-Diole), die Art und Konzentration des Stabilisators (3,0–5,5 gew.-% AAS bzw. DMPS) sowie den Hartsegmentgehalt. Die Dispersionsstabilität wird anhand der kritischen Koagulationskonzentration (ccc) bewertet. Die Ladungseigenschaften werden mittels potentiometrischer Titration und elektrophoretischer Mobilität charakterisiert. Van-der-Waals-Wechselwirkungen werden über Hamaker-Konstanten quantifiziert, abgleitet aus der DLVO- und der van Oss–Chaudhury–Good-Theorie (vOCG). Die Gesamtauswertung erfolgt unter Einbeziehung der DLVO- und XDLVO-Theorie.

Die Dispersionsstabilität steigt mit dem Gehalt an AAS und DMPS, wobei DMPS-stabilisierte Systeme geringere Stabilität aufweisen. Eine Erhöhung des Hartsegmentanteils führt ebenfalls zu einer Stabilitätssteigerung. Unter den untersuchten Strukturparametern zeigt jedoch das Polyol den dominanten Einfluss. PC-basierte PUDs weisen eine deutlich höhere Dispersionsstabilität verglichen mit entsprechenden Systemen basierend auf PolyTHF- oder PE-Diolen auf, was die zentrale Bedeutung der Pololkomponente für die kolloidalen Wechselwirkungen unterstreicht.

Die potentiometrischen Titrationen ergeben Wiederfindungsraten der ionischen Gruppen von lediglich 70–85 % für AAS bzw. 50–75 % für DMPS. Gleichzeitig weisen beide Stabilisatoren ein gegenüber den Monomeren verändertes Dissoziationsverhalten auf. Dementsprechend ist ein erheblicher Anteil der ionischen Gruppen innerhalb der Polymermatrix eingebunden und heterogen verteilt. Die Messungen der elektrophoretischen Mobilität weisen eine von null verschobene Grenzmobilität bei hohen Salzgehalten auf. Während das dafür charakteristische „Soft-Particle“-Modell die Daten nicht adäquat beschriebt, können mit einem erweiterten „Hard-Particle“-Modell unter Berücksichtigung des Relaxationseffektes konsistente Zetapotentiale berechnet werden. Die daraus ermittelten Oberflächenpotentiale sinken mit steigendem Stabilisatorgehalt. Ein Vergleich zwischen elektrokinetischen und titrimetrischen Ladungsdichten weißt Unterschiede auf. Daher wird das Oberflächenpotential als effektives Potential für ein ionenundurchlässiges Teilchen mit gleicher elektrophoretischer Mobilität betrachtet.

Hamaker-Konstanten, die auf Basis der klassischen DLVO-Theorie berechnet wurden, weisen auf das Vorliegen zusätzlicher attraktiver Wechselwirkungen hin. Demgegenüber können aus der vOCG-Theorie konsistentere und typische Werte für wässrige Dispersionen ermittelt werden. Die Interpretation nach XDLVO-Theorie zeigt, dass attraktive, hydrophobe Wechselwirkungen einen erheblichen Beitrag zur Gesamtwechselwirkung leisten und maßgeblich vom Polyoltyp dominiert werden. PolyTHF-basierte PUDs weisen die stärksten hydrophoben Wechselwirkungen auf, gefolgt von PE-basierten Systemen, sowie PC-basierte Dispersionen. Eine Erhöhung des AAS- bzw. DMPS-Gehaltes sowie des Hartsegmentanteils reduziert die attraktiven, hydrophoben Wechselwirkungen. Die Ergebnisse belegen, dass die Dispersionsstabilität elektrostatistisch stabilisierter PUDs nicht ausschließlich durch elektrostatische Abstoßung bestimmt wird, sondern wesentlich von den strukturellen Komponenten von Polyurethanen abhängt. Die Studie liefert damit fundierte Struktur-Eigenschafts-Beziehungen und bietet eine Grundlage für die gezielte Gestaltung stabiler, wasser-basierter Polyurethandispersionen.

Abstract

Water-based polyurethane dispersions (PUDs) are increasingly replacing solvent-based systems, yet the molecular factors governing their stability remain poorly understood. Despite the central role of electrostatic repulsion, growing evidence suggests that dispersion stability is shaped by more than just ionisable groups. This thesis investigates the relationship between molecular structure and dispersion stability in electrostatically stabilized, water-based polyurethane dispersions.

A systematic series of well-defined PUDs is synthesized according to the acetone process to examine the effects of three key structural parameters: the polyol component (polycarbonate, polyester, and polyTHF diols), the type and concentration of hydrophilizing agents (3.0–5.5 wt% AAS and DMPA), and the hard segment content, adjusted through varying amounts of 1,4-butanediol while maintaining constant ionic group content. The dispersion stability is evaluated by critical coagulation concentration (ccc), while electrostatic interactions are characterized by potentiometric titration and electrophoretic mobility, which are analysed using both soft and hard particle models. Van der Waals interactions are quantified through Hamaker constants derived from classical DLVO theory and the van Oss–Chaudhury–Good (vOCG) method. The results are interpreted in terms of DLVO and XDLVO theory.

All dispersions show monomodal particle size distributions, with particle size decreasing asymptotically as stabilizer content increased. Stability improved with higher concentrations of both AAS and DMPA, although DMPA leads to lower dispersion stability. Increasing the hard segment content leads to an improvement in dispersion stability. Among all structural parameters, the polyol component exerts the strongest impact on stability. PC-based PUDs show substantially better stability than those containing PolyTHF or PE diols, indicating that the type soft segment substantially influences particle interactions.

Potentiometric titration reveal that a substantial portion of ionic groups remains cannot be detected, as indicated by recovery rates of 70–85% for AAS and 50–75% for DMPA. In addition, both AAS- and DMPA functional groups show altered dissociation behaviour. Therefore, a substantial portion of ionic groups remains buried within the particle matrix, leading to heterogeneous charge distributions. Electrophoretic mobility measurements show a non-zero limiting mobility at high salt concentrations. While the soft-particle model provides qualitative insights, it fails to describe experimental data at low ionic strength and the charge distribution accurately. In contrast, hard particle model considering relaxation effects yields consistent zeta potentials. Surface potentials decrease with increasing stabilizer content, attributed to greater specific surface area, and shear plane distances align well with literature values. However, electrokinetic surface charge densities are markedly lower than those from titration, reinforcing the existence of an ion-penetrable shell.

Hamaker constants calculated using DLVO theory indicate the presence of additional attractive forces. Hamaker constants derived from vOCG theory based on contact angle measurements are more consistent and typical for aqueous dispersions. Analysing these findings in terms of XDLVO theory reveals hydrophobic attractions that are dominated by the polyol type. PolyTHF based PUDs show the strongest hydrophobic interactions, followed by PE-based systems, while PC-based PUDs demonstrate the lowest hydrophobic contribution. Increasing the AAS and DMPA as well as the hard segment content results in a reduction in hydrophobic interactions in all series. The results demonstrate that the dispersion stability of electrostatically stabilized PUDs is not governed solely by electrostatic repulsion, but is significantly influenced by the structural components of the polyurethanes. This study thus provides fundamental structure–property relationships and establishes a basis for the rational design of stable, water-based polyurethane dispersions.

Contents

1 Introduction

Polyurethanes are used extensively in a variety of industries due to their adaptability, mechanical performance, and durability. These materials can be tailored into various forms, including foams,[1–6] coatings,[6–11] sealants,[6,12–16] and adhesives,[6,15–19] and find application in a range of sectors, like construction, automotive, healthcare, and packaging. A major application is in the production of foam, with flexible foams being utilised in furniture, bedding, and automotive seating, and rigid foams providing insulation in construction and refrigeration. In the field of coatings, polyurethanes are highly favoured for their exceptional resistance to abrasion and their ability to adhere to a wide range of substrates. The utilisation of polyurethane based adhesives and sealants in the automotive, electronics, and construction industries is of particular importance due to their strong bonding and flexibility. Thermoplastic polyurethanes exhibit a combination of elasticity and processability, making them suitable for utilisation in films, tubing, and footwear soles.

Its diverse applications arise from the ability to precisely control their chemical composition. Invented by Otto Bayer, polyurethanes are synthesized through the polyaddition of polyol components and higher functional isocyanates, forming the characteristic urethane linkage.[20] The properties of the resulting material are heavily influenced by the type of polyol used, such as polyester, polyether, and polycarbonate polyols. These polyols differ in their functional groups, which significantly affect the chemical and mechanical properties of the polyurethane. The molecular weight of these polyols ranges from 50 g mol^{-1} (short-chain) to 4000 g mol^{-1} (long-chain). Short-chain polyols increase the density of urethane linkages, often referred to as hard segments, thereby enhancing the polymer's ability to form hydrogen bonds and dipole interactions, resulting in a more rigid, stiff network. In contrast, long-chain polyols reduce the density of urethane linkages, introducing more flexibility into the structure and creating a softer, more elastic material. The choice of isocyanate, such as methylene diphenyl diisocyanate (MDI), toluene diisocyanate (TDI), or hexamethylene diisocyanate (HDI), further influences the final material's rigidity, flexibility, and UV resistance. Additional components, such as chain extenders, crosslinkers, plasticizers, and fillers, are employed to fine-tune the properties of the polyurethane.[6,21–30]

In recent years, increasing environmental concerns and the drive to reduce volatile organic compounds (VOCs) have led to a growing focus on water-based polyurethane dispersions (PUDs), as these systems offer a more sustainable alternative to solvent-based formulations. One technical advantage of aqueous dispersions is the independence of viscosity from molecular weight. Polyurethane dispersions can be synthesised with both a high solids content and a high molecular weight concurrently.[31–37]

The stability of PUDs is crucial throughout synthesis, storage, and application to ensure consistent product performance. Instability can lead to particle agglomeration, phase separation, viscosity drift, and, ultimately, product failure. To maintain dispersion stability, electrostatic stabilization is commonly employed by incorporating acid-functional monomers, such as Dimethylolpropionic acid (DMPA)[38–41] or 2-[(2-aminoethyl)amino]ethanesulfonic acid (AAS),[42,43] into the polymer backbone. During the production process of PUDs, these ionisable groups tend to reorganize themselves in the particle surface region, generating charges that induce electrostatic repulsion between the particles.

A widely accepted theory for describing dispersion stability is the DLVO theory developed by Derjaguin, Landau, Verwey, and Overbeek.[44,45] According to this theory, the total interaction potential between two colloidal particles is characterised by attractive van der Waals forces and repulsive electrostatic interactions. Van der Waals forces are short-range and attractive, while electrostatic forces result from the overlap of electrical double layers formed by surface-functional groups. When two particles approach one another, their double layers begin to overlap, increasing the repulsive energy. If the repulsion is sufficiently strong, an energy barrier forms, which prevents the particles from

aggregating. The height of this energy barrier, and thus the thermal stability of the dispersion, is influenced by surface potential, ionic strength of the medium, pH, and the valence of counterions.[46,47] In low ionic strength environments, the electrical double layer is more effective, increasing repulsive interactions. However, if the ionic strength is too high, the double layer compresses, reducing the energy barrier and destabilizing the system. In particular, above a certain electrolyte concentration, the so called critical coagulation concentration, the energy barrier vanishes, leading to maximum rate of coagulation.

However, the electrostatic forces might also be influenced by the particle character itself. The intrinsic stabilization of PUDs and the complex rearrangement of the charged entities to the particle/water interface during dispersion might lead to variations in the surface structures. Some groups migrate toward the particle-water interface, while others remain embedded within the core or shielded by the surrounding polymer matrix. This reorganization could affect the accessibility, dissociation, and electrostatic contribution of these functional groups.

This raises the question of whether PUD particles should be considered as soft particles. In this context, Ohshima's soft particle model, which describes a hard core surrounded by a polyelectrolyte layer, offers a useful approach for investigating such phenomena.[48,49] To explore this hypothesis, experimental techniques such as potentiometric titration and zeta potential measurements can be used to assess the dissociation behaviour and electrokinetic properties of the particles. Discrepancies between the total ionic group concentration and the measured surface charge might indicate limited accessibility or partial screening effects. Measuring the electrophoretic mobility as a function of ionic strength makes it further possible to distinguish between soft and hard particles.[50] These observations may help clarify whether polyurethane particles exhibit soft-particle-like characteristics, or whether their behaviour is better described by conventional models for hard-spheres.

While DLVO theory provides a valuable framework for understanding colloidal stability, it does not account for interaction types other than van der Waals attraction and electrostatic repulsion. For instance, recent studies using atomic force microscopy (AFM) have uncovered discrepancies between the predicted and measured interparticle forces, suggesting the presence of additional interactions beyond the classical electrostatic and van der Waals forces.[51–58] One of these additional interactions is the hydrophobic force, which can arise when hydrophobic regions or patches on the particle surface come into close contact. The origin of these forces is still an area of current research, but they are thought to involve solvent-mediated interactions, entropic effects, and the ordering of water molecules around hydrophobic surfaces. In PUDs, hydrophobic forces may play an important role due to the amphiphilic nature of the polyurethane polymer and the potential for incomplete hydration or shielding of hydrophilic groups at the particle interface.

Despite extensive studies on the influence of monomer composition on polyurethane properties, a detailed understanding of structure-stability relationships in water-based polyurethane dispersions is still pending. In particular, the role of different types of monomers, surface functional group arrangement, dissociation behaviour, and the particle structure have not been fully explored. This work seeks to address these gaps by systematically investigating the influence of different types of polyols, hydrophilizing components and hard segment content on the dispersion stability of polyurethane dispersion using different types of experimental techniques. By evaluating experimental findings with theoretical models this study aims to offer a more complete understanding of dispersion stability of PUDs.

2 Theoretical Background

2.1 Polyurethane Chemistry

Polyurethanes (PURs) are a broad class of polymers synthesized via the polyaddition of multifunctional isocyanates and hydroxyl-terminated components, a process first discovered by Otto Bayer.[20] The wide variety of suitable monomers is the base for the diverse compositions and a broad spectrum of properties. Compared to other polymers, polyurethanes distinguish through their versatile component selection and the ability to control polymerization through the formation of stable intermediates (prepolymers). This flexibility in composition and processing allows to tailor them to a wide range of application-specific requirements.

All PURs contain urethane functional groups serving as their defining structural unit. Urethanes, being esters of carbamic acid, are primarily synthesized via the addition reaction of isocyanates with alcohols (Figure 2-1a).[6,22,24–29,32,33] If amines are used instead of alcohols, a urea functional group is formed (Figure 2-1b). Such urea functional groups are often considered part of the broader class of polyurethane functionalities, as they share comparable structural and chemical characteristics.

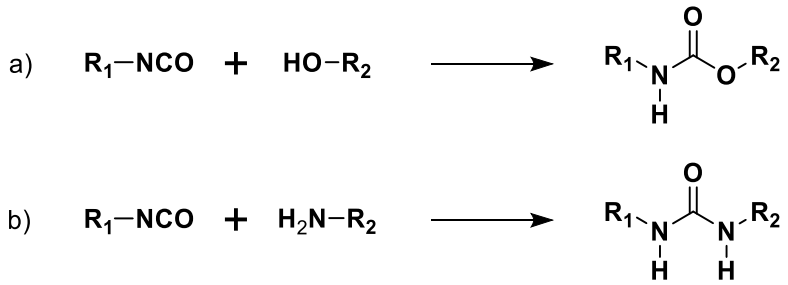

Figure 2-1: Reactions between isocyanates and a) alcohols, b) amines, leading to the characteristic formation of urethane and urea structural groups, respectively.

The use of di- or multifunctional reactants leads to the formation of high-molar mass polyurethanes, as illustrated in Figure 2-2. Compared to other functional groups such as ether, ester or urea groups, the urethane group is generally present to a minor extent. In most cases, two or more closely spaced urethane groups link high-molar mass polyol components. Consequently, the overall properties of the final products are predominantly governed by the polyol structure rather than the urethane groups themselves.[23,27]

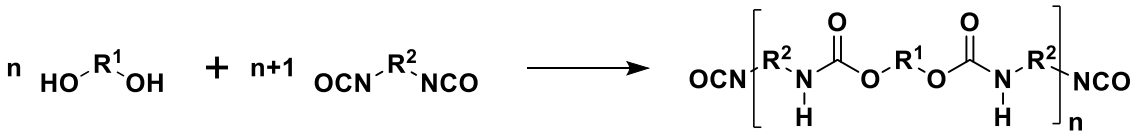

Figure 2-2: Reaction of diisocyanate in excess with a diol component leading to an isocyanate-terminated polyurethane polymer (prepolymer).

This reaction scheme illustrates the fundamental principle of polyaddition, enabling the synthesis of diverse polymer structures. Polyisocyanates used in this reaction include mono- and polycyclic aromatic compounds,[22,27,59–61] as well as aliphatic[22,24,27,62–64] and cycloaliphatic derivatives.[22,27,61,65] On the polyol side, the range of available components is even more diverse. Polyether-[6,27–29] and polyester polyols[29] offer numerous variations in functionality, chain length, and reactivity. Additionally, short-chain diols can be incorporated to fine-tune the final material properties according to specific application requirements. Polyhydroxyl and polyamine compounds are often used in combination to synthesize polyurethanes and polyureas. The reaction of diols with diisocyanates yields linear polyurethanes, while

incorporating higher functional polyols or isocyanates introduces branching and potential crosslinking. The crosslink density is determined by the proportion of higher-functional raw materials. This broad selection of building blocks provides chemists with extensive design flexibility, allowing for the development of polymers with tailored properties to meet specific application requirements. The following sections introduce typical structural components in more detail.

2.1.1 Structural Components

The greatest variety of starting materials is found among the polyol components. Their chemical composition and molar mass have the most significant influence on the properties of the resulting polyurethanes. Polyether polyols[39,59–63,66–80] such as poly(ethylene glycol) diol (PEO), poly(propylene glycol) diol (PPO) and poly(tetrahydrofurane) diol (PolyTHF), represent the largest group used in the production of polyurethanes. Other polyols, notably polyester[38,42,63–65,68,69,75,81–88] polyols, polyacrylate polyols, and polycarbonate[89–93] polyols, are also of industrial importance.[6,22] The polyol components typically have a molar mass ranging from several hundred to a few thousand grams per mole. Figure 2-3 provides an overview of common linear polyol structures.

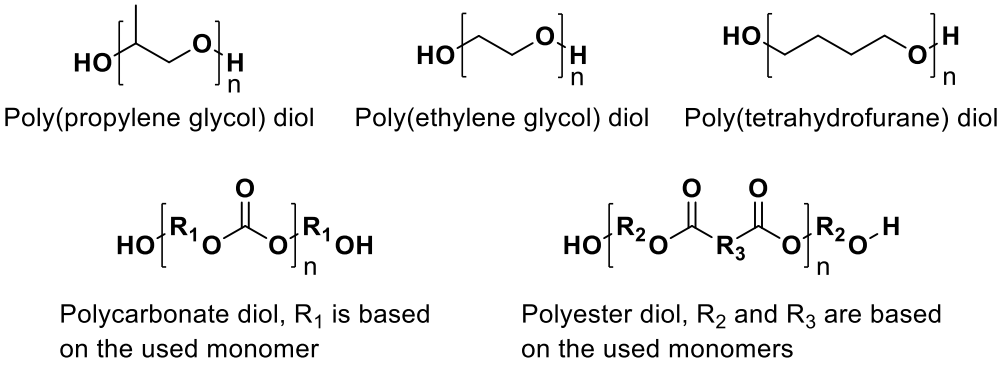

Figure 2-3: Examples of frequently used linear polyol components.

Polyether polyols are well-suited as building blocks for binders and coatings due to their low viscosity, hydrolysis resistance, and flexibility. However, their use is limited to indoor applications because of oxidative degradation of the polyether chains.[6,27,29,71]

Polyester polyols, on the other hand, feature semi-crystalline substructures of ester functionalities. These polyols can form hydrogen bonds with for example urethane or urea groups, which contribute to additional physical crosslinking within the soft segment matrix.[27,28] As a result, the mechanical properties of the polymer film are enhanced. In contrast to aromatic polyester polyols, aliphatic polyester polyols offer several advantages, such as high pigmentability, UV-resistance, and high gloss.[6,24,29] However, their sensitivity to hydrolysis is a significant drawback, leading to reduced chemical resistance with the acid number determining the degree of hydrolytic stability.[27]

Polycarbonate polyols combine the benefits of both polyether and polyester polyols. Aliphatic variants exhibit significantly better hydrolytic and weathering durability compared to polyester polyols.[28,29] The enhanced hydrolytic stability can be attributed to the fact that, unlike polyester polyols, the hydrolysis of polycarbonate polyols does not produce acidic groups that catalyse further hydrolysis reactions. Instead, typical hydrolysis products are carbon dioxide and glycols.[29] The use of polycarbonates or polyesters enhances mechanical properties, such as strength and impact resistance. The presence of carbonate or ester functionalities, along with urethane or urea groups, further contributes to physical crosslinking, resulting in improved mechanical properties.

The use of short-chain di- or triols (Figure 2-4) increases the hard segment content by generating a higher amount of urethane linkages, thereby allowing the mechanical properties of the desired product

to be specifically controlled. When compounds with a functionality > 2 are used, chemical cross-linking takes place, which far exceeds the contribution of physical cross-linking by hard segments. The resulting cross-linking density gives an indication of the subsequent mechanical properties.

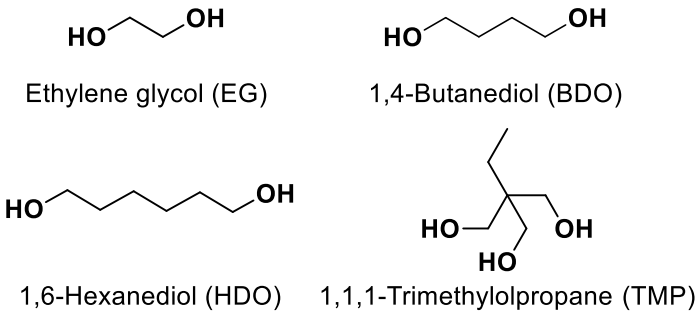

Figure 2-4: Exemplary representation of short chain diol components. Due to its tri functionality, TMP is used as a cross linking agent.

As outlined in chapter 2.1, the formation of polyurethanes require isocyanates with a functionality of two or higher. Aromatic, aliphatic, and cycloaliphatic di- and poly-isocyanates are all suitable for polyurethane chemistry, with aromatic types being more commonly used. An overview about the most common diisocyanates used is illustrated in Figure 2-5. The choice between aromatic and aliphatic isocyanates depends on their reactivity and availability.

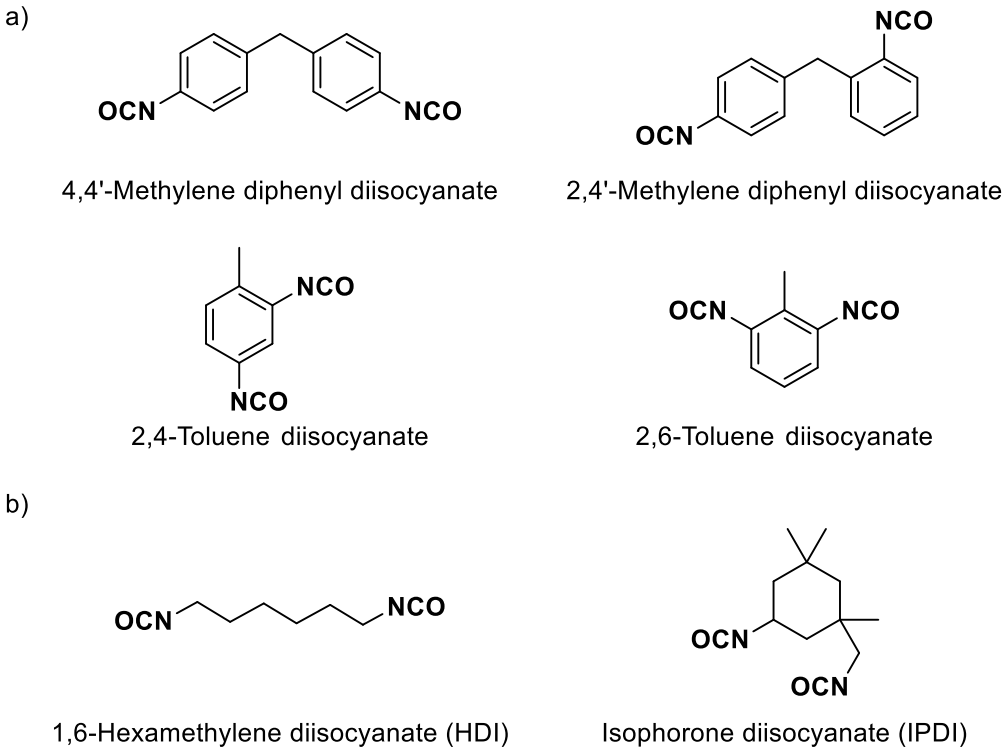

Figure 2-5: Aromatic and aliphatic diisocyanate components.

Aromatic isocyanates are more reactive and more economically accessible, while aliphatic isocyanates are selectively employed if their reactivity aligns with polymer formation requirements or if specific properties are essential for the final products. For instance, aliphatic polyisocyanates are indispensable for producing light-stable coatings. Aromatic polyisocyanates such as toluene diisocyanate (TDI)[66,67,88,94] or methylene diphenyl diisocyanate (MDI)[59–61,71] are mainly employed for the manufacturing of polyurethane foams, but not in paints or coatings due to their susceptibility to

photooxidation.[27,71] Aliphatic polyisocyanates such as hexamethylene diisocyanate (HDI)[62,63,71,93] or isophorone diisocyanate (IPDI)[42,64,68,69,71,77,85–87,89,91,94,95] are much more resistant to photooxidation and are used in paints and coatings.[24,27] In general, aromatic diisocyanates show a higher reactivity than aliphatic, which is the reason why aliphatic diisocyanates are predominantly used to produce water-based dispersions.

In addition to short chain diols, short chain diamines can also be used for chain extension. Their use generates urea groups, resulting in stronger mechanical properties since urea groups result in higher degree of physical cross linking. Typical examples are ethylene diamine (EDA),[61,85,86] hydrazine,[42,61,71] or isophorone diamine (IPDA)[96] (Figure 2-6).[6,27,28,61,94,96]

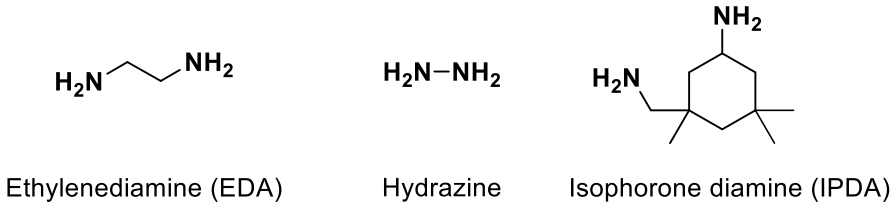

Figure 2-6: Short chain diamine components.

For many applications, especially in the field of binders and coatings, polyurethane dispersions are used due to their lower viscosity at consistently high molecular weights, better processability and water as an environmentally friendly dispersant. Like many polymeric materials, polyurethane is immiscible with water and phase separation occurs even after vigorous mixing. However, NCO-terminated hydrophobic PU prepolymers can be dispersed or emulsified with an appropriate external emulsifier and strong shear forces. Nevertheless, the dispersions obtained by this method tend to be rather coarse and unstable during storage. Therefore, an intrinsic hydrophilic modification of the polymer chains is necessary to achieve good dispersion in aqueous media.[27,31–33] In order to achieve this, ionic groups or hydrophilic chain segments are typically incorporated into the PU structure. An overview of typically used intrinsic stabilizing agents is shown in Figure 2-7.

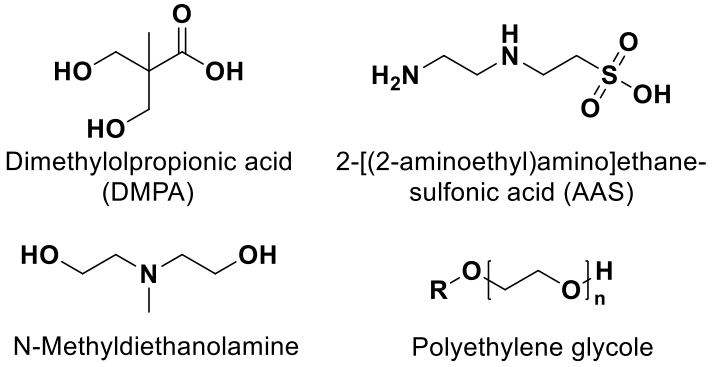

Figure 2-7: Hydrophilizing components.

One strategy to create an internally emulsifiable polyurethanes involves incorporating PEO chain segments.[39,65,84,97] In order to achieve stable dispersions, a significant number of hydrophilic PEO segments has to be incorporated into the polyurethane, resulting in a film that is highly sensitive to water. The dried coatings produced are often swellable or even soluble in water, which is undesired in many applications. Additionally, a noteworthy disadvantage of non-ionic dispersion is the potential for thermocoagulation due to the negative temperature gradient of solubility of hydrophilic PEO segments in water.[31,32] This often poses challenges during the emulsification process.[83,84]

Polyurethanes that contain ionic groups in their backbone are generally described as ionomers.[31,32,60,72,78,80] These can be either of cationic or anionic nature. Cationic polyurethanes can be obtained by the incorporation of tertiary nitrogen components, such as N-Methyldiethanolamine.[59,62,72,76,79] A positive charge is generated by quaternization of the nitrogen molecule with an acid. Nevertheless, anionically stabilized dispersions based on the incorporation of acidic functional groups such as carboxylates[38,66,67,73,85–87] or sulfonates[31,42] are predominantly used. To produce anionic polyurethane ionomers, diols containing a carboxylic acid are typically introduced with subsequent neutralization of the acid groups, e.g., with tertiary amines. Care must be taken in this reaction to avoid side reactions between NCO and COOH groups, which may lead to undesirable branching and crosslinking. Thus, compounds with sterically hindered COOH groups, such as 2,2-bis(hydroxymethyl)propionic acid (DMPA),[38,39,60,61,64–67,69,73,78,80,82–87,95,97–99] are preferred.

Sulfonate groups are usually incorporated via a diaminoalkanesulfonates,[42,92,100] such as 2-[(2-aminoethyl)amino]ethanesulfonic acid (AAS), as these compounds are water-soluble, and their reaction with NCO prepolymers is not adversely affected by water. The type and quantity of ionic groups influence the physical properties as well as the dispersing ability and particle size. Cationic polyurethanes for instance exhibit excellent adhesion properties on various substrates. On the other hand, carboxylate stabilized PUDs impart a good hydrophobic character, while PUDs stabilized by sulfonates give dispersions with excellent stability even under unfavourable conditions, such as low pH values.[31,32]

In this study polyurethanes based on three different polyol components, namely polyether, polyester and polycarbonate polyols of similar molecular weight (1000 g mol^{-1}), are synthesized. IPDI is used as the diisocyanate component due to its aliphatic nature and thus the lower reactivity to suppress side reactions with water. Only anionic groups are used as internal emulsifiers in the prepolymerization (DMPA) or chain extension step (AAS). Due to this specific line up, differences of the incorporation step as well as differences between strong and weak acidic groups can be analysed. To keep other synthesis parameters such as hard segment content, NCO/OH ratio and degree of chain extension constant, appropriate amounts of BDO or IPDA are used in the prepolymerization and chain extension step to compensate the different concentrations of DMPA and AAS, respectively.

2.1.2 Segmented Structure

As outlined in the previous chapter, the production of polyurethanes can involve several different monomers.[22,24] In general, the synthesis results in the formation of urethane and urea groups linking low-molecular weight diisocyanates with polyol blocks in between. Urethane and urea functional groups are particularly important for the properties of polyurethanes because they act as hydrogen bond donors and acceptors. Thus, they strongly influence the structure of polyurethanes due to their ability of physical crosslinking. Hydrogen bonds can be formed between every functional group, which is capable of acting as a hydrogen acceptor or donor, as other urethane or urea groups as well as polyether, polyester or polycarbonate polyol components. Hydrogen bondings between urethane and urea groups are particularly strong and they tend to form associates. The usage of short chain diols or diamines (see Figure 2-4 and Figure 2-6, respectively) leads to local accumulations and the formation of a domain structure, the so called hard segment domains. These hard segment domains are connected through more flexible polyol chains, known as soft segments (cf. Figure 2-8). Between the dissimilar segments, repulsive interactions[101] and a thermodynamically incompatibility[102] lead to a phase separation, resulting in the characteristic segmented structure of polyurethanes.

The magnitude of the phase separation is influenced by the chemical structure of the monomers, the stoichiometric ratio,[103,104] the sequence length of the hard and soft segments,[105] and the molecular weight and its distribution, ultimately effecting the final properties of the polyurethanes.[106] The formation of

domains with urea groups is more pronounced compared to urethane groups. Even individual urea groups can exhibit a hard segment character.[22] The stronger hydrogen bonds of the urea groups lead to a more pronounced segregation of the hard and soft segments. Additionally, the glass transition temperature or the melting range of the hard segment domains increases.[107] As a result, polyureas typically exhibit higher mechanical strength.

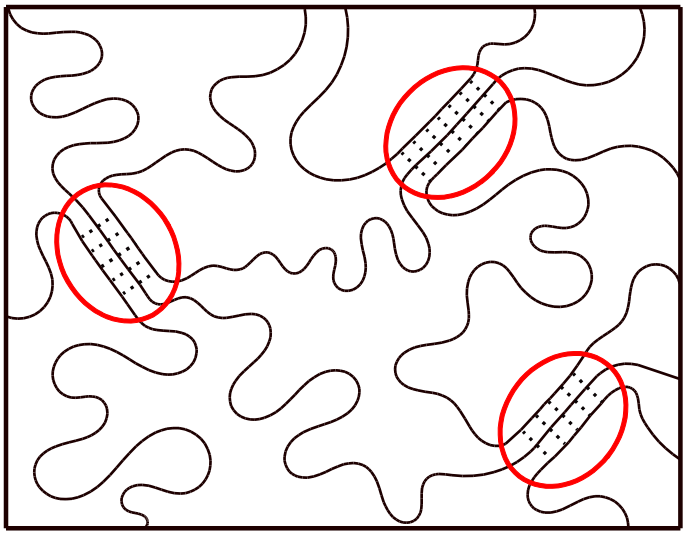

Figure 2-8: Schematic representation of the phase segregation of segmented polyurethanes. Hard segment domains highlighted by red circles connected by soft segments according to Adam et al..[22]

The ratio of urethane to urea groups, as well as the fraction of low-molecular weight diamines and diols are crucial for commercial applications due to their significant influence on domain structures and thus the final properties. In this study, the hard segment content is varied by using different amounts of 1,4-Butanediol within the prepolymerization step within a single synthesis series. Otherwise it was kept constant.

2.1.3 Parameters of Polyurethane Chemistry

Important and relevant parameters used in this work are the ratio between NCO and OH functional groups, the degree of chain extension as well as the hard segment content. The ratio between NCO and OH groups describes whether the polyurethane is terminated by isocyanates or hydroxyl groups. Accordingly, OH-functional prepolymers result with ratios < 1 whereas ratios > 1 lead to polyurethanes terminated by isocyanate groups as given by equation 2-1. The higher the ratio, the greater the excess of isocyanates and the lower the resulting molecular weight. It is especially used to define the intermediate reaction step of the prepolymerization and is the basis for the following reaction step of chain extension.

$$\mathrm{NCO/OH} = \frac{n_{\mathrm{NCO}}}{n_{\mathrm{OH}}} \tag{2-1}$$

In this work, the NCO/ OH ratio was kept constant throughout all synthesis series given by $\mathrm{NCO/OH} = 1.7$. Based on this value the degree of chain extension can be adjusted by addition of proper amounts of diamines according to the available molar quantity of remaining NCO groups after prepolymerization $n_{\mathrm{NCO,Prep}}$ as expressed by equation 2-2.

$$\text{Degree of chain extension} = \frac{n_{\mathrm{NH_2}}}{n_{\mathrm{NCO,Prep}}} \tag{2-2}$$

In general, the higher the degree of chain extension, the higher the molecular weight of the final product. In this work, the degree of chain extension was kept constant throughout all synthesis series at 92 %. As

outlined in the previous chapter, the hard segment content is an important parameter within the polyurethane chemistry and can be expressed by the sum of all short chain components divided by the total mass of polyurethane, as given by equation 2-3.

$$\text{Hard segment content} = \frac{m_{\text{DMPA}} + m_{\text{BDO}} + m_{\text{IPDI}} + m_{\text{AAS}} + m_{\text{IPDA}}}{m_{\text{PU}}} \quad (2\text{-}3)$$

The equation has been adjusted to the used components of this study.

2.2 Polyurethane Dispersions

Originally, polyurethanes are synthesized in organic solvents to handle the increasing viscosity with increasing molecular weight during the reaction and to achieve homogeneous films on substrates after drying. However, these solvents are mostly not recovered, but instead released into the environment in an uneconomical and environmentally questionable manner or combusted in exhaust systems. Consequently, regulations have been introduced to limit the usage of so called volatile organic compounds (VOCs). For this reason, the development of more environmentally friendly water-based polyurethane dispersions has become of great industrial importance.[31–33,108]

Aqueous polyurethane dispersions (PUD) are binary systems of polyurethane particles acting as the dispersed phase in the continuous water phase. PUDs, like every type of polymer dispersion, have a primary benefit in their viscosity, which is typically unaffected by the polymer's molecular weight. This allows the formulation of high solids PUDs with sufficiently high molecular weights to provide films with excellent performance by physical drying alone. This means that film formation occurs solely through the evaporation of water, even at ambient temperatures.[31,64,108] These systems predominantly consist of linear thermoplastic polyurethanes, although recent research also introduced the possibility to use cross linked polymers.[6,32,109]

Polymer dispersions in general are thermodynamically unstable. PUDs typically are dispersions with particles diameters in the range of 10-1000 nm and show therefore a high interfacial area that needs to be stabilized. In contrast to conventional emulsion polymerisation techniques and the predominantly employed stabilisation by external emulsifiers, dispersion stability in the case of PUDs is generally achieved by intrinsic stabilisation. Several strategies regarding the incorporation of hydrophilic monomers into the polymer backbone to achieve anionic, cationic or non-ionic stabilization have been outlined in the previous chapter (refer to chapter 2.1.1 and Figure 2-7). Since the hydrophilic monomers need to be introduced in the system before dispersion takes place a variety of production processes has been established. Of greatest industrial relevance is the so-called acetone process. Besides the acetone process, several other synthesis techniques like the prepolymer mixing process,[6,24,31,33,110–112] ketamine/ketazine process,[6,30,32,33,111,113] or the melt dispersion process[6,24,27,28,30–33,110,111] exist. Since the focus of this work is the acetone process, it will be outlined in more detail in the following section.

2.2.1 Acetone Process

The acetone process is considered to be the most universal technology for the production of PUDs. Its versatility allows it to be used to produce high-quality products for various applications making it of significant industrial interest and the subject of current research. Initially, an isocyanate-terminated prepolymer is synthesized based on the polyaddition reaction of short- and/or long-chain polyol and diisocyanate components. The reaction rate can be controlled by catalysts, such as dibutyltin dilaurate (DBTDL) or triethylenediamine. In the prepolymer step ionomers, preferably hydroxyl terminated, such as DMPA (cf. Figure 2-7), can also be incorporated into the polymer backbone. Since DMPA contains carboxylic acid as functional groups, it needs to be neutralized with, for example, tertiary amines in the subsequent process steps to serve as internal emulsifier.

In contrast to the other processes mentioned above, the acetone process requires a relatively large amount of solvent at the start of the reaction. Besides acetone giving the name of the process, methyl ethyl ketone or tetrahydrofuran can also be used. The solvent must provide a low boiling point and be highly miscible with water, as well as being inert to the reaction components. The synthesized prepolymer is dissolved in the solvent to handle the increasing viscosity in the following reaction step. The isocyanate-terminated prepolymer then reacts in solution with the chain extender to achieve high molecular weight polyurethanes. Since the chain extension solution partly contains water as a solvent, side reactions of isocyanates might also occur. To suppress these side reactions usually diamine components are used for chain extension purpose, as the reactivity towards isocyanates is sufficiently higher than that of water.

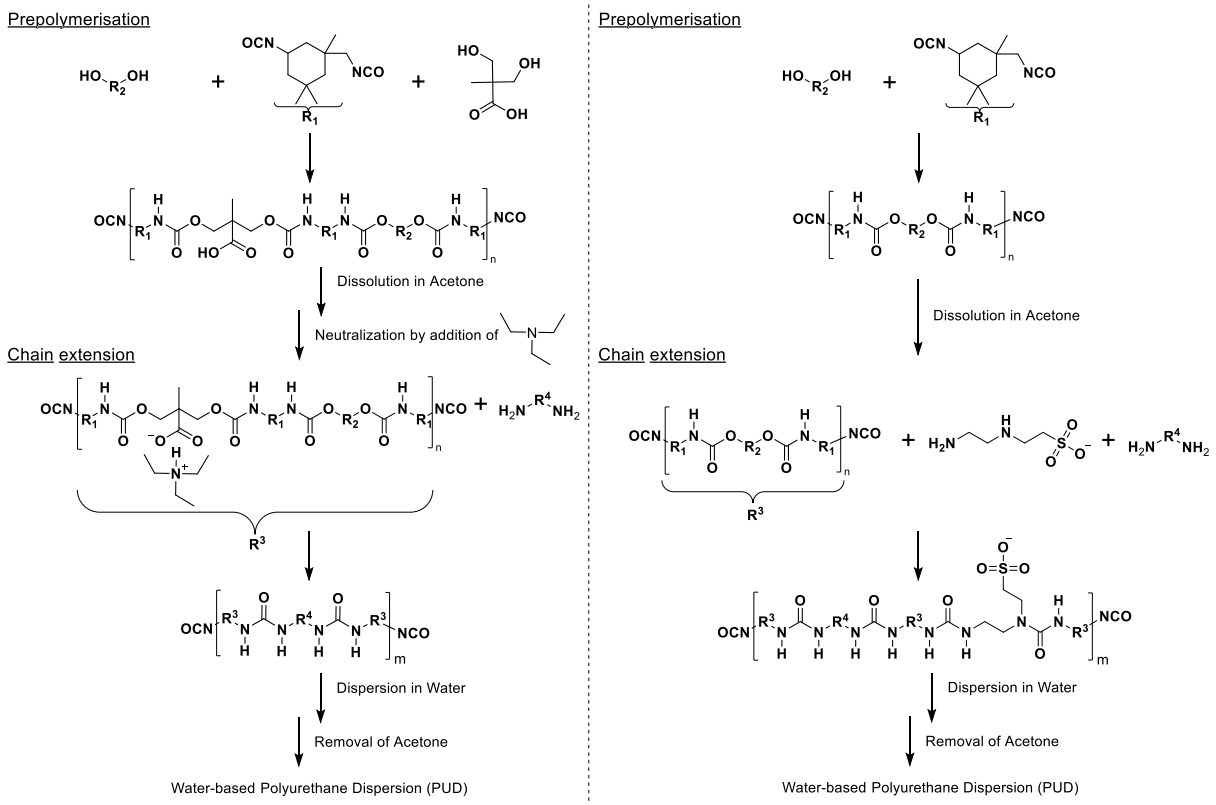

Figure 2-9: Schematic representation of the acetone process. a) ionomer formation within the prepolymerization using DMPA and b) ionomer formation within the chain extension step using AAS.

As an alternative to produce ionomer dispersions, diamines containing sulfonate groups can be introduced in this step. The different steps suitable for incorporation of ionic groups are highlighted in Figure 2-9 by the use of DMPA or AAS, respectively. This is also often referred to as incorporation within the soft segments (prepolymerization) or hard segments (chain extension).[73] Water is added to the polymer solution after the chain extension step has been completed quantitatively. The different stages of the dispersion process are shown in Figure 2-10. The polyurethane is initially dissolved in acetone. In acetone solution the ionic centres are associated, which leads to a high viscosity (Stage 1). With addition of water, solvation of the ionic centres takes place resulting in initially decreasing viscosity of the system (Stage 2). The solution becomes transparent, since the ionomers are molecularly dispersed. Upon further addition of water, the acetone concentration of the system decreases. As a result, an alignment of the hydrophobic chain segments takes places, due to their decreasing solvation sheath (Stage 3).

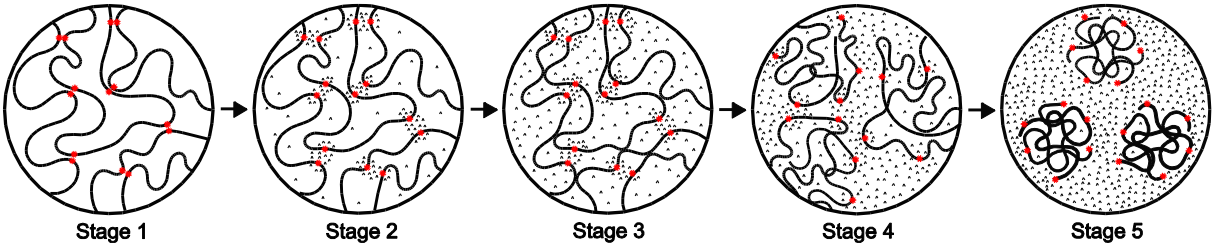

Figure 2-10: Schematic representation of the different stages during the dispersion process. Polymer chains in black, ionic centres are displayed as red circles and water molecules are illustrated with symbol ∧ according to Dieterich.[31]

Further addition of water initiates the formation of the dispersed phase. The hydrophilic ionomer groups orient themselves towards the water interface, resulting in an increase in viscosity. The polymer, which is still dissolved in acetone, is partially swollen with water and cannot absorb any additional water molecules (Stage 4). Once this point is reached and water continues to be added, the system collapses and a phase inversion takes place. As a result, the aqueous phase becomes the matrix in which the solvent-swollen polymer is homogeneously dispersed, causing the viscosity to decrease to a minimum (Stage 5).[31,114–116] The acetone, which is volatile and inert, can be removed after the dispersion step by distillation, dried and recirculated. The acetone process is reproducible and well-defined resulting in aqueous polyurethane dispersions typically characterized by particle size distributions ranging from 10-500 nm.[22,24,31–33,89,90,110–112,117–121]

2.3 Colloidal Dispersions

Colloidal dispersions in general are characterised by a large interfacial area. This leads to a thermodynamically instability of the dispersion and thus to coagulation when the thermal motion of the particles results in particle-particle contact. Additionally, interaction energies like van der Waals forces induce interparticle attraction. These attractive forces can be mitigated through sufficiently high repulsive forces to achieve thermodynamically stable dispersions. Currently, four stabilisation mechanisms are recognised, the electrostatic, hydrophilic, steric and depletion stabilization. Since PUDs are very often intrinsically stabilized by incorporation of ionic groups as outlined in chapter 2.1.1, only the electrostatic stabilization mechanism will be examined in more detail in this work.

2.3.1 Electrochemical Double Layer

In case of electrostatic stabilization, a sufficient amount of ionisable groups needs to be located at the particle surface i.e. the interface between the dispersed and mobile phase generating surface charges. Thus, depending on the amount of surface charges, a characteristic surface charge density or surface potential is generated. The surface charges cause an accumulation of counter ions (charges of opposite sign), at the interface and the nearby environment.[122,123] The concentration of counterions near the surface can be several orders of magnitude higher than that in the bulk solution. However, the concentration of these counterions is limited by their intrinsic volume and their natural repulsive interactions.

The distribution of the counter- and co-ions (charge of similar sign) within the diffuse layer defines the electrostatic potential profile. The potential has its maximum directly at the particle surface i.e. the surface potential ψ_0 and decreases exponentially with distance. The Gouy Chapman model describes the distribution of co- and counter ions within the diffuse layer. The concentration of the co- (c^{CO}) and the counter ions (c^{C}) can be calculated according to equation 2-4 in dependence on the double layer potential ψ at a given distance *x* with the concentration of co- or counterions at large distances from the particle surface $c_0^{\mathrm{CO/C}}$, the valence *z*, the Faraday constant *F*, the ideal gas constant *R* and the temperature *T*.

$$c_{\mathrm{CO/C}} = c_0^{\mathrm{CO/C}} \cdot \exp\left(\frac{zF\psi_{\mathrm{x}}}{RT}\right) \tag{2-4}$$

Thus, the counterion concentration decreases with increasing distance, while the co-ion concentration increases as they are repelled by the similarly charged particle.

The Gouy-Chapman model, however, does not account for the finite size of ions. This limitation was addressed by the Stern model and the basic principles are shown in Figure 2-11.[124] It considers the size of each ion species, resulting in a minimum approach distance to the interface. Furthermore, it accounts for ion saturation at the interface, beyond which additional counterions cannot adsorb. The Stern model divides the diffuse layer into two distinct regions, resulting in the so-called electrical double layer. The Stern layer consists of a fixed, adsorbed layer of counterions directly at the particle surface. Because these ions are immobile, the electrostatic potential decreases linearly within this layer. However, due to thermal energy, hydration shells and steric constraints, not all surface charges are neutralized in the Stern layer. The remaining charge is compensated by a diffuse layer of freely moving counterions surrounding the particle. The boundary between these two layers is characterized by the Stern potential ψ_S.

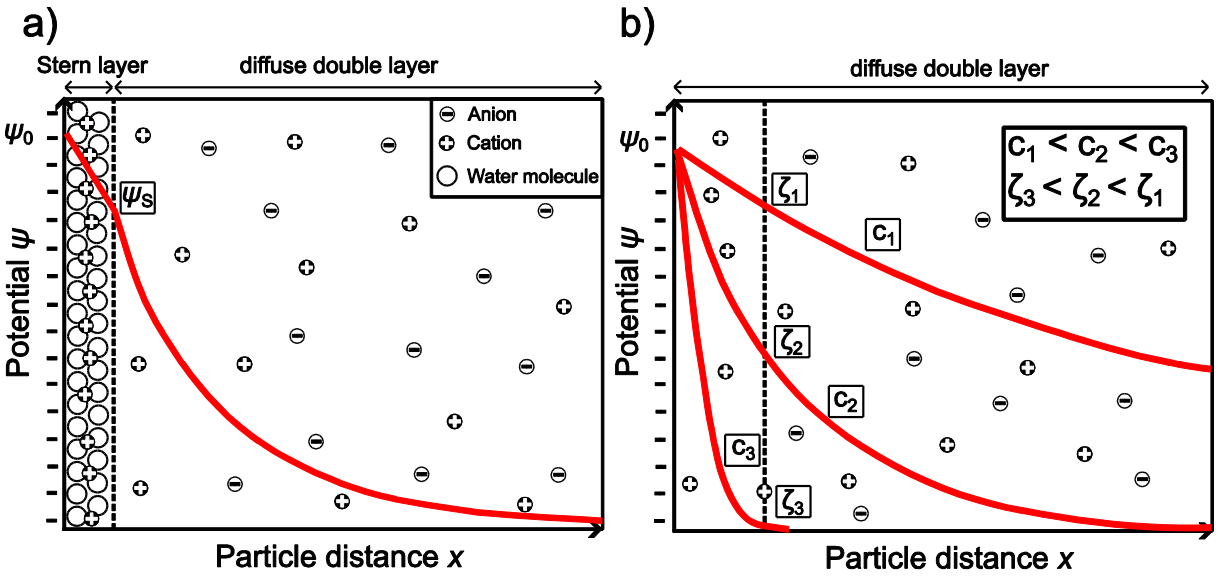

Figure 2-11: a) Exemplary representation of the Stern model for the diffuse double layer of a negatively charged surface according to Stern.[124] b) Potential course around a large, negatively charged, spherical particle for different electrolyte concentrations and thus altering thickness of the diffuse double layer according to Gouy and Chapman.[122,123]

In the diffuse layer, the counter ions are not fixed but can move freely and are subject to diffusion. The concentration of positive counter ions is still high at short distances from the particle surface. With increasing distance, the concentration of co-ions continues to increase until finally the concentration of positive and negative ions is equal. The charge compensation of the particle surface is complete. The corresponding course of the potential is also illustrated in Figure 2-11. The potential drop towards zero occurs in the diffuse layer. In contrast to the linear decay within the stern layer, the potential drop in the diffuse layer is exponential because of the irregular distribution of the counter ions. For a quantitative description of the potential course within the electrical double layer and thus the magnitude of the electrostatic interaction potential, the thickness of the diffuse double layer κ^{-1} (Debye screening length, eq. 2-5) needs to be taken into account.[125]

$$\kappa = \sqrt{\frac{F^2}{\varepsilon_{\mathrm{r}}\varepsilon_0 RT}\sum z_{\mathrm{i}}^2 c_{\mathrm{i}}} \tag{2-5}$$

The Debye-Hückel parameter κ depends on the concentration of ions c_i present in the dispersion medium, their valence and the dielectric constant ε of the dispersion medium, but not on the surface charge density or surface potential. Consequently, the thickness of the diffuse layer is observed to decrease with increasing concentration of an electrolyte, or with increasing valence of the counter ions. As the concentration of the electrolyte or the valence of the counter ions increases, the potential drop in the diffuse layer becomes increasingly steep.

2.3.2 Electrokinetic Properties of Hard Particles

As stated before, the diffuse layer is partially comprised of non-fixed, mobile ions and does therefore not comprise a rigid structure. In the course of a diffusive movement of a particle or in the case of an applied electrical field, the diffuse layer is partially sheared off due to frictional forces. As a result of the loss of an outer part of the diffuse layer, the particle lacks counter ions to compensate for the net charge of the particle surface. Thus, the particle is no longer neutral towards the outside. The removal of the counter ions responsible for the potential difference between the shear plane and the outside of the diffuse layer results in an effective potential, which is often referred to as zeta potential ζ. The zeta potential depends on the thickness of the diffuse double layer and thus on the ionic strength. Increasing ionic strength leads to a compression of the electrical double layer and therefore to lower zeta potentials as highlighted in Figure 2-11 b.

The properties and composition of the electric double layer can be characterised by preferably using electrokinetic investigation methods. In case of an electrical field, the particles are accelerated in the direction of the oppositely charged electrode. The movement of a charged colloidal particle in an electrolyte solution under the influence of an electric field is thereby influenced by four forces, schematically illustrated in Figure 2-12 a.[126,127]

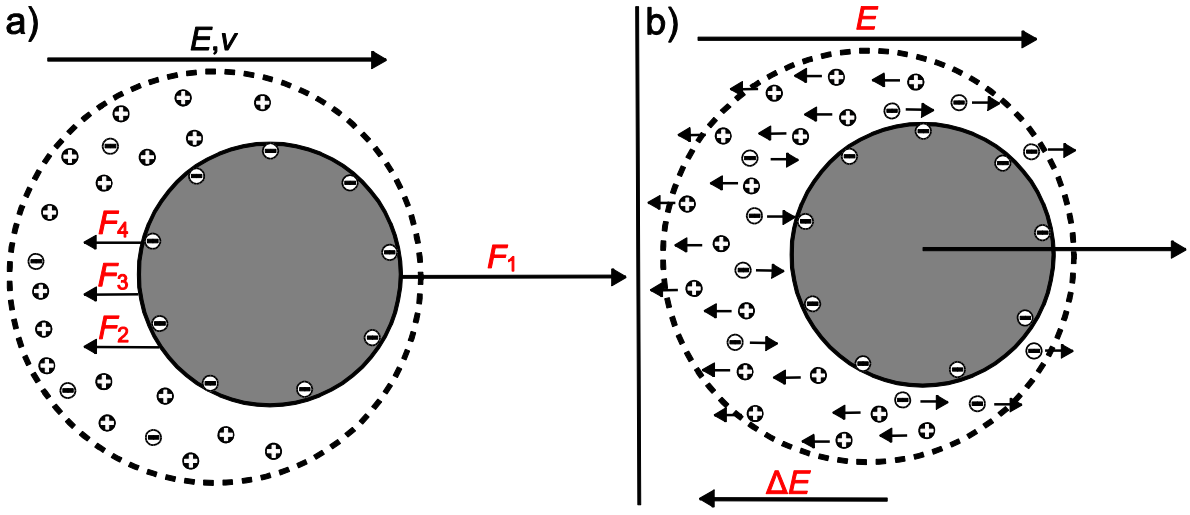

Figure 2-12: a) Forces affecting the particle movement during electrophoresis and b) schematically representation of the relaxation effect according to Overbeek et al..[126]

Two of these forces are fairly straightforward to specify, while the other two affect the particle movement in a highly complex manner. The electrostatic force F_1 is given by the product of the field strength E and the particle charge Q. F_2 is the frictional force of solvent molecules defined by Stokes, which is proportional to the velocity.[128]

The two remaining forces are caused by the diffuse electrical double layer. Due to the application of an electrical field, the hydrated ions within the diffuse double layer are also accelerated in the respective directions. As a result, an additional frictional force F_3 is generated, causing a retardation of the colloidal particles movement. This effect is also known as retardation effect.

Additionally, the distribution of the co- and counterions within the diffuse double layer is deformed under the application of an electrical field, especially in case of a large expansion of the diffuse double layer compared to the particle radius. This phenomenon is caused by the opposing movement of the particle and the counterions leading to an asymmetrical charge distribution. The Coulomb forces between the particle charge Q, and the ions tend to re-establish a symmetrical charge distribution around the particle. However, this process is subject to a finite time, which is referred to as the relaxation time. Therefore, in the stationary state, the centre of the ionic atmosphere is in a state of displacement with respect to the centre of the particle. As a result, an additional electrical force, F_4, is generated in opposite direction to the originally applied electrical field. This force, which decreases the particles velocity, is referred to as the relaxation effect as illustrated in Figure 2-12 b.

If the electrical field is strong enough, the particle velocity is sufficient to shear off almost the complete diffuse double layer, meaning $\zeta \approx \psi_S$. The velocity of a particle v subjected to an electrical field E is referred to as electrophoretic mobility μ as defined by equation 2-6. This parameter can be experimentally determined for example using electrophoretic experiments, for example.

$$\mu = \frac{|v|}{|E|} \tag{2-6}$$

The relation between the electrophoretic mobility μ of a spherical, hard particle and the zeta potential ζ is frequently described by the Helmholtz-Smoluchowski (equation 2-7) with relative permittivity ε_r, permittivity in vacuum ε_0 and the viscosity η.[129] A hard particle is defined as a particle consisting of an ion impermeable core with the charged groups directly located at the particle surface, as schematically illustrated in Figure 2-13.

$$\mu = \frac{\varepsilon_r \varepsilon_0}{\eta} \zeta \tag{2-7}$$

It is a good approximation for the limiting case of particles being much larger than the diffuse double layer, i.e. $\kappa a \gg 1$. Furthermore, additional effects like the relaxation effect are also neglected and thus it is only valid for low zeta potentials (<25-80 mV). On the other hand, an approach to cover the case of $\kappa a \ll 1$ was developed by Hückel[130] and Onsager[131] (eq. 2-8).

$$\mu = \frac{2\varepsilon_r \varepsilon_0}{3\eta} \zeta \tag{2-8}$$

Both theoretical approaches were linked by the Henry theory (eq. 2-9), who additionally considered the hydrodynamic influences, meaning the retardation effect, by introducing the Henry function $f(\kappa a)$.[132]

$$\mu = \frac{\varepsilon_r \varepsilon_0 \zeta}{\eta} f(\kappa a) \tag{2-9}$$

Ohshima derived an accurate expression for Henry's function valid for arbitrary κa values (equation 2-10).[133] For the case of $\kappa a \gg 1$ $f(\kappa a)$ becomes 1.5 leading to equation 2-7 and for $\kappa a \ll 1$ $f(\kappa a)$ becomes 1.0 leading to equation 2-8.

$$f(\kappa a) = \frac{2}{3}\left[1 + \frac{1}{2\left(1+\frac{2.5}{\kappa a\{1+2\exp(-\kappa a)\}}\right)^3}\right] \tag{2-10}$$

To account for the relaxation effect, these basic theories have been extended. Firstly by Overbeek, who additionally considered the relaxation effect for spherical particles, arbitrary κa and low zeta potential $\zeta \ll 25$ mV.[126] Together with Lyklema and Loeb approximate solutions were derived. They clearly showed, that Henrys formula led to too low results for potentials $y = \frac{F\zeta}{RT} > 2$ and small κa values, indicating the necessity to take the relaxation effects into account. The first numerical solution was derived later, by Wiersema, Loeb and Overbeek.[127] Based on this fundamental work, O'Brien and White

established the well-known and often used O'Brien/White theory to describe the relation between the electrophoretic mobility and the zeta potential.[134] Based on this work, Ohshima et al. developed an analytical expression which is in good agreement to the numerical solutions of the aforementioned theory.[135,136] This analytical expression is used within this study and is described in Chapter 4 in detail.

2.3.3 Electrokinetic Properties of Soft Particles

The aforementioned theories describing the relationship between the electrophoretic mobility and the zeta potential can solely be applied to hard particles. However, particles with structured surfaces such as bio colloids or colloids covered with polymers/polyelectrolytes, termed soft particles, these models do not hold. According to Ohshima, a soft particle is defined as a particle consisting of an ion-impenetrable particle core covered by an ion-penetrable surface charge or polyelectrolyte layer. Thus it becomes evident, that the soft particle combines properties of polyelectrolyte like particles as well as hard particles. These fundamental assumption is illustrated in Figure 2-13.

Several theoretical approaches have been discussed in literature for the case of hard particles as already discussed in the previous chapter. Hermans and Fujita demonstrated that the electrophoretic mobility of a spherical polyelectrolyte assuming a uniformly charge distribution at a given volume charge density Q_{fix} can be demonstrated by the following equation.[137]

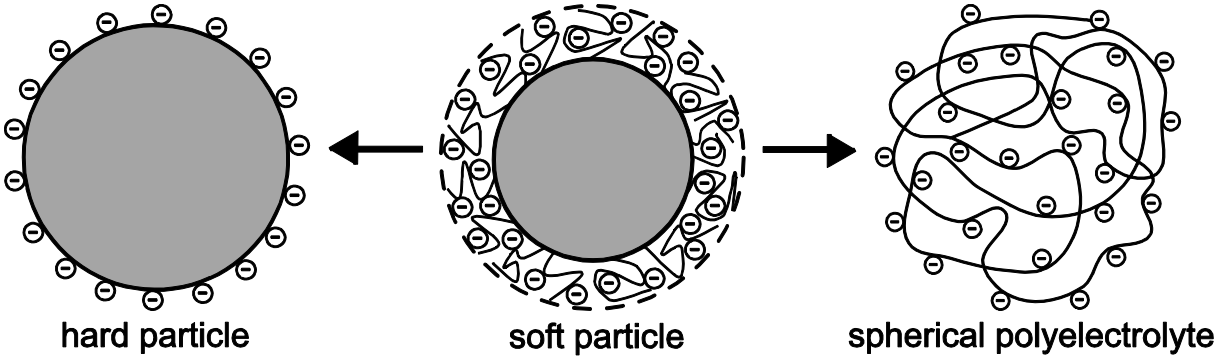

Figure 2-13: Schematic illustration of the different particle structures according to Ohshima.[50,138]

$$\mu = \frac{Q_{\mathrm{fix}}}{\eta {\lambda_{\mathrm{HF}}}^2}\left[1 + \frac{2}{3}\left(\frac{\lambda_{\mathrm{HF}}}{\kappa}\right)^2 \frac{1+\frac{\lambda_{\mathrm{HF}}}{2\kappa}}{1+\frac{\lambda_{\mathrm{HF}}}{\kappa}}\right] \tag{2-11}$$

$$Q_{\mathrm{fix}} = eZN \tag{2-12}$$

Here, λ_{HF} being defined as $\lambda_{\mathrm{HF}} = \sqrt{\frac{\gamma}{\eta}}$ with γ as the frictional coefficient of the ion-penetrable polyelectrolyte layer. Q_{fix} is given by the product of the elementary charge e as well as the valence Z and the number density N of the charged groups inside the polyelectrolyte.

Ohshima, Nakamura and Kondo, developed a theoretical model to describe the electrokinetic properties of a soft particle in a symmetrical $z{:}z$ electrolyte solution of valence z. They considered a spherical particle with an uncharged, ion-impenetrable core of radius a, covered with an ion-penetrable layer of adsorbed charged polymers with the thickness d.[48,139–141] Analogous to the Hermans-Fujita model, they pointed out that the electrokinetic properties of a soft particle is quite different from that described for hard particles. In contrast to the aforementioned hard particle models, the zeta potential loses its physical meaning and is not considered at all. Instead, the electrokinetic behaviour is essentially influenced by the so-called Donnan potential as well as the surface potential at the boundary layer of the polyelectrolyte layer towards the dispersant.[50,142] Both assumptions are shown schematically in Figure

2-14. The Donnan potential is considered as a the potential deep inside the polyelectrolyte layer, which decreases with increasing distance of the order of the Debye length and is given by equation 2-13.

$$\psi_{\mathrm{DON}} = \frac{k_{\mathrm{B}}T}{ze} \ln\left[\frac{ZN}{2zn} + \left\{\left(\frac{ZN}{2zn}\right)^2 + 1\right\}^{0,5}\right] \tag{2-13}$$

The surface potential on the other hand is given by equation 2-14.

$$\psi_0 = \frac{k_{\mathrm{B}}T}{ze}\left(\ln\left[\frac{ZN}{2zn} + \left\{\left(\frac{ZN}{2zn}\right)^2 + 1\right\}^{0,5}\right] + \frac{2zn}{ZN}\left[1 - \left\{\left(\frac{ZN}{2zn}\right)^2 + 1\right\}^{0,5}\right]\right) \tag{2-14}$$

It is important to note that both potentials are dependent on the characteristic volume charge density eZN derived by multiplying the elementary charge e as well as the valence Z and the number density N of the charged groups inside the polyelectrolyte layer. By taking these assumptions into account, Ohshima further developed an analytical expression of the electrophoretic mobility of a soft particle given by the following equations.[49,143–145]

$$\mu = \frac{\varepsilon_{\mathrm{r}}\varepsilon_0}{\eta} \frac{{}^{\psi_0}/_{\kappa_{\mathrm{m}}} + {}^{\psi_{\mathrm{DON}}}/_{\lambda}}{{}^{1}/_{\kappa_{\mathrm{m}}} + {}^{1}/_{\lambda}} f\left({}^{d}/_{a}\right) + \frac{eZN}{\eta\lambda^2} \tag{2-15}$$

λ^{-1} is the so called electrophoretic softness parameter and serves as a measure of the ion permeability of the polyelectrolyte shell. The influence of the ratio of the radius of the particle core a to the thickness of the polyelectrolyte layer d is considered by the function $f\left({}^{d}/_{a}\right)$.

$$f\left({}^{d}/_{a}\right) = \frac{2}{3}\left[1 + \frac{1}{2\left(1 + {}^{d}/_{a}\right)^3}\right] \tag{2-16}$$

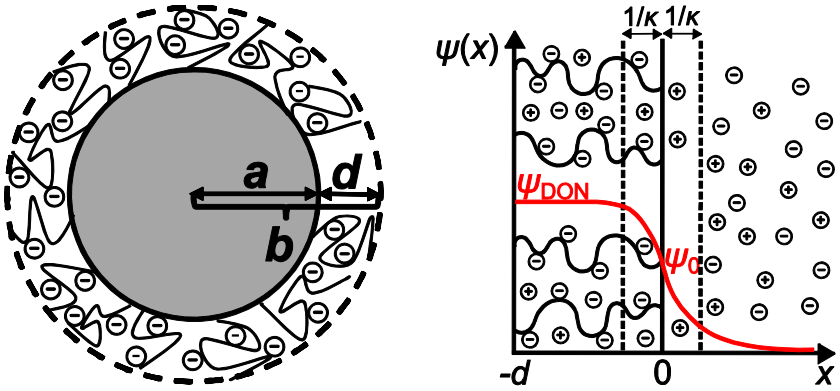

Figure 2-14: General consideration of a soft particle and the potential distribution throughout the polyelectrolyte layer towards the dispersant covering the characteristic Donnan potential as well as the surface potential at the boundary between the polyelectrolyte layer and the dispersion medium according to Ohshima.[50,138]

κ_{m} is the Debye-Hückel parameter of the polyelectrolyte layer and is given by equation 4-25. Equation 2-15 is valid under the assumption of $\lambda a \gg 1$, $\lambda d \gg 1$, $\kappa a \gg 1$ and $\kappa d \gg 1$.[144] In the limiting case of $\lambda \to \infty$ and $d \to 0$ the particle coated by polyelectrolytes shows a behaviour of a hard particle of the radius b. On the other hand, in the limiting case of $a \to 0$, the rigid particle core vanishes and the soft particle equals a spherical polyelectrolyte. In this case and for given low potentials, equation 2-15 approaches the Hermans and Fujita expression (eq. 2-11).

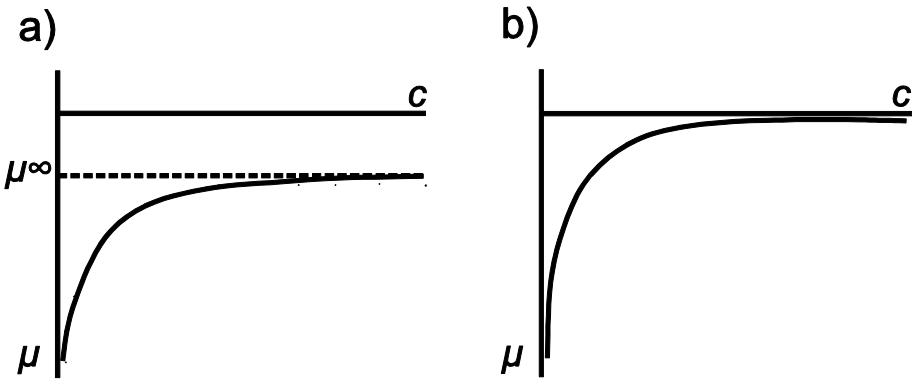

Figure 2-15: Schematic illustration of the electrophoretic mobility as a function of the electrolyte concentration for a a) soft particle and b) hard particle.[50]

Thus, Ohshima has demonstrated that equation 2-15 unites the different electrophoretic theories of hard and polyelectrolyte like particles. Ohshima also extended the theory to highly charged soft particles by taking the relaxation effect into account.[146] This equation is described in detail in chapter 4.2 in formula 4-24 and will be used within this study.

According to Ohshima, soft particles therefore show a characteristic electrolyte dependency of the electrophoretic mobility.[147] He pointed out that equation 2-15 consists out of two terms with κ_{m} being only involved in the first term. For this reason, only the first term depends on the electrolyte concentration of the system and thus tends to zero for high electrolyte concentrations due to shielding effects. The second term is independent of the electrolyte concentration. Thus, in case of high electrolyte concentration ($\kappa \to \infty$), the electrophoretic mobility approaches a non-zero limiting value μ^{∞} as given by equation 2-17.

$$\mu \to \mu^{\infty} = \frac{eZN}{\eta\lambda^2} \tag{2-17}$$

A comparison of the dependency of the electrophoretic mobility on the electrolyte concentration is shown in Figure 2-15. Since the electrophoretic mobility of hard particles approaches zero at higher electrolyte concentrations due to shielding effects, the non-zero limiting value is characteristic for soft particles and makes a differentiation possible.

2.3.4 Stability of Colloidal Dispersions

The stability of colloid dispersions in parallel can be characterized by the well-known DLVO theory, independently developed by Derjaguin and Landau as well as Verwey and Overbeek.[44,45] The theory considers the total interaction energy V_{T} between two particles as the sum of the electrostatic repulsion V_{R} and the attractive interaction energy V_{A} (eq. 2-18) and makes it possible to assess the interaction energies of two charged particles as a function of their separation distance.

$$V_{\mathrm{T}} = V_{\mathrm{R}} + V_{\mathrm{A}} \tag{2-18}$$

The electrostatic repulsive interaction energy can be determined based on the potential course of the particle as described in the previous chapter 2.3.1. Numerous studies deal with expressions for repulsive interaction energies being valid for different cases of ψ_0, κa and κH, but a detailed discussion goes beyond the scope of this thesis and can be found in corresponding literature.[44,148,149] Within this study the approach developed by Sader et al. is used. They derived an analytical expression (eq. 2-19) for the double layer interaction free energy V_{R} in case of two identical spherical particles at constant surface potential and at a given separation distance H, with the relative permittivity ε_{r}, permittivity in vacuum ε_0, molar gas constant R, thermodynamic temperature T, Faraday constant F and the particle radius a. It is valid for large κa, all κH and moderate to high surface potentials ($y_0 \leq 4$).[150]

$$V_{\mathrm{R}}(H) = 4\pi\varepsilon_{\mathrm{r}}\varepsilon_0\left(\frac{RT}{F}\right)^2 \Upsilon^2 \frac{a^2}{2a+H}\ln\left(1+\exp(-\kappa H)\right) \tag{2-19}$$

The function $\Upsilon(H)$ is given by equation 2-20 and includes the reduced surface potential y_0 (eq. 2-21), where z is the valence of the ion species and Ψ_0 the surface potential.

$$\Upsilon(H) = 4\cdot\exp\left(\frac{\kappa H}{2}\right)\tanh^{-1}\left(\exp\left(-\frac{\kappa H}{2}\right)\cdot\tanh\left(\frac{y_0}{4}\right)\right) \tag{2-20}$$

$$y_0 = \frac{ze_0\psi_0}{k_{\mathrm{B}}T} \tag{2-21}$$

According to equation 2-19, the repulsive double layer interaction energy increases with decreasing distance H. Besides it is evident that the expression depends on the surface potential ψ_0 and the Debye-Hückel parameter κ and thus the ionic strength. With increasing ionic strength, the repulsive interaction energy decreases. For this reason, electrostatically stabilized dispersions can be destabilised by increasing the electrolyte concentration of the system.

As stated above, two approaching particles also experience attractive interaction energies. Van-der-Waals forces in general account for the non-covalent bonds between atoms, molecules or colloids. The movement of electrons within an atomic shell result in charge fluctuations, which in turn lead to the formation of molecular dipoles. These dipoles partly attract one another. In this context, there are three different types that are summed up as the overall attractive interaction energy. Keesom interactions between two dipoles, Debye interactions between a dipole and a polarisable molecule and London interactions between two polarisable molecules. The van-der-Waals interaction energy between to spherical particles of the same radius a at a given separation distance H according to Hamaker is given by equation 2-22.[151]

$$V_{\mathrm{A}}(H) = -\frac{A_{131}}{6}\left(\frac{2a^2}{(2a+H)^2-4\cdot a^2}+\frac{2a^2}{(2a+H)^2}+\ln\left(1-\frac{4a^2}{(2a+H)^2}\right)\right) \tag{2-22}$$

It involves the characteristic Hamaker constant A_{131}, which serves as a measure of the magnitude of the van der Waals interaction itself. In a first approximation, the Hamaker constant is independent of the electrolyte concentration and the separation distance of the particles with values for polymer latices in the range of $0.3 - 1.4\cdot10^{-20}$J.[152–154] These values are related to a water-based dispersion and are composed of interactions between the particles of the same type in vacuum A_{11} and the interaction between the molecules of the dispersant in vacuum A_{33}.

$$A_{131} = \left(\sqrt{A_{11}}-\sqrt{A_{33}}\right)^2 \tag{2-23}$$

Lifshitz and co-workers set up a complex method to directly calculate van-der-Waals interaction energies, which has been simplified by Prieve and Russel for the determination of Hamaker constants.[152] It was found that the Hamaker constant is not independent of the separation distance H. For the case of Polystyrene in water it dropped from $1.4\cdot10^{-20}$ J at close separation distances to $0.3\cdot10^{-20}$J towards larger separation distances of $H > 10^2$ nm. Additionally, the Hamaker constant is also not independent of the electrolyte concentration. Therefore, a retardation of the Hamaker constants needs to be taken into account, especially at large separation distances. In this study, the attractive interaction energies will nevertheless be treated as non-retarded according to equation 2-22 as the performed calculations only consider small separation distances.

The sum of the attractive and the repulsive interaction energies result in the overall interaction energy for two spherical particles approaching each other. A schematic illustration is shown in Figure 2-16 a. V_{R} starts at a defined value ($H = 0$) and decays exponentially. Thus it approaches 0 at large separation distances. In contrast to that, V_{A} decays reciprocally with the distance H (equation 2-22) in case of spherical particles and is thus decaying very slow . Therefore, V_{A} will always be larger than V_{R} in two

cases. On the one hand, V_A will always be larger in case of large separation distances because a exponential function approaches zero more rapidly than a function that decreases reciprocally. However, there might be a formation of a secondary minimum depending on the exact conditions. On the other one hand, $V_A \rightarrow \infty$ for very small separation distances and is therefore larger than V_R at close separation distances. Nevertheless, although V_A approaches ∞ for very small separation distances, it is compensated by Born repulsion, which originates from the overlapping of electron clouds. For this reason, the primary thermodynamic minimum is formed at very small separation distances.[44]

In case of sufficiently high surface potentials and low electrolyte concentrations of the system V_R can be larger than V_A at intermediate distances, which may result in the formation of an energy maximum $V_{T,max}$. This energy barrier must be sufficiently high to prevent particle aggregation and thus provide stable dispersions. Since the electrostatic repulsive forces can be effectively decreased by increasing the electrolyte concentration, the course of the total interaction energy curve also changes dependent on the electrolyte concentration, which is illustrated in Figure 2-16 b.

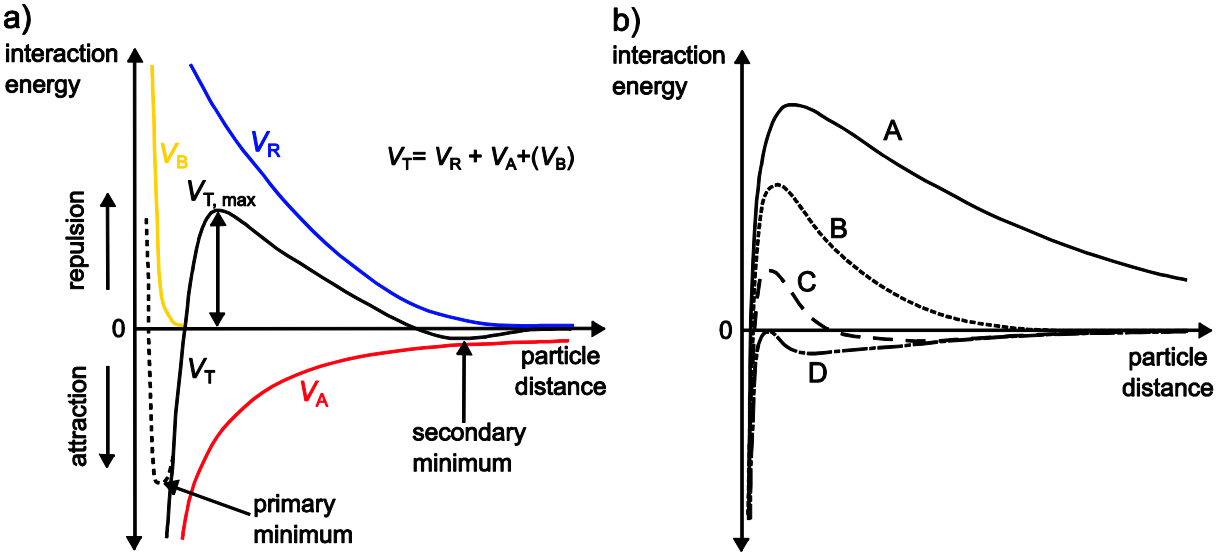

Figure 2-16: a) Interaction energy-distance functions of two spherical particles according to the DLVO theory. The total interaction function V_T (black) is the sum of the electrostatic repulsion V_R (blue) and the van der Waals attraction V_A (red) as well as the Born repulsion V_B (yellow).[148] b) Total interaction energy curves V_T calculated for a spherical particle of radius a=30 nm bearing a surface potential of -40 mV and a Hamaker constant of $0.7 \cdot 10^{-20}$J in a solution of a symmetrical 1:1 electrolyte at different electrolyte concentrations. A: 0.01 M; B: 0.1 M; C: 0.5 M and D: 1.4 M.

For demonstrative purpose, the electrolyte concentration of a symmetrical 1:1 electrolyte is increased from curve A (0.01 M) to D (1.4 M). Obviously, the energy barrier becomes zero at a certain electrolyte concentration, which is commonly referred to as critical coagulation concentration (ccc). Once the energy barrier becomes zero, rapid coagulation of the particles takes place (fast coagulation). This means that every particle collision results in irreversible coagulation, since the particles are trapped within the primary minimum. Nevertheless, due to their thermal energy, particles can still overcome barriers up to the order of $10 - 15\ k_B T$. It is therefore sufficient if $V_{T,max} < 10 - 15\ k_B T$ to induce coagulation (slow coagulation).

The coagulation process is initially based on a bimolecular collision reaction. Further collisions lead to the formation of trimers, tetramers, oligomers and finally larger aggregates. Thus the concentration of particles n_0 decreases with time following the kinetics of a bi-molecular collision reaction.[155]

$$-\frac{dn_0}{dt} = kn_0^2 \qquad (2\text{-}24)$$

Here, k is the reaction rate constant of the collision reaction which attains its maximum value k_0 when $V_{\mathrm{T,max}} \leq 0$. Repulsive interaction energies, or increasing energy barriers will therefore slow down the coagulation process, meaning $k < k_0$. The ratio of both rate constant is defined as the stability factor W.[156]

$$W = \frac{k_0}{k} \tag{2-25}$$

Stable dispersions are typically characterized by $W \geq 10^5$ whereas $W = 1$ for $V_{\mathrm{T,max}} \leq 0$, is characteristic for destabilized systems. The coagulation process can be studied photometrical, since the doublet formation is accompanied by an increase of turbidity τ. The turbidity changes over time according to equation 2-26.[157,158]

$$\tau = A_{\mathrm{oc}} n_0 V_0^2 \left(1 + \frac{k_0}{W} n_0 t\right) \tag{2-26}$$

Here, A_{oc} is an optical constant and V_0 ist the volume of a particle. Therefore, the initial linear change in absorbance $A = \tau L/2.303$ is proportional to the reaction rate constant of the bimolecular collision reaction (eq. 2-27).[156,157,159,160]

$$(\mathrm{d}A/\mathrm{d}t)_{c,t\to 0} = A_{\mathrm{oc}} k_0 c_{\mathrm{s}}^2 / 2.303 W \rho^2 \tag{2-27}$$

In this formula, c_{s} is the solid content of the dispersion and ρ is the density of the particles. In experimental settings, the change in absorbance over time as a function of the salt concentration is measured photometrical at a constant wavelength. As a result, a set of curves that show an initial linear increment is generated. The slope of the linear regime $(\mathrm{d}A/\mathrm{d}t)_{c,t\to 0}$ is determined and its logarithmic reciprocal is plotted against the logarithm of the electrolyte concentration. As a result, a straight line is obtained that bends into parallel to the concentration axis at a certain electrolyte concentration. At this point, the maximum coagulation rate (k_0, fast coagulation) is reached. The intersection point thus provides the critical coagulation concentration ccc.

If the repulsive interaction force (e.g. by means of the surface potential) and the ccc is known, it is possible to calculate the attractive interaction energy. The energy barrier $V_{\mathrm{T,max}}$ becomes zero for this particular electrolyte concentration and the equations $V_{\mathrm{T}} = 0$ and $\mathrm{d}V_{\mathrm{T}}/\mathrm{d}H = 0$ can be simultaneously solved using equation 2-18 to 2-22. Thus, two parameters can be determined, the Hamaker constant A_{131} and necessarily the distance of the energy maximum to the particle surface. When using this approach, it must be kept in mind that all other interactions possibly present are treated in the form of van der Waals forces, with the exception of the electrostatic forces. Accordingly, in this case it is best to speak of an apparent Hamaker constant A_{131}^{app}.

An alternative approach to estimate the Hamaker constant A_{131}^{vOCG} is based on an empirical formula derived by van Oss, Chaudhury and Good (eq. 2-28). It is derived from the apolar surface tension component of the material $\gamma_{\mathrm{S}}^{\mathrm{LW}}$ and is applicable under the condition that the separation distance H is less than 10 nm in order to provide unretarded London-van der Waals interactions. The authors pointed out that the proportionality constant $1.8585 \cdot 10^{-21}$ is accurate with a variance of ± 8 %.[161,162]

$$A_{131}^{\mathrm{vOCG}} = \left(\sqrt{1.8585 \cdot 10^{-21} \cdot \gamma_{\mathrm{S}}^{\mathrm{LW}}} - \sqrt{3.7 \cdot 10^{-20}}\right)^2 \tag{2-28}$$

The apolar surface tension component of the material is related to the contact angle θ of an apolar liquid (index L) by the Young-Good-Girifalco-Fowkes equation (eq. 2-29). For this kind of test liquid, the total surface tension of the liquid γ_{L} is caused by apolar interactions only, i.e. $\gamma_{\mathrm{L}} = \gamma_{\mathrm{L}}^{\mathrm{LW}}$.[163–165]

$$1 + \cos\theta = 2\sqrt{\frac{\gamma_S^{LW}}{\gamma_L^{LW}}} \tag{2-29}$$

Nevertheless, the DLVO theory only considers electrostatic repulsion and van-der-Waals attraction. However, it has been demonstrated that this theory is not always capable of adequately describing experimental results.[166] Recent studies, which were based on AFM force distance measurements, showed evidence that additional interaction parameters might be present.[55,57,58,166,167] The disparity between the experimental data and the theoretical predictions was often attributed to the presence of additional energy contributions hydrophobic or hydrophilic interaction.[51,56,149,168] In order to account for these additional forces, many studies incorporated an additional interaction term V_h into the classical DLVO theory, also known as extended DLVO (XDLVO) approaches.[166,169–173]

$$V_T = V_R + V_A + V_h \tag{2-30}$$

On the one hand, V_h becomes positive for an hydrophilic surface leading to a repulsive interaction energy, often known as hydration force. One the other hand, in case of hydrophobic surfaces, V_h becomes negative, expressing attractive interaction energies, which are usually referred to as hydrophobic attraction. Israelachvili and Parshley analysed the interaction potential between two mica surfaces within a surfactant solution by direct force measurements and were not able to explain the results by the DLVO theory. They found an additional attractive force being much stronger than the van-der-Waals interactions within a range of up to 10 nm and described it by an exponential function.

$$V_h = aC\exp\left(\frac{H}{D_0}\right) \tag{2-31}$$

Here, C is a pre-exponential factor to account for the magnitude of the interaction energy and D_0 is the decay length. Several other functions have been proposed in the literature to be able to describe the found results adequately. However, these approaches are not subject to this study and the interested reader might refer to the literature.[161,162,166,174–181]

Despite substantial experimental evidence, the accurate origin of these additional forces remains uncertain and lacks of a fundamental theoretical description. The precise physical mechanism of this force remains to be elucidated. However, it is hypothesised that it should exhibit a fundamental relationship to the physics of hydrophobicity and hydrophilicity, respectively, of the immersed interface in polar medium, such as water. The experimental evidence of a special, ordered structure of water is first provided by Green-Kelly and Derjaguin by the detection of water layers in sodium montmorillonite.[182] Several studies have further provided evidence indicating that the boundary layers of water exhibit modified physicochemical properties. It is revealed that boundary layers of water show an enhanced viscosity[183] as well as reduced dielectric permittivity[184]. It is evident that the properties of a solid substrate exert a substantial influence on the formation of a distinct structure within the boundary layers of water. The presence of functional groups capable of forming hydrogen bonds and charged sites on the substrate's surface are known to enhance the interaction of water with the surface. Consequently, a potential correlation between the properties of the surface and a structural variation of the boundary layers can be hypothesized. For instance, hydrophilic surfaces are predicted to yield a distinct boundary layer structure compared to hydrophobic substrates, owing to the lack of hydrogen bonds between water and the surface.[185]

Monte Carlo simulation show, that water molecules near a hydrophilic surface tend to align normal, creating a dipole potential and thus reducing the tangential mobility of water molecules. Therefore, the density as well as viscosity within this layer is increased, accompanied by a decrease of the dielectric permittivity. Consequently, the disruption of the ordered water structure requires an excess energy leading to a repulsive interaction potential and additional dispersion stability. In the case of hydrophobic surfaces on the other hand, the dipoles and the planes of the water molecules align mainly in parallel

with the surface. This results in unfavourable decrease of the entropy. Furthermore, the tangential mobility of the aligned water molecules is increased, leading to a decrease in the density and viscosity of the boundary layer. Consequently, water molecules are more easily displaced from the interface and thus might enhance the agglomeration potential of two particles approaching each other.[185] Nevertheless, experimental evidence of the exact mechanism combined with its fundamental theories is still pending and readily discussed within the literature. Polyurethanes contain hydrophobic as well as hydrophilic chain segments. Consequently, it is questionable, whether or in which way these factors also influence the dispersion stability of aqueous PUDs. For this reason, this study also aims to investigate the dispersion stability beyond DLVO theory.

3 Aim and Outline of the Thesis

The fundamental relationships between the molecular structure of polyurethanes and the dispersion stability of water-based PUDs are still insufficiently understood, despite their practical relevance. Therefore, this study aims to identify how different structural components in polyurethane chemistry, including the type and concentration of ionic functional groups, the polyol component and the hard segment content affect dispersion stability of water-based PUDs.

To achieve this, these effects are investigated through systematic synthesis series and characterization of particle properties and interactions. Multiple series of well-defined PUDs are synthesized via the acetone process. Three types of polyols, polyether, polyester and polycarbonate polyols of similar molecular weight (1000 g mol^{-1}), are selected to investigate the influence of the polyol component and thus variations in hydrophilicity or hydrophobicity, respectively. Ionic functional groups are introduced as carboxylate groups (DMPA) or sulfonate groups (AAS) at different mass contents, enabling the study of effects on surface charge, dissociation behaviour and pH dependence. Furthermore, the hard segment content is systematically varied by using different mass fractions of BDO, providing insights on the influence of polymer mobility and varying hydrophilicity.

The experimental characterization focuses on the evaluation of particle properties, interactions, and dispersion stability. Dispersion stability is assessed via the critical coagulation concentration, while particle charge and electrokinetic properties are analysed using titration and electrophoretic mobility measurements. Attractive interactions are investigated using DLVO theory and the vOGC approach based on contact angle measurements. The interpretation of the collected data will be done using DLVO theory and its extensions to reveal a comprehensive picture of the underlying factors governing dispersion stability of water-based PUDs.

Chapter 4 covers a detailed analysis of the particle charge as well as the electrokinetic properties of different PUDs stabilized by AAS. It demonstrates how the polyol type and AAS concentration influence the particle charge content, charge accessibility and dissociation behaviour. Furthermore, the surface potential is determined by an analysis of the electrokinetic properties using hard as well as soft particle models. By combining both techniques insights about the particle character are provided.

Chapter 5 presents a detailed analysis of the dispersion stability of PUDs stabilized by AAS. The dispersion stability is qualitatively assessed by the determination of the ccc. Furthermore, the underlying repulsive as well as attractive interaction potentials are calculated based on experimental data. The results are interpreted using DLVO and XDLVO theory, providing insight into the interplay of the different forces governing stability.

Chapter 6 extends the analysis to DMPA stabilized PUDs, comparing their particle charge characteristics, dissociation behaviour and stability to the AAS systems. It explicitly highlights differences in the charge properties arising between both stabilizing agents and provides a detailed discussion of the findings.

Chapter 7 provides a comprehensive discussion of the most relevant findings and also integrates the influence of the hard segment content. This chapter provides a detailed understanding of how molecular structure influences the stability of water-based PUDs. A detailed description of the experimental procedures can be found in Chapter 9.

By combining precise synthesis, comprehensive characterization, and theoretical analysis, this work deepens the theoretical understanding of colloidal stabilization and provides a basis for designing water-based PUDs with improved stability.

4 Water-Based Polyurethane Dispersions: A Detailed Analysis of the Particle Charge Using Soft and Hard Particle Model

C. Grau [a], A. M. Schmidt [b], J. Wilkens [a]*

[a] *Faculty of Applied Natural Sciences, TH Köln - University of Applied Science, Leverkusen D-51379, Germany*
[b] *Department of Chemistry, University of Cologne, D-50939 Cologne, Germany*
**Corresponding author, E-mail address: jan.wilkens@th-koeln.de*

Remarks on the manuscript in relation to the thesis and declaration of individual contributions

This chapter has been published in *Langmuir* and is reprinted with permission from *Langmuir* 2024, 40, 42, 22123-22135. Numbering of the chapters, figures and formulas has been adjusted to the thesis format.

Article on Request: https://pubs.acs.org/articlesonrequest/AOR-YGI7YXVGXWF82PVTQEHS

DOI: https://doi.org/10.1021/acs.langmuir.4c02498

Here, the detailed analysis of the particle charge by potentiometric acid-base titration as well as electrophoretic measurement techniques of PUDs stabilized by AAS is presented. The obtained results were furthermore analysed by various models, especially focusing on the analysis of the electrophoretic mobility using soft and hard particle theories. For this reason, this publication is fundamental for this thesis, as it provides a detailed discussion of the particle charge of PUD particles stabilized by AAS and thus serves as a basis for further evaluating repulsive interaction energies to analyse the dispersion stability. Based on the comparative approach of different models for the description of the electrokinetic properties as well as proof by independent measurement techniques, namely potentiometric titration, an evaluation procedure is presented, which is makes it suitable to obtain important parameters, such as the surface potential.

The synthesis as well as the analytical experiments were done under my supervision and responsibility. The PUD series PE-X was partly synthesized by *Simon Schösser* and the PUD series PC-X was partly synthesized by *Christoph Pumplün* under my supervision in the context of their bachelor thesis. The remaining dispersions were synthesized by myself. The analytical measurements were mostly conducted by myself. The analysis and interpretation of the results were done by myself and *Prof. Dr. Jan Wilkens*. The manuscript was prepared by myself, following extensive corrections from *Prof. Dr. Jan Wilkens* and *Prof. Dr. Annette M. Schmidt*.

Abstract

Water-based polyurethane dispersions (PUDs) show a characteristic dependency of the electrophoretic mobility on the electrolyte concentration, which can be investigated by hard and soft particle models. For this purpose, additional information can be obtained by determining particle charges and electrostatic potentials. PUDs with different contents of an intrinsic ionic stabilizer and various polyol components were synthesized according to the acetone process. The particle charge was characterized by potentiometric acid−base titration, and the data of the titration curve were fitted assuming multiple functional groups with adaptable acid strengths. To investigate the electrostatic potentials, electrophoretic mobilities were measured as a function of electrolyte concentration and analyzed by soft and hard particle theory. Acid−base titration experiments indicated that not all detected ionic groups are located on the surface but are partly arranged inside the polymer particle, as evidenced by a significant decrease of the corresponding effective dissociation constant. The evaluation of the titration data and the electrokinetic experiments showed that the soft particle model of Ohshima is not suitable to reflect

the actual particle charge. In contrast, the hard particle model can describe the measured electrophoretic mobility of the dispersions very well if the relaxation effect is taken into account. The dependency of the corresponding zeta potentials on the electrolyte concentration can be excellently modelled assuming a constant surface potential ψ_0 and distance of the shear plane x_s. Reasonable results are obtained for both parameters with only minor differences between the PUD series. Nonetheless, the electrokinetic surface charge densities calculated with respect to the surface potential are lower than expected from the titration results. Although our results indicate a more complex charge distribution in a peripheral layer, the hard particle model currently shows the best description of the electrokinetic behavior of the PUDs.

Keywords

Waterbased polyurethane dispersions, electrophoretic mobility, hard particle model, soft particle model, particle charge, surface potential, shear plane

4.1 Introduction

The preparation and handling of water-based polyurethane dispersions (PUDs) is of ever increasing importance due to environmental issues and the necessity to reduce volatile organic compounds. The huge variety of possible building blocks leads to products with different properties and thus makes them applicable for a wide field off possible applications like in coating,[1] adhesive,[2] ink,[3] membrane[4] or textile industry.[5] Produced as a water-based dispersion, polyurethanes are usually stabilized by steric or electrostatic interaction forces in order to prevent particle aggregation. In the latter case, the dispersion can be stabilized by the incorporation of ionic groups, leading to electrostatic repulsion between the identically charged particles. To understand the repulsive interactions and thereby draw conclusions about dispersion stability, knowledge of the effective potentials is of great industrial and scientific interest.

For the production of a water-based PUD, the acetone process is of great industrial relevance.[6–11] Its first step is the prepolymerization, which is the synthesis of low molecular weight polymer based on the polyaddition reaction of polyol and higher functional isocyanate components. Accordingly, the polyol components play a significant role within the polyurethane chemistry. Besides arbitrary molecular weights, they also offer the opportunity to incorporate different functional groups in the polymeric backbone, such as ether,[12,13] ester,[12,14] or carbonate[15] linkages, which have a major impact on the final polymer properties. Acetone is often used to dissolve the prepolymer, as it is non-toxic and can easily be removed due to its low boiling point. Then the prepolymer can be chain extended using short chain diamines or diols in acetone solution to prevent excessive viscosity rise and form a high molecular weight polyurethane. A water-based dispersion is finally obtained by precipitation of the polymer with the addition of water under mechanical stirring and the removal of acetone by evaporation.[9]

Typically, dispersion stability can be achieved by the incorporation of cationic or anionic groups with diol or diamine functionality within the polyurethane backbone. In case of anionically stabilized dispersions, the most referred stabilizing agent is dimethylolpropionic acid (DMPA).[9,16,17] Alternatively, diaminoalkansulfonates, such as 2-[(2-aminoethyl)amino]-ethanesulfonic acid (AAS), can also be used.[9,18,19] During formation of the secondary dispersion a complex rearrangement of the charged groups to the polymer/water interface takes place.[20,21] Conceptually, this rearrangement could lead to a rather complex charge distribution as the hydrophilic groups are part of the polymer backbone and therefore are not freely movable. This gives rise to the assumption that the charges are possibly not only located at the particle surface, but also in a peripheral layer. Moreover, part of the charges could even be trapped within the polymer matrix. For example, Nanda et al. carried out a detailed analysis of several reaction parameters in PUD synthesis.[22] Among others, they investigated the influence of the degree of pre- and

postneutralization on PUDs stabilized by DMPS. They found increasing particle sizes with increasing degree of postneutralization and concluded that some of the carboxylic acid groups are trapped inside the particle. This indicates that it is worth having a closer look at the constitution of charged particles when influencing factors on dispersion stability are investigated in more detail.

Classic techniques for the analysis of charged particles are acid−base titration and the determination of electrokinetic properties. A fundamental understanding of potentiometric and conductometric titration experiments for ionomeric PUD containing strong and weak acidic groups was given by Lorenz et al.[19,23,24] On the other hand, the investigation of electrokinetic properties gives rise to the effective potentials of the particle, which can be set in relation to the results of titration experiments.[25–28] The electrophoretic mobility μ describes the movement of a charged particle in an electrolyte solution when an electric field is applied. It is strongly dependent on the particle radius a, the thickness of the diffuse double layer and the zeta or surface potential, respectively. The zeta potential is the potential at a certain distance x_s to the particle surface, where the velocity of the dispersion medium relative to particle becomes zero. This position is often referred to as the shear plane or hydrodynamic slip plane. The zeta potential can approximately be set equal to the surface potential ψ_0 of the particles and thus be used to characterize electrostatic repulsive forces. The most frequently employed models to describe the relationship of the electrophoretic mobility and the zeta potential are those according to Helmholtz-Smoluchowski,[29,30] Hückel[31] and Henry[32]. All of the corresponding formulas are only valid for certain limiting conditions and for so called hard particles. The concept of a hard particle is essentially based on an ion-impenetrable particle whose charges are solely located at the particle surface (Figure 4-1b).

Since the magnitude of the potential at the shear plane is related to the thickness of the diffuse double layer, the zeta potential usually tends to zero for high electrolyte concentrations. This is due to the compression of the diffuse double layer and hence to an extensive screening of the surface charges. Nevertheless, Ohshima pointed out that highly charged particles show a different behavior because the counterions located next to the particle surface do not contribute to the electrophoretic mobility in this case. Therefore, these particles show a nonzero limiting mobility at high electrolyte concentrations.[33]

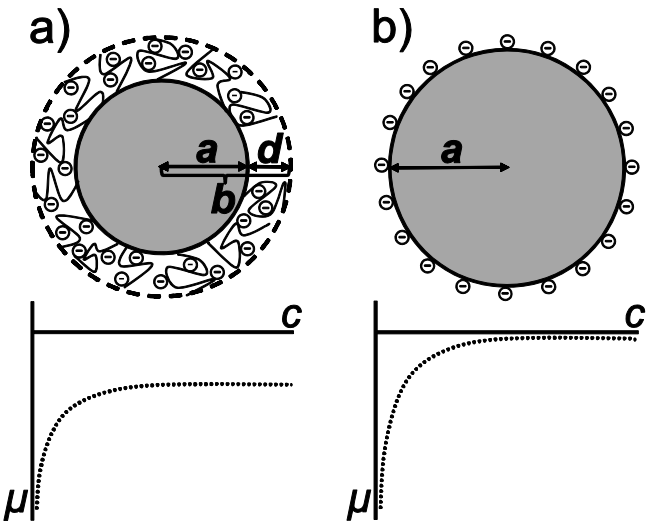

Figure 4-1: Schematic representation of two particles of different character. a) Soft particle consisting of an ion-impenetrable, uncharged core of the radius a surrounded by a polyelectrolyte layer of the thickness d, with $b = a + d$ and its electrophoretic mobility in dependence of the electrolyte concentration, showing a nonzero limiting mobility. b) Hard particle consisting of an ion-impenetrable core of the radius a with the charges located at the particle surface and its electrophoretic mobility in dependence of the electrolyte concentration, showing a limiting mobility of zero.

Since the assumption of a hard particle does not hold for every particle system, Ohshima and Kondo developed a model to describe the electrophoretic mobility of soft particles such as biocolloids.[34] They considered soft particles to have an ion-impenetrable core of the radius a surrounded by a uniformly charged polyelectrolyte layer of the thickness d (Figure 4-1a). The electrokinetic properties of such a soft particle are governed by the Donnan potential (i.e. the potential deep inside the polyelectrolyte layer) and the surface potential (i.e. the potential at the boundary of the polyelectrolyte layer to the dispersion medium).[35] Both potentials are related to the fixed volume charge density ZN, which is a central aspect of the soft particle model together with the electrophoretic softness parameter λ^{-1}. Additionally, Ohshima pointed out that the electrophoretic mobility in dependence of the electrolyte concentration shows a nonzero limiting value for a soft particle, which is just dependent on the volume charge density and the electrophoretic softness parameter. This provides the opportunity to distinguish between soft and hard particle character.

Within this study, we conducted a detailed particle charge analysis of electrostatically stabilized PUDs with different amounts of AAS as intrinsic stabilizing agent and different polyol components. The dispersions were synthesized according to the acetone process. In order to analyze the charge content of the particles, acid−base titrations were performed. The titration curves were evaluated by considering different acidic groups. Additionally, the electrophoretic mobilities were determined as a function of the electrolyte concentration and analyzed by soft and hard particle models, both taking the relaxation effect into account. The obtained model parameters, i.e., volume charge density and surface potential, were compared with their corresponding values obtained by the titration experiments.

4.2 Theory

This section explains the theoretical principles that are used to analyze and interpret the primary measurement results of charge titration and electrophoretic mobility experiments. A distinction is made between the hard and soft particle models, which are based on certain assumptions about the structure of the interface and the charge distribution.

4.2.1 Hard particles

The relationship between electrophoretic mobility μ of a spherical, hard particle and the zeta potential ζ is often described by the Helmholtz-Smoluchowski equation (eq. 4-1), with relative permittivity ε_r, permittivity in vacuum ε_0 and viscosity η.[29,36] It is valid for the limiting case where the particles are much larger than the thickness of the diffuse double layer. Moreover, zeta potentials must be rather low. In this case, the diffuse double layer can be regarded as spherically symmetric during electrophoresis experiments.

$$\mu = \frac{\varepsilon_r \varepsilon_0}{\eta} \zeta \tag{4-1}$$

On the other hand, if the extension of the diffuse double layer is large and potential is high, the double layer can become deformed during electrophoresis because the counterions move in opposite directions with respect to the particle. Then, an asymmetric potential profile and small dipoles are generated as the centers of particle and double layer charge do not coincide anymore. As a result, an additional electrical field is created, which is contrary to the applied external field and hence decelerates the particle movement. This well-known effect is called the relaxation effect, which was first studied by Overbeek and Booth.[37,38] It should be mentioned that it is also associated with the phenomenon of surface conductivity, which can occur in the stagnant layer (hydrodynamically immobile part of the diffuse layer, i.e. within the shear plane) and the diffuse layer (hydrodynamically mobile part of the diffuse layer, i.e. beyond the shear plane).[39,40] On the basis of diffuse layer conductivity only, Ohshima, Healy, and White derived an approximate analytical expression for the electrophoretic mobility of spherical particles in a solution of symmetrical electrolytes.[41] For this purpose, the ionic drag coefficient of the

*i*th ionic species λ_i is given by equation 4-2 with the Avogadro constant N_A, elementary charge e, valence z_i and the limiting molar conductance Λ_i^0 of the ion species.

$$\lambda_\mathrm{i} = \frac{N_\mathrm{A} e^2 |z_\mathrm{i}|}{\Lambda_\mathrm{i}^0} \tag{4-2}$$

It is the basis for the calculation of the scaled drag coefficient m_i (eq. 4-3) of the counterions m_C and co-ions m_CO, respectively, where k_B is the Boltzmann constant and T is the thermodynamic temperature.

$$m_\mathrm{i} = \frac{2\varepsilon_\mathrm{r}\varepsilon_0 k_\mathrm{B} T}{3\eta z_\mathrm{i}^2 e^2}\lambda_\mathrm{i} \tag{4-3}$$

The Debye-Hückel parameter κ is described by equation 4-4 with the Faraday constant F, the molar gas constant R and the concentration of the ionic species c_i.

$$\kappa = \sqrt{\frac{F^2}{\varepsilon_\mathrm{r}\varepsilon_0 RT}\sum z_\mathrm{i}^2 c_\mathrm{i}} \tag{4-4}$$

Finally, the approximate analytical expression between the electrophoretic mobility and zeta potential of a spherical, hard particle can be expressed for different limiting conditions given by the product of the Debye-Hückel parameter κ and the particle radius a. In case of $\kappa a \geq 10$ equation 4-5 is valid with relative error less than 1% for arbitrary values of ζ.[41]

$$\mu = \mathrm{sign}(\zeta)\frac{\varepsilon_\mathrm{r}\varepsilon_0}{\eta}\left(\mathrm{abs}(\zeta)\frac{2F_1}{1+F_1}\frac{k_\mathrm{B}T}{ze}H\right) + \mathrm{sign}(\zeta)\frac{2\varepsilon_\mathrm{r}\varepsilon_0 k_\mathrm{B}T}{3\eta e}\left(\frac{1}{\kappa a}\left(-18\left(t+\frac{t^3}{9}\right)K + \frac{15F_1}{1+F_1}\left(t+\frac{7t^2}{20}+\frac{t^3}{9}\right) - 6(1+3m_\mathrm{CO})\left(1-\exp\left(-\frac{\bar{\zeta}}{2}\right)\right)G + \frac{12F_1}{(1+F_1)^2}H + \frac{9\bar{\zeta}}{1+F}(m_\mathrm{CO}G + m_\mathrm{C}H) - \frac{36F_1}{1+F_1}\left(m_\mathrm{CO}G^2 + \frac{m_\mathrm{C}}{1+F}H^2\right)\right)\right) \tag{4-5}$$

Here, the dimensionless zeta potential $\bar{\zeta}$ and the individual functions F_1, G, H, K and t are given by equations 4-6-4-11.

$$\bar{\zeta} = z_\mathrm{i}\cdot\left|\frac{e\zeta}{k_\mathrm{B}T}\right| \tag{4-6}$$

$$F_1 = \frac{2}{\kappa a}\cdot(1+3m_\mathrm{C})\cdot\left(\exp\left(\frac{\bar{\zeta}}{2}\right)-1\right) \tag{4-7}$$

$$G = \ln\left(\frac{1+\exp\left(-\frac{\bar{\zeta}}{2}\right)}{2}\right) \tag{4-8}$$

$$H = \ln\left(\frac{1+\exp\left(\frac{\bar{\zeta}}{2}\right)}{2}\right) \tag{4-9}$$

$$K = 1 - \frac{25}{3\cdot(\kappa a+10)}\exp\left(-\frac{\kappa a}{6\cdot(\kappa a-6)}\cdot\bar{\zeta}\right) \tag{4-10}$$

$$t = \tanh\left(\frac{\bar{\zeta}}{4}\right) \tag{4-11}$$

Furthermore, Ohshima derived an approximate analytical expression for κa less than 10, which is given by equation 4-12.[42,43] It also considers only diffuse layer conductivity and the relative error is less than 1% for $\bar{\zeta} \leq 7$ at $\kappa a = 0.1$ and $\bar{\zeta} \leq 3$ at $\kappa a = 1$.

$$\mu = \frac{2\varepsilon_r\varepsilon_0\zeta}{3\eta}\left(1 + \frac{1}{2\left(\kappa a\left(1+2\exp(-\kappa a)\right)\right)^3}\right) - \frac{2\varepsilon_r\varepsilon_0\zeta}{3\eta}\bar{\zeta}^2\left(\frac{\kappa a(\kappa a+1.3\exp(-0.18\kappa a)+2.5)}{2(\kappa a+1.2\exp(-7.4\kappa a)+4.8)^3} + \left(\frac{m_{CO}+m_C}{2}\right)\left(\frac{9\kappa a(\kappa a+5.2\exp(-3.9\kappa a)+5.6)}{3(\kappa a+1.55\exp(-0.32\kappa a)+6.02)^3}\right)\right) \quad (4\text{-}12)$$

The knowledge of the surface potential ψ_0 is of fundamental importance as it has a strong impact on the repulsive forces of electrostatically stabilized particles. The surface potential is related to the experimentally determinable zeta potential, which is defined as the potential at the shear plane x_s, i.e. $\zeta = \psi(x_s)$. At this position, the liquid velocity relative to the particle is zero, and the distance to the particle surface is x_s. Ohshima, Healy and White derived an approximate analytical expression for the potential distribution around a spherical hard particle. Accordingly, the potential at the shear plane is then given by equation 4-13-4-16.[43,44]

$$\psi(x_s) = \zeta = \frac{2k_BT}{z_ie}\ln\left(\frac{(1+Bs)\left(1+\frac{Bs}{2\kappa a+1}\right)}{(1-Bs)\left(1-\frac{Bs}{2\kappa a+1}\right)}\right) \quad (4\text{-}13)$$

with

$$B = \frac{\left(a+\frac{\kappa a}{\kappa a+1}\right)\tanh\left(\frac{\gamma_0}{4}\right)}{1+\left(1-\frac{2\kappa a+1}{(\kappa a+1)^2}\tanh\left(\frac{\gamma_0}{4}\right)^2\right)^{0,5}} \quad (4\text{-}14)$$

$$s = \frac{a}{x_s}\exp\left(-\kappa(x_s-a)\right) \quad (4\text{-}15)$$

and the scaled surface potential γ_0.

$$\gamma_0 = \frac{ze\psi_0}{k_BT} \quad (4\text{-}16)$$

If the zeta potential is determined as a function of electrolyte concentration, it is possible to calculate the surface potential and the position of the shear plane according to equation 4-13-4-16 by using a least-squares fitting procedure. Moreover, Ohshima, Healy and White derived an approximate analytic expression for the relation between the surface potential ψ_0 and surface charge density σ_0 (eq. 4-17), which in this study is referred to as the electrokinetic surface charge density σ_0^{ek}. The relative error of equation 4-17 is less than 1% for $\kappa a \geq 0.5$. This expression allows to compare electrokinetic with potentiometric or conductometric titration experiments by calculating the respective corresponding parameter.[43,44]

$$\sigma_0^{ek} = \frac{2\varepsilon_r\varepsilon_0\kappa k_BT}{e}\sinh\left(\frac{\gamma_0}{2}\right)\left(1 + \frac{1}{\kappa a}\frac{2}{\cosh^2\left(\frac{\gamma_0}{4}\right)} + \frac{1}{(\kappa a)^2}\frac{8\ln\left(\cosh\left(\frac{\gamma_0}{4}\right)\right)}{\sinh^2\left(\frac{\gamma_0}{2}\right)}\right)^{0.5} \quad (4\text{-}17)$$

4.2.2 Potentiometric acid-base titration

As already mentioned, potentiometric titration experiments also provide information about the particle charges and thus enable a comparison with the independently measured electrokinetic surface charge density. Based on the work of Masini et al.[45], Alves et al. provided a procedure for the characterization of acid groups, which is derived through a detailed mass and charge balance of all chemical species in the system.[46]

$$f(V, c_{H^+}) = \left(V - V_{HA_0}\right)c_B + \left(c_{H^+} - \frac{K_w}{c_{H^+}}\right)(V_0 - V) - \sum_{n=1}^{N}\left(V_{HA_n} - V_{HA_{n-1}}\right)c_B\frac{K_{HA_n}}{K_{HA_n}+c_{H^+}} \quad (4\text{-}18)$$

This implicit function (eq. 4-18) can be used to analyse potentiometric titration curves by nonlinear regression. The added titrant volume V of concentration c_B is the independent variable, whereas the

proton concentration c_{H^+} is the dependent variable. V_{HA_0} is the volume of the strong acid, V_0 is the initial volume of the solution to be titrated and K_w is the ionization constant of water. The sum describes the contribution of n weak acids to the observed pH value and allows to determine their equivalence volumes V_{HA_n} and their corresponding dissociation constants K_{HA_n}. For more details on the complex, iterative optimisation routine, please refer to the original articles.

The non-linear regression analysis makes it possible to characterise the dissociation behaviour of the incorporated sulfonic acid groups at each detected inflection point. Furthermore, the specific charge content Q_{tit} can be calculated on the basis of the equivalence volumes of the strong and weak acid groups (V_{HA_0} and V_{HA_n}, respectively) and the polymer mass m_p.

$$Q_{tit} = Q_{tit,0} + \sum_{n=1}^{N} Q_{tit,n} = \left(V_{HA_0} + \sum_{n=1}^{N} V_{HA_n}\right) c_B F / m_p \tag{4-19}$$

If the particle radius a and the density of the polymer ρ_p is known, the surface charge density can finally be calculated using equation 4-20.

$$\sigma_0^{tit} = Q_{tit} \frac{\rho_p a}{3} \tag{4-20}$$

4.2.3 Soft particles

Originally, Ohshima, Nakamura and Kondo developed a theoretical model for the description of the electrokinetic properties of a soft particle in symmetrical $z{:}z$ electrolyte solution of valence z by considering a spherical particle with an uncharged, ion-impenetrable core with radius a covered with an ion-penetrable polyelectrolyte layer of thickness d.[47] They showed that the concept of zeta potential is not valid anymore in case of soft particles. Instead, they implemented the following two potentials to describe the electrokinetics of soft particles. The Donnan potential ψ_{DON} (eq. 4-21) and its scaled form γ_{DON} (eq. 4-22) being the potential at the surface of the particle core, and the surface potential ψ_0 (eq. 4-23) being the potential at the boundary of the polyelectrolyte layer to the dispersion medium.

$$\psi_{DON} = \frac{k_B T}{ze} \ln\left[\frac{ZN}{2zn} + \left(\left(\frac{ZN}{2zn}\right)^2 + 1\right)^{0,5}\right] \tag{4-21}$$

$$\gamma_{DON} = \frac{ze\psi_{DON}}{k_B T} \tag{4-22}$$

$$\psi_0 = \frac{k_B T}{ze}\left(\ln\left[\frac{ZN}{2zn} + \left(\left(\frac{ZN}{2zn}\right)^2 + 1\right)^{0,5}\right] + \frac{2zn}{ZN}\left[1 - \left(\left(\frac{ZN}{2zn}\right)^2 + 1\right)^{0,5}\right]\right) \tag{4-23}$$

Here, n is the number density of the electrolyte in the dispersion medium, Z is the valence and N is the number density of the ionized groups in the polyelectrolyte layer, giving a characteristic volume charge density ZN of the polyelectrolyte layer with the assumption of uniformly distributed charges. However, besides other assumptions, which are described in detail elsewhere,[48,49] the original theory only applies for low potentials. Hence, Ohshima extended the soft particle theory and took the relaxation effect into account. Equation 4-24 describes the dependence of the electrophoretic mobility of a soft particle on the electrolyte concentration, where κ_m is the Debye-Hückel parameter of the polyelectrolyte layer (eq. 4-25).[50]

$$\mu = \frac{\varepsilon_r \varepsilon_0}{\eta} \frac{\psi_0/\kappa_m + \psi_{DON}/\lambda}{1/\kappa_m + 1/\lambda} f\left(d/a\right) + \frac{eZN}{\eta\lambda^2}\left(1 - \frac{F_2}{1+F_2}\frac{1}{1+\exp(-|\gamma_{DON}|)}\right) -$$
$$\frac{F_2}{1+F_2}\frac{\varepsilon_r \varepsilon_0}{\eta} f\left(d/a\right)\left(\frac{k_B T}{ze}\right)\left[2\ln\left(\frac{1+\exp\left(\frac{|\gamma_0|}{2}\right)}{2}\right) + \frac{\kappa}{\lambda}\left(\exp\left(\frac{|\gamma_0|}{2}\right) - 1\right) - \frac{\kappa^2}{2\lambda(\lambda+\kappa_m)}\frac{\exp(|\gamma_{DON}|)-1}{1+\exp(-|\gamma_{DON}|)}\right] \tag{4-24}$$

$$\kappa_{\mathrm{m}} = \kappa \left[1 + \left(\frac{ZN}{2zn}\right)^2\right]^{0,25} \tag{4-25}$$

The electrophoretic softness parameter is given by the reciprocal of λ and is a measure of the ion penetrability of the polyelectrolyte layer. The function $f\left(d/a\right)$ depends on the radius of the particle core a and the thickness of the polyelectrolyte layer d. According to equation 4-26, the limiting conditions are $f\left(d/a\right) = 1$ for $a \approx b$ (i.e. hard particle) and $f\left(d/a\right) = \frac{2}{3}$ for $d \approx b$ (i.e. polyelectrolyte particle) with b as the radius of the soft sphere given by $b = a + d$.

$$f\left(d/a\right) = \frac{2}{3}\left(1 + \frac{a^3}{2b^3}\right) = \frac{2}{3}\left(1 + \frac{1}{2\left(1+d/a\right)^3}\right) \tag{4-26}$$

In equation 4-24, all terms involving the function F_2 (eq. 4-27) account for the relaxation effect. The scaled drag coefficient of the counter ions m_{c} refers to equation 4-3.

$$F_2 = \frac{2}{\kappa a}(1 + 3m_{\mathrm{C}})\left(\exp\left(\frac{|\gamma_0|}{2}\right) - 1\right) \tag{4-27}$$

4.3 Experimental

4.3.1 Materials

Polycarbonate (PC; Desmophen C2102, $M_n \sim 1000\ \mathrm{g\ mol^{-1}}$) and polyester diols (PE; Desmophen PE90B, $M_n \sim 1000\ \mathrm{g\ mol^{-1}}$) and a solution of 2-((2-aminoethyl)amino)ethanesulfonate (AAS) were kindly supplied by Covestro AG. Poly(tetrahydrofuran)diol (PTHF; $M_n \sim 1000\ \mathrm{g\ mol^{-1}}$), isophorone diisocynate (IPDI), 1,4-butanediol (BDO), triethylamine (TEA), isophorone diamine (IPDA), dibutyltin dilaurate (DBTL), Amberlite IRN-77 and Amberlite IRA900 were purchased from Merck KGaA. Acetone, 0.1 M standard solutions of hydrochloric acid (HCl), sodium hydroxide (NaOH), potassium nitrate (KNO_3) and magnesium nitrate were purchased from Fisher Scientific. Ultrapure water was used for every sample preparation.

4.3.2 Synthesis of PUDs

Several series of PUDs containing different polyol components and varying AAS mass fractions (see Table 4-1) were synthesized according to the acetone process.[8] Dehydration of polyol components was done in a 500 mL round-bottom four-necked flask equipped with thermometer and mechanical stirrer under nitrogen atmosphere at 100 °C and 200 mbar before each synthesis. The necessary amount of BDO was fed to the polyol component into the four-necked flask, equipped with a mechanical stirrer and condenser. The mixture was preheated up to 70 °C under continuous stirring and DBTL was added into the reaction mixture. When a homogenous reaction mixture was obtained, IPDI was added dropwise through a dropping funnel. The reaction temperature was raised to 100 °C after complete addition. The progress of reaction was controlled by determining NCO content using standard dibutylamine back-titration according to DIN EN ISO 14896:2009-07.[51] Once the theoretical NCO content was reached, the reaction mixture was cooled to 80 °C and acetone was added dropwise through a dropping funnel with approximately 2 mL $\mathrm{min^{-1}}$. After complete addition, the solution was cooled to 40 °C and chain extension was carried out. For this purpose, IPDA and AAS were dissolved in water and added dropwise to the acetone solution through a dropping funnel. The reaction was carried out for 30 minutes. The dispersion process was carried out by adding water constantly with 2.3 mL $\mathrm{min^{-1}}$ using KDS Legato 110 single syringe pumps at 40 °C and 350 rpm. The amount of chain extender and water was adjusted under consideration of the removed mass of prepolymer for the determination of the NCO content. Acetone was removed by distillation at 40 °C and 200 mbar.

4.3.3 Particle size distribution

Particle size distribution of each sample was determined at 25 °C with a Zetasizer Nano ZS from Malvern using a 632.8 nm He-Laser and detecting the signal at 173° backscatter detection. The refractive index of the dispersed polyurethane was set to 1.496 and the absorption at the given wavelength to 0.01. Ultrapure water was used as dispersion medium with a dynamic viscosity of 0.8872 mPa s and a refractive index of 1.3340. For each sample three measurements in poly(methyl methacrylate) (PMMA)-makro cuvettes were carried out, with each single measurement resulting out of 15 measurement sub runs. The samples were diluted to 0.0001 wt % with ultrapure water in order to avoid multiple light scattering while maintaining an appropriate signal-to-noise ratio. The mean particle size is given by the z-average value (intensity mean).

Table 4-1: Synthesis Series of Water-Based PUD with Different Polyol Components and Varying AAS contents.[a]

Sample	PTHF	PE	PC	BDO	IPDI	Acetone	IPDA	AAS	Water
PTHF3.5	24.25	/	/	1.89	17.04	76.78	3.43	3.76	99.96
PTHF4.0	24.25	/	/	1.91	17.05	76.85	3.22	4.30	99.71
PTHF4.5	24.27	/	/	1.91	17.05	76.59	3.00	4.77	102.13
PTHF5.0	24.21	/	/	1.92	17.04	76.66	2.77	5.31	103.08
PTHF5.5	24.34	/	/	1.89	17.03	76.76	2.56	5.86	101.98
PE3.0	/	24.23	/	1.91	17.03	76.68	3.35	3.07	104.80
PE3.5	/	24.25	/	1.90	17.03	76.68	3.24	3.51	104.25
PE4.0	/	24.20	/	1.90	17.00	76.68	3.16	4.17	107.80
PE4.5	/	24.25	/	1.91	17.04	76.92	2.72	4.58	101.90
PE5.0	/	24.24	/	1.91	17.03	76.76	2.40	5.05	104.39
PC3.5	/	/	24.64	2.02	17.04	76.80	3.19	3.45	103.22
PC4.0	/	/	24.28	2.01	17.01	76.82	3.07	4.05	110.06
PC4.5	/	/	24.25	2.03	17.03	77.90	2.90	4.63	107.75
PC5.0	/	/	24.29	2.00	17.0	78.33	2.72	5.18	110.15
PC5.5	/	/	24.42	2.00	17.0	76.90	2.49	5.67	109.73

[a] Series A: poly(tetrahydrofuran) (PTHF), series B: polyester (PE), and series C: polycarbonate (PC) with ratio NCO/OH=1.7, degree of chain extension=92%, and solid content of approx. 30 wt-%. All values in g. The amount of chain extender and water was adjusted under consideration of the removed mass of prepolymer for the determination of the NCO content.

4.3.4 Electrophoretic mobility

Measurements of the electrophoretic mobility in dependence of the electrolyte concentration were performed at 25 °C with a Zetasizer Nano ZS from Malvern. The measurement settings were the same as those for particle size determination. The signal was detected at 17° front scatter detection. Relative permittivity of water was set to 78.5. The samples were measured at 0.1 vol % in order to obtain an appropriate signal-to-noise ratio. Each measurement was performed in a folded capillary cell DTS 1070 as a single measurement consisting out of 15 individual measurement sub runs. Each sample was measured four times using different cells. KNO_3 was used as electrolyte and the electrolyte concentration was varied in the range of 5-300 mM. Samples were left for 12 hours at room temperature for equilibration purpose.

4.3.5 Titration of particle charges

Potentiometric acid-base titration experiments were performed with Metrohm titrator "Ti-Touch 916" using a linear step width of 0.05 mL. The measuring cell was blanketed with nitrogen to avoid the absorption of carbon dioxide. Samples were diluted to a concentration of 5 wt % and treated with a strongly acidic ion-exchange resin Amberlite IRN-77 for 1 h for purification and protonation purpose before titration.

The ion exchange resin was purified and activated according to a procedure described by McCann.[52] It was first washed with preheated water (>80 °C) and then three times with methanol. For activation purpose, the pH value was shifted several times by alternately using 3 M HCl or 3 M NaOH. After each activation cycle, the pH value was set to neutral by washing several times with ultrapure water. The ion exchange resin activated in this way was used for the treatment of the PUD samples and subsequently removed by filtration. Afterwards, the solids content of the protonated polymer was determined for further evaluation purposes. Finally, the potentiometric titration experiment involved two measurements. At first, a blank titration consisting out of 5 mL 0.02 M HCl and 70 mL ultrapure water being titrated with 0.02 M NaOH. Second, sample titration consisting of 10 mL 5 wt % sample, 5 mL 0.02 M HCl and 60 mL ultrapure water. The difference in volume equivalence between the two measurements corresponds to the content of acidic groups of the polymer. The titration curves were further evaluated using the procedure of Alves et al.[46]

4.4 Results and Discussion

To obtain information about the influence of the AAS content and the polyol component on the charge content and the electrokinetic behaviour, defined synthesis series according to the acetone process were carried out. For this purpose, the mass fraction of AAS was varied between 3.0 and 5.5 wt-% for the used polyether, polyester and polycarbonate polyol. Other characteristic parameters were kept constant. Due to the large number of parameters considered, certain symbols are used that specifically address the various aspects examined. A list of important symbols with a brief description can be found in Table 4-2. Detailed explanations are given in subsequent sections.

4.4.1 Particle Size

Particle size distributions of the dispersions under investigation were studied using DLS. The results of particle diameter $2a$ and polydispersity index PDI are shown in Table 4-3. For all series, the particle size decreases asymptotically in all cases with increasing AAS content, reaching a value of about 40 nm to 50 nm at high AAS fraction. The PDI values indicate a monomodal particle size distribution and show no significant differences between the series. The values agree to those given in literature.[53] The minimum AAS content necessary to obtain a stable dispersion was found to be 3.0 wt-% in case of PE and 3.5 wt-% in case of PC and PTHF series. Further reduction of the AAS content led to unstable dispersions with bimodal particle size distribution and phase separation within several hours.

The increasing AAS fraction also increases the charge content of the polymer chains. This is relevant for the acetone process as it enables the stabilization of higher specific surface area, leading to a decrease in particle size. Comparable results were also described in literature.[6,16–19,54] In particular, Nanda and Wicks investigated the influence of several reaction compounds on the particle size distribution. Among others, they varied the DMPA content between 4 and 7 wt-% and found an asymptotic decrease in particle size starting from 140 nm (4.0 wt-%) to 50 nm (7.0 wt %), explaining this with the increase in charges. Nevertheless, the lower boundary of necessary DMPA mass fraction was given with 4.0 wt-% in this study[22], while Lijie et al. also studied the influence of DMPA on PUDs and found the minimum concentration of DMPA to be 2.4 wt-%[55]. In summary, different minimum contents required to obtain a stable dispersion were found. This indicates a significant influence of the entire PUD composition.

Table 4-2: Reference Table of Main Symbols.

Symbol	Description
Q_{max}	maximum amount of specific particle charge calculated from the synthesis recipe
$Q_{\mathrm{tit,0}}$	specific particle charge for the first equivalence point determined by acid-base titration
$Q_{\mathrm{tit,1}}$	specific particle charge for the second equivalence point determined by acid-base titration
Q_{tit}	total specific particle charge determined by acid-base titration, $Q_{\mathrm{tit,0}} + Q_{\mathrm{tit,1}} = Q_{\mathrm{tit}}$
$\mathrm{p}K_{\mathrm{a,0}}$	effective dissociation constant for the first equivalence point
$\mathrm{p}K_{\mathrm{a,1}}$	effective dissociation constant for the second equivalence point
Q_{ek}	specific particle charge determined by electrokinetic data on the basis of the soft particle model using equation 4-28
RR	overall recovery rate of particle charges determined by acid-base titration and the synthesis recipe
σ_0^{tit}	surface charge density determined by acid-base titration
σ_0^{ek}	electrokinetic surface charge density determined by electrokinetic data on the basis of the hard particle model using equation 4-17
ZN	volume charge density according to the soft particle model
ψ_0	surface potential according to the hard particle model determined using equations 4-13-4-16
x_{s}	distance of the shear plane to the particle surface determined using equations 4-13-4-16

4.4.2 Particle charge analysis

In the case of electrostatically stabilized dispersions, knowledge of the charge content of the overall system is of high relevance. For this purpose, each sample was first treated with a strong acidic ion-exchange resin and then titrated with a caustic soda solution. The potentiometric titration curve was analyzed by a nonlinear regression data analysis. Detailed information about this procedure can be found elsewhere.[46] The model allows several acid groups with different acid strength to be considered. As a result, the respective quantities and the effective acid dissociation constants are obtained. Based on these results, the total specific charge Q_{tit} of the system can be calculated with respect to the mass of protonated polymer using equation 4-19. The recovery rate RR is defined as the ratio of the experimentally determined specific particle charge Q_{tit} to the maximum amount of specific particle charge Q_{max}. Q_{max} is given by the theoretical composition, assuming full protonation of the AAS groups. Finally, the surface charge density σ_0^{tit} can be calculated by taking the mean particle diameter $2a$ and a typical value of 1.1 kg L^{-1} for the density ρ_{p} of polyurethanes into account (cf. eq. 4-20). The results are shown in Table 4-3.

As expected, the specific particle charge content Q_{tit} increases with increasing AAS content. Additionally, there is no significant influence of the polyol component observable. The surface charge densities σ_0^{tit} on the other hand, show a slight increase in value for the lowest AAS concentration of each series, followed by nearly constant values for higher AAS concentrations. These results seem to be

counterintuitive at first sight, as more charges are incorporated within the polymer structure, but they can be conclusively explained by the increasing specific surface area of the particles due to the decrease in particle size.

Table 4-3: Characteristic Parameter for All Poly(tetrahydrofuran) (PTHF), Polyester (PE) and Polycarbonate (PC) Based PUDs. [a)]

Sample	$2a$ [nm]	PDI	$Q_{\mathrm{tit},0}$ [C/g]	$Q_{\mathrm{tit},1}$ [C/g]	Q_{tit} [C/g]	Q_{ek} [C/g]	σ_0^{tit} [C/m^2]	σ_0^{ek} [C/m^2]	RR [%]	$\mathrm{p}K_{\mathrm{a},1}$
PTHF3.5	65.7	0.21	-12.2	-2.9	-15.1	-14.5	-0.19	-0.031	72.7	6.0
PTHF4.0	53.3	0.11	-14.8	-3.1	-17.9	-10.4	-0.18	-0.022	76.4	6.1
PTHF4.5	50.7	0.14	-18.1	-3.5	-21.6	-10.0	-0.20	-0.020	83.8	5.6
PTHF5.0	43.7	0.12	-20.9	-3.4	-24.3	-8.1	-0.19	-0.020	85.0	5.6
PTHF5.5	39.3	0.19	-24.3	-3.6	-27.9	-8.4	-0.20	-0.018	84.8	5.7
PE3.0	110.4	0.17	-10.2	-2.5	-12.7	-12.7 [b)]	-0.26	-0.035	73.9	5.8
PE3.5	66.6	0.10	-13.1	-3.3	-16.4	-16.3	-0.20	-0.025	82.3	5.8
PE4.0	56.4	0.11	-16.7	-2.6	-19.3	-9.4	-0.20	-0.020	84.8	6.1
PE4.5	48.4	0.11	-19.3	-2.5	-21.8	-9.4	-0.19	-0.021	84.9	6.7
PE5.0	48.8	0.16	-20.5	-2.7	-23.2	-7.5	-0.20	-0.020	82.0	5.6
PC3.5	113.8	0.25	-10.3	-2.9	-13.2	-13.2	-0.28	-0.022	65.4	6.2
PC4.0	75.0	0.12	-14.3	-2.7	-17.0	-8.9	-0.23	-0.018	74.1	6.4
PC4.5	59.0	0.11	-17.1	-3.2	-20.3	-8.7	-0.22	-0.019	78.9	6.4
PC5.0	53.4	0.12	-21.4	-3.2	-24.6	-9.6	-0.24	-0.020	85.7	6.2
PC5.5	47.2	0.13	-23.7	-3.3	-27.0	-6.2	-0.23	-0.017	85.6	6.2

[a)] The mass concentration of AAS of each system is given by the numbers following the polyol component. Particle diameter $2a$ and polydispersity index PDI are measured using dynamic light scattering. Specific particle charge Q_{tit} (the number in the subscript refers to the first and second equivalence point), recovery rate RR, surface charge density σ_0^{tit} and effective dissociation constant $\mathrm{p}K_{\mathrm{a},1}$ for the second equivalence point are determined by acid-base titration. Electrokinetic data are used for the determination of specific charge Q_{ek} (soft particle model) and electrokinetic surface charge density σ_0^{ek} (hard particle model).

[b)] $f\left(d/a\right) = 0.79$ used for calculation (cf. eq. 4-26), since Q_{tit} is then equal to Q_{ek}.

Looking at the recovery rate RR, all series show values well below 100%. This is especially true at low AAS content, whereas RR increases towards approximately 85% at high AAS content. Although a major part of the incorporated charges could be detected in our charge titration experiments, our findings also clearly indicate that some charges are probably trapped inside the particles, as they cannot participate in the preceding ion exchange process.

This assumption is further supported by the fitting procedure of the potentiometric titration curve (see supporting information Figure S4-1 and Figure S4-2 as well as Table S1). It was found that at least two acidic groups with different effective dissociation constants are necessary to describe the experimental data. Most of the charges ($Q_{\mathrm{tit},0}$) behave like strong acidic groups ($\mathrm{p}K_{\mathrm{a},0} = 0$), as expected by the incorporated sulfonate groups. However, approximately 12 to 22 % of the detectable charges (see $Q_{\mathrm{tit},1}/Q_{\mathrm{tit}}$ in Table S1 in the supporting information) have a weak acidic character ($\mathrm{p}K_{\mathrm{a},1} \approx 6$). The latter can be attributed to additional work required to remove protons from the particle into the bulk

dispersion medium, which lowers the effective dissociation constant. This could occur, for example, if the charged groups are partly located within an ion-penetrable polymer shell with rather small distances to each other, leading to strong electrostatic interactions between the functional groups and the dissociating protons. Conclusively, the analysis of the potentiometric titration curve indicates that the particle charges are not only located on the particle surface but also distributed in a peripheral ion-penetrable layer. This also allows us to understand that the deeper the sulfonate groups are located inside the particles, the less dissociated they are. Ultimately, they can no longer be detected by charge titration experiments.

On closer inspection, it can be seen that an increase in the AAS content hardly affects the amount of weak acidic groups $Q_{\mathrm{tit},1}$, but mainly increases the specific particle charge $Q_{\mathrm{tit},0}$ of the strong acidic groups. As a result, the additionally incorporated charge groups are apparently able to reorganise themselves at the particle surface during secondary dispersion. This finding is in accordance with the increase in interfacial area resulting from the decrease in particle size, which facilitates the rearrangement of the hydrophilic sulfonate groups. It is therefore recommended to investigate the electrophoretic behaviour of the PUDs in detail in order to obtain additional information about the charge structure of the particles.

4.4.3 Electrophoretic behaviour of polyurethane particles

4.4.3.1 Experimental results

The electrophoretic mobility was measured for all synthesised PUD's as a function of the ionic strength using KNO_3 as 1:1 electrolyte. Exemplary results for PE-based dispersion stabilized by different mass concentrations of AAS are shown in Figure 4-2 and are representative for all other synthesised PUDs (for full results refer to supporting information, Figure S4-3-Figure S4-5). Due to the anionic nature of the sulfonate group, all dispersions show negative values of the electrophoretic mobility. In general, the sample with lowest AAS content shows more negative values at low ionic strength compared to samples with high AAS concentration, reflecting the results of the surface charge densities.

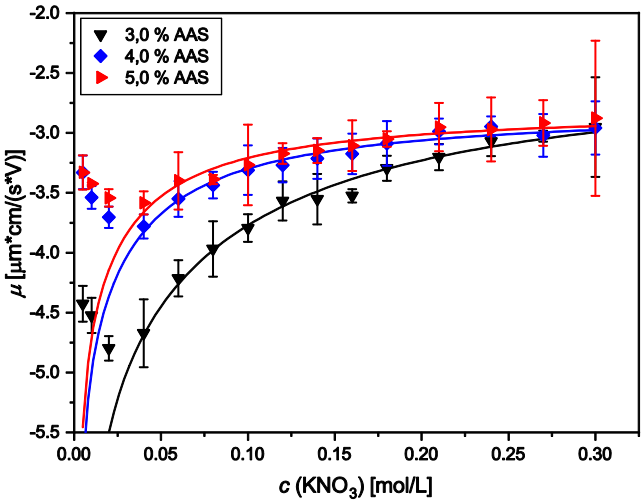

Figure 4-2: Electrophoretic mobility μ as a function of the KNO_3 concentration c for 3.0 wt-% AAS (black), 4.0 wt-% AAS (blue) and 5.0 wt-% of polyester based PUD. The solid symbols represent the average value of the measurement with the error bars corresponding to its standard deviation. The solid lines represent the results of the fit according to equation 4-24 for $d \approx b$ expressed by $f\left(d/a\right) = 2/3$.

In all cases, a distinct extremum of the electrophoretic mobility can be found at low electrolyte concentrations. It is followed by a decrease of the absolute value of electrophoretic mobility, which can

be attributed to the increase of ionic strength, leading to screening of the surface charges and a compression of the diffuse double layer.

However, the electrophoretic mobility does not approach zero, even at high electrolyte concentrations. The nonzero limiting value seems to be independent of the AAS concentration of the system within the range of ionic strength studied. It should be noted that with increasing ionic strength, a degradation of the electrodes of the folded capillary cells due to electrolysis could be observed, which was also mentioned by other authors.[49] A further rise of the ionic strength led to even higher measurement errors and thus to insufficient results. For this reason, the maximum electrolyte concentration used in this study is 300 mM KNO_3. Nevertheless, the observed non-zero limiting value is described as typical for soft particles.[48,56] There are several studies dealing with the soft particle model of Ohshima, but mostly in case of bio colloids like microalgae,[49] humic substances[57] or microbial particles[58] as they are known to have a polyelectrolyte layer surrounding a particle core.

4.4.3.2 Soft particle model

The observed extremum of the electrophoretic mobility at low electrolyte concentration is also mentioned by other authors and is usually caused by relaxation effects of the diffuse double layer, regardless of the particle character being hard or soft.[25,28,49,59] To address this effect, the electrophoretic data were analysed by nonlinear least-squares method according to equation 4-24, which includes the relaxation of soft particles (solid lines shown in Figure 4-2). The characteristic values ZN and λ^{-1} were used as free adjustable variables. The factor $f\left(d/a\right)$ on the other hand, was fixed because it is not very sensitive to the fitting procedure. The course of the fitting curve barely changed and the goodness of the fit did not improve significantly within the range of 1 - 2/3. However it should be recognized, that the factor $f\left(d/a\right)$ has a clear influence on the determined values of ZN and λ^{-1}. It was finally decided to consider the particles as extended polyelectrolytes with a vanishingly small core (i.e. $d \approx b$ and $f\left(d/a\right) = 2/3$), since the determined volume charge densities ZN are not sufficient to match the determined specific particle charge Q_{tit} even under this assumption (with the only exception of sample PE3.0, since Q_{tit} is equal to Q_{ek} if $f\left(d/a\right) = 0.79$). This becomes evident when calculating the specific particle charge Q_{ek} in accordance to equation 4-28 with $N_{\mathrm{p,m}}$ as the specific particle number. The calculated values of ZN and λ^{-1} are shown in Table 4-4, the fitting curves are shown in Figure 4-2 and the values of Q_{ek} are shown in Table 4-3.

$$Q_{\mathrm{ek}} = \frac{\pi}{6}[(2b)^3 - (2a)^3] \cdot N_{\mathrm{p,m}} \cdot ZN \cdot 1000 \cdot F \tag{4-28}$$

The model describes the experimental data well in case of high ionic strengths, but seems to fail for electrolyte concentrations below 40 mM KNO_3. As equation 4-24 takes the relaxation effect into account, it can be excluded as a factor of influence in this study. Deviations at low ionic strength have also been mentioned by other authors.[59–62] According to Gaboriaud et al. the assumption of a homogenous charge distribution is possibly not accurate and might also change in dependence of the ionic strength.

Anyway, characteristic values of the volume charge densities and the electrophoretic softness parameter could be obtained for electrolyte concentrations greater than 40 mM KNO_3 and are shown in Table 4-4. The volume charge density decreases with increasing AAS content. This observation is quite surprising and would imply that the thickness d of the polyelectrolyte layer must concomitantly increase in order to host all charged sulfonate groups. On the other hand, the electrophoretic softness parameter λ^{-1} increases throughout the series. This finding is in good agreement with the increasing recovery rates

found by titration experiments, because increasing ion-penetrability of the charge bearing particle shell would support the proton dissociation.

Table 4-4: Volume charge densities ZN and softness parameter λ^{-1}. *

AAS content [wt-%]	PTHF		PE		PC	
	ZN [mM]	λ^{-1} [nm]	ZN [mM]	λ^{-1} [nm]	ZN [mM]	λ^{-1} [nm]
3.0	/	/	-235**	1.0**	/	/
3.5	-166	1.2	-186	1.2	-153	1.4
4.0	-119	1.5	-107	1.6	-101	1.6
4.5	-114	1.5	-107	1.6	-99	1.7
5.0	-93	1.7	-86	1.8	-110	1.6
5.5	-96	1.6	/	/	-71	1.9

* Results for or all polyTHF (PTHF), polyester (PE) and polycarbonate (PC) based PUDs are obtained by fitting the experimental data with $f\left(d/a\right) = 2/3$ according to equation 4-24 for electrolyte concentrations larger than 40 mM.

** $f\left(d/a\right) = 0.79$ used for calculation (cf. eq. 4-26), since Q_{tit} is then equal to Q_{ek}.

It is known that the electrophoretic mobility of PolyNIPAAm can be described by a soft particle character, which can be strongly controlled by adjusting synthesis parameters like cross-linking density or charge content. PolyNIPAAm particles are thermosensitive and show severe volume shrinkage at higher temperatures. This also affects its electrophoretic properties, making them a perfect reference system for soft particles. Several studies regarding the electrokinetic properties of PolyNIPAAm have been carried out. Several studies regarding the electrokinetic properties of PolyNIPAAm have been done. Among others, López-León et al investigated cationic PolyNIPAAm particles and found the softness parameter to decrease from 4 nm (20 °C) to 1.0 nm (50 °C) and the volume charge density to increase from 1 mM (20 °C) to -23 mM (50 °C) and attributed these effects to the collapse of the polymer structure.[63] Their values of ZN and λ^{-1} are higher and lower, respectively, compared to other studies in this field.[64,65] They attributed this observation to a different composition of the PolyNIPAAm particle, leading to a special cross-linked network and thus more rigid particles. Their determined softness parameter in the collapsed state is in good agreement with the results presented in this study. This suggests a rather dense polymer conformation of the polyurethane particle with a low ion permeability. When comparing the volume charge densities ZN, it is evident that the values determined for PUDs turn out to be quite high. However, as can be seen from the comparison of the specific charge densities in Table 4-3, they are still too low to match the values of the titration. In addition, the trend of the Q_{ek} values is not plausible as it is opposite to that of the Q_{tit} values.

Based on these results and the insufficient description of the electrophoretic mobility data at low ionic strength it can be concluded that the soft particle model of Ohshima is not capable to describe the electrophoretic mobility of polyurethane particles satisfactorily. The characteristic nonzero limiting mobility is not only observed in case of soft particles, but it is also expected for highly charged hard particles. Ohshima pointed out that these disperse systems approach a limiting zeta potential of 35.6 mV in aqueous electrolyte media.[66] Therefore, the experimental data of the PUDs in this study were also investigated with regard to a hard particle model.

4.4.3.3 Hard particle model

In case of hard particles, the zeta potential can be seen as a characteristic value for the electrostatic repulsive forces of the dispersion. Therefore, zeta potentials were calculated according to Helmholtz and Smoluchowski (eq. 4-1) and Ohshima, Healy and White (eq. 4-5 and 4-12, respectively). The results of both models are shown in Figure 4-3 for an exemplary data set (see supporting information for all other results). Since the Helmholtz−Smoluchowski equation does not take the relaxation effect into account, the data are highly erroneous at low ionic strengths.

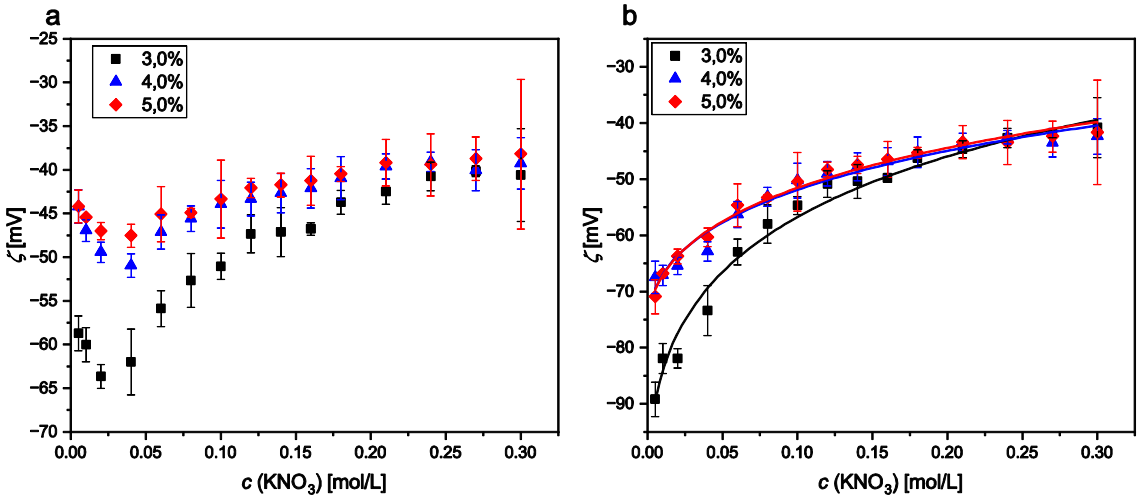

Figure 4-3: Zeta potential ζ as a function of KNO_3 concentration c for polyester based PUDs containing 3.0 wt-% (black), 4.0 wt-% (blue) and 5.0 wt-% (red) AAS. Evaluation according to Helmholtz and Smoluchowski (a) and Ohshima, Healy and White (b). The solid lines represent the results of the fit according to equation 4-13. The solid symbols represent the average value with the error bars corresponding to their standard deviation.

This is clearly seen by the presence of an extremum of the zeta potential at an electrolyte concentration of approximately 20−40 mM. In contrast, the evaluations using the equations of Ohshima, Healy, and White provide much more plausible values, as can be seen from the monotonically decreasing zeta potentials with increasing ionic strength. Exactly this trend is to be expected and can be attributed to compression of the diffuse double layer. The differences between the two evaluations become considerably smaller with increasing ionic strength as the impact of the relaxation effect diminishes. However, one should bear in mind that the zeta potentials according to Helmholtz and Smoluchowski would lead to distinct errors and misinterpretations when the case of a low ionic strength is considered for further interpretation. The necessity to consider the relaxation effect to obtain reliable data has already been described in several other studies.[25,67–69] For example, Hakim et al. recently measured the electrophoretic mobility of different surfactant free polystyrene latices bearing sulfate groups as a function of the ionic strength. They also observed an extremum for the electrophoretic mobility at low ionic strength that could only be explained by means of the relaxation effect. Interestingly, they dealt with dispersions having a surface charge density in the range of -0.006 to -0.096 C/m^2 which is significantly lower than the values for the PUDs (cf. σ_0^{tit} in Table 4-3).This makes the occurrence of relaxation effects in this study much more likely.[28]

Once the zeta potential has been determined as a function of the ionic strength, it is possible to calculate the surface potential ψ_0 and the distance of the shear plane x_s. For this purpose, the dependency of the zeta potentials on the electrolyte concentration is evaluated by nonlinear least-squares fitting procedure according to equation 4-13. Although the sulfonate groups have a strongly acidic character and their dissociation behaviour should therefore only be slightly influenced by the addition of electrolyte, Figure 4-3b shows that the model of a constant surface potential describes the experimentally determined data

very well (diagrams of all other samples are shown in the supporting information, Figure S4-6-Figure S4-8). The results of the two fitting parameters can be seen in Figure 4-4 for all PUD samples.

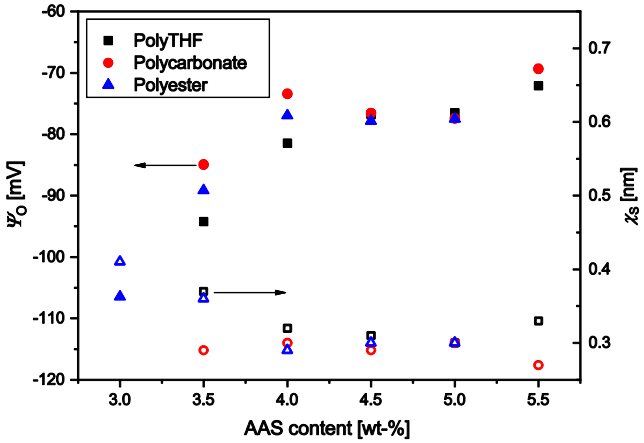

Figure 4-4: Surface potential ψ_0 (solid symbols) and distance of shear plane x_s (empty symbols) as a function of the AAS concentration for polyTHF (black), polyester (blue) and polycarbonate (red) based PUD's obtained by least square fitting procedure according to equation 4-13.

Unexpectedly, the determined surface potentials decrease with increasing AAS content and there are only minor differences between the various polyol components. Taking the polyester based PUDs as an example (Figure 4-4, blue filled symbols) it decreased from -105 mV at 3.0 wt-% AAS to -75 mV at 5.0 wt-% AAS. This distinct trend can again be attributed to the increasing specific surface area of the particles, which compensates the increasing amount of charges incorporated in the system. These results also coincide with the general trend found for the surface charge densities σ_0^{tit} determined by titration experiments.

Additionally, all samples show reasonable distances of shear plane with values between 0.3 nm and 0.4 nm. Recent studies in this field also determined the distance of shear plane to describe electrophoretic mobilities and to draw conclusion about the surface potential.[25,67,68,70,71] For example, Borkovec et al. found values of x_s between 0.3 and 1.0 nm for various charge regulated dispersions.[25] Kobayashi et al. also evaluated electrophoretic mobilities by adjusting x_s and found good agreement by using 0.25 nm.[67,69] A value of 0.25 nm is often attributed to a monolayer of firmly bound water molecules. The values found in this study are a bit larger and therefore indicate a small outward shift of the shear plane. This may be explained by a slight surface roughness, caused, for example, by the presence of a non-uniform, hairy layer of macromolecules.[72,73]

In order to check the data of the hard particle model for plausibility, it is useful to evaluate the surface charge density. By considering the obtained surface potentials, the electrokinetic surface charge density σ_0^{ek} can be calculated according to equation 4-17. A comparison with the surface charge density σ_0^{tit} determined by titration experiments is shown in Table 4-3. Both series show the same trend, but the electrokinetic values σ_0^{ek} are too low by a factor of approximately 10 compared to σ_0^{tit} values, which means that the measured electrophoretic mobilities can hardly be explained by the surface charge densities σ_0^{tit} calculated from titration data. This once again confirms the conclusion drawn from the acid-base titration experiment that the determined charges are not exclusively located on the particle surface, but that they are somehow distributed at the particle surface and in a peripheral ion-penetrable layer. The real particle therefore has a more complex charge arrangement than can be described by the hard particle model. Consequently, the calculated electrokinetic surface charge density σ_0^{ek} (and accordingly the corresponding surface potential ψ_0) should be considered as an equivalent value for an

ion-impenetrable particle with the same electrophoretic mobility, whose charges are completely arranged on the particle surface.

When discussing the charge arrangement, one should also bear in mind that the charged sulfonate groups are not freely mobile but are fixed in the polymer backbone. Therefore, they are subject to a complex rearrangement during the dispersion step. It is thus reasonable to enhance the classical hard particle model when analysing electrophoretic experiments. One of the simplest options is the soft particle model of Ohshima, in which the charges are uniformly distributed in an outer polyelectrolyte layer. However, as demonstrated in this study, this model is unable to explain the experimental results of the PUDs adequately. Unfortunately, other suitable models with complex charge arrangements are currently not available for the analysis of electrophoretic experiments. It can therefore be concluded that the electrophoretic behaviour of PUDs is currently best described with the hard particle model.

4.5 Conclusion

Within this study, PUDs with different amounts of charged intrinsic stabilizer (AAS) and polyol components were prepared. The particle charge content and the electrophoretic behavior of PUDs were analyzed in detail. It was found that the polyol component had no pronounced impact. As expected, the specific particle charges Q_{tit} determined by acid-base titration increase with increasing AAS concentration. These data also indicate that some of the ionic groups are located inside the polymer matrix. Therefore, the soft particle model of Ohshima was tentatively applied to describe the measured electrophoretic mobilities, but the observed dependency on the electrolyte concentration could not be satisfactorily explained. Besides its failure at low ionic strength, the determined volume charge densities ZN and the corresponding specific particle charges Q_{ek} show an implausible trend because they decrease with increasing AAS content.

On the other hand, the electrophoretic mobilities and the corresponding zeta potentials can be well described in terms of a hard particle model taking the relaxation effect into account. In addition, the dependency of the zeta potentials on the electrolyte concentration can be excellently modelled by assuming a constant surface potential ψ_0 and distance of the shear plane x_{s}. These surface potentials show decreasing values with increasing AAS mass fraction, which can be explained by the decreasing particle sizes. Nevertheless, the calculated electrokinetic surface charge densities σ_0^{ek} based on these surface potentials are 1 order of magnitude lower compared to the ones determined by acid-base titration (σ_0^{tit}). Accordingly, this indicates that the particle charges of the PUDs are not entirely arranged on the surface but rather distributed at the particle surface and in a peripheral ion-penetrable layer. However, the results have also shown that a uniform charge distribution, as assumed by the soft particle model, is too simple and does not adequately describe the actual dispersion properties.

This study shows that it is beneficial for in-depth charge characterization of PUDs to perform different investigation methods and compare their results. Thus, additional information about the actual particle charge distribution can be obtained. The results also provide a solid basis for other investigations involving electrostatic interactions, e.g. studies on dispersion stability.

Supporting information

The Supporting Information is available free of charge at https://pubs.acs.org/doi/10.1021/acs.langmuir.4c02498. Exemplary data fits of potentiometric titration curve; detailed data for the specific particle charge and recovery rate for all PUD samples; complete graphics of the measured electrophoretic mobilities and calculated zeta potentials for all PUD samples (PDF).

Author information

Corresponding Author

J. Wilkens − *Faculty of Applied Natural Sciences, TH Köln_ University of Applied Science, Leverkusen D-51379, Germany;* orcid.org/0000-0003-2831-8400;
Email: jan.wilkens@th-koeln.de

Authors

C. Grau − *Faculty of Applied Natural Sciences, TH Köln_ University of Applied Science, Leverkusen D-51379, Germany*
A. M. Schmidt − *Department of Chemistry, University of Cologne, D-50939 Cologne, Germany;* orcid.org/0000-0002-7284-7847
Complete contact information is available at: https://pubs.acs.org/10.1021/acs.langmuir.4c02498

Author contribution

C. Grau: Experimental work, Methodology, Conceptualization, Data evaluation and visualization, Software, Writing – original draft. **A.M. Schmidt:** Supervision, Discussion, Writing – review and editing. **J. Wilkens:** Supervision, Conceptualization, Methodology, Project administration, Discussion, Resources, Funding acquisition, Writing – review and editing.

Notes

The authors declare no competing financial interest.

Acknowledgements

This project has received fundings from the German Ministry of Education and Research (BMBF) as part of the funding program Forschung an Fachhochschulen under contract number 13FH142PX6. We are also very grateful for valuable discussions and financial and material support provided by Covestro AG. We would also like to thank J.P. de Mesquita of the Federal University of the Jequitinhonha and Mucuri Valleys for providing the MATLAB code.

4.6 References

(1) Poussard, L., Lazko, J., Mariage, J., Raquez, J.-M., Dubois, P. Biobased waterborne polyurethanes for coating applications: How fully biobased polyols may improve the coating properties. *Progress in Organic Coatings* **2016**, *97*, 175–183.

(2) Liu, H., Li, C., Sun, X. S. Soy-oil-based waterborne polyurethane improved wet strength of soy protein adhesives on wood. *International Journal of Adhesion and Adhesives* **2017**, *73*, 66–74.

(3) Zhou, X., Li, Y., Fang, C., Li, S., Cheng, Y., Lei, W., Meng, X. Recent Advances in Synthesis of Waterborne Polyurethane and Their Application in Water-based Ink: A Review. *Journal of Materials Science & Technology* **2015**, *31*, 708–722.

(4) Bai, C. Y., Zhang, X. Y., Dai, J. B., Zhang, C. Y. Water resistance of the membranes for UV curable waterborne polyurethane dispersions. *Progress in Organic Coatings* **2007**, *59*, 331–336.

(5) Meng, Q. B., Lee, S.-I., Nah, C., Lee, Y.-S. Preparation of waterborne polyurethanes using an amphiphilic diol for breathable waterproof textile coatings. *Progress in Organic Coatings* **2009**, *66*, 382–386.

(6) Chinwanitcharoen, C., Kanoh, S., Yamada, T., Tada, K., Hayashi, S., Sugano, S. Preparation and Shelf-Life Stability of Aqueous Polyurethane Dispersion. *Macromolecular Symposia* **2004**, *216*, 229–240.

(7) García-Pacios, V., Jofre-Reche, J. A., Costa, V., Colera, M., Martín-Martínez, J. M. Coatings prepared from waterborne polyurethane dispersions obtained with polycarbonates of 1,6-hexanediol of different molecular weights. *Progress in Organic Coatings* **2013**, *76*, 1484–1493.

(8) García-Pacios, V., Costa, V., Colera, M., Martín-Martínez, J. M. Waterborne polyurethane dispersions obtained with polycarbonate of hexanediol intended for use as coatings. *Progress in Organic Coatings* **2011**, *71*, 136–146.

(9) Dieterich, D. Aqueous emulsions, dispersions and solutions of polyurethanes; synthesis and properties. *Progress in Organic Coatings* **1981**, *9*, 281–340.

(10) Sardon, H., Irusta, L., Fernández-Berridi, M. J., Luna, J., Lansalot, M., Bourgeat-Lami, E. Waterborne polyurethane dispersions obtained by the acetone process: A study of colloidal features. *Journal of Applied Polymer Science* **2011**, *120*, 2054–2062.

(11) Wicks, Z. W., Wicks, D. A., Rosthauser, J. W. Two package waterborne urethane systems. *Progress in Organic Coatings* **2002**, *44*, 161–183.

(12) Cakić, S. M., Ristić, I. S., Krakovský, I., Stojiljković, D. T., Bělský, P., Kollová, L. Crystallization and thermal properties in waterborne polyurethane elastomers: Influence of mixed soft segment block. *Materials Chemistry and Physics* **2014**, *144*, 31–40.

(13) Hourston, D. J., Williams, G., Satguru, R., Padget, J. D., Pears, D. Structure-property study of polyurethane anionomers based on various polyols and diisocyanates. *Journal of Applied Polymer Science* **1997**, *66*, 2035–2044.

(14) Gündüz, G., Kısakürek, R. R. Structure–Property Study of Waterborne Polyurethane Coatings with Different Hydrophilic Contents and Polyols. *Journal of Dispersion Science and Technology* **2004**, *25*, 217–228.

(15) Lee, D.-K., Tsai, H.-B., Wang, H.-H., Tsai, R.-S. Aqueous polyurethane dispersions derived from polycarbonatediols. *Journal of Applied Polymer Science* **2004**, *94*, 1723–1729.

(16) Lee, S. K., Kim, B. K. High solid and high stability waterborne polyurethanes via ionic groups in soft segments and chain termini. *Journal of Colloid and Interface Science* **2009**, *336*, 208–214.

(17) Pérez-Limiñana, M. A., Arán-Aís, F., Torró-Palau, A. M., César Orgilés-Barceló, A., Miguel Martín-Martínez, J. Characterization of waterborne polyurethane adhesives containing different amounts of ionic groups. *International Journal of Adhesion and Adhesives* **2005**, *25*, 507–517.

(18) Mequanint, K., Sanderson, R. Hydrolytic stability of nano-particle polyurethane dispersions: Implications to their long-term use. *European Polymer Journal* **2006**, *42*, 1145–1153.

(19) Lorenz, O., Budde, V., Reinmöller, K.-H. Wäßrige Dispersionen anionischer Polyurethane mit Sulfonatgruppen. *Angewandte Makromolekulare Chemie* **1980**, *87*, 35–48.

(20) Saw, L. K., Brooks, B. W., Carpenter, K. J., Keight, D. V. Catastrophic phase inversion in region II of an ionomeric Polymer-water system. *Journal of Colloid and Interface Science* **2004**, *279*, 235–243.

(21) Wei, Y., Luo, Y., Li, B., Li, B. Phase inversion of UV-curable anionic polyurethane in the presence of acetone solvent. *Colloid & Polymer Science* **2005**, *283*, 1289–1297.

(22) Nanda, A. K., Wicks, D. A., Madbouly, S. A., Otaigbe, J. U. Effect of ionic content, solid content, degree of neutralization, and chain extension on aqueous polyurethane dispersions prepared by prepolymer method. *Journal of Applied Polymer Science* **2005**, *98*, 2514–2520.

(23) Lorenz, O., Budde, V., Wirtz, W. Investigation of the particle surface of anionic polyurethane dispersions with COO−-groups. *Angewandte Makromolekulare Chemie* **1979**, *83*, 113–127.

(24) Lorenz, O., Reinmöller, K.-H., Hellendahl, K. Über den Kationenaustausch bei anionischen Polyurethan-Dispersionen mit Natriumsulfonat-gruppen. *Angewandte Makromolekulare Chemie* **1981**, *101*, 29–34.

(25) Borkovec, M., Behrens, S. H., Semmler, M. Observation of the Mobility Maximum Predicted by the Standard Electrokinetic Model for Highly Charged Amidine Latex Particles. *Langmuir the ACS journal of surfaces and colloids* **2000**, *16*, 5209–5212.

(26) Trefalt, G., Behrens, S. H., Borkovec, M. Charge Regulation in the Electrical Double Layer: Ion Adsorption and Surface Interactions. *Langmuir the ACS journal of surfaces and colloids* **2016**, *32*, 380–400.

(27) Trefalt, G., Cao, T., Sugimoto, T., Borkovec, M. Heteroaggregation between Charged and Neutral Particles. *Langmuir the ACS journal of surfaces and colloids* **2020**, *36*, 5303–5311.

(28) Hakim, A., Nishiya, M., Kobayashi, M. Charge reversal of sulfate latex induced by hydrophobic counterion: Effects of surface charge density. *Colloid & Polymer Science* **2016**, *294*, 1671–1678.

(29) Smoluchowski, M. v. Elektrische Endosmose und Strömungsströme. In *Handbuch der Elektrizität und des Magnetismus*; Graetz, L., Ed.; Johann Ambrosius: Barth, Leipzig, 1921; Vols. 2, pp. 366–428.

(30) Graetz L., Ed. *Handbuch der Elektrizität und des Magnetismus*; Johann Ambrosius: Barth, Leipzig, 1921.

(31) E. Hückel. Die Kataphorese der Kugel. *Physikalische Zeitschrift* **1924**, 204–210.

(32) Henry, D. C. The Cataphoresis of Suspended Particles. Part I. The Equation of Cataphoresis. *Proceedings of the Royal Society A: Mathematical, Physical and Engineering Sciences* **1931**, *133*, 106–129.

(33) Ohshima, H. On the limiting electrophoretic mobility of a highly charged colloidal particle in an electrolyte solution. *Journal of Colloid and Interface Science* **2003**, *263*, 337–340.

(34) Ohshima, H., Kondo, T. Electrophoresis of large colloidal particles with surface charge layers. Position of the slipping plane and surface layer thickness. *Colloid & Polymer Science* **1986**, *264*, 1080–1084.

(35) Ohshima, H. Electrokinetics of soft particles. *Colloid & Polymer Science* **2007**, *285*, 1411–1421.

(36) Lyklema, J. Electrokinetics after Smoluchowski. *Colloids and Surfaces A: Physicochemical and Engineering Aspects* **2003**, *222*, 5–14.

(37) Overbeek, J. Th. G. Theorie der Elektrophorese: Der Relaxationseffekt. *Kolloid-Beihefte* **1943**, *54*, 287–364.

(38) Booth, F. The cataphoresis of spherical, solid non-conducting particles in a symmetrical electrolyte. *Proceedings of the Royal Society of London. Series A. Mathematical and Physical Sciences* **1950**, *203*, 514–533.

(39) International Organization for Standardization. *Colloidal systems - Methods for zeta-potential determination - Part 1: Electroacoustic and electrokinetic phenomena*, 2012(13099-1:2012-06).

(40) Delgado, A. V., González-Caballero, F., Hunter, R. J., Koopal, L. K., Lyklema, J. Measurement and interpretation of electrokinetic phenomena. *Journal of Colloid and Interface Science* **2007**, *309*, 194–224.

(41) Ohshima, H., Healy, T. W., White, L. R. Approximate analytic expressions for the electrophoretic mobility of spherical colloidal particles and the conductivity of their dilute suspensions. *Journal of the Chemical Society, Faraday Transactions 2* **1983**, *79*, 1613.

(42) Ohshima, H. Approximate Analytic Expression for the Electrophoretic Mobility of a Spherical Colloidal Particle. *Journal of Colloid and Interface Science* **2001**, *239*, 587–590.

(43) Ohshima H. *Theory of colloid and interfacial electric phenomena*, 1st ed.; Elsevier Academic Press: Amsterdam, Boston, 2006.

(44) Ohshima, H., Healy, T. W., White, L. R. Accurate analytic expressions for the surface charge density/surface potential relationship and double-layer potential distribution for a spherical colloidal particle. *Journal of Colloid and Interface Science* **1982**, *90*, 17–26.

(45) Masini, J. C., Godinho, O. E. S., Aleixo, L. M. Determination of ionizable groups of proteins by potentiometric titration in concentrated solutions of guanidine hydrochloride. *Fresenius' Journal of Analytical Chemistry* **1998**, *360*, 104–111.

(46) Alves, L. A., Castro, A. H. de, Mendonça, F. G. de, Mesquita, J. P. de. Characterization of acid functional groups of carbon dots by nonlinear regression data fitting of potentiometric titration curves. *Applied Surface Science* **2016**, *370*, 486–495.

(47) Ohshima, H., Nakamura, M., Kondo, T. Electrophoretic mobility of colloidal particles coated with a layer of adsorbed polymers. *Colloid & Polymer Science* **1992**, *270*, 873–877.

(48) Ohshima, H. Electrophoresis of soft particles: analytic approximations. *Electrophoresis* **2006**, *27*, 526–533.

(49) Gomes, P. A., d'Espinose de Lacaillerie, J.-B., Lartiges, B., Maliet, M., Molinier, V., Passade-Boupat, N., Sanson, N. Microalgae as Soft Permeable Particles. *Langmuir the ACS journal of surfaces and colloids* **2022**, *38*, 14044–14052.

(50) Ohshima, H. Electrophoretic mobility of a highly charged soft particle: Relaxation effect. *Colloids and Surfaces A: Physicochemical and Engineering Aspects* **2011**, *376*, 72–75.

(51) DIN Deutsches Institut für Normung e. V. *Determination of isocyanate content*, 07th ed. (ISO 14896:2009);).

(52) Lagaly G., Schulz O., Zimehl R. *Dispersionen und Emulsionen: Eine Einführung in die Kolloidik feinverteilter Stoffe einschließlich der Tonminerale*; Steinkopff: Heidelberg, 1997.

(53) Bullermann, J., Friebel, S., Salthammer, T., Spohnholz, R. Novel polyurethane dispersions based on renewable raw materials—Stability studies by variations of DMPA content and degree of neutralisation. *Progress in Organic Coatings* **2013**, *76*, 609–615.

(54) Kim, B. K., Lee, J. C. Waterborne polyurethanes and their properties. *Journal of Polymer Science Part A: Polymer Chemistry* **1996**, *34*, 1095–1104.

(55) Lijie, H., Yongtao, D., Zhiliang, Z., Zhongsheng, S., Zhihua, S. Synergistic effect of anionic and nonionic monomers on the synthesis of high solid content waterborne polyurethane. *Colloids and Surfaces A: Physicochemical and Engineering Aspects* **2015**, *467*, 46–56.

(56) Dukhin, S. S., Zimmermann, R., Werner, C. Electrophoresis of soft particles at high electrolyte concentrations: An interpretation by the Henry theory. *Journal of Colloid and Interface Science* **2007**, *313*, 676–679.

(57) Duval, J. F. L., Wilkinson, K. J., van Leeuwen, H. P., Buffle, J. Humic Substances Are Soft and Permeable: Evidence from Their Electrophoretic Mobilities †. *Environ. Sci. Technol.* **2005**, *39*, 6435–6445.

(58) Duval, J. F., Gaboriaud, F. Progress in electrohydrodynamics of soft microbial particle interphases. *Current Opinion in Colloid & Interface Science* **2010**, *15*, 184–195.

(59) Gaboriaud, F., Gee, M. L., Strugnell, R., Duval, J. F. L. Coupled electrostatic, hydrodynamic, and mechanical properties of bacterial interfaces in aqueous media. *Langmuir* **2008**, *24*, 10988–10995.

(60) Kerchove, A. J. de, Elimelech, M. Relevance of electrokinetic theory for "soft" particles to bacterial cells: implications for bacterial adhesion. *Langmuir* **2005**, *21*, 6462–6472.

(61) Sonohara, R., Muramatsu, N., Ohshima, H., Kondo, T. Difference in surface properties between Escherichia coli and Staphylococcus aureus as revealed by electrophoretic mobility measurements. *Biophysical Chemistry* **1995**, *55*, 273–277.

(62) Wolf, T., Grau, C., Rosengarten, J. F., Stitz, J., Wilkens, J., Barbe, S. Investigation of the Electrokinetic Properties of HIV-Based Virus-Like Particles. *Langmuir* **2024**, *40*, 4762–4771.

(63) López-León, T., Ortega-Vinuesa, J. L., Bastos-Gonzalez, D., Elaïssari, A. Cationic and anionic poly(N-isopropylacrylamide) based submicron gel particles: electrokinetic properties and colloidal stability. *The journal of physical chemistry. B* **2006**, *110*, 4629–4636.

(64) Daly, E., Saunders, B. R. Temperature–dependent electrophoretic mobility and hydrodynamic radius measurements of poly(N-isopropylacrylamide) microgel particles: structural insights. *Physical Chemistry Chemical Physics* **2000**, *2*, 3187–3193.

(65) Makino, K., Yamamoto, S., Fujimoto, K., Kawaguchi, H., Ohshima, H. Surface Structure of Latex Particles Covered with Temperature-Sensitive Hydrogel Layers. *Journal of Colloid and Interface Science* **1994**, *166*, 251–258.

(66) Ohshima, H. Limiting electrophoretic mobility of a highly charged soft particle in an electrolyte solution: Solidification effect. *Journal of Colloid and Interface Science* **2010**, *349*, 641–644.

(67) Kobayashi, M. Electrophoretic mobility of latex spheres in the presence of divalent ions: experiments and modeling. *Colloid & Polymer Science* **2008**, *286*, 935–940.

(68) Kobayashi, M., Nitanai, M., Satta, N., Adachi, Y. Coagulation and charging of latex particles in the presence of imogolite. *Colloids and Surfaces A: Physicochemical and Engineering Aspects* **2013**, *435*, 139–146.

(69) Kobayashi, M., Sasaki, A. Electrophoretic mobility of latex spheres in mixture solutions containing mono and divalent counter ions. *27th European Colloid and Interface Society conference (27th ECIS 2013)* **2014**, *440*, 74–78.

(70) Behrens, S. H., Christl, D. I., Emmerzael, R., Schurtenberger, P., Borkovec, M. Charging and Aggregation Properties of Carboxyl Latex Particles: Experiments versus DLVO Theory. *Langmuir* **2000**, *16*, 2566–2575.

(71) Antonietti, M., Vorwerg, L. Examination of the atypical electrophoretic mobility behavior of charged colloids in the low salt region using the O'Brian-White theory. *Colloid & Polymer Science* **1997**, *275*, 883–887.

(72) Peula-García, J. M., Hidalgo-Alvarez, R., las Nieves, F. J. de. Colloid stability and electrokinetic characterization of polymer colloids prepared by different methods. *27th European Colloid and Interface Society conference (27th ECIS 2013)* **1997**, *127*, 19–24.

(73) Tamai, H., Niino, K., Suzawa, T. Surface characterization of styrene/sodium styrenesulfonate copolymer latex particles. *Journal of Colloid and Interface Science* **1989**, *131*, 1–7.

For Table of Contents Only (Graphical Abstract)

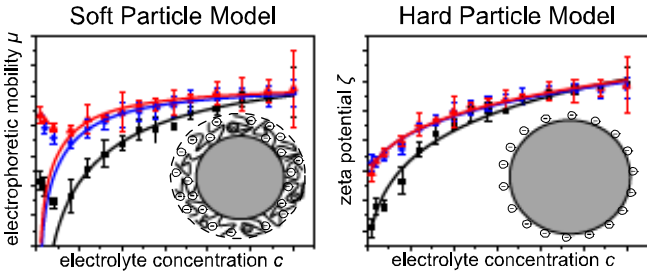

4.7 Supporting Information

Water-based Polyurethane Dispersions: A Detailed Analysis of the Particle Charge Using Soft and Hard Particle Model

C. Grau [a], A. M. Schmidt [b], J. Wilkens [a]*

[a] *Faculty of Applied Natural Sciences, TH Köln - University of Applied Science, Leverkusen D-51379, Germany*
[b] *Department of Chemistry, University of Cologne, D-50939 Cologne, Germany*
**Corresponding author, E-mail address: jan.wilkens@th-koeln.de*

Potentiometric Acid/Base Titration

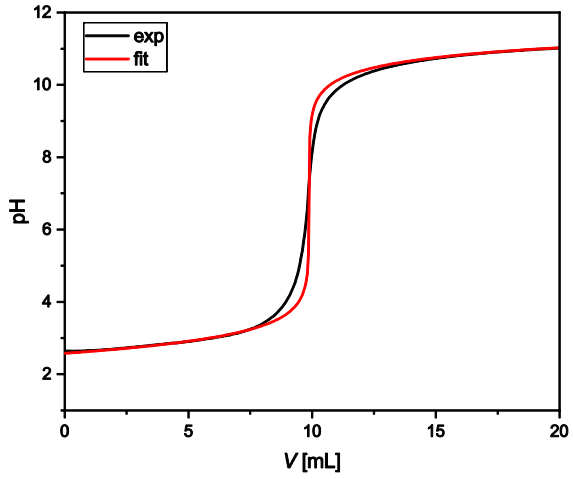

Figure S4-1: Experimental (black) and calculated (red) titration curve of the exemplary sample PE4.5 assuming a strongly acidic functional group.

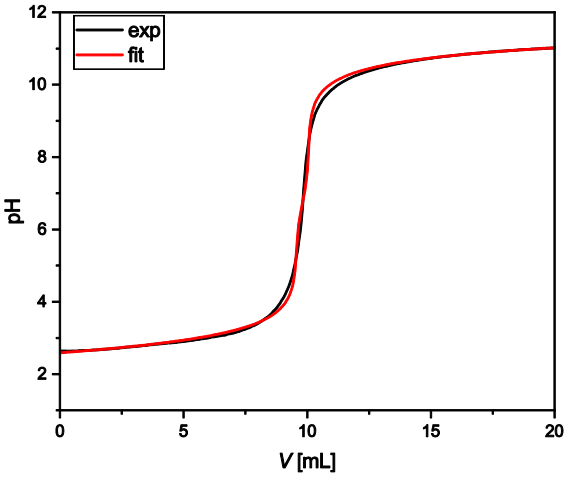

Figure S4-2: Experimental (black) and calculated (red) titration curve of the exemplary sample PE4.5 assuming a strongly acidic and a weak acidic group.

It is clearly shown that the experimental data cannot be modelled by assuming highly acidic functional groups alone (c.f. Figure S4-1). In contrast, it is necessary to take additional functional groups of lower acid strength into account (c.f. Figure S4-2). The inclusion of two or more weak acidic groups barely improved the residual sum of squares and was therefore not considered a significant improvement. The data in Table S1 are obtained by evaluation of two functional groups, one strong (index 0) and one weak acidic (index 1).

Table S1: Specific particle charges $Q_{\mathrm{tit},i}$ and recovery rates RR_i of each equivalence point *

Sample	$Q_{\mathrm{tit},0}$ [C/g]	$Q_{\mathrm{tit},1}$ [C/g]	Q_{tit} [C/g]	Q_{max} [C/g]	$Q_{\mathrm{tit},0}/Q_{\mathrm{ti}}$ [%]	$Q_{\mathrm{tit},1}/Q_{\mathrm{ti}}$ [%]	RR_0 [%]	RR_1 [%]	RR [%]
PTHF3.5	-12.3	-2.8	-15.1	-20.8	81.5	18.5	58.8	13.9	72.7
PTHF4.0	-14.8	-3.1	-17.9	-23.5	82.7	17.3	62.9	13.5	76.4
PTHF4.5	-18.1	-3.5	-21.6	-25.8	83.8	16.2	70.0	13.8	83.8
PTHF5.0	-20.9	-3.4	-24.3	-28.6	86	14	72.8	12.1	84.9

Sample	$Q_{tit,0}$ [C/g]	$Q_{tit,1}$ [C/g]	Q_{tit} [C/g]	Q_{max} [C/g]	$Q_{tit,0}/Q_{tit}$ [%]	$Q_{tit,1}/Q_{tit}$ [%]	RR_0 [%]	RR_1 [%]	RR [%]
PTHF5.5	-24.3	-3.6	-27.9	-33.0	87.1	12.9	73.8	11.0	84.8
PE3.0	-10.2	-2.5	-12.7	-17.2	80.3	19.7	59.4	14.5	73.9
PE3.5	-13.1	-3.3	-16.4	-19.9	79.9	20.1	65.6	16.7	82.3
PE4.0	-16.7	-2.6	-19.3	-22.7	86.5	13.5	73.4	11.4	84.8
PE4.5	-19.3	-2.5	-21.8	-25.7	88.5	11.5	74.9	10.0	84.9
PE5.0	-20.5	-2.7	-23.2	-28.3	88.4	11.6	72.2	9.8	82.0
PC3.5	-10.2	-2.9	-13.2	-20.1	77.9	22.1	50.9	14.5	65.4
PC4.0	-14.3	-2.7	-17.0	-23.0	84.1	15.9	62.0	12.1	74.1
PC4.5	-17.1	-3.3	-20.3	-25.8	83.8	16.2	66.4	12.5	78.9
PC5.0	-21.4	-3.2	-24.6	-28.8	87	13	74.3	11.4	85.7
PC5.5	-23.7	-3.3	-27.0	-31.5	87.8	12.2	75.2	10.4	85.6

* The equivalence points are indicated by the given indices $i = 0, 1$. The overall recovery rate RR is calculated as $RR = RR_0 + RR_1$

Electrophoretic Mobility and Zeta Potential

Complete data sets of the measured electrophoretic mobilities of each series are shown in Figure S4-3 - Figure S4-5.

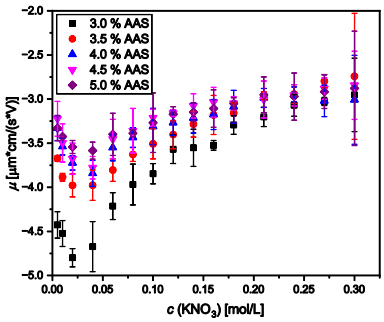

Figure S4-3: Electrophoretic mobility of PE based PUDs with different concentrations of AAS. Error bars correspond to the standard deviation.

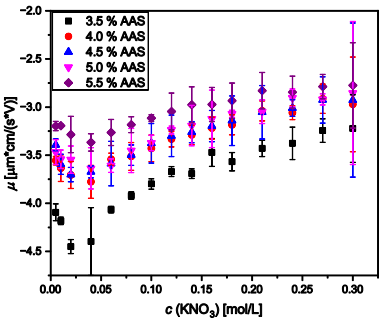

Figure S4-4 Electrophoretic mobility of PC based PUDs with different concentrations of AAS. Error bars correspond to the standard deviation.

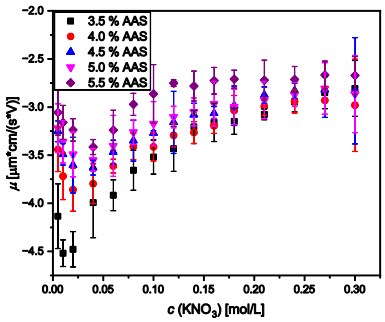

Figure S4-5: Electrophoretic mobility of PTHF based PUDs with different concentrations of AAS. Error bars correspond to the standard deviation.

Zeta potentials calculated thereof by considering the relaxation effect are shown in Figure S4-6 - Figure S4-8 and the model fit is based on a constant surface potential ψ_0 for all ionic strengths.

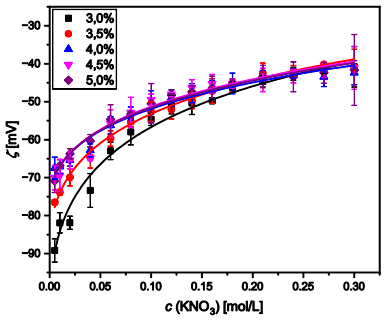

Figure S4-6: Zeta potential of PE based PUDs with different concentrations of AAS. Solid symbols symbolize the mean value with its error bars corresponding to the standard deviation. Solid lines represent the fit assuming a constant surface potential.

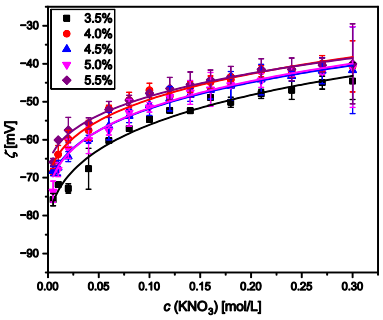

Figure S4-7: Zeta potential of PC based PUDs with different concentrations of AAS. Solid symbols symbolize the mean value with its error bars corresponding to the standard deviation. Solid lines represent the fit assuming a constant surface potential.

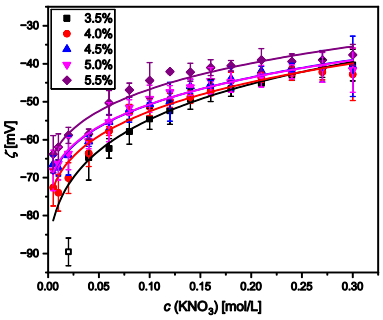

Figure S4-8: Zeta potential of PTHF based PUDs with different concentrations of AAS. Solid symbols symbolize the mean value with its error bars corresponding to the standard deviation. Empty symbols are not used for fitting procedure. Solid lines represent the fit.

5 Water-Based Polyurethane Dispersions: Analysis of the Dispersion Stability in Terms of DLVO and XDLVO Theories

C. Grau [a], A. M. Schmidt [b], J. Wilkens [a]*

[a] *Faculty of Applied Natural Sciences, TH Köln - University of Applied Science, Leverkusen D-51379, Germany*
[b] *Department of Chemistry, University of Cologne, D-50939 Cologne, Germany*
* *Corresponding author, E-mail address: jan.wilkens@th-koeln.de*

Remarks on the manuscript in relation to the thesis and declaration of individual contributions

This chapter has been published in *Langmuir* and is reprinted with permission from *Langmuir* 2025, 41 (25), 16263-16273. Numbering of the chapters, figures and formulas has been adjusted to the thesis format.

Article on Request: https://pubs.acs.org/articlesonrequest/AOR-NJAIJDB46CBNIIBKRCJ4

DOI: https://doi.org/10.1021/acs.langmuir.5c01517

Here, the detailed analysis of the dispersion stability of PUDs stabilized by AAS is presented. The experimentally observed dispersion stabilities are further analysed by using DLVO as well as XDLVO approaches. Based on the previously determined surface potentials it was possible to calculate the repulsive interaction energies. Additionally, it was possible to further assess the attractive interaction energies in terms of the Hamaker constant following DLVO as well as the XDLVO approaches. A comparison of both led to the conclusion, that the XDLVO approach based on contact angle data led to more realistic values for the Hamaker constant. Further analysis according to the stated XDLVO theory revealed a major influence on the dispersion stability by an additional attractive interaction parameter based on hydrophobic forces. Thus it was possible to explain the influence of the polyol component as well as the functional surface groups on the dispersion stability and its underlying interaction contributions. For this reason, this publication is fundamental for this thesis, as it provides a detailed discussion of dispersion stability of PUD particles stabilized by AAS.

The analytical experiments were done under my supervision and responsibility. The PUD series characterised in this study were similar to chapter 4. PE-X was partly synthesized by *Simon Schösser* and the PUD series PC-X was partly synthesized by *Christoph Pumplün* under my supervision in the context of their bachelor thesis. The dispersion stability of the synthesis series PE-X was also done by *Simon Schösser*. Further analytical experiments were done by myself. The analysis and interpretation of the results were done by myself and *Prof. Dr. Jan Wilkens*. The manuscript was prepared by myself, following extensive corrections from *Prof. Dr. Jan Wilkens* and *Prof. Dr. Annette M. Schmidt*.

Abstract

Although water-based polyurethane dispersions (PUDs) are predominantly stabilized through the incorporation of ionic groups, a comprehensive investigation of the dispersion stability of PUDs is still pending. For this reason, the structure−stability relationship of a series of PUDs with different soft segments (polyether, polyester, and polycarbonate polyols) and variable contents of sulfonate groups is examined in detail.

The dispersion stability was characterized by time-resolved photometric determination of the critical coagulation concentration (ccc) and analyzed in terms of DLVO and XDLVO theories. Hamaker constants were determined based on contact angle data of PUD films with an apolar test liquid using the van Oss−Chaudhury−Good theory.

As expected, it was found that the ccc increases with increasing 2-((2-aminoethyl)amino)ethanesulfonate (AAS) content. Moreover, the results indicate a strong influence of the nature of the polyol component on dispersion stability. The polycarbonate-based PUDs have the highest electrolyte stability, followed by polyester- and polyether-based PUDs. The apparent Hamaker constants A_{131}^{app} calculated according to the DLVO theory show nonconstant and unexpected high values for water-based polymer dispersions. Therefore, the observed dispersion stabilities cannot be adequately described by electrostatic and van der Waals interaction energies alone, so additional attractive interaction forces are likely to occur. On the other hand, Hamaker constants A_{131}^{vOCG} determined from contact angle data are found to be in the range of $0.6 \cdot 10^{-20}$ J for all samples, which is in good agreement with typical values for water-based polymer dispersions. Using this Hamaker constant and extending the DLVO theory with an additional, exponentially decaying interaction term, the observed dispersion stabilities can be explained very well. This additional interaction is attractive, as the negative sign of the pre-exponential factor shows, and is presumably hydrophobic in nature. The magnitude of this factor also reveals clear differences between the different polyol components and the AAS contents of the PUDs.

Keywords

Water-based polyurethane dispersions, dispersion stability, critical coagulation concentration, Hamaker constant, hydrophobic interactions, DLVO, XDLVO

5.1 Introduction

Polyurethanes, as one of the most versatile and widely used classes of polymer materials, are nowadays frequently processed as water-based polyurethane dispersions (PUDs) due to their environmental benefits. The dispersion stability plays a crucial role, not only within the production process but also for their shelf life, storability, and final application. To obtain stable PUDs, they are often electrostatically stabilized by the incorporation of ionic groups in order to prevent particle aggregation.

Polyurethanes are obtained from the polyaddition reaction of one or more polyol components with bi- or higher-functional isocyanates, forming characteristic urethane linkages in the main chain. The choice of the polyol component is well known to determine important product properties, such as softness, glass transition temperature, and hydrophobicity. Thus, they play a significant role in polyurethane chemistry. Frequently used polyols are polyester,[1] polyether, and polycarbonates,[2–4] which all have different functional groups leading to different properties in the final product. The molar mass can vary between 50 g mol^{-1} (short chain polyol) and 4000 g mol^{-1} (long chain polyol). On the one hand, the incorporation of short-chain diols leads to higher fraction of urethane linkages, which are often referred to as hard segments. As a result, the capability of creating hydrogen bonds or dipole interactions increases, leading to enhanced stiffness of the polymer network. On the other hand, the use of long-chain polyols leads to more flexibility within the structure.

Several industrially relevant processes for the production of PUDs.[5] In addition to the prepolymer mixing process, the acetone process is frequently used.[6–8] First step is the reaction of polyol and diisocyanate components to build a low-molecular-weight prepolymer. The prepolymer is then dissolved in acetone, which is commonly used as a solvent within polyurethane chemistry because it can be easily removed. Afterward, the chain extension is performed in solution. For this purpose, typically, diamines are used to build up a high-molecular-weight polyurethane.[9] Secondary dispersion takes place with the addition of water to the polymer solution under vigorous stirring.[10–12] Acetone is finally removed by distillation to yield the water-based dispersion.

Since the polyurethane as a whole is normally of hydrophobic nature, it has to be stabilized. This can be achieved by the incorporation of cationic, anionic, or non-ionic groups.[13–15] In case of anionically stabilized dispersions, the most referred agents are dimethylolpropionic or dimethylolbutanoic acid, which are typically incorporated within the prepolymerization step.[8,14,16,17] However, the dissociation behavior of carboxyl groups and thus the dispersion stability are directly related to the pH value. As an alternative, diamino alkanesulfonates, such as 2-[(2- aminoethyl)amino]ethanesulfonic acid (AAS), can also be used and are usually incorporated within the chain extension step.[8,18]

The renowned DLVO theory describes the nature of dispersion stability on the basis of repulsive electrostatic and attractive van der Waals forces.[19–21] If the repulsive force is much stronger than the attractive force, a distinct energy barrier results at a certain distance, preventing coagulation of two approaching particles. The magnitude of this energy barrier can be decreased by addition of electrolytes, since the extension of the electrical double layer (EDL) is compressed and the electrostatic repulsion is weakened. The concentration at which the energy barrier just vanishes is known as the critical coagulation concentration (ccc) or the critical coagulation ionic strength (ccis) and provides valuable insights into the stabilization conditions.

The DLVO theory has been successfully used to assess the interaction potentials for various systems, including micelles,[22] proteins,[23–25] inorganic systems,[26–29] as well as different types of polymer dispersions.[30–32] Recently, Zeng and Kobayashi studied the influence of ciprofloxacin on the aggregation behavior of Na-montmorillonite. Although they found that the measured ccis values could be adequately described by the DLVO theory, they also pointed out that differences in the determined Hamaker constants may be attributed to additional hydrophobic attraction by the adsorbed ciprofloxacin molecules.[29] Therefore, it is important to note that the classical DLVO theory does not take into account other interactions, such as hydrophilic repulsion or hydrophobic attraction forces.[33] However, these effects can play an important role in dispersion stability, especially for water-based systems. In such cases, extended versions of the DLVO theory, usually termed XDLVO theories, should be used to account for these additional interactions.

To the best of our knowledge, an in-depth analysis of the dispersion stability of PUDs based on DLVO or XLDVO approaches is still pending. However, recent studies have shown that a minimum amount of anionic groups in a quite wide range between 2.5 and 5.0 wt % DMPA is required to obtain stable dispersions.[17,34–36] These findings already indicate that the PU dispersion stability is rather complex and is not simply dependent on the content of ionic groups. Kim and Lee performed a detailed analysis of several reaction compounds and parameters They used DMPA as a stabilizing agent for all of their samples. Among others, they investigated the influence of DMPA content and different polyester polyol components on the dispersion stability and described it in terms of particle size. They found that the particle size decreased with an increasing DMPA content from roughly 300 nm (2.5 wt %) to 84 nm (4.0 wt %). They attributed this decrease to an increase in electrostatic repulsion. They also found differences in the particle size between the polyol components and explained them by different amounts of water swellability.[34] Nevertheless, the characteristics of dispersion stability were only described in terms of particle size, and they do not show a detailed analysis of the corresponding repulsive and attractive forces.

Mohanty and Krishnamurti determined the critical coagulation concentration of cationically stabilized polyurethane dispersions with different amounts of N-methyldiethanolamine (N-MDEA). They found increasing ccc values with an increasing amount of N-MDEA but did not analyze the contribution of repulsive and attractive forces of the system.[37]

Tielemans et al. carried out calculations on the dispersion stability of radiation-curable polyurethane dispersions. They determined the ccc and found nearly similar values for different amounts of DMPA.

Based on these values, they calculated the repulsive and attractive forces to describe the observed electrolyte stability. Nevertheless, they determined the surface potential by making rough assumptions about the Hamaker constant in the range of $1 \cdot 10^{-19}$ to $1 \cdot 10^{-22}$ J and already pointed out that independently determined values of both variables are required to describe the observed electrolyte stability.[31]

In a recent study, we performed a comprehensive analysis of the particle charge and potentials of water-based polyurethane dispersions.[38] One of the key factors examined was the effective surface potential and the distance of the shear plane, which were determined by using the dependency of electrokinetic measurements on the electrolyte concentration. For this purpose, zeta potentials were calculated by taking the relaxation effect into account. Our detailed analysis indicates that the surface potential can be assumed to be constant at different ionic strengths. These findings can therefore serve as a solid basis for the description of repulsive electrostatic interaction forces in the analysis of the dispersion stability.

In this study, we investigate the structure−stability relationship of PUDs on the basis of DLVO and non-DLVO interactions. For this purpose, several PUDs were synthesized using the acetone process. The quantity of particle charges was controlled by varying the amount of sulfonate groups via different AAS contents. In order to assess the potential influence of modifications in the hydrophobicity of the PUD particles, different types of polyol components were studied employing polyether, polyester, and polycarbonate polyols of similar molecular weight. The critical coagulation concentration was determined by time-resolved photometric measurements of the absorbance[39] In order to interpret the dispersion stability, calculations were performed according to the classical DLVO theory. Additionally, the Hamaker constant was determined by means of contact angle measurements of PUD films with an apolar test liquid using the van Oss−Chaudhury−Good (vOCG) theory.[40] The plausibility of these data was subsequently checked with calculations based on the XDLVO theory in order to obtain information about the influence of hydrophobicity on dispersion stability

5.2 Theory

Dispersion stability is commonly described by means of DLVO theory.[19,20] When two particles approach each other, they experience repulsive and attractive interaction forces. In order to take the influence of particle shape into account, different approaches can be used to describe the interaction energies between spherical,[27,41] plate like,[33] cylindrical,[42,43] or rod-like[23] particles. As it has been established in various studies and confirmed by TEM images, water-based polyurethane dispersions generally have a spherical particle shape.[44–49] Accordingly, this study makes use of expressions that are valid for spherical particles.

In the DLVO theory, the repulsion of the particles is solely governed by electrostatic interaction forces, i.e., the aggregation of the particles is prevented due to the same nature of the particle charges. Sader et al. derived an analytical expression (eq. 5-1) for the repulsive double layer interaction free energy V_R as a function of the separation distance H for the case of two identical spherical particles with constant surface potential Ψ_0, with the relative permittivity ε_r, permittivity in vacuum ε_0, molar gas constant R, thermodynamic temperature T, Faraday constant F and the particle radius a. It is valid for large κa, all κH and moderate-to-high surface potentials ($y_0 \leq 4$).[50]

$$V_\mathrm{R}(H) = 4\pi\varepsilon_\mathrm{r}\varepsilon_0\left(\frac{RT}{F}\right)^2 \Upsilon^2 \frac{a^2}{2a+H}\ln\left(1+\exp(-\kappa H)\right) \tag{5-1}$$

The function $\Upsilon(H)$ is given by equation 5-2 and includes the reduced surface potential y_0 (eq. 5-3), where z is the valence of the ion species and Ψ_0 the surface potential.

$$\Upsilon(H) = 4 \cdot \exp\left(\frac{\kappa H}{2}\right)\tanh^{-1}\left(\exp\left(-\frac{\kappa H}{2}\right)\cdot\tanh\left(\frac{y_0}{4}\right)\right) \tag{5-2}$$

$$y_0 = \frac{zF\Psi_0}{RT} \tag{5-3}$$

According to equations 5-1-5-3, the repulsive double layer interaction energy depends particularly on the surface potential, the Debye-Hückel parameter κ and thus the ionic strength. The Debye-Hückel parameter κ is described by equation 5-4, with the electrolyte concentration c_i and the valence z_i for the i-th ion species.

$$\kappa = \sqrt{\frac{F^2}{\varepsilon_\mathrm{r}\varepsilon_0 RT}\sum_\mathrm{i} z_\mathrm{i}^2 c_\mathrm{i}} \tag{5-4}$$

Attractive interaction energies are based on dipole-dipole, dipole-dipole induced and dispersion forces and are commonly summed up as van der Waals forces. Hamaker derived an analytical expression (eq. 5-5) for two spherical particles.[21] Here, the influence of the dispersed material (index 1) and the dispersant (index 3) is characterised by the Hamaker constant A_{131}.

$$V_\mathrm{A}(H) = -\frac{A_{131}}{6}\left(\frac{2a^2}{(2a+H)^2-4a^2} + \frac{2a^2}{(2a+H)^2} + \ln\left(1-\frac{4a^2}{(2a+H)^2}\right)\right) \tag{5-5}$$

The total interaction free energy V_T (eq. 5-6) is then given by the sum of the repulsive and attractive interaction energies.

$$V_\mathrm{T} = V_\mathrm{R} + V_\mathrm{A} \tag{5-6}$$

However, it should be emphasized that the DLVO theory only considers electrostatic and van der Waals interaction forces between two particles and experimental results cannot always be satisfactorily described with this approach.[51] The relevance of other interaction forces has been demonstrated in several studies using AFM force−distance measurements.[52–54] Therefore, recent studies aimed to extend the DLVO theory (so called XDLVO theory) by introducing an additional interaction parameter V_h.[33,51,55–57]

$$V_\mathrm{T} = V_\mathrm{R} + V_\mathrm{A} + V_\mathrm{h} \tag{5-7}$$

These interaction forces can be attributed to either hydrophilic repulsion or hydrophobic attraction and arise from the specific structural arrangement of water molecules at the particle interface. Hydrophilic surfaces have highly ordered hydration layers with many hydrogen bonds, which results in a repulsive force when two interfaces interact with each other. On the other hand, hydrophobic surfaces lead to a specific orientation of the water molecules in the near vicinity, which reduces the conformational entropy and results in fewer hydrogen bonds. When two hydrophobic surfaces interact with each other, dewetting or hydrophobic attraction occurs.[55] Nevertheless, a comprehensive theory to address these effects has not been developed yet. For instance, Israelachvili and Pashley suggested an expression involving an exponential dependence on the distance *H*. The pre-exponential factor *C* characterizes the strength of the hydrophilic or hydrophobic interaction.[56] Equation 5-8 has also been used by several other authors.[56–58]

$$V_\mathrm{h}(H) = aC \cdot \exp\left(-\frac{H}{\lambda}\right) \tag{5-8}$$

The range of these interaction forces is governed by the characteristic decay length λ. It is noteworthy that the span of experimentally determined values for the decay length is quite broad, and values between 0.3 nm to several nm have been reported.[51,53,54,59]

Stable dispersions are obtained if the repulsive interaction forces are sufficiently stronger than the attractive interaction forces. Repulsive electrostatic interaction forces can be relatively long-range depending on the electrolyte content of the dispersant. In comparison, the attractive van der Waals interaction forces are often larger and rather short-range; therefore, they are particularly effective at

small separation distances *H*. This may lead to the formation of a characteristic energy barrier at a certain separation distance, which prevents particle aggregation. In case of electrostatically stabilized dispersions, coagulation can be induced by increasing the electrolyte concentration of the system. This becomes evident as equation 5-1 depends on the Debye-Hückel parameter κ and thus on the ionic strength. By increasing the ionic strength, the repulsive interaction force decreases due to the compression of the diffuse electrical double layer. As a result, the energy barrier also decreases. The electrolyte concentration at which the energy barrier just vanishes is called the critical coagulation concentration (ccc).

If the surface potential and thus the repulsive electrostatic interaction energy is known, the corresponding attractive interaction energy can be calculated taking the ccc into account. For this particular electrolyte concentration, the equations $V_\mathrm{T} = 0$ and $\mathrm{d}V_\mathrm{T}/\mathrm{d}H = 0$ can be simultaneously solved using equations 5-1-5-6. This allows two parameters to be determined, the Hamaker constant A_{131} and necessarily the distance of the energy maximum to the particle surface. When applying this approach, it must be kept in mind that all forms of interaction that are not electrostatic in nature are treated as van der Waals forces and are finally summed up in the Hamaker constant. In this work, we take this into account by referring to the according result as the apparent Hamaker constant A_{131}^{app}.

As an alternative way to determine the Hamaker constant, an empirical formula derived by van Oss, Chaudhury and Good can be used (A_{131}^{vOCG}, eq. 5-9). It is based on the contact angle determination of a film with an apolar test liquid. In the evaluation, the apolar surface tension component of the material $\gamma_\mathrm{S}^{\mathrm{LW}}$ is used. Equation 5-9 is valid under the condition that H is less than 10 nm in order to provide unretarded London-van der Waals interactions. The authors pointed out that the accuracy of the proportionality constant $1.8585 \cdot 10^{-21}$ is about ± 8 %.[33,40]

$$A_{131}^{\mathrm{vOCG}} = \left(\sqrt{1.8585 \cdot 10^{-21} \cdot \gamma_\mathrm{S}^{\mathrm{LW}}} - \sqrt{3.7 \cdot 10^{-20}}\right)^2 \tag{5-9}$$

The apolar surface tension component of the material is related to the contact angle θ of an apolar liquid (index *L*) by the Good-Girifalco-Fowkes equation 5-10. For this kind of test liquid, the total surface tension of the liquid γ_L is caused by apolar interactions only, i.e. $\gamma_\mathrm{L} = \gamma_\mathrm{L}^{\mathrm{LW}}$.[60–62]

$$1 + \cos\theta = 2\sqrt{\frac{\gamma_\mathrm{S}^{\mathrm{LW}}}{\gamma_\mathrm{L}^{\mathrm{LW}}}} \tag{5-10}$$

Based on the Hamaker constant A_{131}^{vOCG} and assuming a reasonable value for the decay constant λ, equations 5-1-5-5 and 5-7-5-8 can be used to estimate the pre-exponential factor C by solving the conditions $V_\mathrm{T} = 0$ and $\mathrm{d}V_\mathrm{T}/\mathrm{d}H = 0$ again.

5.3 Experimental

5.3.1 Materials

Polycarbonate (Desmophen C2102, $M_n \sim 1000$ g mol^{-1}, PC) and polyester diols (Desmophen PE90B, $M_n \sim 1000$ g mol^{-1}, PE) and a solution of 2-((2-aminoethyl)amino)ethanesulfonate (AAS) were kindly supplied by Covestro AG. Poly(tetrahydrofuran)diol ($M_n \sim 1000$ g mol^{-1}, PTHF), isophorone diisocyanate (IPDI), butanediol (BDO), triethylamine (TEA), isophorone diamine (IPDA), dibutyltin dilaurate (DBTL) were purchased from Merck KGaA. Acetone, sodium chloride (NaCl), potassium nitrate (KNO_3), magnesium nitrate ($Mg(NO_3)_2$) and diiodomethane were purchased from Fisher Scientific. Ultrapure water (Millipore) was used for every sample preparation.

5.3.2 Synthesis of PUDs

Several series of PUDs containing different polyol components and varying AAS mass fractions were synthesized according to the acetone process, which is illustrated in Figure 5-1. A detailed description of the synthesis routine and a table containing the monomer masses used can be found in a previous study.[38] The dehydrated polyol component (R_1) and BDO (R_2) were fed into a four-necked round-bottom flask, equipped with a mechanical stirrer and condenser under nitrogen atmosphere. Once the reaction mixture reached 70 °C, DBTL was added and homogenised. IPDI (R_3) was added dropwise using a dropping funnel. After complete addition, the temperature was raised to 100 °C and reaction was carried out until the theoretical NCO content was reached. The reaction mixture (prepolymer R_4) was cooled to 80 °C and dissolved by addition of acetone. The solution was cooled to 40 °C and an aqueous solution of IPDA (R_5) and AAS was added for chain extension. Once the reaction was completed, water was added using a syringe pump. Acetone was finally removed by distillation to yield a water-based dispersion.

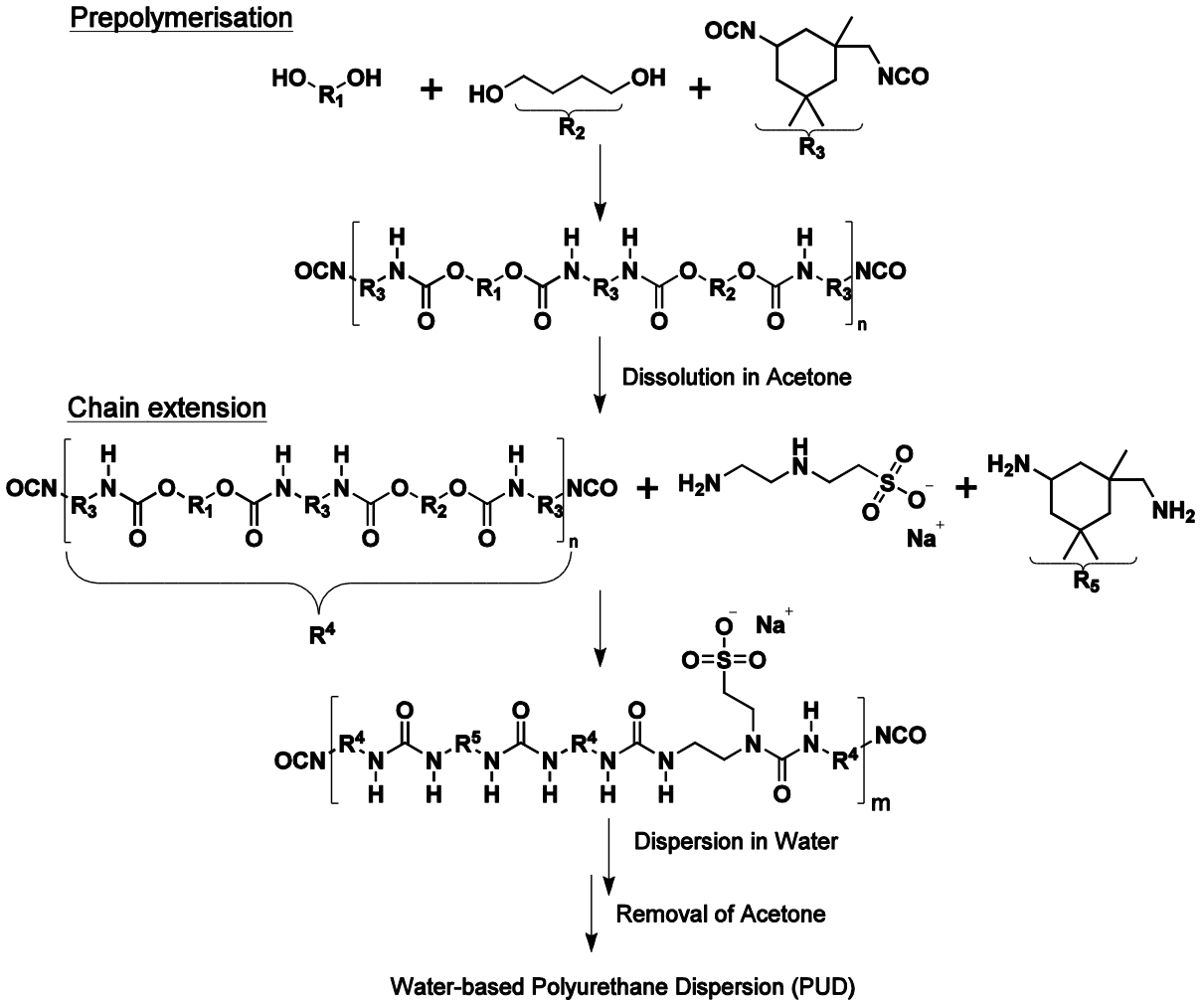

Figure 5-1: Illustration of the synthesis scheme of water-based PUDs according to the acetone process. Prepolymerisation of the polyol component (R_1) and butanediol (R_2) with an excess of IPDI (R_3) leads to an NCO terminated prepolymer (R_4), which is followed by dissolution in acetone and chain extension with diamine components (R_5 and AAS). Secondary dispersion is achieved by addition of water. Finally, the acetone is removed by vacuum distillation.

5.3.3 Particle size distribution and electrophoretic mobility

Particle size distribution and electrophoretic mobility of each sample were determined at 25 °C with a Zetasizer Nano ZS from Malvern using a 632.8 nm He-Laser. Particle size was determined with a concentration of 0.0001 wt % and its signal was detected at 173° backscatter detection. Electrophoretic mobility was measured at 0.1 wt % as a function of ionic strength (KNO3) using folded capillary cells DTS 1070 detecting the signal at 17° front scatter detection. Multiple measurements were performed for each determination purpose. A detailed description of the measurement parameter and the data evaluation can be found in a previous study.[38]

5.3.4 Critical coagulation concentration

Following the procedure of Reerink and Overbeek,[39] the critical coagulation concentration was determined photometrically with a UV/vis spectrophotometer Evolution 220 (Thermo Scientific) using a wavelength of 500 nm. Absorbance A was measured for 30 s at 0.1 s intervals in PMMA cuvettes. Blank measurements were done with ultrapure water. Each sample was measured at 0.075 wt % and sodium chloride (NaCl) was used as an electrolyte in a concentration range of 0.5 mol L−1−4.5 mol L^{-1} in the final dispersion. Sample and electrolyte solutions were mixed immediately before starting the measurement. The measurement at different electrolyte concentrations finally led to a set of curves for each sample The initial slope $\mathrm{d}A/\mathrm{d}t$ of each curve was determined and the logarithmic reciprocal $\log(\mathrm{d}t/\mathrm{d}A)$ was plotted against $\log(c)$. The values obtained decrease with increasing electrolyte concentration in the slow coagulation regime, while they remain constant in the fast coagulation regime. The intercept of the two sections gives the critical coagulation concentration. An example of the described evaluation can be found in the supporting information.

5.3.5 Contact angle measurements

Static contact angles were measured using the Contact Angle System OCA (Dataphysics) in accordance to DIN 55660-2.[63] Diiodomethane (γ_L: 50.8 mN m^{-1}, γ_L^{AB}: 0 mN m^{-1}, γ_L^{LW}: 50.8 mN m^{-1}) was used as test liquid.[51] At least six contact angles were measured 15 s after dispensing the droplet with a volume of 3 µL on different positions of the polyurethane film. The contact angles were evaluated using Young-Laplace equation.

Polyurethane films were prepared on glass substrate with a wet film thickness of 200 µm, dried at 80°C and stored at a constant relative humidity of approximately 50 % over a saturated $Mg(NO_3)_2$ solution at room temperature for at least 16 h prior to measurement.

5.4 Results and Discussion

This study aims to identify the role of the chemical composition of polyurethanes in the dispersion stability in the case of electrostatically stabilized water-based PUDs. For this purpose, PUDs based on polyurethanes with three different polyol components, a variation of AAS mass fractions, and otherwise analogous composition were synthesized. The AAS content was varied between 3.0 and 5.5 wt %. Lower AAS fractions resulted in unstable dispersions To examine the influence of the polyol component, we employed polyether, polyester, and polycarbonate polyols with similar molar mass. The remaining synthesis parameters were kept constant, including NCO/OH ratio of 1.7 for the prepolymer, degree of chain extension of 92 %, solid content of about 30 wt%, and a hard segment content of approximately 54 %.[38] To ensure a constant degree of chain extension while adjusting the AAS amount, AAS was balanced with the appropriate quantity of IPDA.

5.4.1 Dispersion stability

Coagulation of electrostatically stabilized dispersions can be induced by increasing the electrolyte concentration of the system. We have monitored this process using time-resolved absorbance measurements at various ionic strengths. The determined ccc values are shown in Table 5-1 and Figure 5-2 for all samples. It is evident that an increase in AAS content leads to an enhancement in dispersion stability with a similar trend for all polyol series. For PTHF-based PUDs, the ccc increases from 1.1 M (3.5 wt% AAS) to 1.6 M at (5.5 wt% AAS), while the PE-based PUDs show rising values from 1.5 M (3.0 wt% AAS) to 1.9 M (5.0 wt-% AAS). Interestingly, the observed dispersion stability of the PC-based PUDs increases from 3.7 M (3.5 wt% AAS) up to 4.3 M (5.5 wt% AAS), far exceeding that of PTHF and PE diols.

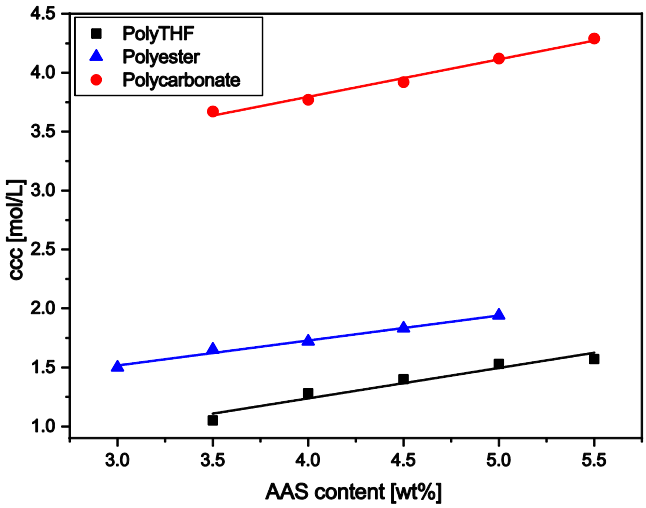

Figure 5-2: Critical coagulation concentration ccc as a function of the AAS content for PTHF (black), PE (blue) and PC (red) based PUDs. Solid lines are a guide to the eye.

The results indicate two major factors influencing the observed dispersion stability. First, the AAS content, which leads to a rather moderate enhancement of stability. Second, the influence of the polyol component clearly surpasses that of the AAS content. These findings highlight the complex interplay between the AAS content and the type of polyol component on the interparticle forces within the dispersions. To gain deeper insights into the causes of the observed differences, it is important to investigate the contributions of the repulsive and attractive interaction forces more closely

5.4.2 Determination of interaction forces according to DLVO theory

For a better understanding of the dispersion stability, the repulsive electrostatic interaction energy V_R of two particles approaching each other must be determined. V_R is particularly governed by the particle charge, as well as the particle size of the colloid. To describe this relationship, various expressions have been derived using different approaches. On the one hand, they are based on the assumption that the surface charge density remains constant as the EDLs overlap. The alternative limiting case, on the other hand, assumes a constant surface potential. Both approaches have proven to be successful in the past for describing experimentally determined dispersion stabilities.[27–29,64–67]

We have recently published detailed results on the investigation of the particle charge of the PUDs used in this study.[38] Among others, we determined the dependence of the zeta potential on the electrolyte concentration. The measured values could be described very well by a least-squares fit assuming a constant surface potential and gave reasonable values for the distance of the shear plane (approximately

0.3 nm). Based on these findings, we therefore follow the constant surface potential approach for calculating the electrostatic interaction potential in this study (cf. equations 5-1 to 5-4).

The results for the effective surface potential Ψ_0 and the particle radius a are summarized in Table 5-1. It can be seen that as the AAS content increases, both the particle size and the effective surface potential decrease. This trend is attributed to the enhanced number of charges within the system, enabling the stabilization of a larger interfacial area.[14,34] Consequently, this leads to a decrease in particle size and surface potential. It is also remarkable that the polyol component has only a minor impact on either of these values when comparing PUDs with the same content of AAS. It turns out that the particle sizes of polycarbonate-based PUDs are slightly larger than those of PE- and PolyTHF-based PUDs. However, these differences disappear almost completely at high AAS concentrations.

Table 5-1: Characteristic parameters for all PTHF, PE and PC based PUDs *

AAS content [wt%]	PTHF based PUD					PE based PUD					PC based PUD				
	a [nm]	Ψ_0 [mV]	ccc [M]	θ [°]	γ_S^{LW} [mN/m]	a [nm]	Ψ_0 [mV]	ccc [M]	θ [°]	γ_S^{LW} [mN/m]	a [nm]	Ψ_0 [mV]	ccc [M]	θ [°]	γ_S^{LW} [mN/m]
3.0	/	/	/	/	/	55.2	-106.5	1.5	48.0 ± 0.5	35.4	/	/	/	/	/
3.5	32.9	-94.2	1.1	34.0 ± 0.1	42.5	33.3	-89.2	1.6	49.3 ± 0.3	34.7	56.9	-84.9	3.7	43.7 ± 0.5	37.7
4.0	26.7	-81.5	1.3	35.7 ± 0.5	41.7	28.2	-77.0	1.7	49.0 ± 0.8	34.8	37.5	-75.4	3.8	42.1 ± 0.3	38.6
4.5	25.4	-76.8	1.4	35.7 ± 1.6	41.7	24.2	-77.8	1.8	48.3 ± 0.6	35.2	29.5	-76.6	3.9	42.9 ± 0.4	38.1
5.0	21.9	-76.5	1.5	38.6 ± 0.2	40.3	24.4	-77.5	1.9	48.8 ± 0.2	34.9	26.7	-77.4	4.1	45.3 ± 0.2	36.8
5.5	19.7	-72.1	1.6	35.2 ± 1.1	41.9	/	/	/	/	/	23.6	-69.3	4.3	47.9 ± 0.6	35.4

* Particle radius a, effective surface potential Ψ_0, critical coagulation concentration ccc, contact angle θ for diiodmethane and the apolar surface tension component of the material γ_S^{LW} calculated on the basis of the Good-Girifalco-Fowkes equation 5-10. No PUD was synthesized in the case of empty data records.

Utilizing this dataset, the repulsive electrostatic interaction energy V_R can be computed as a function of the separation distance H according to equations 5-1 to 5-4. Knowledge of this energy and the ccc value serves as the basis for calculating the attractive interaction energy V_A (cf. eq 5-5) within the framework of DLVO theory (cf. eq 5-6), in particular the apparent Hamaker constant A_{131}^{app}, as explained in the theoretical section. These results are shown in Table 5-2 and Figure 5-3 (exemplary interaction energy curves according to the DLVO theory are given in the Supporting Information). Obviously, the apparent Hamaker constants exhibit substantial differences between the polyol components, and most values are remarkably high for water-based polymer dispersions. This is particularly evident for PTHF- and PE-based PUDs, which display values between with $2.0 \cdot 10^{-20}$ and $3.5 \cdot 10^{-20}$ J for both series. Typical values for aqueous polymer dispersions are in the range of $0.3 \cdot 10^{-20}$ to $1.4 \cdot 10^{-20}$ J.[68–71] In this

regard, only the PC-based PUDs can be considered as reasonable at first glance, since their determined values lie between $1.1 \cdot 10^{-20}$ and $1.5 \cdot 10^{-20}$ J.

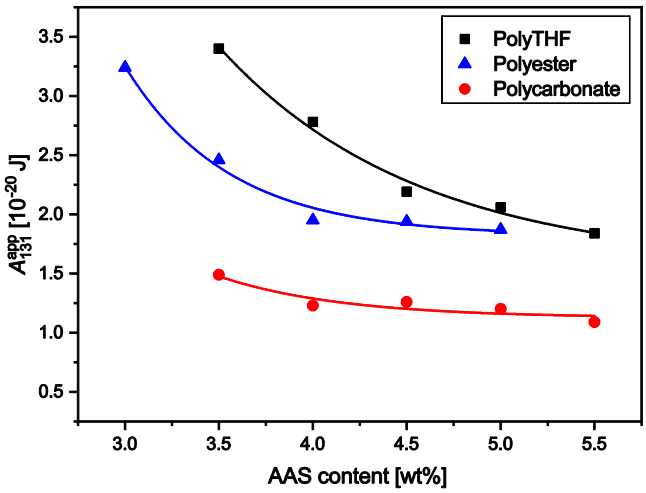

Figure 5-3: Apparent Hamaker constant A_{131}^{app} as a function of the AAS content for PTHF (black), PE (blue) and PC (red) based PUDs. Values are calculated according to DLVO theory. Solid lines are a guide to the eye.

Moreover, the absence of constant values for different AAS contents within each series is an unexpected outcome, especially considering the largely unchanged polymer composition of the PUD series. Modifications were exclusively confined to the variation of the AAS content and its corresponding substitution by an appropriate quantity of IPDA. Therefore, only the amount of charged groups changed, whereas other characteristic parameters like the hard segment content and the degree of chain extension are kept approximately constant. Consequently, it is reasonable to anticipate only marginal variations in the Hamaker constant within a specific polyol series. In view of these observations, it is reasonable to assume that the attractive interactions in the PUDs studied are not solely due to van der Waals forces but are most likely influenced by other attractive interaction forces.

Table 5-2: Hamaker constants and hydrophobicity for all PTHF, PE and PC based PUDs *

AAS content [wt%]	PTHF based PUD			PE based PUD			PC based PUD		
	A_{131}^{app} [10^{-20} J]	A_{131}^{vOCG} [10^{-20} J]	C [10^{-12} N]	A_{131}^{app} [10^{-20} J]	A_{131}^{vOCG} [10^{-20} J]	C [10^{-12} N]	A_{131}^{app} [10^{-20} J]	A_{131}^{vOCG} [10^{-20} J]	C [10^{-12} N]
3.0	/	/	/	3.21	0.41	-21.0	/	/	/
3.5	3.37	0.79	-19.3	2.46	0.38	-14.1	1.48	0.52	-8.4
4.0	2.50	0.74	-13.2	1.95	0.39	-9.9	1.24	0.57	-5.8
4.5	2.18	0.74	-11.1	1.94	0.40	-9.9	1.25	0.54	-5.9
5.0	2.09	0.66	-10.5	1.87	0.39	-9.5	1.25	0.48	-5.9
5.5	1.90	0.75	-9.0	/	/	/	1.03	0.41	-3.8

* The apparent Hamaker constant A_{131}^{app} is calculated using the DLVO theory. The Hamaker constant A_{131}^{vOCG} is based on contact angle data and evaluated according to the van Oss-Chaudhury-Good theory. The pre-exponential factor C as a measure of hydrophobicity is determined using XDLVO calculations.

Since A_{131}^{app} is obtained by solving the system of equations $V_{\mathrm{T}} = 0$ and $\mathrm{d}V_{\mathrm{T}}/\mathrm{d}H = 0$, essentially taking into account the electrostatic repulsive forces and the ccc, it sums up all forms of interaction that are not electrostatic in nature. Therefore, it is worth considering an alternative approach to determine the Hamaker constant based on an independent measurement technique. This can be achieved by measuring the contact angle θ of an apolar test liquid, which is related to the apolar surface tension component of the material $\gamma_{\mathrm{S}}^{\mathrm{LW}}$, as given by the Good-Girifalco-Fowkes equation, equation 5-10. The results obtained for all PUDs are summarized in Table 5-1. Based on these values, the Hamaker constants A_{131}^{vOCG} can be calculated according to van Oss-Chaudhury-Good theory and equation 5-9. All results are shown in Table 5-2 and Figure 5-4.

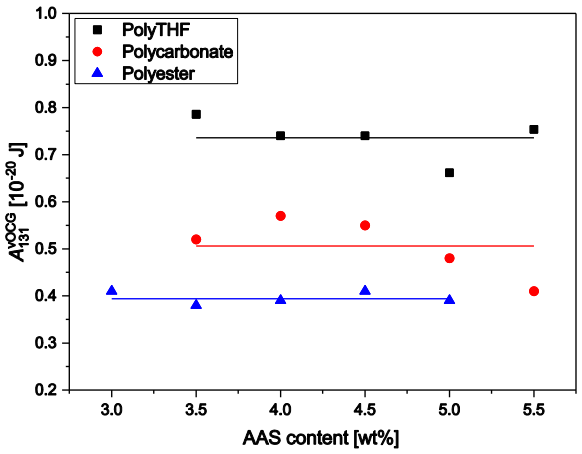

Figure 5-4: Hamaker constant A_{131}^{vOCG} as a function of the AAS content for PTHF (black), PE (blue) and PC (red) based PUDs. Values are based on contact angle data. Solid lines refer to the average value for each PUD series.

Hamaker constants A_{131}^{vOCG} obtained by this approach were found to be in the range of approximately $0.4 \cdot 10^{-20}$ J (PE-based PUDs) to $0.75 \cdot 10^{-20}$ J (PTHF-based PUDs). These values are in good accordance with the above-mentioned characteristic range for water-based polymer dispersions. Furthermore, they show only minor variations within the individual series and thus meet expectations arising from the marginal modifications in the polymer composition. The Hamaker constants A_{131}^{vOCG} can thus be considered as quite reasonable. However, absolute accuracy of these values should not be overrated, as the determination of contact angles is sensitive to several factors, e.g. static or dynamic measuring techniques, liquid drop volume, drop spreading time or surface roughness of the investigated solid.[72,73] Moreover, we have observed minor inconsistencies with so far unpublished results from PUDs based on the same polyol components but employing DMPA as intrinsic stabilizer. It was therefore decided to use an average value $\overline{A_{131}^{\mathrm{vOCG}}}$ of $(0.6 \pm 0.1) \cdot 10^{-20}$ J for the Hamaker constant of all PUDs in the subsequent calculations.

As outlined above, the apparent Hamaker constants A_{131}^{app} are too high for aqueous polymer dispersions. Since these values were determined using an approach based on DLVO theory, they represent the cumulative interaction of all attractive forces. Conversely, the Hamaker constants A_{131}^{vOCG}, which are based on contact angle data, are significantly lower and more in line with expectations. These results suggest the presence of additional attractive interactions that are not due to van der Waals forces. This possibility can be taken into account by XDLVO theory and is considered in more detail below.

5.4.3 Assessment according to XDLVO theory

As outlined in the theory section, many studies aimed to extend the DLVO within the so-called XDLVO approaches, taking into account additional interactions that are often ascribed to the hydrophobicity or hydrophilicity of the material. For the PUDs studied, our results so far indicate the presence of an additional attractive interaction force, which might be attributed to hydrophobic effects. To describe this additional energy term V_h by means of the XDLVO theory, knowledge of two parameters is required according to 5-8. These are the decay length λ and the pre-exponential factor C. Using equations 5-1-5-5 and 5-7-5-8, the known ccc and considering the conditions $V_T = 0$ as well as $dV_T/dH = 0$, again only one of these two parameters can be estimated. In order to estimate the pre-exponential factor, which characterizes the strength of the hydrophobic interaction, we decided to look for a reasonable literature value for the decay constant. As described in the theoretical section, several studies have so far addressed the topic of hydrophobic attraction and determined a rather wide spectrum of λ values, ranging from a few tens to several nanometers.[51,53,54,59]

According to Donaldson et al. a plausible range of 0.3 nm - 1 nm can be assumed. They pointed out that the variation in the data given in the literature can be attributed to difficulties in creating uniform hydrophobic surfaces.[55] For example, long-range attraction has been observed for anionic mica surfaces that were modified by adsorbed cationic surfactants or lipids. It was finally determined in various studies that the local structure of these surfaces shows domains of bilayers and bare mica. The long-range attraction could therefore be attributed to electrostatic interactions between these oppositely charged patches.[74–77] Moreover, the existence of long-range attractive forces has been demonstrated to result from the bridging of nanobubbles.[78–80] On the other hand, Tabor et al. and Moazzami-Gudarzi et al. analyzed the hydrophobic interaction of oil droplets and polystyrene particles in detail. Both groups found a decay length of about 0.3 nm.[58,81] Tabor et al. further concluded that this value is very reasonable for hydrophobic interactions, which are solely due to the orientation of water molecules at hydrophobic surfaces.[54] Therefore, we also opted for a short-range hydrophobic attraction in our study, which is characterized by a decay length of $\lambda = 0.3$ nm. Based on this assumption and considering the determined effective surface potential Ψ_0 (cf. Table 5-1) as well as the average Hamaker constant $\overline{A_{131}^{vOCG}} = 0.6 \cdot 10^{-20}$ J, the pre-exponential factor C can be calculated. The results are shown in Table 5-2 and Figure 5-5 (exemplary interaction energy curves according to the XDLVO theory are given in the Supporting Information).

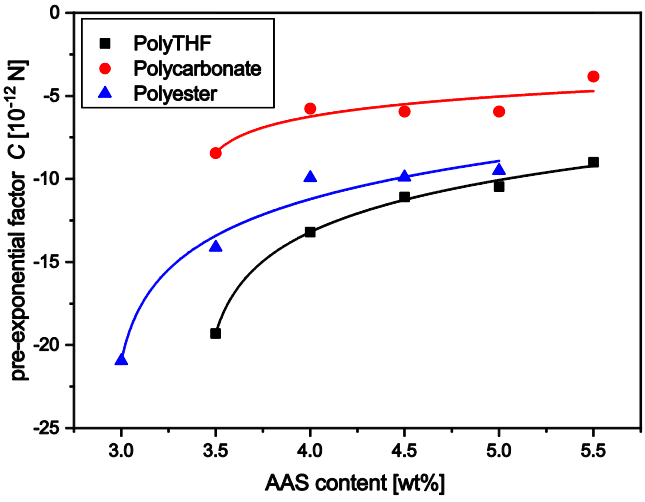

Figure 5-5: Pre-exponential factor C as a function of the AAS content for PTHF (black), PE (blue) and PC (red) based PUDs. Values are calculated according to XDLVO theory. Solid lines are a guide to the eye.

Our results indicate that the consideration of an additional attractive interaction parameter can adequately describe the observed dispersion stability. The PTHF-based PUDs show the most hydrophobic character of our dispersion series, followed by the PE-based PUDs. The least hydrophobic ones are the PC-based PUDs. It is also evident that the incorporation of hydrophilic sulfonate groups attenuates the extent of hydrophobic attraction with an increasing AAS content, but the overall character remains clearly hydrophobic. It is noteworthy in this context that the influence of this additional parameter on the particle sizes formed during secondary dispersion is rather small. As already mentioned, the most hydrophobic, PTHF-based PUDs have the smallest particles relative to the other PUD samples examined. On the basis of hydrophobicity, however, the opposite effect would have been expected, as the interface to the dispersant would then be minimized. Accordingly, the influence of the particle charge already discussed must be regarded as much stronger. Although the exact background is not yet fully understood, it is currently assumed that the destabilizing hydrophobic effect is at least partly due to a specific orientation of water molecules near the interface so that these water molecules lose conformational entropy and form fewer hydrogen bonds. This situation represents an energetically unfavourable state that would be reduced by particle aggregation.[54,68] In light of this, the impact of the polyol component, as well as the influence of the AAS content on the dispersion stability of the PUDs, can be properly understood. Nevertheless, one should bear in mind that our XDLVO calculations are subject to a certain shortcoming. The decay length λ cannot be determined with the help of the measured ccc values alone. Instead, a physically reasonable value had to be adopted, as stated in the literature. Therefore, the utilization of alternative investigation methods would be of great interest. For example, force−distance measurements using atomic force microscopy provide detailed information about the decay behavior of the total interaction energy between two approaching interfaces.[53,68] The analysis of these curves would allow a more accurate assessment of the additional attractive interaction force between the PUD particles.

5.5 Conclusion

In this study, the dispersion stability of water-based PUDs was investigated using the critical coagulation concentration (ccc) and analyzed in terms of DLVO and XDLVO theories. The determined ccc values indicate a considerable influence of the polyol component on the dispersion stability, whereas the effect of the variation in the AAS content is relatively moderate. These distinct differences cannot be ascribed to electrostatic interactions, because the surface potentials determined for each polyol series are quite similar. Moreover, it is evident that the variations in dispersion stability cannot be explained by attractive van der Waals interaction energies alone. The apparent Hamaker constants, determined by means of the DLVO theory, are not consistent for different AAS contents within each PUD series. They are also unusually high for aqueous polymer dispersions, whereas values based on contact angle data and the van Oss−Chaudhury−Good theory led to reasonable results in the range o $(0.6 \pm 0.1) \cdot 10^{-20}$ J. These discrepancies indicate the need to consider additional attractive interaction forces.

Accordingly, XDLVO calculations were performed by taking an exponentially decaying extra term into account. For this purpose, we used a short-range decay length λ of 0.3 nm. As a result, we obtained reasonable values with a negative sign for the pre-exponential factor C. This parameter can be interpreted as a measure of the hydrophobic interactions of the PUD particles. The magnitudes of these values reveal strong differences between the polyol components. In addition, they are found to decrease as the content of hydrophilic AAS increases within each polyol series. Therefore, we conclude the presence of additional attractive interaction forces is probably due to hydrophobic effects. Our study could therefore serve as a basis for further investigations of PUDs, e.g., for force−distance measurements using AFM methods.

Supporting information

The Supporting Information is available free of charge at https://pubs.acs.org/doi/10.1021/acs.langmuir.5c01517?goto=supporting-info

Exemplary description for the determination of the critical coagulation concentration and interaction energy curves according to DLVO and XDLVO theories.

Author information

Corresponding Author

J. Wilkens − *Faculty of Applied Natural Sciences, TH Köln_ University of Applied Science, Leverkusen D-51379, Germany;* orcid.org/0000-0003-2831-8400;
Email: jan.wilkens@th-koeln.de

Authors

C. Grau − *Faculty of Applied Natural Sciences, TH Köln_ University of Applied Science, Leverkusen D-51379, Germany*
A. M. Schmidt − *Department of Chemistry, University of Cologne, D-50939 Cologne, Germany;* orcid.org/0000-0002-7284-7847
Complete contact information is available at: https://pubs.acs.org/doi/10.1021/acs.langmuir.5c01517

Credit authorship contribution statement

C. Grau: experimental work, methodology, conceptualization, data evaluation and visualization, software, writing – original draft. **A.M. Schmidt:** supervision, discussion, writing – review and editing. **J. Wilkens:** supervision, conceptualization, methodology, project administration, discussion, resources, funding acquisition, writing – review and editing.

Notes

The authors declare no competing financial interest.

Acknowledgements

This project has received fundings from the German Ministry of Education and Research (BMBF) as part of the funding program Forschung an Fachhochschulen under contract number 13FH142PX6. We are also very grateful for valuable discussions and financial and material support provided by Covestro AG.

5.6 References

(1) Athawale, V. D., Kulkarni, M. A. Polyester polyols for waterborne polyurethanes and hybrid dispersions. *Prog. Org. Coat.* **2010**, *67*, 44–54.

(2) García-Pacios, V., Jofre-Reche, J. A., Costa, V., Colera, M., Martín-Martínez, J. M. Coatings prepared from waterborne polyurethane dispersions obtained with polycarbonates of 1,6-hexanediol of different molecular weights. *Prog. Org. Coat.* **2013**, *76*, 1484–1493.

(3) García-Pacios, V., Costa, V., Colera, M., Martín-Martínez, J. M. Waterborne polyurethane dispersions obtained with polycarbonate of hexanediol intended for use as coatings. *Prog. Org. Coat.* **2011**, *71*, 136–146.

(4) Lee, D.-K., Tsai, H.-B., Wang, H.-H., Tsai, R.-S. Aqueous polyurethane dispersions derived from polycarbonatediols. *J. Appl. Polym. Sci.* **2004**, *94*, 1723–1729.

(5) Barni, A., Levi, M. Aqueous polyurethane dispersions: A comparative study of polymerization processes. *J. Appl. Polym. Sci.* **2003**, *88*, 716–723.

(6) Harjunalanen, T., Lahtinen, M. The effects of altered reaction conditions on the properties of anionic poly(urethane-urea) dispersions and films cast from the dispersions. *Eur. Polym. J.* **2003**, *39*, 817–824.

(7) Sardon, H., Irusta, L., Fernández-Berridi, M. J., Luna, J., Lansalot, M., Bourgeat-Lami, E. Waterborne polyurethane dispersions obtained by the acetone process: A study of colloidal features. *J. Appl. Polym. Sci.* **2011**, *120*, 2054–2062.

(8) Dieterich, D. Aqueous emulsions, dispersions and solutions of polyurethanes; synthesis and properties. *Prog. Org. Coat.* **1981**, *9*, 281–340.

(9) Jhon, Y.-K., Cheong, I.-W., Kim, J.-H. Chain extension study of aqueous polyurethane dispersions. *Colloids Surf. A: Physicochem. Eng.* **2001**, *179*, 71–78.

(10) Saw, L. K., Brooks, B. W., Carpenter, K. J., Keight, D. V. Different dispersion regions during the phase inversion of an ionomeric polymer–water system. *J. Colloid Interface Sci.* **2003**, *257*, 163–172.

(11) Saw, L. K., Brooks, B. W., Carpenter, K. J., Keight, D. V. Catastrophic phase inversion in region II of an ionomeric polymer-water system. *J. Colloid Interface Sci.* **2004**, *279*, 235–243.

(12) Wei, Y., Luo, Y., Li, B., Li, B. Phase inversion of UV-curable anionic polyurethane in the presence of acetone solvent. *Colloid Polym. Sci.* **2005**, *283*, 1289–1297.

(13) Lijie, H., Yongtao, D., Zhiliang, Z., Zhongsheng, S., Zhihua, S. Synergistic effect of anionic and nonionic monomers on the synthesis of high solid content waterborne polyurethane. *Colloids Surf. A: Physicochem. Eng.* **2015**, *467*, 46–56.

(14) Lee, S. K., Kim, B. K. High solid and high stability waterborne polyurethanes via ionic groups in soft segments and chain termini. *J. Colloid Interface Sci.* **2009**, *336*, 208–214.

(15) Chinwanitcharoen, C., Kanoh, S., Yamada, T., Tada, K., Hayashi, S., Sugano, S. Preparation and Shelf-Life Stability of Aqueous Polyurethane Dispersion. *Macromol. Symp.* **2004**, *216*, 229–240.

(16) Pérez-Limiñana, M. A., Arán-Aís, F., Torró-Palau, A. M., César Orgilés-Barceló, A., Miguel Martín-Martínez, J. Characterization of waterborne polyurethane adhesives containing different amounts of ionic groups. *Int. J. Adhes. Adhes.* **2005**, *25*, 507–517.

(17) Bullermann, J., Friebel, S., Salthammer, T., Spohnholz, R. Novel polyurethane dispersions based on renewable raw materials—Stability studies by variations of DMPA content and degree of neutralisation. *Prog. Org. Coat.* **2013**, *76*, 609–615.

(18) Mequanint, K., Sanderson, R. Hydrolytic stability of nano-particle polyurethane dispersions: Implications to their long-term use. *Eur. Polym. J.* **2006**, *42*, 1145–1153.

(19) Derjaguin, B., Landau, L. Theory of the stability of strongly charged lyophobic sols and of the adhesion of strongly charged particles in solutions of electrolytes. *Prog. Surf. Sci.* **1993**, *43*, 30–59.

(20) Verwey E. J. W., Overbeek J. T. G. *Theory of the Stability of Lyophobic Colloids*: New York, 1948.

(21) Hamaker, H. C. The London—van der Waals attraction between spherical particles. *Physica* **1937**, *4*, 1058–1072.

(22) Galantini, L., Giampaolo, S. M., Mannina, L., Pavel, N. V., Viel, S. Study of Intermicellar Interactions and Micellar Sizes in Ionic Micelle Solutions by Comparing Collective Diffusion and Self-Diffusion Coefficients. *The Journal of Physical Chemistry B* **2004**, *108*, 4799–4805.

(23) Zuev, Y. F., Kusova, A. M., Sitnitsky, A. E. Protein translational diffusion as a way to detect intermolecular interactions. *Biophysical reviews* **2023**, *15*, 1111–1125.

(24) Kusova, A. M., Sitnitsky, A. E., Uversky, V. N., Zuev, Y. F. Effect of Protein-Protein Interactions on Translational Diffusion of Spheroidal Proteins. *International journal of molecular sciences* **2022**, *23*.

(25) Kusova, A. M., Sitnitsky, A. E., Zuev, Y. F. Impact of intermolecular attraction and repulsion on molecular diffusion and virial coefficients of spheroidal and rod-shaped proteins. *Journal of Molecular Liquids* **2021**, *323*, 114927.

(26) Li, Y., Yang, X., Wang, Z., Xia, W., Wu, F., Sun, Y., Sun, X., Liu, S. The influence of Ca2+/Mg2+ concentration on the rheological properties of kaolinite slurry: An experiment and DLVO calculation study. *Minerals Engineering* **2025**, *227*, 109296.

(27) Li, M., Kobayashi, M. The aggregation and charging of natural clay allophane: Critical coagulation ionic strength in the presence of multivalent counter-ions. *Colloids Surf. A: Physicochem. Eng.* **2021**, *626*, 127021.

(28) Li, M., Sugimoto, T., Yamashita, Y., Kobayashi, M. Aggregation and charging of natural allophane particles in the presence of oxyanions. *Colloids Surf. A: Physicochem. Eng.* **2022**, *649*, 129413.

(29) Zeng, C., Kobayashi, M. Charging and Aggregation of Nano-Clay Na-Montmorillonite in the Presence of Ciprofloxacin. *Nanomaterials (Basel, Switzerland)* **2025**, *15*.

(30) Schneider, C., Hanisch, M., Wedel, B., Jusufi, A., Ballauff, M. Experimental study of electrostatically stabilized colloidal particles: colloidal stability and charge reversal. *J. Colloid Interface Sci.* **2011**, *358*, 62–67.

(31) Tielemans, M., Roose, P., Groote, P. de, Vanovervelt, J.-C. Colloidal stability of surfactant-free radiation curable polyurethane dispersions. *Prog. Org. Coat.* **2006**, *55*, 128–136.

(32) Behrens, S. H., Christl, D. I., Emmerzael, R., Schurtenberger, P., Borkovec, M. Charging and Aggregation Properties of Carboxyl Latex Particles: Experiments versus DLVO Theory. *Langmuir* **2000**, *16*, 2566–2575.

(33) van Oss C. J. *The properties of water and their role in colloidal and biological systems*, 1st ed.; Elsevier/Acad. Press: Amsterdam, 2008.

(34) Kim, B. K., Lee, J. C. Waterborne polyurethanes and their properties. *J. Polym. Sci., Part A:Polym. Chem.* **1996**, *34*, 1095–1104.

(35) Saalah, S., Abdullah, L. C., Aung, M. M., Salleh, M. Z., Awang Biak, D. R., Basri, M., Jusoh, E. R., Mamat, S. Colloidal stability and rheology of jatropha oil-based waterborne polyurethane (JPU) dispersion. *Prog. Org. Coat.* **2018**, *125*, 348–357.

(36) Nurdin, N. S., Saalah, S., Lim, A. T., Francis, A. Y., Abdullah, L., SaifulAzry, S. Effect of DMPA Content on Colloidal Stability of Jatropha Oil-based waterborne Polyurethane Dispersion. *IOP Conf. Ser. Mater. Sci. Eng.* **2020**, *778*, 12107.

(37) Mohanty, S., Krishnamurti, N. Synthesis and characterization of aqueous cationomeric polyurethanes and their use as adhesives. *J. Appl. Polym. Sci.* **1996**, *62*, 1993–2003.

(38) Grau, C., Schmidt, A. M., Wilkens, J. Water-Based Polyurethane Dispersions: A Detailed Analysis of the Particle Charge Using Soft and Hard Particle Model. *Langmuir* **2024**, *40*, 22123–22135.

(39) Reerink, H., Overbeek, J. T. G. The rate of coagulation as a measure of the stability of silver iodide sols. *Discuss. Faraday Soc.* **1954**, *18*, 74–84.

(40) van Oss, C. J., Chaudhury, M. K., Good, R. J. Interfacial Lifshitz-van der Waals and polar interactions in macroscopic systems. *Chem. Rev.* **1988**, *88*, 927–941.

(41) Trefalt, G., Szilagyi, I., Téllez, G., Borkovec, M. Colloidal Stability in Asymmetric Electrolytes: Modifications of the Schulze-Hardy Rule. *Langmuir* **2017**, *33*, 1695–1704.

(42) M. J. Sparnaay. The interaction between two cylinder shaped colloidal particles. *Recueil des Travaux Chimiques des Pays-Bas* **1959**, *78*, 680–709.

(43) Gu, Y. The Electrical Double-Layer Interaction between a Spherical Particle and a Cylinder. *J. Colloid Interface Sci.* **2000**, *231*, 199–203.

(44) Chai, C., Ma, Y., Li, G., Ge, Z., Ma, S., Luo, Y. The preparation of high solid content waterborne polyurethane by special physical blending. *Progress in Organic Coatings* **2018**, *115*, 79–85.

(45) Zhou, X., Hao, Y., He, X., Zhou, D., Xie, L., Liu, S., Qiao, B. Protean morphology of waterborne polyurethane dispersion: An overview of nanoparticles from sphere to irregular elongated shape. *Progress in Organic Coatings* **2020**, *146*, 105742.

(46) Kang, S.-Y., Ji, Z., Tseng, L.-F., Turner, S. A., Villanueva, D. A., Johnson, R., Albano, A., Langer, R. Design and Synthesis of Waterborne Polyurethanes. *Advanced materials (Deerfield Beach, Fla.)* **2018**, *30*, e1706237.

(47) Li, Q.-A., Sun, D.-C. Synthesis and characterization of high solid content aqueous polyurethane dispersion. *Journal of Applied Polymer Science* **2007**, *105*, 2516–2524.

(48) Madbouly, S. A., Otaigbe, J. U. Recent advances in synthesis, characterization and rheological properties of polyurethanes and POSS/polyurethane nanocomposites dispersions and films. *Progress in Polymer Science* **2009**, *34*, 1283–1332.

(49) Quane, E. J., Elders, N., Newman, A. S., van Mourik, S., Williams, N. S. J., van den Berg, K. J., Ryan, A. J., Mykhaylyk, O. O. Synthesis, Morphology, and Particle Size Control of Acidic Aqueous Polyurethane Dispersions. *Macromolecules* **2024**, *57*, 10623–10634.

(50) Sader, J. E., Carnie, S. L., Chan, D. Y. Accurate Analytic Formulas for the Double-Layer Interaction between Spheres. *J. Colloid Interface Sci.* **1995**, *171*, 46–54.

(51) van Oss, C. J. Acid—base interfacial interactions in aqueous media. *Colloids Surf. A: Physicochem. Eng.* **1993**, *78*, 1–49.

(52) Brant, J. A., Childress, A. E. Colloidal adhesion to hydrophilic membrane surfaces. *J. Membr. Sci.* **2004**, *241*, 235–248.

(53) Butt, H.-J., Cappella, B., Kappl, M. Force measurements with the atomic force microscope: Technique, interpretation and applications. *Surf. Sci. Rep.* **2005**, *59*, 1–152.

(54) Tabor, R. F., Grieser, F., Dagastine, R. R., Chan, D. Y. C. The hydrophobic force: measurements and methods. *Phys. Chem. Chem. Phys.* **2014**, *16*, 18065–18075.

(55) Donaldson, S. H., Røyne, A., Kristiansen, K., Rapp, M. V., Das, S., Gebbie, M. A., Lee, D. W., Stock, P., Valtiner, M., Israelachvili, J. Developing a general interaction potential for hydrophobic and hydrophilic interactions. *Langmuir* **2015**, *31*, 2051–2064.

(56) Israelachvili, J., Pashley, R. The hydrophobic interaction is long range, decaying exponentially with distance. *Nature* **1982**, *300*, 341–342.

(57) Smith, A. M., Borkovec, M., Trefalt, G. Forces between solid surfaces in aqueous electrolyte solutions. *Adv. Colloid Interface Sci.* **2020**, *275*, 102078.

(58) Moazzami-Gudarzi, M., Trefalt, G., Szilagyi, I., Maroni, P., Borkovec, M. Nanometer-ranged attraction induced by multivalent ions between similar and dissimilar surfaces probed using an atomic force microscope (AFM). *Phys. Chem. Chem. Phys.* **2016**, *18*, 8739–8751.

(59) Ducker, W. A., Mastropietro, D. Forces between extended hydrophobic solids: Is there a long-range hydrophobic force? *Curr. Opin. Colloid Interface Sci.* **2016**, *22*, 51–58.

(60) Fowkes, F. M. Determination of interfacial tensions, contact angles and dispersion forces in surfaces by assuming additivity of intermolecular interactions in surfaces. *J. Phys. Chem.* **1962**, *66*, 382.

(61) Good, R. J., Girifalco, L. A. A theory for estimation of surface and interfacial energies. III. Estimation of surface energies of solids from contact angle data. *J. Phys. Chem.* **1960**, *64*, 561–565.

(62) Girifalco, L. A., Good, R. J. A Theory for the Estimation of Surface and Interfacial Energies. I. Derivation and Application to Interfacial Tension. *J. Phys. Chem.* **1957**, *61*, 904–909.

(63) Deutsches Institut für Normung e. V. *Beschichtungsstoffe –Benetzbarkeit –Teil 2: Bestimmung der freien Oberflächenenergie fester Oberflächen durch Messung des Kontaktwinkels*, 2011, *87.040*(55660-2).

(64) Zhao, D., Li, Z., Yang, H., Yang, W., Tian, Y., Tan, L., Chen, N., Feng, H. Salt-Responsive Phenol Formaldehyde Resin: Changes of Interface Energy on the Aggregation Process. *Langmuir* **2023**, *39*, 395–402.

(65) Volkova, A. V., Ermakova, L. E., Golikova, E. V. Peculiarities of coagulation of the pseudohydrophilic colloids: Aggregate stability of the positively charged γ-Al2O3 hydrosol in NaCl solutions. *Colloids Surf., A* **2017**, *516*, 129–138.

(66) Takeshita, C., Masuda, K., Kobayashi, M. The effect of monovalent anion species on the aggregation and charging of allophane clay nanoparticles. *Colloids Surf. A: Physicochem. Eng.* **2019**, *577*, 103–109.

(67) Puertas, las, N. F. J. de. Colloidal Stability of Polymer Colloids with Variable Surface Charge. *J. Colloid Interface Sci.* **1999**, *216*, 221–229.

(68) Israelachvili J. N. *Intermolecular and surface forces*, 3rd ed.; Academic Press: Amsterdam, 2012.

(69) Prieve, D. C., Russel, W. B. Simplified predictions of Hamaker constants from Lifshitz theory. *J. Colloid Interface Sci.* **1988**, *125*, 1–13.

(70) Hough, D. B., White, L. R. The calculation of hamaker constants from liftshitz theory with applications to wetting phenomena. *Adv. Colloid Interface Sci.* **1980**, *14*, 3–41.

(71) Lyklema J. *Fundamentals of Interface and Colloid Science: Volume V Soft Colloids*; Elsevier Academic Press: Amsterdam, 2005.

(72) Rudawska, A., Jacniacka, E. Evaluating uncertainty of surface free energy measurement by the van Oss-Chaudhury-Good method. *Int. J. Adhes. Adhes.* **2018**, *82*, 139–145.

(73) Siboni, S., Della Volpe, C. Acid-Base Theory of Adhesion: A Critical Review. *Rev. Adhes. Adhes.* **2015**, *3*, 253–310.

(74) Meyer, E. E., Lin, Q., Hassenkam, T., Oroudjev, E., Israelachvili, J. N. Origin of the long-range attraction between surfactant-coated surfaces. *Proc. Natl. Acad. Sci. U S A* **2005**, *102*, 6839–6842.

(75) Jho, Y. S., Brewster, R., Safran, S. A., Pincus, P. A. Long-range interaction between heterogeneously charged membranes. *Langmuir* **2011**, *27*, 4439–4446.

(76) Silbert, G., Ben-Yaakov, D., Dror, Y., Perkin, S., Kampf, N., Klein, J. Long-ranged attraction between disordered heterogeneous surfaces. *Phys. Rev. Lett.* **2012**, *109*, 168305.

(77) Perkin, S., Kampf, N., Klein, J. Long-range attraction between charge-mosaic surfaces across water. *Phys. Rev. Lett.* **2006**, *96*, 38301.

(78) Attard, P. Nanobubbles and the hydrophobic attraction. *Adv. Colloid Interface Sci.* **2003**, *104*, 75–91.

(79) Parker, J. L., Claesson, P. M., Attard, P. Bubbles, cavities, and the long-ranged attraction between hydrophobic surfaces. *J. Phys. Chem.* **1994**, *98*, 8468–8480.

(80) Stevens, H., Considine, R. F., Drummond, C. J., Hayes, R. A., Attard, P. Effects of degassing on the long-range attractive force between hydrophobic surfaces in water. *Langmuir* **2005**, *21*, 6399–6405.

(81) Tabor, R. F., Wu, C., Grieser, F., Dagastine, R. R., Chan, D. Y. C. Measurement of the Hydrophobic Force in a Soft Matter System. *J. Phys. Chem. Lett.* **2013**, *4*, 3872–3877.

For Table of Contents only (Graphical Abstract)

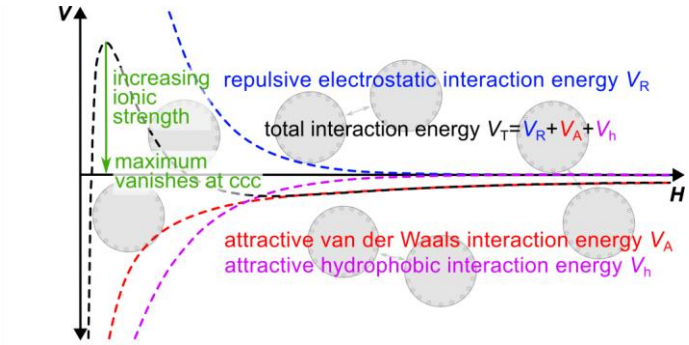

5.7 Supporting Information

Water-based Polyurethane Dispersions: Analysis of the Dispersion Stability in Terms of DLVO and XDLVO Theory

C. Grau [a], A. M. Schmidt [b], J. Wilkens [a]*

[a] Faculty of Applied Natural Sciences, TH Köln - University of Applied Science, Leverkusen D-51379, Germany
[b] Department of Chemistry, University of Cologne, D-50939 Cologne, Germany
* Corresponding author: E-Mail: jan.wilkens@th-koeln.de; Address: Campusplatz 1, D-51379 Leverkusen, Germany

Table of Contents

Determination of the critical coagulation concentration

Following the procedure of Reerink and Overbeek[1], the critical coagulation concentration was determined photometrically with an UV/Vis spectrophotometer Evolution 220 (ThermoScientific) using a wavelength of 500 nm. Absorbance A was measured for 30 s at 0.1 s intervals in PMMA cuvettes. Blank measurements were done with ultra-pure water. Each sample was measured at 0.075 wt% and sodium chloride (NaCl) was used as electrolyte in a concentration range c of 0.5 – 4.5 mol L^{-1} in the final dispersion. Sample and electrolyte solution were mixed immediately before starting the measurement. The measurement at different electrolyte concentrations leads to a set of curves for each sample, as shown in Figure S 5-1.

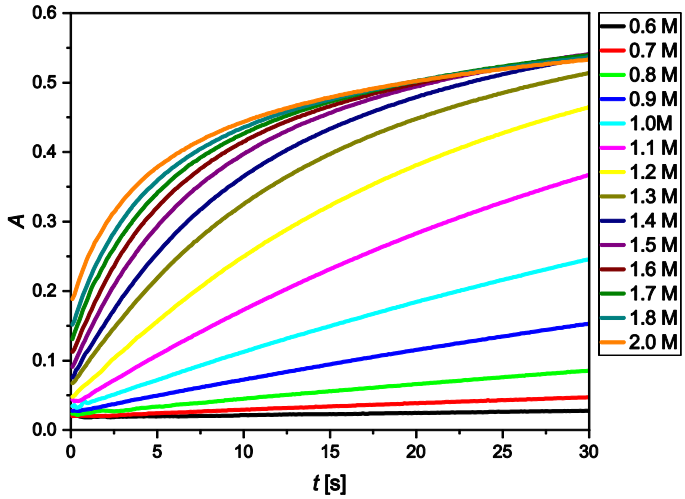

Figure S 5-1: Exemplary set of curves of sample PTHF4.5%: Absorbance A vs. measuring time t.

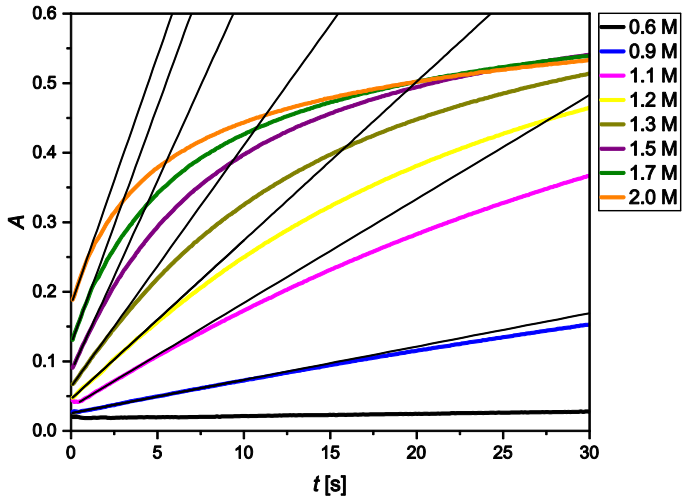

Figure S 5-2: Exemplary determination of the initial slope $\mathrm{d}A/\mathrm{d}t$ for several electrolyte concentrations. Solid black lines represent the initial linear slope.

The initial slope $\mathrm{d}A/\mathrm{d}t$ of each curve was determined (cf. Figure S 5-2) and the logarithmic reciprocal $\log(\mathrm{d}t/\mathrm{d}A)$ was plotted against $\log(c)$, as shown in Figure S 5-3. The values obtained decrease in the slow coagulation regime, while they remain constant in the fast coagulation regime. The intercept of the two sections gives the critical coagulation concentration ccc.

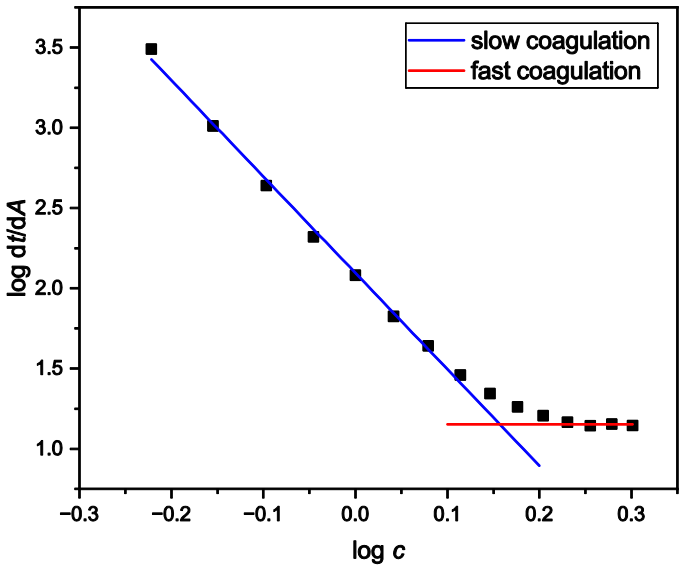

Figure S 5-3: Logarithmic reciprocal $\log(\mathrm{d}t/\mathrm{d}A)$ vs. $\log(c)$. The blue line represents the slow coagulation regime and the red line represents the fast coagulation regime. The intercept of the two sections gives the critical coagulation concentration.

Interaction energy curves according to DLVO theory

In case of the DLVO theory, the interaction energy curves were calculated using eqs 5-1-5-6, as described in the main article. The repulsive electrostatic interaction energy V_R can be calculated according to equation 5-1-5-4 using the effective surface potential Ψ_0. The attractive Van der Waals interaction energy V_A is given by eq 5. If the electrolyte concentration equals the ccc value, the barrier of the total interaction energy V_T (cf. eq 5-6) just vanishes so that the system of equations $V_\mathrm{T} = 0$ and $\mathrm{d}V_\mathrm{T}/\mathrm{d}H = 0$ can be simultaneously solved. Based on this approach, two parameters are obtained, the distance H of the total interaction energy maximum as well as the apparent Hamaker constant A_{131}^{app}. Thus, the following interaction energy curves are obtained, with one example for each polyol component at the same AAS content, as depicted in Figure S5-4 - Figure S5-6.

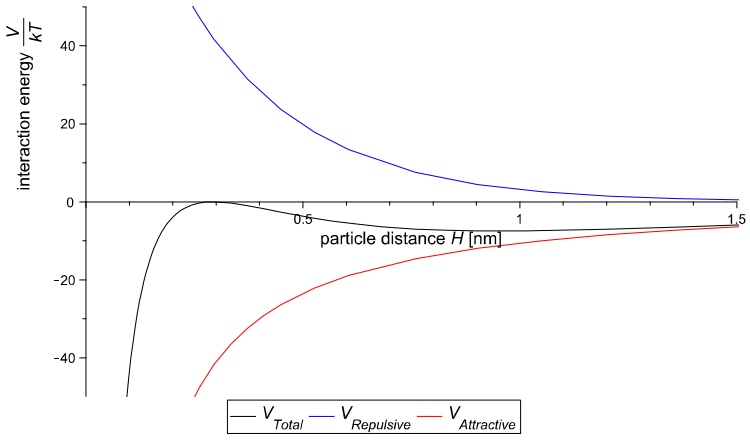

Figure S5-4: Exemplary interaction energy curves for PolyTHF-based PUD with 4.0 wt% AAS according to the DLVO theory. The blue line represents the electrostatic interaction energy V_R, the red line the Van der Waals interaction energy V_A and the black line the total interaction energy V_T.

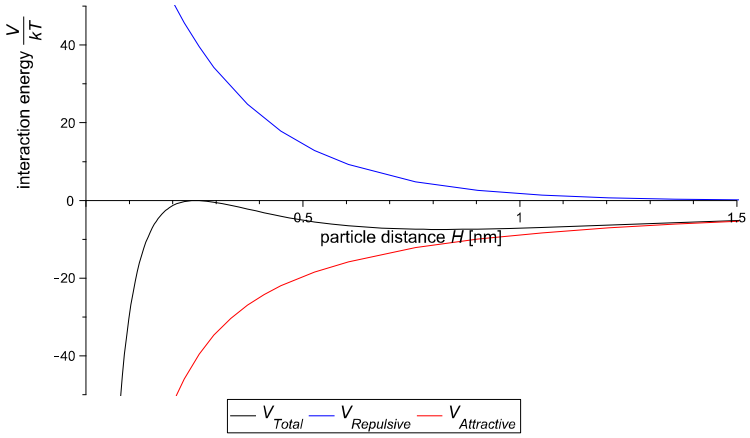

Figure S5-5: Exemplary interaction energy curves for PE-based PUD with 4.0 wt% AAS according to the DLVO theory. The blue line represents the electrostatic interaction energy V_R, the red line the Van der Waals interaction energy V_A and the black line the total interaction energy V_T.

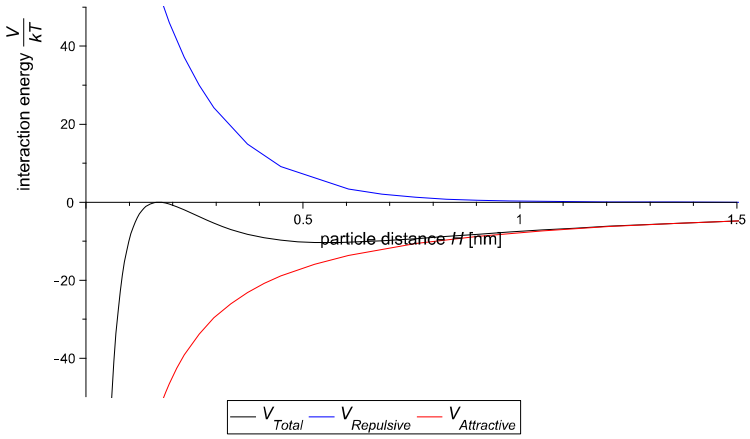

Figure S5-6: Exemplary interaction energy curves for PC-based PUD with 4.0 wt% AAS according to the DLVO theory. The blue line represents the electrostatic interaction energy V_R, the red line the Van der Waals interaction energy V_A and the black line the total interaction energy V_T.

Interaction energy curves according to XDLVO theory

The summation of the total interaction energy V_T according to the XDLVO theory includes an additional term for the hydrophobic interaction energy V_h (cf. eqs 5-7 and 5-8 in the main article). As described in section 2 of the Supporting Information, the effective surface potential Ψ_0 as well as the ccc value were again used as input parameters for the calculations. However, the Van der Waals interaction energy V_A was now calculated on the basis of the Hamaker constant A_{131}^{vOCG}, which was determined from contact angle data using the theory of van Oss, Chaudhury and Good.[2,3]

The system of equations $V_T = 0$ and $dV_T/dH = 0$ can be simultaneously solved using eqs 5-1-5-5 and 5-7-5-8 in order to determine the distance H of the total interaction energy maximum and the pre-exponential factor C, which serves as a measure of the magnitude of the additional hydrophobic interaction energy. The corresponding interaction energy curves of the same samples as in section 2 are presented in Figure S5-7 - Figure S5-9.

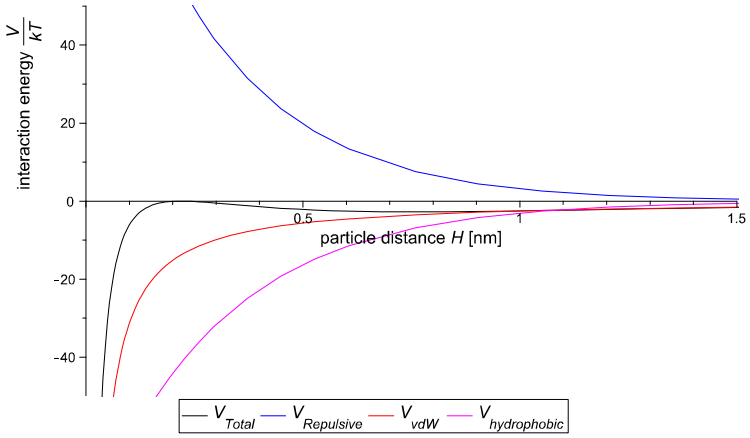

Figure S5-7: Exemplary interaction energy curves for PolyTHF-based PUD with 4.0 wt% AAS according to the XDLVO theory. The blue line represents the electrostatic interaction energy V_R, the red line the Van der Waals interaction energy V_A, the magenta line the hydrophobic interaction energy V_h and the black line the total interaction energy V_T.

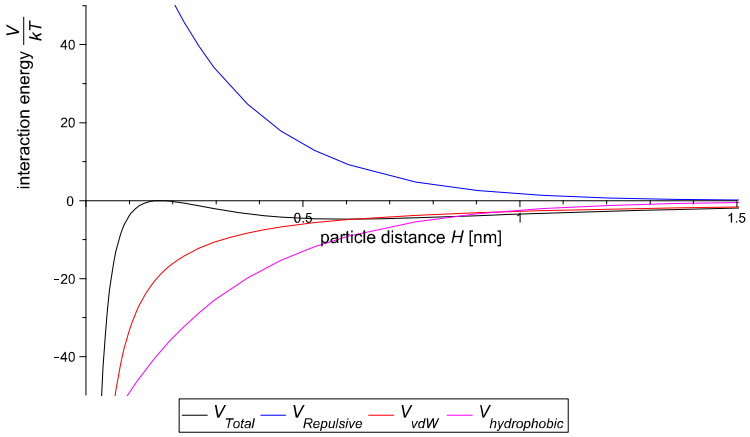

Figure S5-8: Exemplary interaction energy curves for PE-based PUD with 4.0 wt% AAS according to the XDLVO theory. The blue line represents the electrostatic interaction energy V_R, the red line the Van der Waals interaction energy V_A, the magenta line the hydrophobic interaction energy V_h and the black line the total interaction energy V_T.

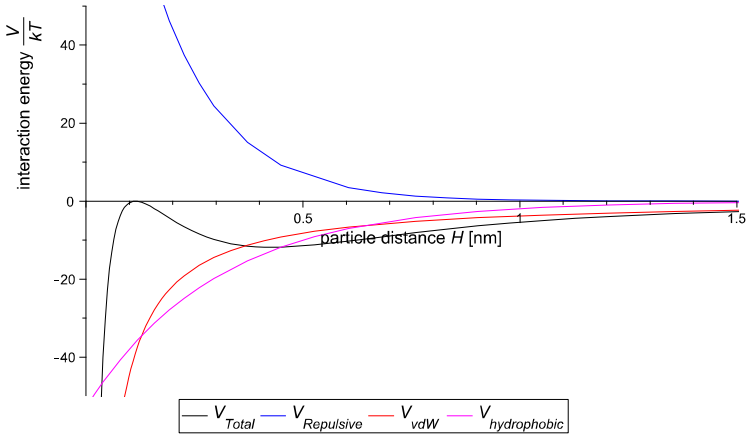

Figure S5-9: Exemplary interaction energy curves for PC-based PUD with 4.0 wt% AAS according to the XDLVO theory. The blue line represents the electrostatic interaction energy V_R, the red line the Van der Waals interaction energy V_A, the magenta line the hydrophobic interaction energy V_h and the black line the total interaction energy V_T.

References

(1) Reerink, H., Overbeek, J. T. G. The rate of coagulation as a measure of the stability of silver iodide sols. *Discuss. Faraday Soc.* **1954**, *18*, 74–84.

(2) van Oss, C. J., Chaudhury, M. K., Good, R. J. Interfacial Lifshitz-van der Waals and polar interactions in macroscopic systems. *Chem. Rev.* **1988**, *88*, 927–941.

(3) van Oss C. J. *The properties of water and their role in colloidal and biological systems*, 1st ed.; Elsevier/Acad. Press: Amsterdam, 2008.

6 Water-Based Polyurethane Dispersions: New Insights into the Intrinsic Stabilization Using Carboxylate Groups

C. Grau [a], A. M. Schmidt [b], J. Wilkens [a]*

[a] *Faculty of Applied Natural Sciences, TH Köln - University of Applied Science, Leverkusen D-51379, Germany*
[b] *Department of Chemistry, University of Cologne, D-50939 Cologne, Germany*
* *Corresponding author, E-mail address: jan.wilkens@th-koeln.de*

Remarks on the manuscript in relation to the thesis and declaration of individual contributions

This chapter has been published in *Langmuir* and is reprinted with permission from *Langmuir* 2026, 42 (26), 18775-18787. Numbering of the chapters, figures and formulas has been adjusted to the thesis format.

Article on Request: https://pubs.acs.org/articlesonrequest/AOR-ZJTXCPDNXGAHUWUBVAEH

DOI: https://doi.org/10.1021/acs.langmuir.6c00992

The chapter presents a comprehensive analysis of both the particle charge and dispersion stability of PUDs stabilized by DMPA. The results are evaluated using corresponding theoretical models, with particular emphasis on interpreting electrophoretic mobility through soft and hard particle theories. Potentiometric titration data revealed, that the majority of the carboxylate groups are dissociation limited and potentially located throughout a peripheral, charge carrying layer. The dispersion stability was analysed in terms of critical coagulation concentration. Additionally, dispersion stability was examined in the context of DLVO and XDLVO frameworks, allowing repulsive interaction energies to be derived from the determined surface potentials. Attractive interaction energies were quantified via the Hamaker constant, calculated according to both DLVO and XDLVO approaches. The comparison showed that the XDLVO approach, based on contact angle data, yielded more realistic Hamaker constant values. Moreover, XDLVO analysis identified a significant contribution of hydrophobic attraction as an additional interaction parameter, enabling an explanation of the influence of polyol components and surface functional groups on dispersion stability. As such, this publication is fundamental to this thesis, providing detailed insight into both the electrokinetic properties and colloidal interaction mechanisms governing the stability of DMPA-stabilized PUDs.

The synthesis and analytical work were carried out under my supervision and responsibility. The PUD series PE-DMPA and PC-DMPA were synthesized by *Tobias Wagner* within the scope of his master thesis under my supervision. I synthesized the remaining dispersions and conducted most of the analytical measurements myself, except for the contact angle measurements also done by *Tobias Wagner*. The analysis and interpretation of the results were carried out collaboratively by myself and *Prof. Dr. Jan Wilkens*. I prepared the manuscript with extensive feedback and corrections from *Prof. Dr. Jan Wilkens* and *Prof. Dr. Annette M. Schmidt*.

Abstract

To achieve sufficient dispersion stability, ionizable groups such as dimethylolpropionic acid (DMPA) are often incorporated into the framework of water-based polyurethane dispersions (PUDs). As a weak acid, this group exhibits pH-dependent dissociation, which directly influences the degree of electrostatic repulsion between two particles. To gain deeper insights into the structure-stability relationship of PUDs, we synthesized numerous samples with different soft segments (polyether, polyester and

polycarbonate polyols) and varying contents of DMPA according to the acetone process. The dissociation behaviour of the carboxyl groups and the particle charge were characterized by potentiometric acid-base titration, and the corresponding titration curves were fitted assuming multiple functional groups with adaptable acid strengths. To determine the surface potentials, electrokinetic measurements as a function of electrolyte concentration were performed and analyzed by hard particle theory considering the relaxation effect. Dispersion stability was examined by means of the critical coagulation concentration (ccc) and evaluated according to the DLVO and XDLVO theory. Hamaker constants were determined based on contact angle data of the respective PU films with an apolar test liquid using the van Oss-Chaudhury-Good theory.

The study shows that not all carboxyl groups incorporated into the polymer backbone can be detected by potentiometric titration. In addition, data from titration curves are best fitted when at least two functional groups with different acid strengths are assumed, indicating a non-uniform charge distribution in a peripheral layer and hindered dissociation. Interestingly, early DMPA incorporation during the prepolymerization step has a significant effect on the charge localisation in the PUD particles. Compared to PUDs, in which the ionisable groups were incorporated during the final chain extension step, the proportion of charge groups in the particle interior increases significantly. However, these differences hardly affect the determined surface potentials and dispersion stabilities. Similar to a recent study, the surface potentials decrease slightly with increasing DMPA content, which is a result of the decreasing particle size. As expected, the ccc values increase with rising DMPA content, but in particular they show a strong influence of the polyol component. The analysis of our data indicates that the DLVO approach should be extended by considering an additional attractive interaction energy, which is probably based on the hydrophobicity of the polymer components.

Keywords

Water-based polyurethane dispersions, dimethylolpropionic acid, acid strength, particle charge, surface potential, shear plane, dispersion stability, critical coagulation concentration, Hamaker constant, van Oss-Chaudhury-Good theory, hydrophobic interaction, DLVO, XDLVO

6.1 Introduction

Nowadays, polyurethanes are often produced as water-based polyurethane dispersions (PUDs), meeting environmental requirements. For this reason, a sufficient dispersion stability is required for the production process, storage, transportation and final application. Typically, the essentially hydrophobic macromolecules are stabilized by the incorporation of hydrophilizing or ionic functional groups. In the latter case, knowledge of the electrostatic potentials and the resulting interaction energies is of crucial importance.

Besides non-ionic stabilization by polyethylene glycol segments[1,2] or cationic stabilization by ammonium salts, such as N-methyldiethanolamine,[3–7] anionic groups are frequently used. For instance, diamino alkane sulfonic acids, such as 2-[(2-aminoethyl)amino]ethanesulfonic acid (AAS),[8–10] or carboxylic acids, such as dimethylolpropionic acid (DMPA)[11–16] or dimethylolbutanoic acid (DMBA)[17], can be incorporated in the polymer backbone to achieve sufficient dispersion stability. In this regard, water-based PUDs stabilized by DMPA are often the focus of scientific research. Numerous studies have been carried out to investigate the influence of the DMPA content on the properties of the final PUDs. Since DMPA usually needs to be neutralized during synthesis, the degree of neutralization has also received attention in various studies.

Among others, Kim et al. analyzed the impact of the DMPA content on the dispersion stability and expressed it in terms of particle size. They found that the particle size decreases with increasing DMPA content, as this generally allows larger interfacial areas to be stabilized.[18] Nanda and Wicks investigated

the influence of DMPA content as well as the degree of neutralization. When the neutralization degree of the carboxyl groups decreased during dispersion, the particle size increased, which was attributed to the lower hydrophilicity of the carboxyl groups compared to the carboxylate groups. In addition, they also investigated the effect of postneutralization, meaning that partially neutralized PUDs during dispersion were completely neutralized by subsequent addition of an organic base. Interestingly, they found the particle size to increase. They concluded that some of the functional groups are trapped within the polymer matrix and some of them can be neutralized after particle formation. As a result, the subsequently gained hydrophilicity within the polymer matrix leads to water-swelling and thus to an increase of particle size.[14]

This already points to a complex structure of the particle charges in PUD systems and suggests the need of a comprehensive investigation of the ionic groups of the PU particles. For this purpose, acid-base titration is well suited to provide information about the detectable charges of the DMPA moiety and their dissociation behaviour. In a well-known study, Stone-Masui and Watillon analyzed monodispersed polystyrene latices stabilized by surfactants using potentiometric and conductometric titration.[19] They found that the pK_a value of potassium stearate significantly increases when adsorbed on the particle surface. This decrease in the effective acid strength was attributed to electrostatic interactions of the dissociated protons with neighbouring carboxylate groups. In case of PUDs, a complex rearrangement of the polymer network takes place during secondary dispersion, with the hydrophobic parts being arranged inside the particle, while the hydrophilic parts move to the particle surface.[20–23] Consequently, an influence on the localisation of the ionic groups and the associated dissociation behaviour is to be expected, since their fixed position within the polymer backbone allows only limited conformational changes.

In a recent study, Alves et al. characterized acidic groups of oxidized carbon dots by data fitting of potentiometric titration curves with nonlinear regression.[24] This approach is capable of considering various acidic species with different pK_a values and is therefore well suited to gain detailed insights into the peripheral charge distribution of PU particles.

The arrangement of charges at the particle interface and the dissociation behaviour of the carboxyl groups may have an influence on the dispersion stability, which is often characterised by the critical coagulation concentration (ccc). This is the minimum electrolyte concentration, at which aggregation of particles is not hindered by a repulsive energy barrier and is thus limited solely by the particle diffusion. Determined ccc values are commonly described by the renowned DLVO theory, which takes repulsive electrostatic and attractive van der Waals forces into account.[25–27] This in turn means that any other interaction forces, such as hydrophilic repulsion or hydrophobic attraction forces,[28–31] are not considered. However, it is increasingly recognised that these effects can play an important role in the stability of aqueous dispersions. Therefore, it can be necessary to extend the DLVO theory by considering these additional interaction forces.[30–35] These approaches are often referred to as XDLVO theory.

In this study, we analyze the influence of the DMPA content and polyol components on the electrostatic and electrodynamic properties of water-based polyurethane dispersions. For this purpose, PUDs based on polycarbonate, polyester and polyether polyols with DMPA mass fractions between 3.0 and 5.0 wt % are synthesized according to the acetone process. A detailed analysis of the particle charge is performed by potentiometric and electrophoretic investigations. The data of the potentiometric acid-base titration curves are fitted with nonlinear regression to determine the amount and acid strength of the carboxyl groups. The electrophoretic mobility is analyzed as a function of ionic strength, providing values for the distance of the shear plane and the surface potential of the particles. Furthermore, the dispersion stability is investigated using time-resolved photometric measurement of the critical coagulation concentration.

These results are interpreted based on the DLVO and XDLVO theory. For this purpose, Hamaker constants are determined using contact angle measurements of the respective PU films with an apolar test liquid and the van Oss-Chaudhury-Good (vOCG) theory.[28,36]

6.2 Theory

The following section introduces the theoretical principles employed in the analysis and interpretation of the primary measurement results. The theories used to evaluate the electrophoretic mobility of hard particles are presented. It is also shown how the surface potential and the position of the shear plane can be determined. Furthermore, the evaluation of the particle charge by analyzing the potentiometric titration curves is described in detail. Finally, we outline the analysis of the dispersion stability in terms of DLVO and XDLVO theory.

6.2.1 Electrokinetic properties of hard particles

An early description of the relationship between the electrophoretic mobility μ and the zeta potential ζ was given by Helmholtz and Smoluchowski.[37] It is valid for low zeta potentials and particles of radius a much larger than the thickness of the diffuse double layer, which can be characterized by the reciprocal of the Debye-Hückel parameter κ. This parameter is given by eq 6-1 with the Faraday constant F, relative permittivity ε_r, permittivity in vacuum ε_0, molar gas constant R, thermodynamic temperature T and the valence z_i and concentration c_i of the i-th ion species.

$$\kappa = \sqrt{\frac{F^2}{\varepsilon_\mathrm{r}\varepsilon_0 RT}\sum z_\mathrm{i}^2 c_\mathrm{i}} \tag{6-1}$$

In case of high potentials and large diffuse double layers, the relaxation effect needs to be taken into account.[38,39] The double layer can be deformed during electrophoresis leading to an asymmetrically ion distribution, since the counter ions move in the opposite direction to the particle. As a result, the particle centre and centre of the surrounding ion cloud do not coincide anymore. This generates an additional electrical polarisation field that is opposite to the applied field and slows down the particle movement. The relaxation effect is associated with the phenomenon of surface conductivity, which can occur in the stagnant layer (hydrodynamically immobile part of the diffuse layer, i.e. within the shear plane) and the diffuse layer (hydrodynamically mobile part of the diffuse layer, i.e. beyond the shear plane).[39] To account for this effect, the scaled drag coefficient m_i (eq 6-2) of the co-ions (m_C) and counter ions (m_CO) needs to be considered. It is based on the ionic drag coefficient of the i-th ionic species λ_i (eq 6-3) with the Boltzmann constant k_B, Avogadro constant N_A, elementary charge e, viscosity η and the limiting conductance Λ_i^0.[40]

$$m_\mathrm{i} = \frac{2\varepsilon_\mathrm{r}\varepsilon_0 k_\mathrm{B} T}{3\eta z_\mathrm{i}^2 e^2}\lambda_\mathrm{i} \tag{6-2}$$

$$\lambda_\mathrm{i} = \frac{N_\mathrm{A} e^2 |z_\mathrm{i}|}{\Lambda_\mathrm{i}^0} \tag{6-3}$$

Ohshima, Healy and White developed an approximate analytical expression (eq 6-4) to describe the electrophoretic mobility of spherical, hard particles in a solution of symmetrical z-z electrolytes, which is valid for arbitrary values of the zeta potential and shows an error of less than 1% for $\kappa a \geq 10$.[40]

$$\mu = \mathrm{sign}(\zeta)\frac{\varepsilon_r\varepsilon_0}{\eta}\left(\mathrm{abs}(\zeta)\frac{2F}{1+F}\frac{k_B T}{ze}H\right) + \mathrm{sign}(\zeta)\frac{2\varepsilon_r\varepsilon_0 k_B T}{3\eta e}\left(\frac{1}{\kappa a}\left(-18\left(t+\frac{t^3}{9}\right)K + \frac{15F}{1+F}\left(t+\frac{7t^2}{20}+\frac{t^3}{9}\right) - 6(1+3m_{CO})\left(1-\exp\left(-\frac{\bar{\zeta}}{2}\right)\right)G + \frac{12F}{(1+F)^2}H + \frac{9\bar{\zeta}}{1+F}(m_{CO}G + m_C H) - \frac{36F}{1+F}\left(m_{CO}G^2 + \frac{m_C}{1+F}H^2\right)\right)\right) \quad (6\text{-}4)$$

The equations for the functions H, t, K, $\bar{\zeta}$, F and G have been described elsewhere in detail,[9,40] but can also be found in the supporting information. Additionally, Ohshima developed an approximate analytical expression (eq 6-5) for the case of $\kappa a < 10$ with a relative error less than 1% for $e|\zeta|/k_B T \leq 3$ at $\kappa a = 1$.[41]

$$\mu = \frac{2\varepsilon_r\varepsilon_0\zeta}{3\eta}\left(1+\frac{1}{2\left(\kappa a\left(1+2\exp(-\kappa a)\right)\right)^3}\right) - \frac{2\varepsilon_r\varepsilon_0\zeta}{3\eta}\bar{\zeta}^2\left(\frac{\kappa a(\kappa a+1.3\exp(-0.18\kappa a)+2.5)}{2(\kappa a+1.2\exp(-7.4\kappa a)+4.8)^3} + \left(\frac{m_{CO}+m_C}{2}\right)\left(\frac{9\kappa a(\kappa a+5.2\exp(-3.9\kappa a)+5.6)}{3(\kappa a+1.55\exp(-0.32\kappa a)+6.02)^3}\right)\right) \quad (6\text{-}5)$$

It should be noted here that both equations 6-4 and 6-5 only account for the diffuse layer part of surface conductivity so that inaccuracies may occur if stagnant layer conductivity is significant. However, Frangenberg et al. recently showed for a PUD sample similar to those in this study that the error caused by neglecting the stagnant layer conductivity was acceptable (< 10 %).[42]

Ohshima, Healy and White also derived an approximate analytical expression (eqs 6-6 to 6-9) to describe the relationship between the surface potential ψ_0 and the potential ψ at a certain distance x to the particle surface.[43,44] This potential can also be related to the zeta potential, since the zeta potential is defined as the potential at the shear plane x_s, i.e. $\zeta = \psi(x_s)$.

$$\psi(x) = \frac{2k_B T}{ze}\ln\left(\frac{(1+Bs)\left(1+\frac{Bs}{2\kappa a+1}\right)}{(1-Bs)\left(1-\frac{Bs}{2\kappa a+1}\right)}\right) \quad (6\text{-}6)$$

with

$$B = \frac{\left(1+\frac{\kappa a}{\kappa a+1}\right)\tanh\left(\frac{y_0}{4}\right)}{1+\left(1-\frac{2\kappa a+1}{(\kappa a+1)^2}\tanh\left(\frac{y_0}{4}\right)^2\right)^{0,5}} \quad (6\text{-}7)$$

$$s = \frac{a}{x+a}\exp(-\kappa x) \quad (6\text{-}8)$$

The surface potential is included by the scaled surface potential y_0.

$$y_0 = \frac{ze\psi_0}{k_B T} \quad (6\text{-}9)$$

Using equations 6-6 to 6-9, the surface potential and the distance of the shear plane can be calculated by a least-squares fitting procedure, if the zeta potential is determined as a function of ionic strength.

Moreover, the electrokinetic charge density σ_0^{ek} can be calculated based on electrokinetic measurements, as given by the approximate analytical expression in equation 6-10 derived by Ohshima, Healy and White. For $\kappa a \geq 0.5$ the relative error is less than 0.5 %.[43]

$$\sigma_0^{\mathrm{ek}} = \frac{2\varepsilon_\mathrm{r}\varepsilon_0\kappa k_\mathrm{B}T}{e}\sinh\left(\frac{\gamma_0}{2}\right)\left(1+\frac{1}{\kappa a}\frac{2}{\cosh^2\left(\frac{\gamma_0}{4}\right)}+\frac{1}{(\kappa a)^2}\frac{8\ln\left(\cosh\left(\frac{\gamma_0}{4}\right)\right)}{\sinh^2\left(\frac{\gamma_0}{2}\right)}\right)^{0.5} \quad (6\text{-}10)$$

6.2.2 Potentiometric acid-base titration

The potentiometric acid-base titration also enables the determination of particle charges. Based on the work of Masini et al.,[45] Alves et al. have provided a procedure for the quantitative analysis of titration curves. It essentially considers the neutralization of one strong acid and N weak acids of different acid strengths with a strong base. The implicit function given in eq 6-11 is an integral part of the non-linear regression analysis of the titration curve.[24]

$$f(V, c_{\mathrm{H}^+}) = \left(V - V_{\mathrm{HA}_0}\right)c_\mathrm{B} + \left(c_{\mathrm{H}^+} - \frac{K_\mathrm{w}}{c_{\mathrm{H}^+}}\right)(V_0 - V) - \sum_{n=1}^{N}\left(V_{\mathrm{HA}_\mathrm{n}} - V_{\mathrm{HA}_{\mathrm{n}-1}}\right)c_\mathrm{B}\frac{K_{\mathrm{HA}_\mathrm{n}}}{K_{\mathrm{HA}_\mathrm{n}} + c_{\mathrm{H}^+}} \quad (6\text{-}11)$$

It involves several quantities and parameters, such as the initial volume V_0 of the solution to be titrated, the volume V of the added base, its concentration c_B and the ionization constant K_w of water. The equivalence volumes of the strongly acidic (V_{HA_0}) and the N weakly acidic groups (V_{HA_n}) as well as their corresponding dissociation constants K_{HA_n} can be determined, since they are related to the measured proton concentrations c_{H^+} of the titrated system.

The knowledge of these equivalence volumes and of the corresponding polymer mass m_p enables the calculation of the specific particle charge Q_tit.

$$Q_\mathrm{tit} = Q_{\mathrm{tit,0}} + \sum_{n=1}^{N} Q_{\mathrm{tit,n}} = \left(V_{\mathrm{HA}_0} + \sum_{n=1}^{N} V_{\mathrm{HA}_\mathrm{n}}\right)c_\mathrm{B}F/m_\mathrm{p} \quad (6\text{-}12)$$

Taking the particle radius a and the density of the polymer ρ_p into account, the surface charge density σ_0^{tit} based on the titration experiment can finally be calculated.

$$\sigma_0^{\mathrm{tit}} = Q_\mathrm{tit}\frac{\rho_\mathrm{p}\,a}{3} \quad (6\text{-}13)$$

The equations 6-10 and 6-13 now allow a comparison of charge values determined using independent measurement methods.

6.2.3 Dispersion stability

The stability of colloidal dispersions is often described by the renowned DLVO theory, which is based on the sum of the repulsive electrostatic interaction energy V_R and the attractive van der Waals interaction energy V_A.[25,27] Sader et. al developed an analytical expression (eq 6-14) for the repulsive interaction energy of two identical spherical particles with constant surface potentials as a function of the separation distance H. It is accurate for moderate to high surface potentials, large κa as well as all κH.[46]

$$V_\mathrm{R}(H) = 4\pi\varepsilon_\mathrm{r}\varepsilon_0\left(\frac{RT}{F}\right)^2\Upsilon^2\frac{a^2}{2a+H}\ln\left(1+\exp(-\kappa H)\right) \quad (6\text{-}14)$$

Here, the function Υ includes the scaled surface potential according to equation 6-9.

$$\Upsilon(H) = 4\,\exp\left(\frac{\kappa H}{2}\right)\tanh^{-1}\left(\exp\left(-\frac{\kappa H}{2}\right)\tanh\left(\frac{y_0}{4}\right)\right) \quad (6\text{-}15)$$

An analytical expression for the attractive van der Waals interaction energy of two spherical particles was given by Hamaker (eq 6-16). The influence of the dispersed material (index 1) and the dispersant (index 3) is included in the Hamaker constant A_{131}.[26]

$$V_\mathrm{A}(H) = -\frac{A_{131}}{6}\left(\frac{2a^2}{(2a+H)^2-4a^2}+\frac{2a^2}{(2a+H)^2}+\ln\left(1-\frac{4a^2}{(2a+H)^2}\right)\right) \quad (6\text{-}16)$$

In terms of DLVO theory, the sum of the electrostatic and the van der Waals interaction energy give the total interaction energy V_T. Nevertheless, recent studies have suggested to extend the DLVO theory (so-called XDLVO theory) by including an additional interaction term V_h (eq 6-17).[28–31,47]

$$V_T = V_R + V_A + V_h \tag{6-17}$$

This term is based on hydrophilic or hydrophobic interactions between the particles and the dispersion medium and can therefore be either repulsive or attractive. The existence of these interaction forces has especially been proven by force-distance measurements using AFM.[33,48,49] Israelachvili and Pashley introduced an exponential function with a pre-exponential factor C decaying with distance H to address these effects (eq 6-18).[29] The characteristic decay length λ describes the range of the interaction forces. In case of hydrophilic repulsive interactions, the factor C has a positive sign, whereas it becomes negative for hydrophobic attractive interactions.

$$V_h(H) = a\ C \exp\left(-\frac{H}{\lambda}\right) \tag{6-18}$$

If the repulsive interaction energies are sufficiently stronger than the attractive interaction energies, an energy barrier $V_{T,max}$ at a certain distance H_{max} to the particle surface results. Depending on the magnitude of this barrier, kinetically stable dispersions can be obtained. Since eqs 6-14 and 6-15 depend on the ionic strength, electrostatically stabilized dispersions can be destabilized by increasing the electrolyte concentration. The concentration at which the energy barrier ceases to exist is referred to as the critical coagulation concentration (ccc).

Based on the values determined for the ccc and the surface potential, two unknowns can be calculated by simultaneously solving equations $V_T = 0$ and $dV_T/dH = 0$. One of them is necessarily the distance of the energy barrier H_{max}. The other one is the Hamaker constant, which can be obtained by means of DLVO theory using eqs 6-14 to 6-16. Since all other interactions that may be present in the system are consequently treated as van der Waals forces, it is best to refer to the characteristic parameter as the apparent Hamaker constant A_{131}^{app}.

An alternative approach to determine the Hamaker constant involves the van Oss-Chaudhury-Good (vOCG) theory.[28,31,36] It is based on contact angle measurements of the material with apolar test liquids and uses the Good-Girifalco-Fowkes equation (eq 6-19) with the apolar surface tension component of the liquid γ_L^{LW} and the material γ_S^{LW}, respectively.[50–52] γ_S^{LW} in turn is related to the Hamaker constant A_{131}^{vOCG} (eq 6-20).

$$1 + \cos\theta = 2\sqrt{\frac{\gamma_S^{LW}}{\gamma_L^{LW}}} \tag{6-19}$$

$$A_{131}^{vOCG} = \left(\sqrt{1.8585 \cdot 10^{-21}\ \gamma_S^{LW}} - \sqrt{3.7 \cdot 10^{-20}}\right)^2 \tag{6-20}$$

Knowledge of this Hamaker constant A_{131}^{vOCG} and assuming a reasonable value for the decay constant λ offers the opportunity to estimate the pre-exponential factor C by simultaneously solving the equations $V_T = 0$ and $dV_T/dH = 0$ on the basis of equations 6-14 to 6-18.

6.3 Experimental

6.3.1 Materials

Polycarbonate (PC; Desmophen C2102, $M_n \sim 1060\ g\ mol^{-1}$, OH value of dehydrated polyol: 105.8 mg KOH/g) and polyester diols (PE; Desmophen PE90B, $M_n \sim 1011\ g\ mol^{-1}$, OH value of dehydrated polyol: 111.0 mg KOH/g) and dimethylolpropionic acid (DMPA) were kindly supplied by

Covestro AG. Polytetrahydrofurane diol (PTHF; M_n~984 g mol^{-1}, OH value of dehydrated polyol: 112.0 mg KOH/g), isophorone diisocynate (IPDI), 1,4-butanediol (BDO), triethylamine (TEA), isophorone diamine (IPDA), dibutyltin dilaurate (DBTL), Amberlite IRN-77 and Amberlite IRA900 were purchased from Merck KGaA. Acetone, 0.1 M standard solutions of hydrochloric acid, sodium hydroxide, potassium nitrate and magnesium nitrate were purchased from Fisher Scientific. Triton X-165 was purchased from Sigma Aldrich. Ultrapure water was used for every sample preparation.

6.3.2 Synthesis of PUDs

The acetone process[20] was used to synthesize a series of PUDs with different polyol components and varying DMPA mass fractions (see Table 6-1). To reliably control the intended NCO/OH ratio of 1.7, the OH values of the dehydrated polyols were determined by the p-toluenesulfonyl isocyanate (TSI) method in accordance with DIN EN 15168:2006.[53] Changes in the DMPA content were balanced by an equivalent adjustment of the BDO content. The degree of chain extension (i.e., degree of conversion of the NCO groups remaining after prepolymerization) was adjusted to 92% by adding an appropriate amount of IPDA.

Prior to each synthesis, the polyol components were dehydrated at 100 °C and 200 mbar in a 500 mL round bottom four-necked flask equipped with a thermometer and blade stirrer. The required quantities of DMPA and BDO were then added to the polyol component under a nitrogen atmosphere. DBTL was added to the reaction system after homogenisation at 70 °C under continuous stirring at 70 rpm. The prepolymerization step was then started by dropwise addition of IPDI using a dropping funnel. After complete addition, the reaction temperature was raised to 100 °C.

Table 6-1: Synthesis series of water-based PUDs with different polyol components and varying DMPA content.[a]

Sample	PolyTHF	PE	PC	DMPA	BDO	IPDI	Acetone	TEA	IPDA	Water
PTHF3.0	24.20	/	/	1.49	0.88	17.00	77.5	1.12	4.93	115.8
PTHF3.5	24.20	/	/	1.75	0.71	17.00	77.6	1.32	4.93	116.4
PTHF4.0	24.20	/	/	2.01	0.53	17.00	77.8	1.51	4.93	117.1
PTHF4.5	24.20	/	/	2.27	0.35	17.00	77.9	1.71	4.93	117.8
PTHF5.0	24.20	/	/	2.54	0.17	17.00	78.1	1.92	4.93	118.4
PE3.0	/	24.20	/	1.49	0.90	17.00	77.5	1.12	4.93	115.8
PE3.5	/	24.20	/	1.75	0.72	17.00	77.6	1.32	4.93	116.5
PE4.0	/	24.20	/	2.01	0.55	17.00	77.8	1.51	4.93	117.1
PE4.5	/	24.20	/	2.27	0.37	17.00	77.9	1.71	4.93	117.8
PE5.0	/	24.20	/	2.54	0.19	17.00	78.3	1.92	4.93	118.5
PC3.5	/	/	24.20	1.75	0.82	17.00	77.8	1.32	4.93	116.7
PC4.0	/	/	24.20	2.01	0.65	17.00	78.0	1.52	4.93	117.4
PC4.5	/	/	24.20	2.28	0.47	17.00	78.1	1.72	4.93	118.1
PC5.0	/	/	24.20	2.54	0.29	17.00	78.3	1.92	4.93	118.7

[a] All weights are given in grams. Polytetrahydrofurane (PTHF), Polyester (PE) and Polycarbonate (PC) diol with the mass fraction of DMPA for each dispersion indicated in the sample identifier by the number following the polyol component. Intended constraints: ratio NCO/OH=1.7, degree of chain extension = 92%, and solid content of approx. 30 wt %. Note: The actual amounts of chain extender, TEA and water used had to be adjusted to account for the prepolymer mass taken for determining the NCO content.

The NCO content was determined by standard dibutylamine back-titration according to DIN EN ISO 14896:2009 to monitor the progress of the reaction.[54] The reaction mixture was cooled to 80 °C once the target NCO content, based on the desired NCO/OH ratio, had been reached (typical reaction time ~1.5 h). Acetone was added dropwise through a dropping funnel at approximately 2 ml min^{-1}. When the prepolymer had completely dissolved, the temperature was lowered to 40°C, and an equivalent molar amount of TEA, solved in a 10-fold amount of acetone, was added for neutralization. After 30 min, the chain extension step was initiated by dropwise addition of an aqueous solution of IPDA using a dropping funnel. The reaction was carried out for 30 minutes. Secondary dispersion was achieved by continuous addition of water using a KDS Legato 110 single syringe pump (dosing rate 2.3 ml min^{-1}) at 40 °C. The stirring speed was kept at 350 rpm. Finally, acetone was removed by distillation at 40 °C and 200 mbar.

6.3.3 Particle Size distribution and electrophoretic mobility

A Malvern Zetasizer Nano ZS equipped with a 632.8 nm He-laser was used to determine particle size and electrophoretic mobility at 25 °C. Particle size was measured at 173° backscatter detection at a concentration of 0.0001 wt % and given as the *z*-average value. Electrophoretic mobility was analyzed at 0.1 wt % as a function of ionic strength (KNO_3) using DTS 1070 folded capillary cells, with the signal detected at 17° front scatter detection. Multiple measurements were done for each determination. Due to the pH sensitivity of the carboxyl groups, the pH was adjusted to pH 10.4 using a sodium carbonate/bicarbonate buffer with a concentration of 2 mM to ensure complete dissociation. A detailed description of the measurement parameters can be found in a previous study.[9]

6.3.4 Potentiometric titration

A Metrohm Ti-Touch 916 titrator was employed for the potentiometric acid-base titrations using a linear step size of 0.05 mL. The next dosing step was initiated as soon as the signal drift fell below 15 mV/min, but no later than 180 seconds. The measuring cell was blanketed with nitrogen to prevent the absorption of carbon dioxide. Samples were prepared at a concentration of 5 wt % in a solution of 3 vol% Triton X-165 and treated with a strongly basic ion-exchange resin Amberlite IRA900 followed by a strongly acidic ion-exchange resin Amberlite IRN-77 for 1 h each for purification and protonation purposes prior to titration. The addition of Triton X-165 was necessary to ensure sufficient dispersion stability in the presence of the protonated carboxylate groups following ion-exchange treatment.[55]

Following a procedure described by McCann, the ion-exchange resin was purified and activated.[56] The resin was washed with pre-heated water (> 80 °C) and then washed three times with methanol. For the purpose of activation, the pH value was shifted several times by alternately using 3 M HCl and 3 M NaOH. After each activation cycle, the pH was neutralized by repeated washing with ultrapure water. This preconditioned ion-exchange resin was used to treat the PUD samples and subsequently separated again by filtration. For further evaluation, the total solids content of the dispersion was determined after the ion-exchange treatment. Finally, the potentiometric titration experiment consisted out of two measurements. First, a blank titration consisting of 5 mL 0.02 M HCl and 70 mL ultrapure water being titrated with 0.02 M NaOH. Second, a sample titration consisting of 10 mL 5 wt % sample, 5 mL 0.02 M HCl and 60 mL ultrapure water. The difference in volume equivalence between the two measurements corresponds to the content of acidic groups of the polymer. The titration curves were further evaluated using the model function of Alves et al.[24]

6.3.5 Critical coagulation concentration

The method of Reerink and Overbeek was used to determine the critical coagulation concentration.[57] The change in absorbance *A* was measured for 30 s at 0.1 s intervals in PMMA cuvettes using a UV/Vis spectrophotometer Evolution 220 (ThermoScientific) operating at a wavelength of 500 nm. Blank measurements were made with ultrapure water. Each sample was measured at 0.075 wt % and sodium

chloride (NaCl) was used as electrolyte in a concentration range of 0.5 – 4.5 mol L^{-1} in the final dispersion. Sample and electrolyte solution were mixed immediately prior to measurement. By measuring at different electrolyte concentrations c, a series of curves was obtained for each sample and the initial slope $\mathrm{d}A/\mathrm{d}t$ of each curve was determined. The logarithmic reciprocal $\log(\mathrm{d}t/\mathrm{d}A)$ was then plotted against $\log(c)$. The values obtained decrease with increasing electrolyte concentration in the slow coagulation regime, while they remain constant in the fast coagulation regime. The intercept of the two sections gives the critical coagulation concentration. An example of the evaluation is described in detail in the Supporting Information.

6.3.6 Contact angle measurements

Static contact angles were measured using the Contact Angle System OCA (Dataphysics) in accordance to DIN EN ISO 19403-2:2024.[58] Diiodomethane (γ_L: 50.8 mN m^{-1}, γ_L^{LW}: 50.8 mN m^{-1}, γ_L^{AB}: 0 mN m^{-1}) was used as test liquid.[28] At least six contact angles were measured 15 s after dripping a volume of 3 µL at different points on the polyurethane film. The contact angles were evaluated using the Young-Laplace equation.

Polyurethane films were prepared on glass substrate with a wet film thickness of 200 µm. They were dried at 80°C and stored at a constant relative humidity of approximately 50 % over a saturated magnesium nitrate solution at room temperature for at least 16 h before measurement.

6.4 Results and Discussion

The aim of this study is to identify the dissociation behaviour of carboxyl groups incorporated within the polymer backbone and thus their influence on the particle charge and correspondingly on the dispersion stability. For this reason, PUDs with different polyol components but similar molecular weight were synthesized. The DMPA content was adjusted between 3.0 and 5.0 wt %.

6.4.1 Particle size

The influence of the DMPA content and the polyol component on the particle diameter $2a$ was analyzed by dynamic light scattering and the results are shown in Table 6-2. In all synthesis series investigated, an eventually asymptotic reduction in particle size is observed with increasing DMPA content, starting at 140 nm (3.0 wt % PTHF and PE) and 120 nm (3.5 wt % PC) and reaching a value of approximately 40 nm at high DMPA fractions. The lower threshold fraction of DMPA is found to be 3.5 wt % for PC and 3.0 wt % for PTHF and PE series. Any further reduction in DMPA content resulted in destabilization of the dispersions, as evidenced by rapid sedimentation of coagulated particles.

The observed reduction in particle size can be attributed to the increase in DMPA content and consequently the greater number of charges, which enables the stabilization of a larger interfacial area. Correspondingly, the particle size decreases. In a previous study, we found a similar behaviour of PUDs based on the same polyol components but stabilized by sulfonate groups.[9] The minimum mass fraction required to obtain stable dispersions, was also found to be in the range of 3.0 to 3.5 wt % AAS, which is in line with expectations, since the remaining polymer composition was kept unchanged. Comparable results were also reported in literature.[2,14,15,59–61] However, certain differences in the final particle size (45 – 70 nm) and the minimum content of stabilizing agent (2.5 – 4.0 wt % DMPA) are evident. This indicates that the particle formation cannot solely be attributed to the number of charges, but is also influenced by the total PUD composition.

6.4.2 Particle charge analysis

Since this study focuses on dispersions that are electrostatically stabilized by carboxylates, the pH-dependence of the particle charge is of great importance. For further insights into the dissociation

behaviour of the surface functional groups, the potentiometric titration data were fitted with nonlinear regression based on eq 6-11. A detailed description of the MATLAB code for this procedure is described elsewhere.[24] It is possible to fit the titration curve by varying the number n of weak acidic groups along with their volume equivalence V_{HA_n} and their acid strength $\mathrm{p}K_\mathrm{a}$. Figure 6-1 a and b provide exemplary diagrams illustrating the influence of one ($n = 1$) and two ($n = 2$) weak acidic groups. Both diagrams display the equivalence point of the strong acid HCl (V_{HA_0}), which was consistently set at 5 mL according to the titration procedure. It becomes evident that considering just one additional weak acidic group (Figure 6-1 a, $n = 1$) is insufficient to describe the experimental results. A better description of our findings could be achieved by introducing another weak acidic group (Figure 6-1 b, $n = 2$). A further increase in the number of considered weak acidic groups would naturally lead to even lower residuals, but does not substantially improve the accuracy. If the measurement error is also taken into account, it becomes reasonable to carry out the modelling with just two weak acidic groups of different acid strength. The results for all PUDs investigated are shown in Table 6-2.

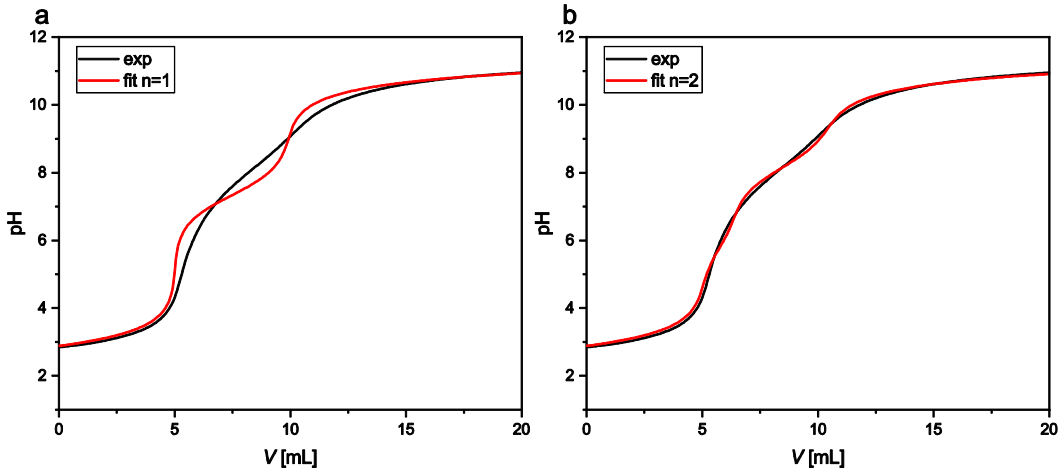

Figure 6-1: Example for the fitting results of the experimental potentiometric titration curve of PTHF 4.5 wt% DMPA (solid black line) with a) one weak acidic group $n = 1$ and b) two weak acidic groups $n = 2$ (solid red lines).

Based on the determined equivalence points V_{HA_n}, the specific particle charge Q_{tit} can be calculated with respect to the used mass of polymer. Furthermore, it is possible to calculate the recovery rate RR, because the maximum amount of charges Q_{max} is known from the synthesis recipe. RR is given by the ratio $RR = \frac{Q_{\mathrm{tit}}}{Q_{\mathrm{max}}}$.

Table 6-2: Characteristic parameters based on titration experiments for all PTHF-, PE- and PC-based PUDs [a]

Sample	$2a$ [nm]	$Q_{\mathrm{tit,1}}$ [C/g]	$Q_{\mathrm{tit,2}}$ [C/g]	Q_{tit} [C/g]	RR [%]	$\mathrm{p}K_{\mathrm{a1}}$	$\mathrm{p}K_{\mathrm{a2}}$	σ_0^{tit} [C/m^2]	σ_0^{ek} [C/m^2]
PTHF3.0	142.9	-2.8	-8,0	-10.8	50.1	5.9	8.1	-0.30	-0.025
PTHF3.5	112.4	-4.0	-10.2	-14.2	55.6	6.0	8.4	-0.33	-0.021
PTHF4.0	72.5	-4.8	-13.9	-18.7	63.3	5.8	8.1	-0.27	-0.017
PTHF4.5	53.4	-5.2	-16.2	-21.4	63.1	5.7	8.1	-0.23	-0.019
PTHF5.0	45.5	-6.3	-19.4	-25.8	69.9	6.0	8.2	-0.25	-0.017
PE3.0	144.9	-3.5	-8.9	-12.4	57.6	6.4	8.8	-0.33	-0.025

PE3.5	58.4	-3.7	-10.8	-14.5	57.6	6.0	8.4	-0.16	-0.021
PE4.0	46.4	-5.7	-13.9	-19.6	68.3	6.1	8.4	-0.17	-0.019
PE4.5	44.5	-5.4	-17.4	-22.9	70.6	5.9	8.2	-0.19	-0.018
PE5.0	36.8	-6.6	-20.3	-26.9	74.3	5.9	8.2	-0.20	-0.019
PC3.5	119.7	-2.9	-10.4	-13.2	54.8	5.9	8.2	-0.29	-0.018
PC4.0	74.0	-3.5	-12.3	-15.8	55.0	5.8	8.2	-0.21	-0.019
PC4.5	41.2	-4.8	-14.6	-19.4	57.0	5.7	8.2	-0.15	-0.020
PC5.0	41.5	-5.2	-19.0	-24.2	67.9	5.6	8.2	-0.18	-0.019

[a] Particle diameter $2a$ and polydispersity index PDI determined by dynamic light scattering. Specific particle charge $Q_{\mathrm{tit},1}$ and $Q_{\mathrm{tit},2}$ related to the first and second equivalence point and the total specific particle charge Q_{tit}. Recovery rate RR, dissociation constant $\mathrm{p}K_{\mathrm{a}1}$ and $\mathrm{p}K_{\mathrm{a}2}$ of the first and second inflection point. Surface charge density σ_0^{tit} determined by titration and surface charge density σ_0^{ek} based on electrokinetic data.

As the DMPA content increases, the specific particle charge Q_{tit} also increases, in line with expectations due to the rising number of carboxyl groups in the system. Furthermore, comparable results are found for all series indicating that the polyol component does not have a major effect on particle charge. Besides, the surface charge densities σ_0^{tit} show decreasing values with increasing DMPA content. This effect becomes comprehensible if the trend in particle sizes and the corresponding increase in specific surface area is taken into account as well.

While the aforementioned findings essentially correspond to expectations, it should be noted that not all charges of the incorporated carboxyl groups are found by titration experiments. This is evident as the recovery rate RR in all series ranges between 50 % and 75 %, despite DMPA being fully neutralized during synthesis. It implies that parts of the carboxyl groups must be hidden inside the polymer matrix and are therefore not accessible to the ion-exchange pre-treatment. Similar findings were already obtained in our previous study concerning PUDs with sulfonate groups (AAS). In this case, however, a higher recovery rate of approximately 70 to 85 % was observed.[9]

In this context, a careful analysis of the acid strength and the equivalent volumes of the hypothesized two acid groups provides further insights into the charge structure of the PUD particles. The two dissociation constants of the carboxyl groups determined (cf. Table 6-2), $\mathrm{p}K_{\mathrm{a}1}$ and $\mathrm{p}K_{\mathrm{a}2}$) are significantly lower than the corresponding dissociation constant of the monomeric DMPA molecule ($\mathrm{p}K_{\mathrm{a}}$ value of 4.41), similar to the dissociation constants found for AAS-stabilised PUDs. Consequently, this indicates that the dissociation of the acid groups integrated into the polymer backbone is hampered.

Comparable results to our $\mathrm{p}K_{\mathrm{a}1}$ values have already been found in former studies. For instance, Stone-Masui and Watillon extensively investigated the particle charge of monodisperse latices stabilized by surfactants.[19] Their study also employed potentiometric acid-base titration. For potassium stearate, they found $\mathrm{p}K_{\mathrm{a}}$ values in the range of 6.7 to 8.7 depending on the added electrolyte concentration, which are much higher than the corresponding value of stearic acid itself ($\mathrm{p}K_{\mathrm{a}}$ value of 4.8[19]). They explained it by electrostatic interactions with neighbouring charged groups at the particle surface. Consequently, additional work is required to remove the protons and the dissociation of the carboxyl groups effectively decreases.

In case of PUDs, the carboxyl groups are fixed in the polymer backbone. It is therefore very likely that not all groups can rearrange themselves on the particle surface during the secondary dispersion step. As a result, some of them will be located inside the polymer matrix, meaning that their dissociation is additionally affected or in some cases is no longer possible at all. On the one hand, this explains the recovery rate, which is well below 100 %. On the other hand, the need to include at least one additional,

weaker acid group in the fit of the titration curve becomes comprehensible. However, it should be kept in mind that these carboxyl groups inside the polymer matrix probably do not have a uniform pK_{a2} value, but rather a distribution of values depending on their actual position within the particle.

Additional information on the charge structure of the particles can be obtained by comparing the equivalence points of the hypothesized two acid groups. In case of DMPA as intrinsic stabiliser, merely about 25 % of the total specific charge content Q_{tit} is detected at the first equivalence point, characterised by pK_{a1}. Accordingly, the vast majority of the charges (approx. 75 %) are located inside the particle. This result is contrary to what we have previously observed for PUDs stabilised by AAS. It was found that about 85 % of the specific particle charge is detected at the first equivalence point, i.e. near the particle surface, and only 15 % at the second equivalence point.[9]

At first sight, a possible explanation for this considerable discrepancy could be due to the different acid strength of the carboxylic and sulfonic acid groups. However, the carboxyl groups were 100 % neutralised during synthesis by stoichiometric addition of TEA, meaning no differences in the degree of dissociation are to be expected. Instead, the charge distribution may be more affected by the synthesis protocol, since DMPA is already incorporated into the polymer backbone during the prepolymerization step. The initial polyaddition of IPDI thus proceeds by reaction with short-chain DMPA and BDO components as well as with the polyol. AAS, on the other hand, is incorporated later in the chain extension step by reaction with the NCO-terminated prepolymers, meaning that the polymer blocks located between the AAS units are of higher molecular weight and are thus larger and more flexible. When the polyurethane macromolecules dissolved in acetone are dispersed in water, they are folded and coiled. While hydrophobic segments tend to organize themselves inside the particle, hydrophilic segments are preferably located on the particle surface. However, due to the polymer constitution described above, the DMPA units cannot arrange themselves on the particle surface as easily as it is possible for the widely spaced AAS units. Accordingly, it is evident that in the potentiometric titration the higher DMPA content was determined at low acid strength, i.e. at pK_{a2}.

Based on these variations in particle structure, the differences in the recovery rates determined can now also be better understood. As already mentioned, approximately 10-20 % less charge is determined for the DMPA-stabilised PUDs compared to the AAS-stabilised variants. This outcome is in line with the finding just discussed that the titratable carboxyl groups are predominantly located within the particle. As a result, it is also quite likely that they are increasingly buried in the polymer matrix. To obtain further information on the particle charge structure, it is helpful to use other independent investigation methods. Electrokinetic measurements, for example, are particularly suitable for this purpose, especially if they are carried out at various electrolyte concentrations.

6.4.3 Electrokinetic properties

The electrophoretic mobility was measured as a function of ionic strength using KNO_3 as a symmetrical 1-1 electrolyte up to a concentration of 0.3 mol/L. Higher electrolyte concentrations could not be studied due to Joule heating of the dispersion and degradation of the electrodes. The results obtained for all PUD samples can be found in the supporting information.

An extremum at low ionic strength has been found for all PUDs investigated. It is followed by a steep decrease, caused by the compression of the diffuse double layer and the screening of the particle charges. The same behaviour was observed in our previous study for AAS-stabilised PUDs.[9] Since there were also indications of a charge distribution in a peripheral layer, the measurement data were analyzed by means of the Ohshima soft particle model.[62] However, the model did not provide plausible results at low ionic strengths. In particular, it could not explain the observed extremum, even though it takes the relaxation effect into account. Possible reasons, such as inhomogeneous charge distribution in the

peripheral layer, were discussed in detail in our previous study.[9] Nonetheless, complete data sets of the electrophoretic mobility as a function of ionic strength along with the results of nonlinear least squares fitting and an explanation of the used soft particle model of Ohshima can be found in the supporting information. In the absence of a more suitable model, the investigated PUDs are described in the following by the hard particle model, knowing that this represents certainly a simplification of the actual particle structure.

The occurrence of an extremum in the electrophoretic mobility at low ionic strength is often attributed to the relaxation effect.[63–66] For this reason, we calculated the zeta potentials based on the method of Ohshima, Healy and White using eqs 6-4 and 6-5. . In this way, plausible values are obtained, since the zeta potentials decrease monotonically with increasing electrolyte concentrations, as exemplarily shown in Figure 6-2.

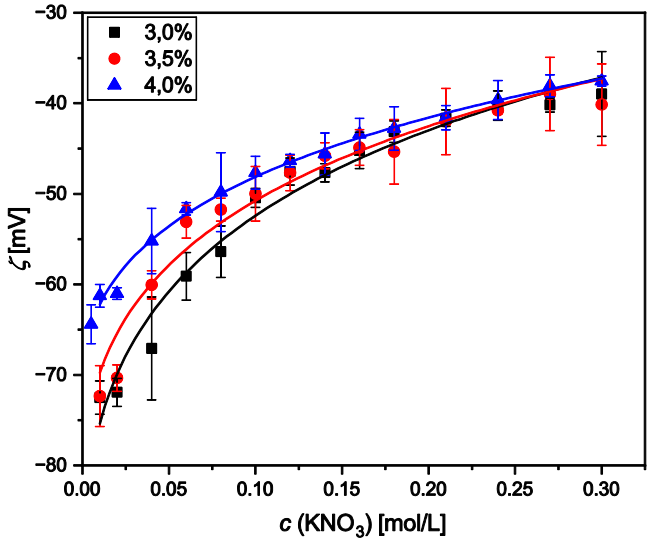

Figure 6-2: Zeta potential ζ as a function of KNO_3 concentration c for PTHF-based PUDs containing 3.0 wt-% (black), 3.5 wt-% (red) and 4.0 wt-% (blue) DMPA. The solid lines result from the fitting procedure. The solid symbols represent the average value with the error bars corresponding to their standard deviation.

When the zeta potential is determined as a function of ionic strength, it is possible to calculate the surface potential ψ_0 and the position of shear plane x_s by a least squares fitting procedure based on eqs 6-6 to 6-9 The results of the fitting procedure assuming a constant surface potential with varying ionic strength are also shown in Figure 6-2 (solid lines) Obviously, the fits agree well with the experimentally determined zeta potentials. The surface potential and the distance of the shear plane for all PUD samples are shown in Figure 6-3. Interestingly, as the charge content of the polymer increases, the surface potential decreases with increasing DMPA content from -92 mV (3.0 wt % PE and PTHF) to -73 mV (5.0 wt % PE and PTHF). This trend can be attributed to the decreasing particle size and thus the increasing specific surface area of the system. Additionally, only minor variations among the polyol components can be observed, indicating no significant impact of the polyol component on the electrokinetic properties of the PUDs.

The determined values for the distance of shear plane provide reasonable results within the range of 0.3 to 0.4 nm. Values ranging from 0.25 to 1.0 nm have also been found in literature.[63,67–71] Several studies employed 0.25 nm as the assumed position of shear plane when describing their experimentally observed electrophoretic mobility data. For instance, Behrens et al. used this value to describe the electrophoretic mobility of carboxyl latex particles.[68] Similarly, Kobayashi et al. varied the position of shear plane to describe the observed electrophoretic mobilities of polystyrene sulfate latex particles as

a function of ionic strength and found the best agreement for 0.25 nm.[70] The value of x_s represents the thickness of a hydrodynamically immobile fluid layer surrounding the particle surface. Consequently, 0.25 nm is often utilized to describe experimental results, because it approximately corresponds to the thickness of a single layer of water molecules. However, since our values are slightly larger than 0.25 nm, they suggest a small outward shift of the shear plane. This is consistent with the presumed surface structures deduced from the results of the potentiometric titration, as the charges appear to be partially arranged in a permeable surface layer.

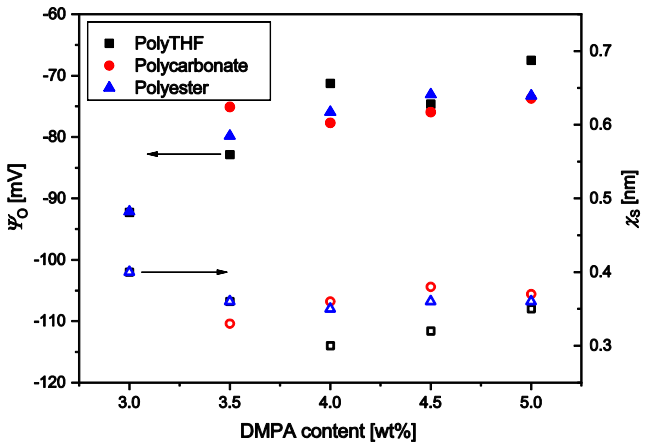

Figure 6-3: Surface potential ψ_0 (solid symbols) and distance of shear plane x_s (empty symbols) as a function of the DMPA concentration for PTHF (black), PE (blue) and PC (red) based PUD's obtained by least square fitting procedure.

To evaluate the plausibility of the determined surface potentials, we calculated the electrokinetic surface charge density σ_0^{ek} according to eq 6-10 and compared it to the surface charge density σ_0^{tit} determined by potentiometric titration. These values are presented in Table 6-2. While both values show a comparable trend, the electrokinetic surface charge densities are approximately one order of magnitude lower than the ones determined by potentiometric titration. Similar observations have been made in literature. Kobayashi et al. analyzed amidine latex particles bearing a surface charge density of 0.21 C/m^2 and studied the electrophoretic mobility as a function of ionic strength. [69] They found the electrokinetic surface charge density to be 0.032 C/m^2 and attributed the differences to a structure possibly based on a hairy or porous particle surface. Accordingly, the deviation between σ_0^{ek} and σ_0^{tit} likewise underlines the charge structure of the PUD particles assumed by us, as it indicates that the charges are not located entirely on the particle surface but rather in a surface layer.

Finally, the results determined by the evaluation of the electrokinetic properties are comparable to the results obtained for PUDs stabilized by AAS.[9] This applies to the values of the surface potential, the position of shear plane and the electrokinetic surface charge density. Accordingly, the discussed differences in the charge arrangement at the particle surface have no decisive influence on the electrokinetic properties at all. However, since charge quantities and charge localisation can have a significant influence on the dispersion stability, it is examined in more detail in the following chapter.

6.4.4 Dispersion stability

Proper addition of electrolyte to a colloidal dispersion system can lead to coagulation of electrostatically stabilised dispersions. We studied this behaviour by performing time-resolved absorbance measurements at different ionic strengths. The critical coagulation concentrations (ccc) determined in this way are plotted in Figure 6-4 for all samples.

The ccc of PTHF-based PUDs increases from roughly 1.0 M (3.0 wt % DMPA) to 1.25 M (5.0 wt % DMPA) and in the case of PE-based PUDs from 1.3 M (3.0 wt % DMPA) to 1.7 M (5.0 wt % DMPA).

It is noteworthy that the observed dispersion stability of the PC-based PUDs significantly surpasses the stability of PTHF- and PE-based PUDs with values rising from 2.9 M (3.5 wt % DMPA) to 3.3 M (5.0 wt % DMPA). These results align again with the findings of our previous study, which dealt with the analysis of the dispersion stability of PUDs stabilized by sulfonate groups.

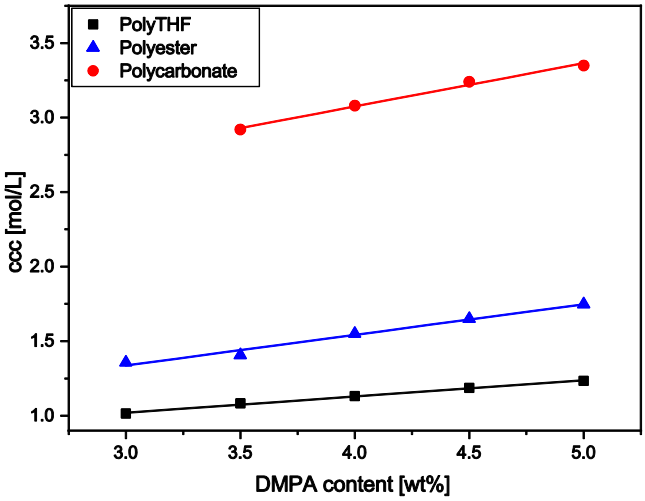

Figure 6-4: Critical coagulation concentration ccc as a function of the DMPA content for PTHF (black), PE (blue) and PC (red) based PUDs. Solid lines are a guide to the eye.

Two factors obviously influence the dispersion stability. On the one hand, the stability to electrolyte addition increases slightly with increasing DMPA content. On the other hand, the polyol component leads to strong differences that clearly exceeds those associated with the DMPA content. To analyse the various factors influencing dispersion stability in more detail, it is recommended to apply the DLVO and XDLVO theory, respectively.

6.4.5 Interaction energies

To gain further insights into the experimentally determined differences of dispersion stability, we started with an analysis of the repulsive V_R and attractive interaction energies V_A according to DLVO theory. The repulsive electrostatic interaction energy V_R can be calculated as a function of the separation distance H according to eqs 6-14 and 6-15. It is primarily influenced by the surface potential Ψ_0 (cf. Figure 6-3) and the particle radius a (cf. Table 6-2). The attractive van der Waals interaction energy can be described with equation 6-16. If the ccc value is known, the apparent Hamaker constant A_{131}^{app} can be calculated by simultaneously solving $V_T = V_R + V_A = 0$ and $dV_T/dH = 0$. The values obtained are remarkably high ranging from $1.4 \cdot 10^{-20}$ to $3.2 \cdot 10^{-20}$ J (cf. supporting information). Typical values for aqueous polymer dispersions are known to be about $0.4 \cdot 10^{-20}$ to $1.2 \cdot 10^{-20}$ J.[72] In addition, another important observation is that the Hamaker constants A_{131}^{app} in each PUD series actually decrease with increasing DMPA content. Since the general composition of our PUDs is kept constant and changes are solely done by varying the amount of DMPA with BDO, only slight variations of the Hamaker constant are to be expected. These outcomes are once again in line with our previous study.

Due to these inconsistencies, we have also applied an alternative approach suggested by van Oss et al.[28] It is essentially based on contact angle measurements using an apolar test liquid and the Hamaker constant A_{131}^{vOCG} is related to the apolar surface tension component of the material γ_S^{LW} (cf. eqs 6-19 and 6-20). Contact angles and calculated values of γ_S^{LW} are shown in the supporting information and the results of A_{131}^{vOCG} are illustrated in Figure 6-5.

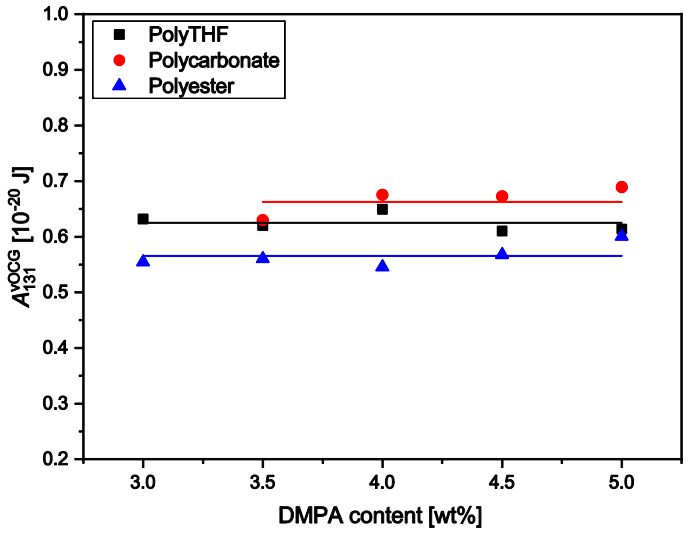

Figure 6-5: Hamaker constant A_{131}^{vOCG} as a function of the DMPA content for PTHF (black), PE (blue) and PC (red) based PUDs. Values are based on contact angle data. Solid lines refer to the average value for each PUD series.

Hamaker constants A_{131}^{vOCG} range from $0.56 \cdot 10^{-20}$ (PE-based PUDs) to $0.66 \cdot 10^{-20}$ J (PC-based PUDs) and correspond well to typical values for aqueous polymer dispersions given in literature.[30,56,73,74] Moreover, they show only slight variations within each series as expected due to the nearly constant polymer composition. Consequently, Hamaker constants A_{131}^{vOCG} can be considered to be more reasonable than the A_{131}^{app} values.

However, it is important to note that the accuracy of these values should not be overestimated, since the measurement of contact angles is very sensitive to various influences, e.g. surface roughness.[75] For PUDs stabilized by sulfonate groups, we found Hamaker constants A_{131}^{vOCG} to be approximately $0.4 \cdot 10^{-20}$ J for PE-, $0.5 \cdot 10^{-20}$ J for PC- and $0.7 \cdot 10^{-20}$ J for PTHF-based PUDs. [10] These values do not exactly match the values determined for DMPA-stabilized PUDs in this study. They also show a different trend between the individual polyol series. It is therefore best to average the determined Hamaker constants A_{131}^{vOCG} of all PUDs in our studies and continue the further analyses with a uniform Hamaker constant $\overline{A_{131}^{\mathrm{vOCG}}}$ of approximately $0.6 \cdot 10^{-20}$ J.

Since the DLVO theory cannot coherently explain the experimentally observed dispersion stabilities, the so-called extended DLVO (XDLVO) theory might be a useful approach. Especially, as the apparent Hamaker constants A_{131}^{app} are too high, it makes sense to consider an additional attractive force that is due to the hydrophobicity of the polymer. The corresponding interaction energy can be calculated with eq 6-18. Here, we decided to use a value for the decay length λ of 0.3 nm, which is well-known from the literature.[10,34] By applying eqs 6-14 to 6-18 and taking the conditions $V_{\mathrm{T}} = 0$ and $\mathrm{d}V_{\mathrm{T}}/\mathrm{d}H = 0$ into account, it is possible to estimate the pre-exponential factor C, which is a key indicator for the hydrophobic interaction.

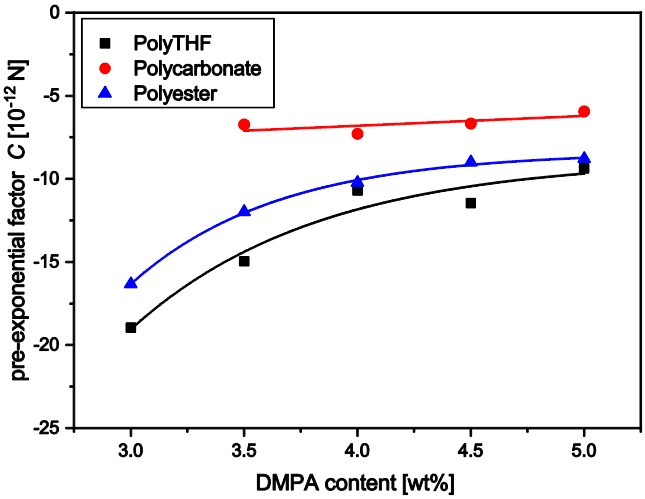

Figure 6-6: Pre-exponential factor C as a function of the DMPA content for PTHF (black), PE (blue) and PC (red) based PUDs. Values are calculated according to XDLVO theory. Solid lines are a guide to the eye.

Our results are presented in Figure 6-6 and in Table S3 in the supporting information (for comparison purposes, the pre-exponential factors calculated for a decay length of 0.4 nm are also listed there). Among the different dispersion series, PTHF-based PUDs exhibit the most hydrophobic behaviour, followed by PE-based PUDs, while PC-based PUDs are the least hydrophobic. Furthermore, it becomes evident that the incorporation of hydrophilic carboxylate groups lowers the hydrophobicity of the polymer. Although the exact mechanism is not yet fully understood, it is currently assumed that the attractive hydrophobic effect results from perturbations in the arrangement of water molecules near the interface. These water molecules adopt a specific orientation leading to a loss of conformational entropy and hydrogen bonds. This situation represents an energetically unfavourable state, which can be reduced by the aggregation of particles, as the interface area becomes smaller.[30,76] Accordingly, the observed stability of our aqueous PUDs can be properly understood if not only the electrostatic and van der Waals interaction but also the hydrophobicity of the polymers is taken into account. This conclusion is further supported by the fact that we obtained comparable results for the PUDs stabilised with sulfonate groups in our previous study.[10]

6.5 Conclusion

In this study, we performed a detailed charge analysis of polyurethane dispersions (PUDs), which were intrinsically stabilized by the carboxylic acid DMPA incorporated into the polymer backbone. The interpretation of the potentiometric acid-base titration data revealed the necessity to consider at least two different weak acidic groups. The corresponding pK_a values are much higher than the one of monomeric DMPA. Consequently, the dissociation of the incorporated acidic groups is impeded. The analysis of the total charge quantities further revealed that 25-50 % of the total amount of carboxyl groups could not be determined at all. Accordingly, a considerable proportion of the functional groups cannot dissociate because they are presumably buried in the polymer matrix. Moreover, we found that about 75 % of the detectable charges tend to be located inside the polymer matrix, whereas only 25 % are arranged at the particle surface. This is in contrast to a former study of sulfonate-stabilised PUDs, in which the majority of the charges were detectable and were found particularly near the particle exterior. Accordingly, the influence of the synthesis protocol becomes apparent, since DMPA, unlike the sulfonate groups, is incorporated early on during the prepolymerization step. This leads to the important conclusion for PUD chemistry that the incorporation of hydrophilic functional groups should preferably take place in the final chain extension step.

Potentiometric titration has provided clear indications of charge distribution in a peripheral polymer layer. Nevertheless, the dependency of the electrophoretic mobility on the electrolyte concentration could not be adequately explained using the soft particle model of Ohshima. However, the assumption of a hard particle with charges located on the particle surface was far more successful and we obtained plausible values for an effective surface potential and the distance of the shear plane. Our study has also shown that the influence of increasing DMPA content on the critical coagulation concentration (i.e. dispersion stability) is surprisingly low, while the impact of the polyol component proved to be much stronger. Evaluations according to DLVO and XDLVO theory revealed the need to extend the DLVO approach by considering an additional attractive interaction parameter, which is probably based on the hydrophobicity of the polymer components. The findings of this study can therefore make a valuable contribution to the design and optimization of PU dispersion synthesis.

Author information

Corresponding Author

J. Wilkens − *Faculty of Applied Natural Sciences, TH Köln_ University of Applied Science, Leverkusen D-51379, Germany;* orcid.org/0000-0003-2831-8400;
Email: jan.wilkens@th-koeln.de

Authors

C. Grau − *Faculty of Applied Natural Sciences, TH Köln_ University of Applied Science, Leverkusen D-51379, Germany*
A. M. Schmidt − *Department of Chemistry, University of Cologne, D-50939 Cologne, Germany;* orcid.org/0000-0002-7284-7847
Complete contact information is available at: https://pubs.acs.org/doi/10.1021/acs.langmuir.6c00992

Supporting Information

The Supporting Information is available free of charge at https://pubs.acs.org/doi/10.1021/acs.langmuir.6c00992.

Supporting information on the theory of hard and soft particles; complete graphs of the measured electrophoretic mobilities, the calculated zeta potentials and the soft particle fits; exemplary description for the determination of the critical coagulation concentration; graph of the apparent Hamaker constants A_{131}^{app}, calculated on the basis of DLVO theory; contact angles for diiodomethane and apolar components of the surface tension γ_S^{LW}; values for the pre-exponential factor using a decay length of 0.3 or 0.4 nm.

Acknowledgements

This project has received fundings from the German Ministry of Education and Research (BMBF) as part of the funding program Forschung an Fachhochschulen under contract number 13FH142PX6. We are also very grateful for valuable discussions and financial and material support provided by Covestro AG. We would also like to thank J.P. de Mesquita of the Federal University of the Jequitinhonha and Mucuri Valleys for providing the MATLAB code.

Author Contributions

C. Grau: Experimental work, Methodology, Conceptualization, Data evaluation and visualization, Software, Writing – original draft. **A.M. Schmidt:** Supervision, Discussion, Writing – review and

editing. **J. Wilkens:** Supervision, Conceptualization, Methodology, Project administration, Discussion, Resources, Funding acquisition, Writing – review and editing.

Notes

The authors declare no competing financial interest.

6.6 References

(1) Kim, B. K., Lee, Y. M. Aqueous dispersion of polyurethanes containing ionic and nonionic hydrophilic segments. *J. Appl. Polym. Sci.* **1994**, *54*, 1809–1815.

(2) Lijie, H., Yongtao, D., Zhiliang, Z., Zhongsheng, S., Zhihua, S. Synergistic effect of anionic and nonionic monomers on the synthesis of high solid content waterborne polyurethane. *Colloids Surf. A: Physicochem. Eng. Asp.* **2015**, *467*, 46–56.

(3) Cao, H., Qi, F., Liu, R., Wang, F., Zhang, C., Zhang, X., Chai, Y., Zhai, L. The influence of hydrogen bonding on N-methyldiethanolamine-extended polyurethane solid–solid phase change materials for energy storage. *RSC Adv.* **2017**, *7*, 11244–11252.

(4) Chan, W.-C., Chen, S.-A. Polyurethane ionomers: effects of emulsification on properties of hexamethylene diisocyanate-based polyether polyurethane cationomers. *Polymer* **1988**, *29*, 1995–2001.

(5) Hsu, S. L., Xiao, H. X., Szmant, H. H., Frisch, K. C. Polyurethane ionomers. I. Structure–properties relationships of polyurethane ionomers. *J. Appl. Polym. Sci.* **1984**, *29*, 2467–2479.

(6) Wang, H., Shen, Y., Fei, G., Li, X., Liang, Y. Micromorphology and phase behavior of cationic polyurethane segmented copolymer modified with hydroxysilane. *J. Colloid Interface Sci.* **2008**, *324*, 36–41.

(7) Xin, H., Shen, Y., Li, X. Novel cationic polyurethane-fluorinated acrylic hybrid latexes: Synthesis, characterization and properties. *27th ECIS 2013* **2011**, *384*, 205–211.

(8) Cao, X., Ge, X., Chen, H., Li, W. Effects of trimethylol propane and AAS salt on properties of waterborne polyurethane with low gloss. *Prog. Org. Coat.* **2017**, *107*, 5–13.

(9) Grau, C., Schmidt, A. M., Wilkens, J. Water-Based Polyurethane Dispersions: A Detailed Analysis of the Particle Charge Using Soft and Hard Particle Model. *Langmuir* **2024**, *40*, 22123–22135.

(10) Grau, C., Schmidt, A. M., Wilkens, J. Water-based Polyurethane Dispersions: Analysis of the Dispersion Stability in Terms of DLVO and XDLVO Theory. *Langmuir* **2025**, *41*, 16263–16273.

(11) Barikani, M., Valipour Ebrahimi, M., Seyed Mohaghegh, S. M. Preparation and characterization of aqueous polyurethane dispersions containing ionic centers. *J. Appl. Polym. Sci.* **2007**, *104*, 3931–3937.

(12) Delpech, M. C., Coutinho, F. M. Waterborne anionic polyurethanes and poly(urethane-urea)s: influence of the chain extender on mechanical and adhesive properties. *Polym. Test.* **2000**, *19*, 939–952.

(13) Santamaria-Echart, A., Arbelaiz, A., Saralegi, A., Fernández-d'Arlas, B., Eceiza, A., Corcuera, M. Relationship between reagents molar ratio and dispersion stability and film properties of waterborne polyurethanes. *Colloids Surf. A: Physicochem. Eng. Asp.* **2015**, *482*, 554–561.

(14) Nanda, A. K., Wicks, D. A. The influence of the ionic concentration, concentration of the polymer, degree of neutralization and chain extension on aqueous polyurethane dispersions prepared by the acetone process. *Polymer* **2006**, *47*, 1805–1811.

(15) Nanda, A. K., Wicks, D. A., Madbouly, S. A., Otaigbe, J. U. Effect of ionic content, solid content, degree of neutralization, and chain extension on aqueous polyurethane dispersions prepared by prepolymer method. *J. Appl. Polym. Sci.* **2005**, *98*, 2514–2520.

(16) Fuensanta, M., Khoshnood, A., Martín-Martínez, J. M. Structure-Properties Relationship in Waterborne Poly(Urethane-Urea)s Synthesized with Dimethylolpropionic Acid (DMPA) Internal Emulsifier added before, during and after Prepolymer Formation. *Polymers* **2020**, *12*, 2478.

(17) Lee, S. K., Kim, B. K. High solid and high stability waterborne polyurethanes via ionic groups in soft segments and chain termini. *J. Colloid Interface Sci.* **2009**, *336*, 208–214.

(18) Kim, B. K., Lee, J. C. Waterborne polyurethanes and their properties. *J. Polym. Sci. A Polym. Chem.* **1996**, *34*, 1095–1104.

(19) Stone-Masui, J., Watillon, A. Characterization of surface charge on polystyrene latices. *J. Colloid Interface Sci.* **1975**, *52*, 479–503.

(20) Dieterich, D. Aqueous emulsions, dispersions and solutions of polyurethanes; synthesis and properties. *Prog. Org. Coat.* **1981**, *9*, 281–340.

(21) Saw, L. K., Brooks, B. W., Carpenter, K. J., Keight, D. V. Different dispersion regions during the phase inversion of an ionomeric polymer-water system. *J. Colloid Interface Sci.* **2003**, *257*, 163–172.

(22) Saw, L. K., Brooks, B. W., Carpenter, K. J., Keight, D. V. Catastrophic phase inversion in region II of an ionomeric polymer-water system. *J. Colloid Interface Sci.* **2004**, *279*, 235–243.

(23) Wei, Y., Luo, Y., Li, B., Li, B. Phase inversion of UV-curable anionic polyurethane in the presence of acetone solvent. *Colloid. Polym. Sci.* **2005**, *283*, 1289–1297.

(24) Alves, L. A., Castro, A. H. de, Mendonça, F. G. de, Mesquita, J. P. de. Characterization of acid functional groups of carbon dots by nonlinear regression data fitting of potentiometric titration curves. *Appl. Surf. Sci.* **2016**, *370*, 486–495.

(25) Verwey E. J. W., Overbeek J. T. G. *Theory of the Stability of Lyophobic Colloids*; Elsevier: New York, 1948.

(26) Hamaker, H. C. The London—van der Waals attraction between spherical particles. *Physica* **1937**, *4*, 1058–1072.

(27) Derjaguin, B., Landau, L. Theory of the stability of strongly charged lyophobic sols and of the adhesion of strongly charged particles in solutions of electrolytes. *Prog. Surf. Sci.* **1993**, *43*, 30–59.

(28) van Oss, C. J. Acid—base interfacial interactions in aqueous media. *Colloids Surf. A: Physicochem. Eng. Asp.* **1993**, *78*, 1–49.

(29) Israelachvili, J., Pashley, R. The hydrophobic interaction is long range, decaying exponentially with distance. *Nature* **1982**, *300*, 341–342.

(30) Israelachvili J. N. *Intermolecular and surface forces*, 3rd ed.; Elsevier/Academic Press: Amsterdam, 2012.

(31) van Oss C. J. *The properties of water and their role in colloidal and biological systems*, 1st ed.; Elsevier/Academic Press: Amsterdam, 2008.

(32) Grasso*, D., Subramaniam, K., Butkus, M., Strevett, K., Bergendahl, J. A review of non-DLVO interactions in environmental colloidal systems. *Rev. Environ. Sci. Biotechnol.* **2002**, *1*, 17–38.

(33) Butt, H.-J., Cappella, B., Kappl, M. Force measurements with the atomic force microscope: Technique, interpretation and applications. *Surf. Sci. Rep.* **2005**, *59*, 1–152.

(34) Donaldson, S. H., Røyne, A., Kristiansen, K., Rapp, M. V., Das, S., Gebbie, M. A., Lee, D. W., Stock, P., Valtiner, M., Israelachvili, J. Developing a general interaction potential for hydrophobic and hydrophilic interactions. *Langmuir* **2015**, *31*, 2051–2064.

(35) Smith, A. M., Borkovec, M., Trefalt, G. Forces between solid surfaces in aqueous electrolyte solutions. *Adv. Colloid Interface Sci.* **2020**, *275*, 102078.

(36) van Oss, C. J., Chaudhury, M. K., Good, R. J. Interfacial Lifshitz-van der Waals and polar interactions in macroscopic systems. *Chem. Rev.* **1988**, *88*, 927–941.

(37) Smoluchowski, M. v. Elektrische Endosmose und Strömungsströme. In *Handbuch der Elektrizität und des Magnetismus*; Graetz, L., Ed.; Johann Ambrosius: Barth, Leipzig, 1921; Vols. 2, pp. 366–428.

(38) Overbeek, J. Th. G. Theorie der Elektrophorese: Der Relaxationseffekt. *Kolloid-Beihefte* **1943**, *54*, 287–364.

(39) Delgado, A. V., González-Caballero, F., Hunter, R. J., Koopal, L. K., Lyklema, J. Measurement and interpretation of electrokinetic phenomena. *J. Colloid Interface Sci.* **2007**, *309*, 194–224.

(40) Ohshima, H., Healy, T. W., White, L. R. Approximate analytic expressions for the electrophoretic mobility of spherical colloidal particles and the conductivity of their dilute suspensions. *J. Chem. Soc., Faraday Trans. 2* **1983**, *79*, 1613.

(41) Ohshima, H. Approximate Analytic Expression for the Electrophoretic Mobility of a Spherical Colloidal Particle. *J. Colloid Interface Sci.* **2001**, *239*, 587–590.

(42) Frangenberg, M., Schmidt, A. M., Wilkens, J. New Experimental Approach for the Proper Consideration of Stagnant and Diffuse Layer Conductivity in the Zeta Potential Determination. *Langmuir* **2025**, *41*, 5188–5201.

(43) Ohshima, H., Healy, T. W., White, L. R. Accurate analytic expressions for the surface charge density/surface potential relationship and double-layer potential distribution for a spherical colloidal particle. *J. Colloid Interface Sci.* **1982**, *90*, 17–26.

(44) Ohshima H. *Theory of colloid and interfacial electric phenomena*, 1st ed.; Elsevier/Academic Press: Amsterdam, Boston, 2006.

(45) Masini, J. C., Godinho, O. E. S., Aleixo, L. M. Determination of ionizable groups of proteins by potentiometric titration in concentrated solutions of guanidine hydrochloride. *Fresenius J. Anal. Chem.* **1998**, *360*, 104–111.

(46) Sader, J. E., Carnie, S. L., Chan, D. Y. Accurate Analytic Formulas for the Double-Layer Interaction between Spheres. *J. Colloid Interface Sci.* **1995**, *171*, 46–54.

(47) Ducker, W. A., Mastropietro, D. Forces between extended hydrophobic solids: Is there a long-range hydrophobic force? *Curr. Opin. Colloid Interface Sci.* **2016**, *22*, 51–58.

(48) Brant, J. A., Childress, A. E. Colloidal adhesion to hydrophilic membrane surfaces. *J. Membr. Sci.* **2004**, *241*, 235–248.

(49) Moazzami-Gudarzi, M., Trefalt, G., Szilagyi, I., Maroni, P., Borkovec, M. Nanometer-ranged attraction induced by multivalent ions between similar and dissimilar surfaces probed using an atomic force microscope (AFM). *Phys. Chem. Chem. Phys.* **2016**, *18*, 8739–8751.

(50) Fowkes, F. M. Determination of interfacial tensions, contact angles and dispersion forces in surfaces by assuming additivity of intermolecular interactions in surfaces. *J. Phys. Chem.* **1962**, *66*, 382.

(51) Girifalco, L. A., Good, R. J. A Theory for the Estimation of Surface and Interfacial Energies. I. Derivation and Application to Interfacial Tension. *J. Phys. Chem.* **1957**, *61*, 904–909.

(52) Good, R. J., Girifalco, L. A. A theory for estimation of surface and interfacial energies. III. Estimation of surface energies of solids from contact angle data. *J. Phys. Chem.* **1960**, *64*, 561–565.

(53) DIN Deutsches Institut für Normung e. V. *Grenzflächenaktive Stoffe - Bestimmung der Hydroxylzahl - p-Toluolsulfonylisocyanat-(TSI-)Verfahren und potentiometrische Titration mit Tetrabutylammoniumhydroxid: Deutsche Fassung EN 15168:2006*; DIN Media GmbH: Berlin, *71.100.40*(15168:2007-02).

(54) DIN Deutsches Institut für Normung e. V. *Kunststoffe - Polyurethanrohstoffe - Bestimmung des Isocyanatanteils (ISO_14896:2009): Deutsche Fassung EN ISO 14896:2009*; DIN Media GmbH: Berlin, *83.080.20*(14896:2009-07).

(55) Lorenz, O., Breidenich, N., Denter, U., Reinmöller, K.-H., Rose, G. Bestimmung von starker neben schwacher Säure in Polyurethan-Dispersionen mit SO3- und COO -Gruppen. *Angew. Makromol. Chemie* **1982**, *103*, 159–185.

(56) Lagaly G., Schulz O., Zimehl R. *Dispersionen und Emulsionen: Eine Einführung in die Kolloidik feinverteilter Stoffe einschliesslich der Tonminerale*; Steinkopff: Darmstadt, op. 1997.

(57) Reerink, H., Overbeek, J. Th. G. The rate of coagulation as a measure of the stability of silver iodide sols. *Discuss. Faraday Soc.* **1954**, *18*, 74.

(58) DIN Deutsches Institut für Normung e. V. *Beschichtungsstoffe_- Benetzbarkeit_- Teil_2: Bestimmung der freien Oberflächenenergie fester Oberflächen durch Messung des Kontaktwinkels (ISO_19403-2:2024): Deutsche Fassung EN ISO 19403-2:2024*; DIN Media GmbH: Berlin, *87.040*(19403-2:2024-11).

(59) Bullermann, J., Friebel, S., Salthammer, T., Spohnholz, R. Novel polyurethane dispersions based on renewable raw materials—Stability studies by variations of DMPA content and degree of neutralisation. *Prog. Org. Coat.* **2013**, *76*, 609–615.

(60) Kim, C. K., Kim, B. K. IPDI-based polyurethane ionomer dispersions: Effects of ionic, nonionic hydrophilic segments, and extender on particle size and physical properties of emulsion cast film. *J. Appl. Polym. Sci.* **1991**, *43*, 2295–2301.

(61) Gündüz, G., Kısakürek, R. R. Structure–Property Study of Waterborne Polyurethane Coatings with Different Hydrophilic Contents and Polyols. *J. Dispers. Sci. Technol.* **2004**, *25*, 217–228.

(62) Ohshima, H. Electrophoretic mobility of a highly charged soft particle: Relaxation effect. *Colloids Surf. A: Physicochem. Eng. Asp.* **2011**, *376*, 72–75.

(63) Borkovec, M., Behrens, S. H., Semmler, M. Observation of the Mobility Maximum Predicted by the Standard Electrokinetic Model for Highly Charged Amidine Latex Particles. *Langmuir* **2000**, *16*, 5209–5212.

(64) Gaboriaud, F., Gee, M. L., Strugnell, R., Duval, J. F. L. Coupled electrostatic, hydrodynamic, and mechanical properties of bacterial interfaces in aqueous media. *Langmuir* **2008**, *24*, 10988–10995.

(65) Hakim, A., Nishiya, M., Kobayashi, M. Charge reversal of sulfate latex induced by hydrophobic counterion: effects of surface charge density. *Colloid. Polym. Sci.* **2016**, *294*, 1671–1678.

(66) Gomes, P. A., d'Espinose de Lacaillerie, J.-B., Lartiges, B., Maliet, M., Molinier, V., Passade-Boupat, N., Sanson, N. Microalgae as Soft Permeable Particles. *Langmuir* **2022**, *38*, 14044–14052.

(67) Antonietti, M., Vorwerg, L. Examination of the atypical electrophoretic mobility behavior of charged colloids in the low salt region using the O'Brian-White theory. *Colloid. Polym. Sci.* **1997**, *275*, 883–887.

(68) Behrens, S. H., Christl, D. I., Emmerzael, R., Schurtenberger, P., Borkovec, M. Charging and Aggregation Properties of Carboxyl Latex Particles: Experiments versus DLVO Theory. *Langmuir* **2000**, *16*, 2566–2575.

(69) Kobayashi, M., Nitanai, M., Satta, N., Adachi, Y. Coagulation and charging of latex particles in the presence of imogolite. *Colloids Surf. A: Physicochem. Eng. Asp.* **2013**, *435*, 139–146.

(70) Kobayashi, M., Sasaki, A. Electrophoretic mobility of latex spheres in mixture solutions containing mono and divalent counter ions. *Colloids Surf. A: Physicochem. Eng. Asp.* **2014**, *440*, 74–78.

(71) Kobayashi, M. Electrophoretic mobility of latex spheres in the presence of divalent ions: experiments and modeling. *Colloid. Polym. Sci.* **2008**, *286*, 935–940.

(72) Lyklema J. *Fundamentals of Interface and Colloid Science: Volume V Soft Colloids*; Elsevier/Academic Press: Amsterdam, 2005.

(73) Hough, D. B., White, L. R. The calculation of hamaker constants from liftshitz theory with applications to wetting phenomena. *Adv. Colloid Interface Sci.* **1980**, *14*, 3–41.

(74) Prieve, D. C., Russel, W. B. Simplified predictions of Hamaker constants from Lifshitz theory. *J. Colloid Interface Sci.* **1988**, *125*, 1–13.

(75) Xu, Y., Han, B., Xiao, K., Yu, J., Zheng, J., Liang, S., Wang, X., Xu, G., Huang, X. Revisiting the Surface Energy Parameters of Standard Test Liquids with a Corrected Contact Angle Method over Rough Surfaces. *Langmuir* **2022**, *38*, 10760–10767.

(76) Tabor, R. F., Grieser, F., Dagastine, R. R., Chan, D. Y. C. The hydrophobic force: measurements and methods. *Phys. Chem. Chem. Phys.* **2014**, *16*, 18065–18075.

6.7 Supporting Information

Water-based polyurethane dispersions: New insights into the intrinsic stabilisation using carboxylate groups

C. Grau [a], A. M. Schmidt [b], J. Wilkens [a]*

[a] *Faculty of Applied Natural Sciences, TH Köln – University of Applied Sciences, Leverkusen D-51379, Germany*
[b] *Department of Chemistry, University of Cologne, D-50939 Cologne, Germany*

* Corresponding author; E-Mail: jan.wilkens@th-koeln.de; Address: Campusplatz 1, D-51379 Leverkusen, Germany

Theory

Table of Contents

Hard particle model

In the main article, an approximate analytical expression (eq 6-4) was shown to describe the electrophoretic mobility μ of spherical, hard particles in a solution of symmetrical z-z electrolytes.[1] For the sake of completeness, we provide the entire set of equations involved below.

$$\mu = \mathrm{sign}(\zeta)\frac{\varepsilon_\mathrm{r}\varepsilon_0}{\eta}\left(\mathrm{abs}(\zeta)\frac{2F}{1+F}\frac{k_\mathrm{B}T}{ze}H\right) + \mathrm{sign}(\zeta)\frac{2\varepsilon_\mathrm{r}\varepsilon_0 k_\mathrm{B}T}{3\eta e}\left(\frac{1}{\kappa a}\left(-18\left(t+\frac{t^3}{9}\right)K + \frac{15F}{1+F}\left(t+\frac{7t^2}{20}+\frac{t^3}{9}\right) - 6(1+3m_\mathrm{CO})\left(1-\exp\left(-\frac{\bar{\zeta}}{2}\right)\right)G + \frac{12F}{(1+F)^2}H + \frac{9\bar{\zeta}}{1+F_1}(m_\mathrm{CO}G + m_\mathrm{C}H) - \frac{36F}{1+F}\left(m_\mathrm{CO}G^2 + \frac{m_\mathrm{C}}{1+F}H^2\right)\right)\right) \quad \text{(S 1)}$$

The individual functions F, G, H, K and t as well as the dimensionless zeta potential $\bar{\zeta}$ are given by eqs S 2-S 7.[1]

$$\bar{\zeta} = z_\mathrm{i}\cdot\left|\frac{e\zeta}{k_\mathrm{B}T}\right| \quad \text{(S 2)}$$

$$F = \frac{2}{\kappa a}\cdot(1+3m_\mathrm{C})\cdot\left(\exp\left(\frac{\bar{\zeta}}{2}\right)-1\right) \quad \text{(S 3)}$$

$$G = \ln\left(\frac{1+\exp\left(-\frac{\bar{\zeta}}{2}\right)}{2}\right) \quad \text{(S 4)}$$

$$H = \ln\left(\frac{1+\exp\left(\frac{\bar{\zeta}}{2}\right)}{2}\right) \quad \text{(S 5)}$$

$$K = 1 - \frac{25}{3\cdot(\kappa a+10)}\exp\left(-\frac{\kappa a}{6\cdot(\kappa a-6)}\cdot\bar{\zeta}\right) \quad \text{(S 6)}$$

$$t = \tanh\left(\frac{\bar{\zeta}}{4}\right) \quad \text{(S 7)}$$

Soft particle model

The soft particle model, developed by Ohshima, Nakamura and Kondo, describes the electrokinetic properties of a spherical particle comprising an uncharged ion-impermeable core of radius a, covered by an ion-permeable polyelectrolyte layer of thickness d. Consequently, the total radius b of the particle is given by $a + d = b$.[2]

To account for the particular features of the surface structure, the Donnan potential ψ_DON (eq S 8; scaled version γ_DON, eq S 9) at the surface of the particle core as well as the surface potential ψ_0 (eq S 10) at the interface of the polyelectrolyte layer and dispersion medium were introduced.

$$\psi_\mathrm{DON} = \frac{k_\mathrm{B}T}{ze}\ln\left[\frac{ZN}{2zn} + \left\{\left(\frac{ZN}{2zn}\right)^2 + 1\right\}^{0,5}\right] \quad \text{(S 8)}$$

$$\gamma_\mathrm{DON} = \frac{ze\psi_\mathrm{DON}}{k_\mathrm{B}T} \quad \text{(S 9)}$$

$$\psi_0 = \frac{k_\mathrm{B}T}{ze}\left(\ln\left[\frac{ZN}{2zn} + \left\{\left(\frac{ZN}{2zn}\right)^2 + 1\right\}^{0,5}\right] + \frac{2zn}{ZN}\left[1 - \left\{\left(\frac{ZN}{2zn}\right)^2 + 1\right\}^{0,5}\right]\right) \quad \text{(S 10)}$$

Here, n is the number density and z is the valence of the symmetrical electrolyte. The capital letters N and Z denote the number density and valence of the ionised groups that are embedded within the polyelectrolyte layer. Consequently, the product ZN is the characteristic volume charge density assuming a uniform charge distribution.

Ohshima derived an expression for the dependence of the electrophoretic mobility on the electrolyte concentration of a soft particle, considering the relaxation effect (eq S 11). It includes the Debye-Hückel parameter κ_m of the polyelectrolyte layer (eq S 12).[3]

$$\mu = \frac{\varepsilon_\mathrm{r}\varepsilon_0}{\eta}\frac{{}^{\psi_0}/_{\kappa_\mathrm{m}}+{}^{\psi_\mathrm{DON}}/_{\lambda}}{{}^{1}/_{\kappa_\mathrm{m}}+{}^{1}/_{\lambda}} f\left({}^{d}/_{a}\right) + \frac{eZN}{\eta\lambda^2}\left(1 - \frac{F_1}{1+F_1}\frac{1}{1+\exp(-|\gamma_\mathrm{DON}|)}\right) - \frac{F_1}{1+F_1}\frac{\varepsilon_\mathrm{r}\varepsilon_0}{\eta} f\left({}^{d}/_{a}\right)\left(\frac{k_\mathrm{B}T}{ze}\right)\left[2\ln\left(\frac{1+\exp\left(\frac{|\gamma_0|}{2}\right)}{2}\right) + \frac{\kappa}{\lambda}\left(\exp\left(\frac{|\gamma_0|}{2}\right) - 1\right) - \frac{\kappa^2}{2\lambda(\lambda+\kappa_\mathrm{m})}\frac{\exp(|\gamma_\mathrm{DON}|)-1}{1+\exp(-|\gamma_\mathrm{DON}|)}\right] \quad \text{(S 11)}$$

$$\kappa_\mathrm{m} = \kappa\left[1 + \left(\frac{ZN}{2zn}\right)^2\right]^{0,25} \quad \text{(S 12)}$$

The electrophoretic softness parameter λ^{-1} describes the ion permeability of the polyelectrolyte layer. The function $f\left({}^{d}/_{a}\right)$ (eq S 13) includes the limiting conditions with $f\left({}^{d}/_{a}\right) = 1$ for $a \approx b$ (i.e. hard particle) and $f\left({}^{d}/_{a}\right) = \frac{2}{3}$ for $d \approx b$ (i.e. polyelectrolyte particle).

$$f\left({}^{d}/_{a}\right) = \frac{2}{3}\left(1 + \frac{a^3}{2b^3}\right) = \frac{2}{3}\left[1 + \frac{1}{2\left(1+{}^{d}/_{a}\right)^3}\right] \quad \text{(S 13)}$$

In eq S 11, all terms involving the function F_1 (eq S 14) account for the relaxation effect and include the scaled drag coefficient of the counter ions m_C (eq S 15) including the ionic drag coefficient λ_C (eq S 16).

$$F_1 = \frac{2}{\kappa a}(1 + 3m_\mathrm{C})\left(\exp\left(\frac{|\gamma_0|}{2}\right) - 1\right) \quad \text{(S 14)}$$

$$m_\mathrm{C} = \frac{2\varepsilon_\mathrm{r}\varepsilon_0 k_\mathrm{B}T}{3\eta z_\mathrm{C}^2 e^2}\lambda_\mathrm{C} \quad \text{(S 15)}$$

$$\lambda_\mathrm{C} = \frac{N_\mathrm{A}e^2|z_\mathrm{C}|}{\Lambda_\mathrm{C}^0} \quad \text{(S 16)}$$

An overview of all symbols used in the expressions can be found in the following table.

Table S 2: Overview of the used symbols and their meaning.

Symbol	Meaning	Symbol	Meaning
μ	Electrophoretic mobility	m_CO	Scaled drag coefficient co ions
ζ	Zeta potential	m_C	Scaled drag coefficient of counter ions
$\bar{\zeta}$	Scaled zeta potential	ψ_DON	Donnan potential
ε_r	relative permittivity	γ_DON	Scaled Donnan potential
ε_0	permittivity in vacuum	ψ_0	Surface potential
η	viscosity	γ_0	Scaled surface potential

k_B	Boltzmann constant	n	Number density of electrolyte
T	Thermodynamic temperature	Z	Valence of ionic groups within the polyelectrolyte layer
z	Valence of ionic species	N	Number density of ionic groups within the polyelectrolyte layer
e	Elementary charge	κ_m	Debye-Hückel parameter of the polyelectrolyte layer
κ	Debye-Hückel parameter	λ^{-1}	Electrophoretic softness parameter
a	Radius of the particle core	N_A	Avogadro constant
d	Radius of the polyelectrolyte layer	λ_C	Ionic drag coefficient
b	Total radius of the soft particle	Λ_C^0	Limiting molar conductance

Results

Hard particle model

Complete data sets of the measured electrophoretic mobilities of each series are shown in Figure S6-1 - Figure S6-3.

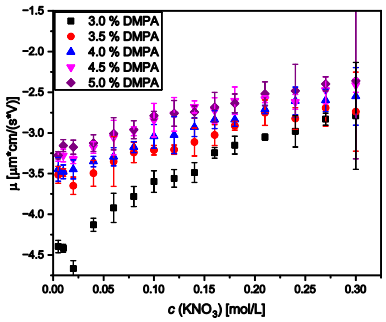

Figure S6-1: Electrophoretic mobility of PE-based PUDs with different concentrations of DMPA. Error bars correspond to the standard deviation.

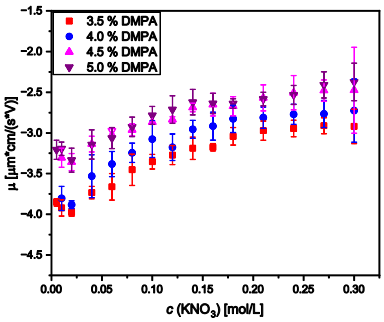

Figure S6-2: Electrophoretic mobility of PC-based PUDs with different concentrations of DMPA. Error bars correspond to the standard deviation.

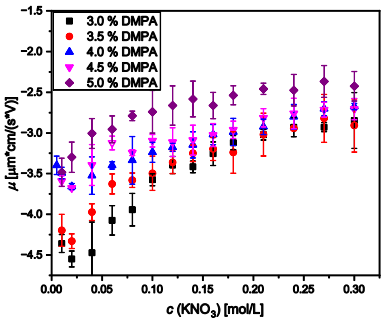

Figure S6-3: Electrophoretic mobility of PTHF-based PUDs with different concentrations of DMPA. Error bars correspond to the standard deviation.

The corresponding zeta potentials calculated according to the Helmholtz-Smoluchowski theory (Figure S6-4 - Figure S6-6) as well as taking the relaxation effect into account (Figure S6-7 - Figure S6-9) are shown below. The model fit is based on a constant surface potential ψ_0 for all ionic strengths.

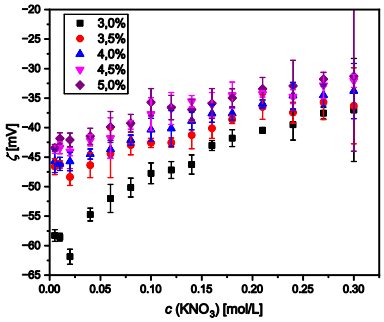

Figure S6-4:Zeta potential according to Helmholtz-Smoluchowski theory of PE-based PUDs with different concentrations of DMPA. Solid symbols correspond to the mean value and the error bars to the standard deviation.

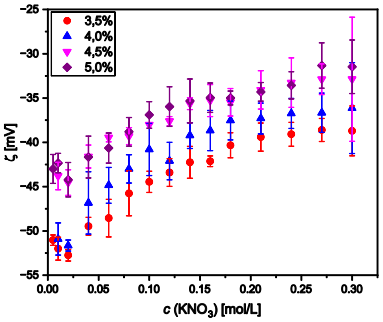

Figure S6-5: Zeta potential according to Helmholtz-Smoluchowski theory of PC-based PUDs with different concentrations of DMPA. Solid symbols correspond to the mean value and the error bars to the standard deviation.

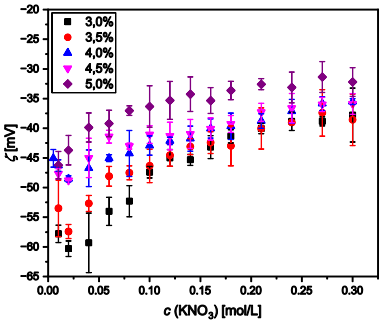

Figure S6-6: Zeta potential according to Helmholtz-Smoluchowski theory of PTHF-based PUDs with different concentrations of DMPA. Solid symbols correspond to the mean value and the error bars to the standard deviation.

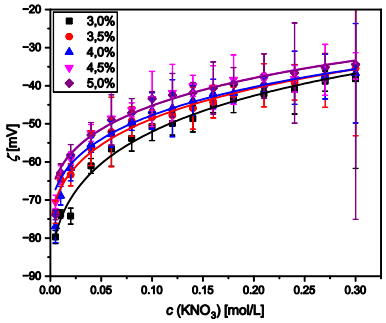

Figure S6-7: Zeta potential considering relaxation effects of PE-based PUDs with different concentrations of DMPA. Solid symbols correspond to the mean value and the error bars to the standard deviation. Solid lines represent the fit assuming a constant surface potential.

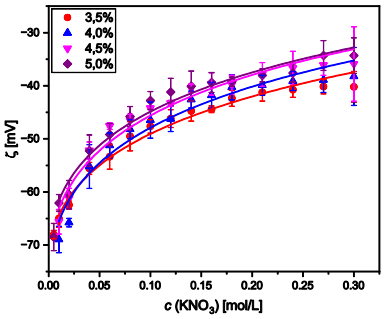

Figure S6-8: Zeta potential considering relaxation effects of PC-based PUDs with different concentrations of DMPA. Solid symbols correspond to the mean value and the error bars to the standard deviation. Solid lines represent the fit assuming a constant surface potential

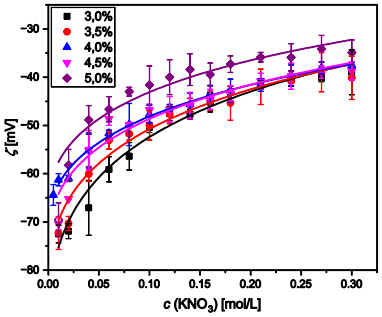

Figure S6-9: Zeta potential considering relaxation effects of PolyTHF based PUDs with different concentrations of DMPA. Solid symbols correspond to the mean value and the error bars to the standard deviation. Empty symbols were not used for fitting procedure. Solid lines represent the fit assuming a constant surface potential.

Soft particle model

The experimentally determined electrophoretic mobilities were also evaluated according to the soft particle model for electrolyte concentrations ≥ 40 mM. The corresponding data fits are shown in Figure S6-10 - Figure S6-12. The inclusion of concentrations below 40 mM led to a poorer description of the experimental data. In any case, the extrema found at electrolyte concentrations between 20 and 40 mM could not be confirmed by the soft particle model, although the relaxation effect was taken into account.

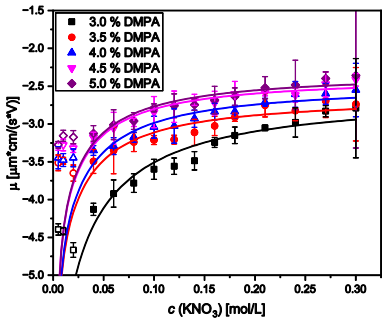

Figure S6-10: Electrophoretic mobility of PE based PUDs with different concentrations of DMPA. Error bars correspond to the standard deviation. Solid lines symbolize the fit according to the soft particle model. Empty symbols were not used for fitting procedure.

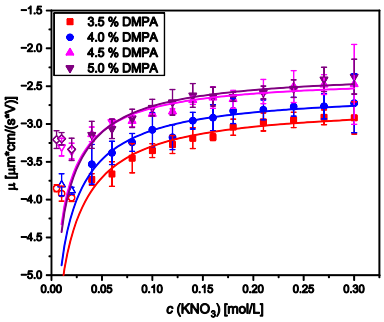

Figure S6-11 Electrophoretic mobility of PC based PUDs with different concentrations of DMPA. Error bars correspond to the standard deviation. Solid lines symbolize the fit according to the soft particle model. Empty symbols were not used for fitting procedure.

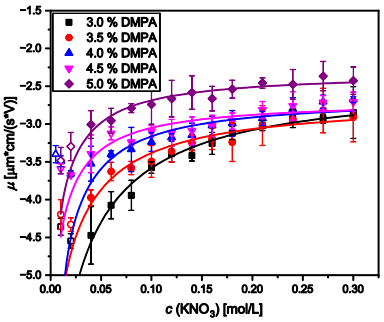

Figure S6-12: Electrophoretic mobility of PTHF based PUDs with different concentrations of DMPA. Error bars correspond to the standard deviation. Solid lines symbolize the fit according to the soft particle model. Empty symbols were not used for fitting procedure.

Determination of the critical coagulation concentration

According to the procedure described by Reerink and Overbeek[4], the critical coagulation concentration (ccc) was photometrically determined using a UV/Vis spectrophotometer Evolution 220 (ThermoScientific) employing a wavelength of 500 nm. The absorbance *A* was measured for 30 seconds in 0.1 s intervals in PMMA cuvettes. Blank measurements were done with ultra-pure water. The pH value of each sample was adjusted to 10.4 using a sodium carbonate/bicarbonate buffer system with a concentration of 2 mM and allowed to equilibrate for 12 hours prior to measurement. Finally, sodium chloride was added as electrolyte in a concentration range of 0.5 – 4.5 mol L^{-1} in the final dispersion, while adjusting a solids content of 0.075 wt%. The sample and the electrolyte solution were mixed immediately before the measurement. An exemplary set of measurement curves is shown in Figure S 6-13 for a polycarbonate-based PUD with 4.0 wt% DMPA.

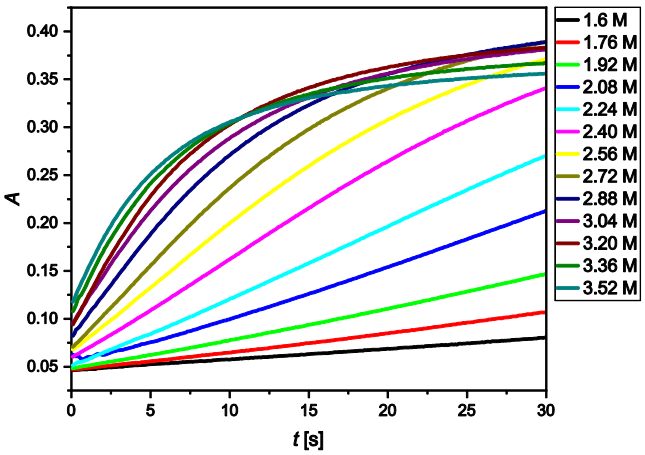

Figure S 6-13: Exemplary set of measurement curves of sample PC4.0%: Absorbance *A* vs. measuring time *t*.

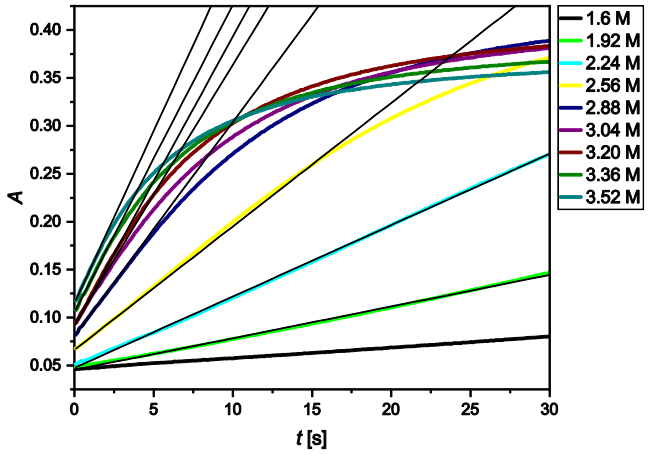

Figure S 6-14: Exemplary determination of the initial slope $\mathrm{d}A/\mathrm{d}t$ for several electrolyte concentrations. Black lines represent the initial linear slope.

The initial slope $\mathrm{d}A/\mathrm{d}t$ of each curve was determined, as shown in Figure S 6-14. Its logarithmic reciprocal $\log(\mathrm{d}t/\mathrm{d}A)$ was plotted against $\log(c)$. The graph obtained shows two characteristic regimes. The slow coagulation regime with decreasing values and the fast coagulation regime with nearly constant values. The intercept of both regimes gives the critical coagulation concentration.

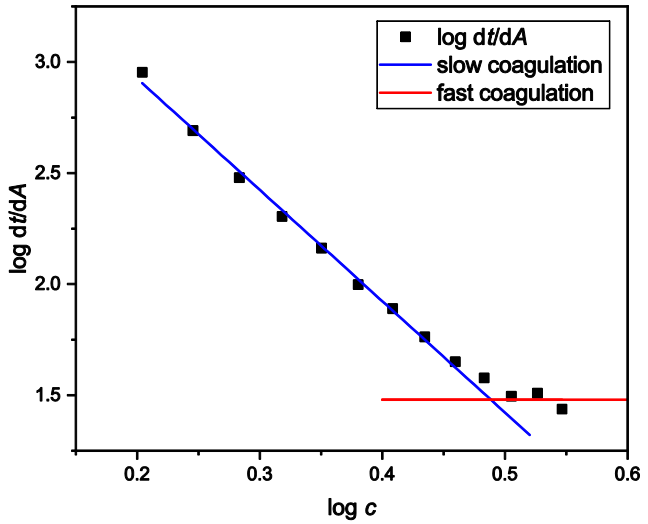

Figure S 6-15: Logarithmic reciprocal $\log(\mathrm{d}t/\mathrm{d}A)$ vs. $\log(c)$. The blue line represents the slow coagulation regime and the red line represents the fast coagulation regime. The intercept of the two sections gives the critical coagulation concentration.

Apparent Hamaker constants A_{131}^{app}

The apparent Hamaker constants A_{131}^{app} were calculated using the DLVO theory and are shown in Figure S 6-16. For a better understanding, a brief description of the procedure follows below (please refer to the main article for the equations used). The repulsive electrostatic interaction energy V_{R} and the attractive van der Waals interaction energy V_{A} can be calculated as a function of the particle separation distance H. If the surface potential Ψ_0 and the ccc value have been determined, the apparent Hamaker constant A_{131}^{app} can be calculated by simultaneously solving $V_{\mathrm{T}} = V_{\mathrm{R}} + V_{\mathrm{A}} = 0$ and $\mathrm{d}V_{\mathrm{T}}/\mathrm{d}H = 0$.

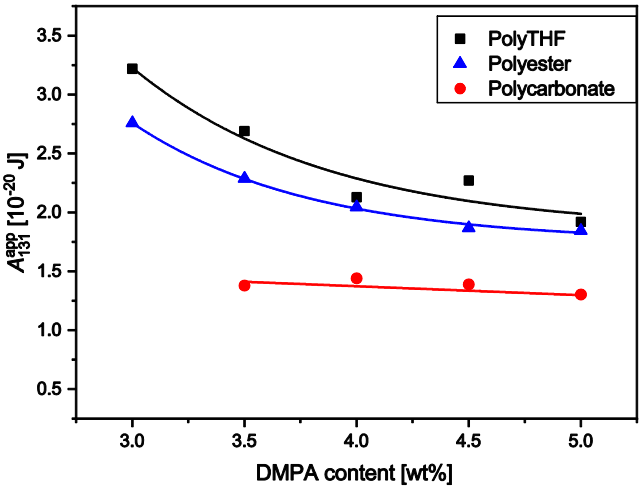

Figure S 6-16: Apparent Hamaker constant A_{131}^{app} of all PUD series at different DMPA mass fractions.

Contact angles for diiodomethane and apolar surface tension component γ_S^{LW}

Contact angles were measured for diiodomethane as test liquid at 6 different positions on the polyurethane film. The values were averaged and used to calculate the apolar component of the surface tension γ_S^{LW}. The results are shown in Table S 3.

Table S 3: Average contact angles and the apolar surface tension component γ_S^{LW}.

DMPA content [wt%]	PTHF based PUD		PE based PUD		PC based PUD	
	θ [°]	γ_S^{LW} [mN/m]	θ [°]	γ_S^{LW} [mN/m]	θ [°]	γ_S^{LW} [mN/m]
3.0	39.7 ± 0.1	39.8	42.6 ± 1.6	38.3	/	/
3.5	40.1 ± 0.7	39.5	42.3 ± 1.4	38.4	39.8 ± 0.4	39.7
4.0	39.1 ± 0.5	40.1	42.9 ± 1.2	38.1	38.1 ± 0.5	40.6
4.5	40.5 ± 0.3	39.4	42.1 ± 1.3	38.6	38.2 ± 0.4	40.5
5.0	40.4 ± 0.3	39.4	40.9 ± 1.4	39.2	37.6 ± 0.5	40.8

Pre-exponential Factor C using Different Decay Lengths λ

Hydrophilic or hydrophobic interactions between particles and the dispersion medium can make a significant contribution to the total interaction energy V_T. They can be described by an exponential function decaying with distance H. The range of these interaction forces is determined by the decay length λ, and their magnitude by the pre-exponential factor C. In this study, we calculated the factor C for various PUD series using the XDLVO theory and two different values for the decay length λ. The results are shown in

For a better understanding, a brief description of the procedure follows below (please refer to the main article for the equations used). The repulsive electrostatic interaction energy V_R, the attractive van der Waals interaction energy V_A and the attractive hydrophobic interaction energy V_h can be calculated as a function of the particle separation distance H. If the surface potential Ψ_0, the Hamaker constant A_{131} and the critical coagulation concentration ccc have been determined, and a reasonable value for the

decay length λ is assumed, the pre-exponential factor C can be calculated by simultaneously solving $V_T = V_R + V_A + V_h = 0$ and $dV_T/dH = 0$.

Table S4: Sensitivity of the pre-exponential factor C to variations in the decay length λ *

DMPA mass fraction	for $\lambda = 0.3$ nm			for $\lambda = 0.4$ nm		
	PTHF	PE	PC	PTHF	PE	PC
3.0%	-19.0	-16.3	/	-16.2	-14.6	/
3.5%	-15.0	-12.0	-6.7	-12.6	-10.4	-6.1
4.0%	-10.7	-10.2	-7.3	-8.8	-8.9	-6.6
4.5%	-11.5	-8.8	-6.7	-9.6	-7.8	-6.1
5.0%	-9.4	-9.0	-5.9	-7.8	-7.7	-5.4

* All values are given in 10^{-12} N. Water-based PUDs containing Polytetrahydrofurane (PTHF), Polyester (PE) and Polycarbonate (PC) diol, as well as various mass fractions of DMPA.

References

(1) Ohshima, H., Healy, T. W., White, L. R. Approximate analytic expressions for the electrophoretic mobility of spherical colloidal particles and the conductivity of their dilute suspensions. *Journal of the Chemical Society, Faraday Transactions 2* **1983**, *79*, 1613.

(2) Ohshima, H., Nakamura, M., Kondo, T. Electrophoretic mobility of colloidal particles coated with a layer of adsorbed polymers. *Colloid & Polymer Science* **1992**, *270*, 873–877.

(3) Ohshima, H. Electrophoretic mobility of a highly charged soft particle: Relaxation effect. *Colloids and Surfaces A: Physicochemical and Engineering Aspects* **2011**, *376*, 72–75.

(4) Reerink, H., Overbeek, J. T. G. The rate of coagulation as a measure of the stability of silver iodide sols. *Discuss. Faraday Soc.* **1954**, *18*, 74.

7 Comprehensive discussion

The central objective of this thesis is to obtain insights into potential structure-stability relationships of water-based polyurethane dispersions. Polyurethanes exhibit a vast array of potential monomers, including different polyols, short-chain diols, diamines, and higher functional isocyanates. The incorporation of surface functional groups, such as carboxylic or sulfonic acids, is typically employed to achieve dispersion stability in contemporary practice. However, it is important to note that additional factors, such as structural differences within the building blocks or the final product, may also influence dispersion stability. Understanding how molecular design governs colloidal stability is crucial for developing predictive relationships that enable the tailored design of stable water-based polyurethane systems. To address this, a series of well-defined PUDs is synthesised via the acetone process, systematically varying the polyol component, hydrophilising agent, and hard-segment content. This experimental design enables isolation of individual structural effects on dispersion behaviour and provides a framework for linking molecular parameters to dispersion stability.

The central focus of this work lies on dispersion stability in electrostatically stabilised systems. Such dispersions are sensitive to destabilisation by increasing electrolyte concentration. Accordingly, the coagulation process is monitored through time-resolved absorbance measurements at various ionic strengths, following the established procedure of Reerink and Overbeek.[47] From these measurements, the critical coagulation concentration is determined, providing a quantitative measure of dispersion stability (Chapter 7.2).

To interpret these results in terms of DLVO and XDLVO theory, detailed knowledge of the particle interaction energies is required. Since the incorporation of ionic functional groups results in the formation of a surface potential, the particle charges are investigated in detail by potentiometric titration as well as electrophoretic analysis. These measurements provide insights into how surface chemistry and charge distribution influence the electrostatic component of colloidal stability. The intrinsic stabilization of PUDs and the complex rearrangement of the charged entities to the particle/water interface during dispersion might lead to variations in the peripheral particle structure. Some functional groups may migrate toward the particle-water interface, while others may remain embedded within the core or shielded by the surrounding polymer matrix. This reorganization can affect the accessibility, dissociation, and electrostatic interaction of these functional groups. This effect is analysed by potentiometric titration experiments in detail. Additionally, since such charge carrying layers alter the electrophoretic properties, the electrophoretic mobility is analysed in dependence of the ionic strength using the respective soft and hard particle models outlined in section 2.3.2 and 2.3.3. A comprehensive discussion of the overall outcomes follows in chapter 7.3.

In addition to repulsive electrostatic interactions, attractive van der Waals forces also play a decisive role in dispersion behaviour. These are typically addressed by the Hamaker constant, which serves as a measure of the attractive van der Waals interaction potential. Hamaker constants are therefore determined based on the DLVO approach and compared to the alternative vOCG-approach, which is based on contact angle measurements. The dispersion stability is theoretically described in terms of DLVO and XDLVO theory (chapter 7.4). Building upon these analyses, the subsequent discussion integrates experimental findings and theoretical evaluations to derive structure–stability correlations across the investigated systems.

7.1 Particle Size of PUDs

In this thesis, PUDs with varying structural components are synthesized using the acetone process. The synthesis parameters are systematically adjusted to investigate the influence of different polyol components, specifically polycarbonate, polyester, and polytetrahydrofurane polyols of similar molecular weight. Additionally, the impact of the hydrophilizing agent is studied by incorporating either AAS or DMPA at concentrations ranging from 3.0 wt% to 5.5 wt%. Furthermore, the hard segment content is modified by varying the amount of 1,4-butanediol while maintaining a constant charge content of 4.0 wt% AAS and using a polyester polyol component.

Figure 7-1 shows the average particle size as a function of the AAS- (a), DMPA- (b) and hard segment content (c). All samples are characterized by a monomodal particle size distribution. Increasing the concentration of AAS or DMPA leads to an asymptotic decrease in particle size, reaching a lower limit of approximately 40 nm (Figure 7-1a and b) A minimum stabilizer concentration of 3.0–3.5 wt% is required to maintain dispersion stability, while further reduction leads to rapid sedimentation and instability. No significant differences in particle formation are observed between AAS- and DMPA-stabilized PUDs.

The influence of hard segment content on the particle size is comparatively minor (Figure 7-1c). Across the studied range, the average particle diameter remains approximately constant at (58.4 ± 4.5) nm. This suggests that, within the studied range, the hard segment content does not significantly influence the average particle size. Notably, the particle sizes of these samples are consistent with those of the 4.0 wt% sample obtained from the AAS series (Figure 7-1a), indicating consistent particle sizes across various formulations.

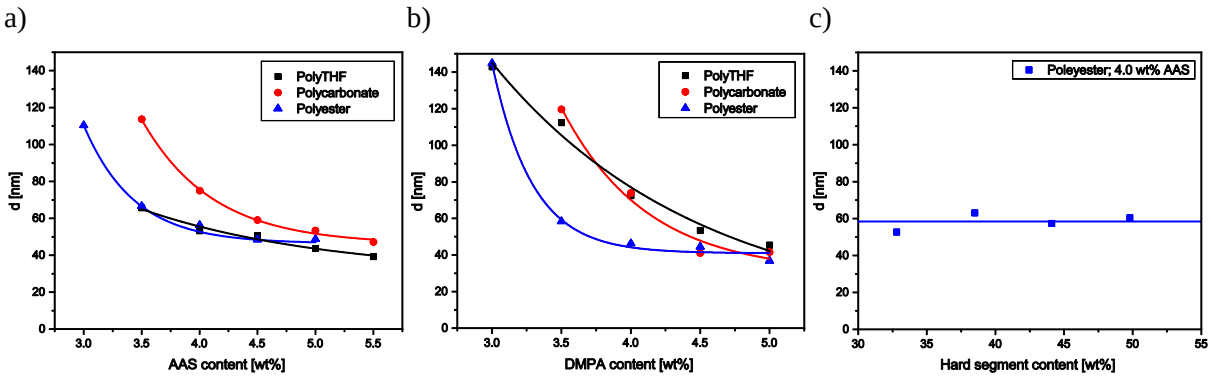

Figure 7-1: Average particle diameter as a function of a) AAS concentration, b) DMPA concentration and c) the hard segment content for polycarbonate (red), polyester (blue) and polyTHF (black) polyol components.

Similar observations are also reported in literature.[38,39,69,84,98,186] For instance, Nanda and Wicks find decreasing particle sizes from 140 nm (4.0 wt-%) to 50 nm (7.0 wt %) for PUDs stabilized by DMPA.[38,186] Kim et al on the other hand observed decreasing values from approximately 200 nm (3.0 wt-%) to 90 nm (4.5 wt-%) also for PUDs stabilized by DMPA.[84] Lijie et al. also studied the influence of DMPA on PUDs and found the minimum concentration of DMPA to be 2.4 wt-%.[39] While the asymptotic decrease with increasing stabilizer content can be confirmed by literature, the minimum concentration necessary to produce stable dispersion deviates. Since the polyurethane composition is different for the mentioned studies, it indicates a significant influence of the entire PUD composition.

The overall composition, including polyol type, hard segment content, and stabilizer concentration, governs particle formation mechanisms. This suggests that charge content alone is not the sole determinant of particle size distribution, emphasizing the need to consider multiple structural factors when analysing dispersion behaviour.

7.2 Dispersion stability

A central focus of this work is the characterization of the dispersion stability of the synthesized PUDs, which is crucial for their practical application and performance. Dispersion stability is primarily governed by the interactions between the particles, which can often be understood using the DLVO theory, as outlined in chapter 2.3.4. Electrostatic repulsion plays a key role in preventing aggregation, but its effectiveness can be weakened by the presence of electrolytes, reducing the dispersion stability. In this context, the critical coagulation concentration ccc represents the minimum electrolyte concentration required to induce rapid coagulation and serves as a characteristic measure of dispersion stability.

To determine the ccc for the synthesized PUDs, time-resolved photometric analysis of the coagulation process is done. The results demonstrate how varying AAS (Figure 7-2 a) and DMPA (Figure 7-2 b) mass fractions, as well as the hard segment content (Figure 7-2 c) influence dispersions stability. A more detailed discussion for AAS can be found in chapter 5.4.1 and for DMPA in chapter 6.4.4.

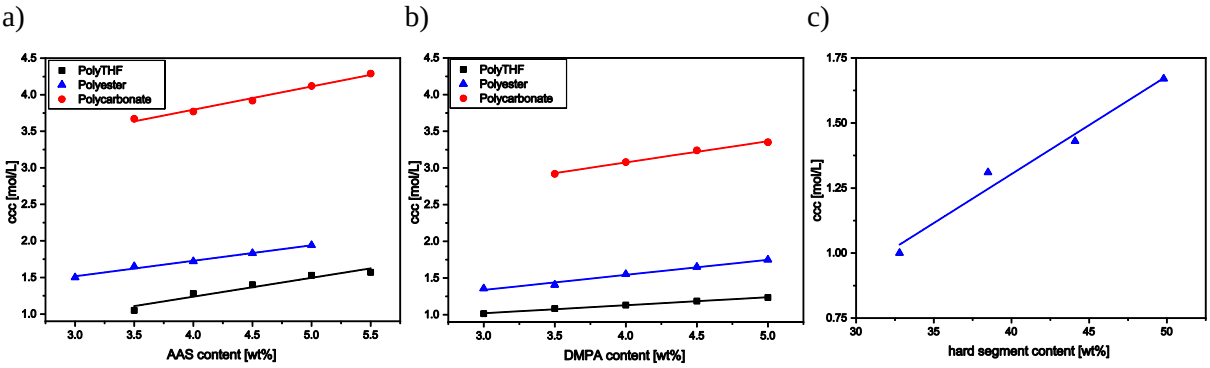

Figure 7-2: Critical coagulation concentration (ccc) of the synthesized PUDs as a function of a) AAS concentration, b) DMPA concentration and c) hard segment content for polycarbonate (red), polyester (blue) and polyTHF (black) polyol components.

The stability trends observed across the different synthesis series highlight that dispersion stability in water-based PUDs is governed by a combined influence of ionic stabilization, polyol chemistry, and hard-segment architecture. Across all systems, higher concentrations of ionic functional groups generally enhance colloidal stability. Differences between AAS and DMPA stabilized PUDs are evident, particularly for PC-based PUDs, where DMPA-stabilized dispersions show ccc values approximately 0.5 M lower than those stabilized by AAS. Increasing the hard segment content leads to an improvement in dispersion stability, with the ccc rising from 1.0 M (32.8 wt%) to 1.7 M NaCl (49.8 wt%). Since the AAS content is kept constant at 4.0 wt%, this change is not expected to arise from differences in electrostatic repulsion. Among all structural parameters, the polyol component exerts the strongest impact on stability. PC-based PUDs show substantially better stability than those containing PolyTHF or PE diols, indicating that the type soft segment substantially influences particle interactions.

The ccc results provide a clear, comparative overview of stability trends, but they do not yet explain the mechanistic origin of the observed differences. To fully rationalize these trends, the interplay between surface charge, dissociation behaviour, and attractive forces must be examined. The following sections therefore analyse electrokinetic properties and interaction potentials in detail to establish a more complete understanding of the factors governing dispersion stability in water-based PUDs.

7.3 Analysis of the surface charges and electrokinetic properties

In case of electrostatically stabilized PUDs, the characterization of the charge content and the corresponding surface potential is crucial to assess the magnitude of electrostatic repulsive forces. In this study sulfonate and carboxylate functional groups are incorporated into the polymer structure as ionisable moieties to generate surface charges and induce electrostatic repulsion. A quantitative assessment of the charge content, the distribution of the functional groups throughout the particle as well as the dissociation behaviour is investigated using potentiometric titration experiments. The results are summarized in chapter 7.3.1. Since surface charge characteristics directly affect the electrophoretic mobility of dispersed particles, ELS measurements are done to assess the electrokinetic properties. The resulting data are analysed using the theoretical models introduced in chapter 2.3.2 and 2.3.3 as well as 4.2, with a comprehensive discussion shown in chapter 7.3.2.

7.3.1 Characteristics of the surface functional groups

The PUDs synthesized in this study contain both sulfonic and carboxyl groups, whose differing acid strengths can influence the particle's surface charge and, consequently, its electrokinetic potential. Due to the intrinsic stabilization of PUDs the functional groups are covalently bond within the polymer backbone, which limits their ability to reorganize at the particle/water interface during dispersion. As a consequence, only a fraction of the stabilizing groups contributes directly to the measurable surface charge, while others remain partially shielded within the particle interior. This structural constraint likely affects both the magnitude of the particle charge and the apparent acid–base behaviour of the system.

Characteristic values obtained by evaluation of the potentiometric titration experiments for PUDs stabilized by AAS and DMPA can be found in Table 4-3 (AAS) and Based on the determined equivalence points V_{HA_n}, the specific particle charge Q_{tit} can be calculated with respect to the used mass of polymer. Furthermore, it is possible to calculate the recovery rate RR, because the maximum amount of charges Q_{max} is known from the synthesis recipe. RR is given by the ratio $RR = \frac{Q_{\mathrm{tit}}}{Q_{\mathrm{max}}}$.

Table 6-2 (DMPA), respectively. A more detailed comparison of the results for DMPA and AAS stabilized PUDs can be found in chapter 6.4.2. The specific particle charge content Q_{tit} increases with increasing AAS or DMPA content, reflecting the higher amount of charges incorporated into the system. While the general trend in charge content follows the expected increase with higher stabilizer concentrations, the titration experiments reveal that not all charges can be detected. This is reflected by the incomplete recovery rate RR for both AAS- and DMPA-stabilized systems. This suggests that a significant portion of the charges are not participating in the ion-exchange procedure. As the progress of the synthesis was monitored until complete conversion, it can be anticipated that some of the charges might be trapped inside the particle or the polymer matrix itself.

The theoretical evaluation (c.f. chapter 4.2.2 for details on the mathematical model) of the titration curves supports this interpretation. For both stabilizing agents, the experimental data cannot be described by a single acidic species. Instead, both require at least one additional acid group of lower acidity, suggesting partially hindered dissociation of the functional groups caused by the chemical environment within the polymer matrix. The altered dissociation can be attributed to additional work required to remove protons from the particle into the bulk dispersion medium. Stone-Masui and Watillon analysed monodisperse latex particles stabilized by potassium stearate. Their results reveal $\mathrm{p}K_{\mathrm{a}}$ values in the range of 6.7 to 8.7 depending on the added electrolyte concentration, significantly higher than the natural $\mathrm{p}K_{\mathrm{a}}$ value of stearic acid (4.8). The discrepancy is attributed to electrostatic interactions between neighbouring charged groups at the particle surface, which increase the electrostatic work required to remove protons from the surface functional groups.[187] Additionally, the surface functional groups are expected to be partially embedded within the polymer matrix, introducing diffusion limitations for

protons to reach the bulk medium, which further alters dissociation behaviour. Thus, both electrostatic effects and proton diffusion constraints contribute to the effective pK_a values and reduced dissociation observed, highlighting the complexity of ionization behaviour in intrinsically stabilized latex systems.

Figure 7-3 shows a schematically representation of a DMPA-stabilized particle, highlighting the anticipated distribution of charges and the corresponding dissociation range of each class of functional groups detected in the potentiometric titration.

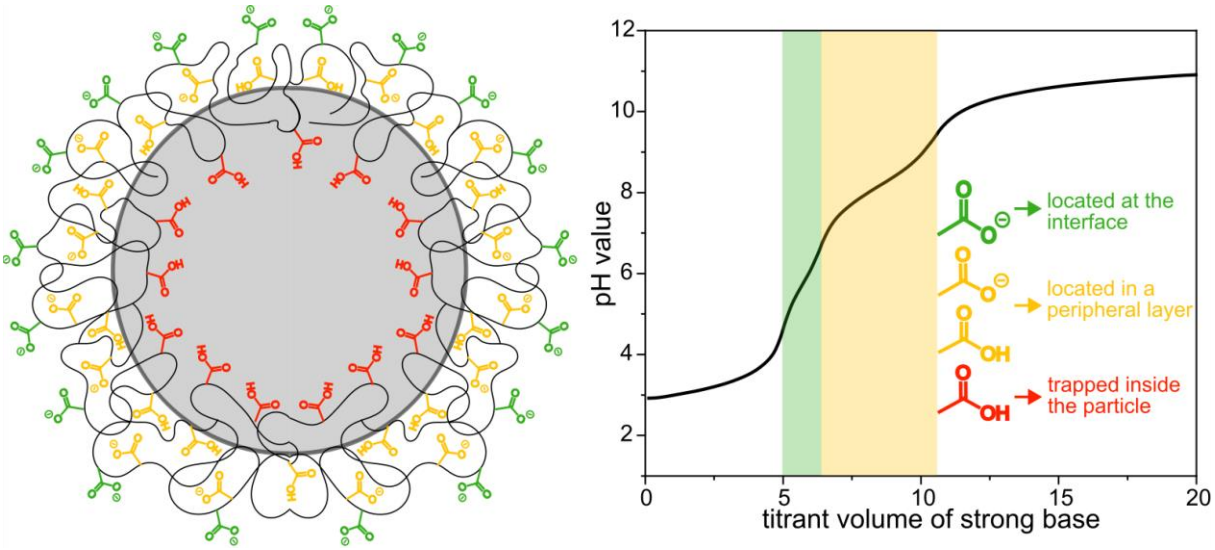

Figure 7-3: Schematic illustration of the anticipated charge distribution of a particle stabilized by DMPA and the corresponding titration curve highlighting the different dissociation regions of the groups characterised by different dissociation constants.

Comparing the two stabilizers reveals notable differences in the charge distribution within the particle. In DMPA-stabilized dispersions, only about 25% of the total specific charge content is located in close proximity to the particle surface (first equivalence point, pK_{a1}), while the remaining 75% are located inside the particle (second equivalence point, pK_{a2}). In contrast, AAS-stabilized systems show the opposite trend with 85% of the specific charge content located near the particle surface and only 15% embedded within the particle. The relative changes in the amount of charges detected at the first and second equivalence point are different in the case of AAS. While no consistent changes can be observed in case of increasing DMPA content (appr. 25% at $Q_{tit,1}$ and 75% at $Q_{tit,2}$) rising AAS mass fractions predominantly influence the first equivalence point corresponding to the strong acidic groups. The relative amount detected at the first equivalence point increases while the relative amount at the second equivalence point decreases from approximately 20% to 13 %.

The differences likely arise from the synthesis protocol, as DMPA is incorporated early during prepolymerization, whereas AAS is added in the chain extension step. During the transition from acetone solution to a water-based dispersion a complex rearrangement takes place. The hydrophobic segments of the polymer tend to cluster in the particle's interior, minimizing their exposure to the polar aqueous environment. Conversely, the hydrophilic segments preferentially migrate toward the particle's surface. Due to the early-stage incorporation of DMPA into the polymer backbone, these units are less mobile and less likely to migrate to the particle surface. In contrast, AAS units, incorporated later into a more flexible polymer structure, can more easily migrate to the particle surface. This structural constraint is reflected in the results of potentiometric titration, where the higher DMPA content is detected at lower acid strength, specifically at pK_{a2} as well as the increasing amount of charges characterised by p$K_{a,0} = 0$ in case of AAS. These findings and explanations are furthermore supported by the results obtained for the variation of the hard segment content, which are shown in Table 7-1.

Table 7-1: Characteristic parameters based on titration experiments for all PE based PUDs stabilized by 4.0 wt% AAS with varying hard segment content.

Sample	$Q_{\mathrm{tit},0}$ [C/g]	$Q_{\mathrm{tit},1}$ [C/g]	Q_{tit} [C/g]	RR_1 [%]	RR_2 [%]	RR [%]	$\mathrm{p}K_{\mathrm{a},1}$
PE49.8	-15.6	-3.0	-18.6	68.2	13.1	81.3	6.2
PE44.1	-16.0	-2.2	-18.2	70.1	9.3	79.4	6.5
PE38.5	-17.2	-2.0	-19.2	74.8	8.7	83.5	7.1
PE32.8	-16.1	-1.8	-17.9	70.3	8.1	78.4	7.2

The specific particle charge Q_{tit} remains essentially constant at $(-18.5 \pm 0.6)\ \mathrm{Cg}^{-1}$ on average, resulting in only minor differences in the total recovery rate RR with (80.7 ± 2.3) %. These findings meet the theoretical expectations, as the AAS mass fraction is kept constant at 4.0 wt%. Notably, the results are in great accordance to the similar sample PE4.0 (see Table 4-3) underlining the reproducibility of the synthesis as well as the characterization procedure. Similar to the other AAS stabilized dispersions, two types of functional groups are relevant to describe the titration curve satisfactorily. Most of the surface functional groups are characterised by $\mathrm{p}K_{\mathrm{a},0} = 0$ and thus a strongly acidic behaviour. Further insights emerge from analyzing the recovery rates at the first and second equivalence points $RR_1$and RR_2 as a function of the hard segment content. As the hard segment content decreases, the fraction of charges detected at the first equivalence point increases, while the amount detected at the second equivalence point decreases. This trend suggests that less rigid polymer chains allow the hydrophilic sulfonate groups to more easily migrate to the particle surface, supporting the discussed effect of polymer flexibility on charge rearrangement during dispersion.

Conclusively, the analysis of the potentiometric titration curve indicates that the particle charges are not only located on the particle surface but also distributed in a peripheral ion-penetrable layer. This also allows us to understand that the deeper the functional groups are located inside the particles, the more limited is their dissociation. Ultimately, they can no longer be detected by charge titration experiments. The latter seems to be even more pronounced in case of DMPA. Both effects are potentially influenced by the synthesis protocol.

7.3.2 Electrokinetic properties of the polyurethane particles

The results of the potentiometric titration experiments give rise to the assumption that the charges of the polyurethane particles are distributed throughout the particle and potentially in an ion-penetrable polyelectrolyte layer. This is expected to affect the electrokinetic properties as well. To get further insights the electrophoretic mobility of each dispersion is analysed as a function of ionic strength. To draw further conclusions about the particle structure, the results are analysed by models according to hard as well as soft particle theories (c.f. chapter 2.3.2, 2.3.3 and 4.2). The electrophoretic mobility is measured for all synthesised PUDs as a function of the ionic strength using KNO_3 as 1: 1 electrolyte. The results for AAS are discussed in chapter 4.4.3 and for DMPA in chapter 0 and 6.6. The data for the hard segment content are included within this section.

Representative results are shown in Figure 7-4 for each polyol component at a constant mass fraction of 4.0 wt% of either AAS (Figure 7-4 a) or DMPA (Figure 7-4 b) as well as variations in hard segment content (Figure 7-4 c). Due to the anionic nature of the sulfonate and carboxylate group, all dispersions show negative values of the electrophoretic mobility with only minor differences between the used polyol component. In all cases, a distinct extremum of the electrophoretic mobility can be found at low electrolyte concentrations. Such extrema at low ionic strength are commonly attributed to relaxation effects of the diffuse double layer, regardless of the particle character being hard or soft.[188–192] It is

followed by a decrease of the absolute value of electrophoretic mobility, which can be attributed to the increasing ionic strength, leading to screening of the surface charges and a compression of the diffuse double layer. Notably, the mobility is still of finite value, even at high ionic strengths. This is characteristic for soft particles and the experimental data are subsequently analysed with the corresponding soft particle theory, considering the relaxation effect.

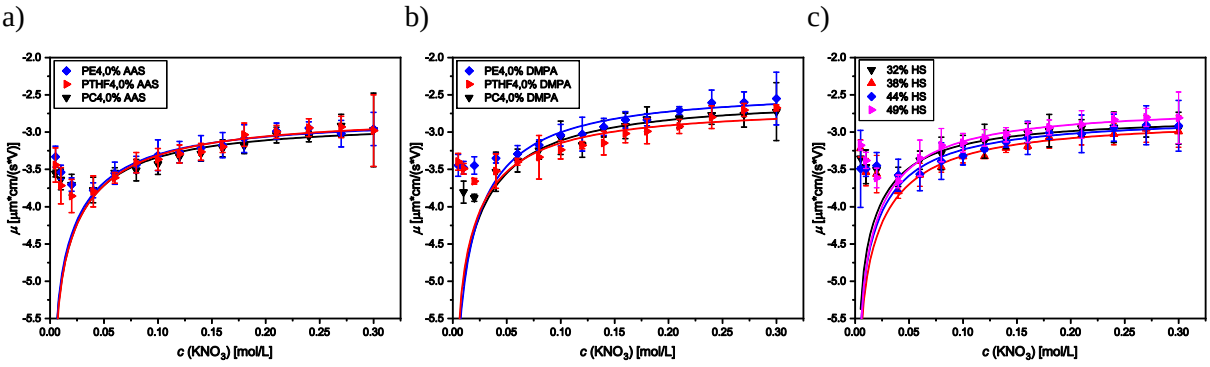

Figure 7-4: Exemplary diagrams of the electrophoretic mobility μ as a function of the KNO_3 concentration c for a) polycarbonate, polyester and polyTHF based PUD stabilized by 4.0 wt% AAS, b) polycarbonate, polyester and polyTHF based PUD stabilized by 4.0 wt% DMPA and c) for the synthesis series with different hard segment at a constant AAS concentration of 4.0 wt%. The solid symbols represent the average value of the measurement with the error bars corresponding to its standard deviation. The solid lines represent the results of the fit according to the soft particle model considering relaxation effects for $d \approx b$ expressed by $f\left(d/a\right) = 2/3$.

The fits are illustrated in Figure 7-4 by the solid lines. The model describes the experimental data well in case of high ionic strength, but fails at lower electrolyte concentrations (<40 mM KNO_3). Similar deviations at low ionic strength are also mentioned by other authors, analysing various colloidal systems.[188,193–195] According to Gaboriaud et al. the assumption of a homogenous charge distribution is possibly not accurate and might also change in dependence of the ionic strength. The results obtained by potentiometric titration support this explanation. The charge carrying layer of the PUDs is not homogenous but characterised by a gradient, which increases towards the dispersion medium. Nevertheless, the characteristic volume charge density ZN and the electrophoretic softness parameter λ^{-1} are determined for electrolyte concentration higher than 40 mM as illustrated in Figure 7-5, considering the particles to be polyelectrolytes with a vanishingly small core (i.e. $d \approx b$ and $f\left(d/a\right) = 2/3$).

ZN decreases with increasing stabilizer content, which implies that the thickness d of the polyelectrolyte layer must increase in order to accommodate charged groups. Based on the determined volume charge densities the specific particle charge Q_{ek} is calculated with a comparison of Q_{ek} and Q_{tit} for PUDs stabilized by AAS shown in chapter 4.4. Even when assuming a polyelectrolyte-like particle structure, the calculated volume charge densities ZN and corresponding specific particle charge Q_{ek} are insufficient to account for the specific particle charge Q_{tit} determined by titration, except for samples with the lowest stabilizer concentration of 3.0 wt% for both stabilizing agents.

The electrophoretic softness parameter λ^{-1} increases across the series, consistent with the results of titration experiments. Higher recovery rates imply improved ion-permeability, which support proton dissociation. However, the dissociation constants remain largely unchanged, suggesting that local electrostatic interactions between neighbouring charges have a stronger influence on the effective ionization than the polymer network density. The hard segment content on the other hand shows only minor effects and the corresponding results show slightly fluctuating results for both ZN as well as the softness parameter.

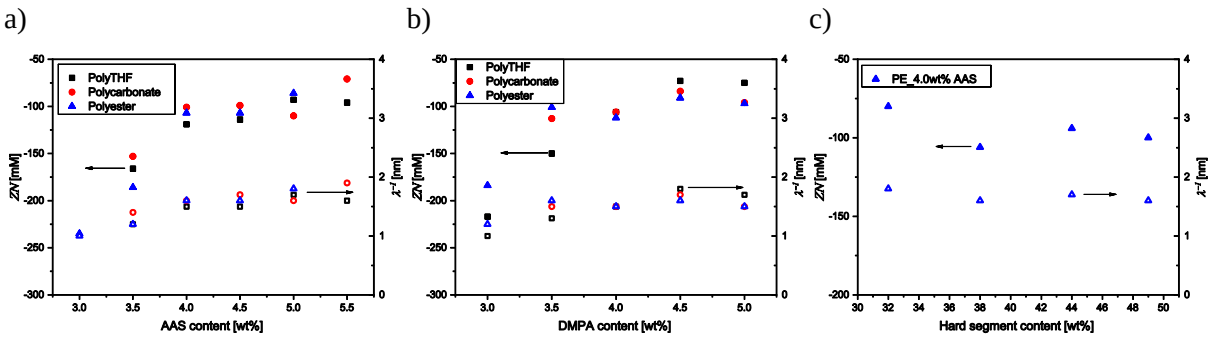

Figure 7-5: Volume charge densities ZN and softness parameter λ^{-1} determined according to the soft particle model for electrolyte concentrations larger than 40 mM for a). PolyTHF, polyester and polycarbonate based PUDs stabilized by AAS are obtained by fitting the experimental data with $f\left(d/a\right) = 2/3$. $f\left(d/a\right) = 0.79$ used for calculation in case of PE_3.0wt% AAS, since Q_{tit} is then equal to Q_{ek}. b) PolyTHF, polyester and polycarbonate based PUDs stabilized by DMPA obtained by fitting the experimental data with $f\left(d/a\right) = 2/3$. $f\left(d/a\right) = 0.74$ used for calculation in case of PE_3.0wt% DMPA and $f\left(d/a\right) = 0.81$ used for calculation in case of PolyTHF_3.0wt% DMPA, since Q_{tit} is then equal to Q_{ek}. c) different hard segment for PE based PUD at a constant AAS concentration of 4.0 wt% obtained by fitting the experimental data with $f\left(d/a\right) = 2/3$.

Based on these results and the insufficient description of the electrophoretic mobility data at low electrolyte concentrations, it is concluded that the soft particle model of Ohshima is insufficient to satisfactorily describe the electrophoretic mobility of polyurethane particles analysed in this study. Most likely, the assumption of a homogenous charge distribution within the polyelectrolyte layer is the main reason for its failure. Since the non-zero limiting mobility is also characteristic for highly charged hard particles,[196] the experimental data of the PUDs in this study are also investigated by hard particle models.

In case of hard particles, the zeta potential is generally considered as the particles effective potential. Therefore, the electrophoretic mobility data are converted to zeta potentials using two different models. Graphic illustrations of the results of all PUDs stabilized by AAS and DMPA can be found in chapter 4.4.3.3 and 0, respectively. The results obtained by the Helmholtz-Smoluchowski model as well as the model according to Ohshima et al. for varying hard segment contents are shown in Figure 7-6.

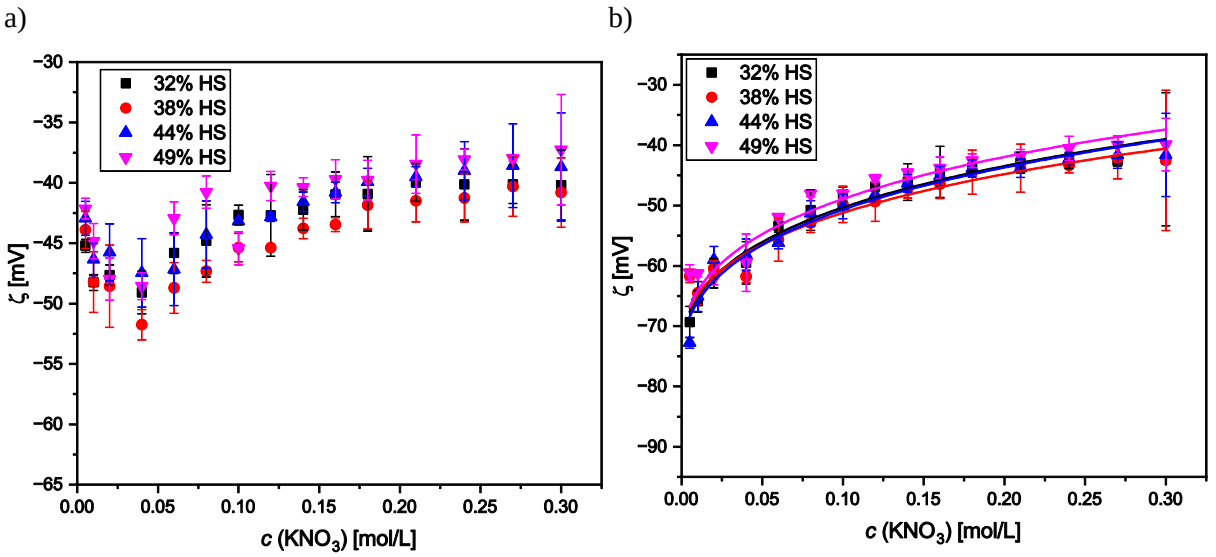

Figure 7-6: Zeta potential ζ as a function of KNO_3 concentration c for polyester based PUDs containing containing different hard segment contents stabilized by 4.= wt% AAS Evaluation according to Helmholtz and Smoluchowski (a) and Ohshima, Healy and White (b). The solid lines represent the results of the fit to determine the surface potential with respect to the position of the shear plane. The solid symbols represent the average value with the error bars corresponding to their standard deviation.

The widely used Helmholtz-Smoluchowski model proves inadequate, particularly at low electrolyte concentrations, as it neglects the relaxation effect (c.f. chapter 4.4.3.3 for AAS and 6.6 for DMPA). To account for the relaxation effect, the approximate analytical expression proposed by Ohshima et. al.[135,136] is used. The model provides much more plausible values, as evidenced by the monotonically decreasing zeta potentials with increasing electrolyte concentration, reflecting the compression of the diffuse double layer (Figure 7-6b, Figure 4-3 and Figure 6-2).

Based on these zeta potentials, it is possible to calculate the surface potential ψ_0 and the distance of the shear plane x_s. For this purpose, the dependency of the zeta potentials on the electrolyte concentration is evaluated by using the corresponding expression for a potential distribution around a particle derived by Ohshima, Healy and White.[138,197] This model assumes a constant surface potential with increasing ionic strength and can be successfully applied to describe all PUDs of this work, as evidenced by the quality of the fitting curve illustrated by the solid line in Figure 7-6 b, as well as Figure 4-3 (AAS) and Figure 6-2 (DMPA). Especially for PUDs stabilized by AAS this is observation is interesting, as the sulfonate groups have a strongly acidic character and their dissociation behaviour should therefore only be slightly influenced by the addition of electrolyte. The results for the surface potential and the position of the shear plane are shown in Figure 7-7.

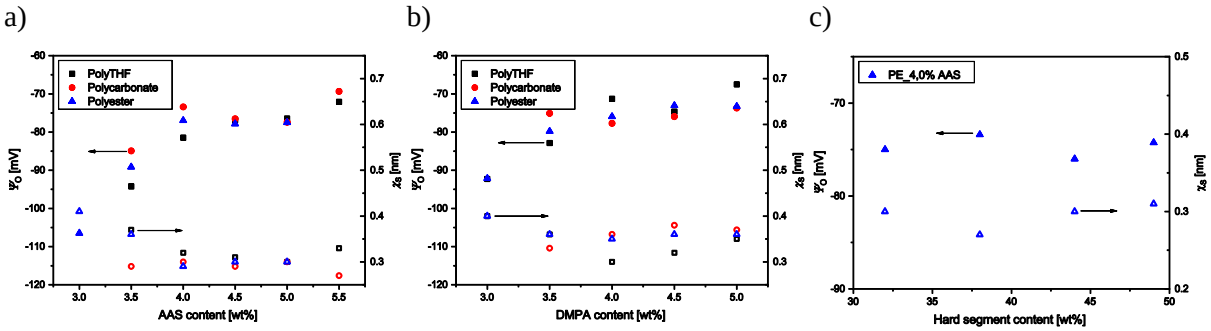

Figure 7-7: Surface potential ψ_0 (solid symbols) and distance of shear plane x_s (empty symbols) for a) PUDs stabilized by AAS, b)PUDs stabilized by DMPA and c) PUDs based on PE at a constant mass fraction of 4.0 wt% AAS witch different hard segment content.

The surface potentials ψ_0 decrease with increasing AAS as well as DMPA content. This trend can be explained by the increasing specific surface area of the system, compensating for the higher number of incorporated charges. The polyol component has only minor influence on the surface potential, which becomes evident by comparing results of similar AAS and DMPA mass fractions. For the series with varying hard segment content, the surface potential remains essentially constant, as expected from the same AAS mass fraction. All samples show reasonable shear plane distances with values between of 0.2 nm and 0.4 nm, which aligns with results from recent studies.[190,198–201] For example, Borkovec et al. found x_s values between 0.3 and 1.0 nm for highly charged amidine latex particles,[190] while Kobayashi et al. achieved excellent agreement in mobility calculations using 0.25 nm for polystyrene sulfate latex particles.[198,202] Since a value of 0.25 nm is often attributed to a monolayer of firmly bound water molecules, the slightly higher values of this study may indicate surface roughness, caused, for example, by the presence of a non-uniform, hairy layer of macromolecules.[203,204]

In order to check the data of the hard particle model for plausibility, the electrokinetic surface charge density is evaluated according to analytical expression for the surface potential/surface charge density relationship proposed by Ohshima et al.[197] and compared to the surface charge density obtained by titration experiments. As shown for AAS in Table 4-3 and DMPA in Based on the determined equivalence points V_{HA_n}, the specific particle charge Q_{tit} can be calculated with respect to the used mass

of polymer. Furthermore, it is possible to calculate the recovery rate RR, because the maximum amount of charges $Q_{\max}$ is known from the synthesis recipe. RR is given by the ratio $RR = \frac{Q_{\mathrm{tit}}}{Q_{\max}}$.

Table 6-2, σ_0^{ek} is not sufficient to describe σ_0^{tit} determined by titration. This means that the measured electrophoretic mobilities can hardly be explained by the surface charge densities σ_0^{tit} calculated from titration data. The particle has a more complex charge arrangement than can be described by the hard particle model. Consequently, the calculated electrokinetic surface charge density σ_0^{ek} and the corresponding surface potential ψ_0 should be considered as an equivalent value for an ion-impenetrable particle with the same electrophoretic mobility, whose charges are completely arranged on the particle surface.

7.3.3 Conclusive remarks regarding the charge properties of PUDs

These results indicate that neither the soft particle model of Ohshima nor the conventional hard particle models are able to satisfactorily describe the observed particle properties. Instead, the fixed position of the charged groups within the polymer backbone and the corresponding limited mobility during the dispersion process, are likely to create a distribution of the surface functional groups in a peripheral layer in vicinity of the particle interface. This hypothesis is supported by the results obtained by titration experiments, revealing an altered dissociation of the surface functional groups. A distinction between different types of surface functional groups is necessary. By that it is concluded that the functional groups are located in a peripheral layer. The extend of this ordering is furthermore influenced by the synthesis procedure, as the differences between AAS and DMPA indicate. It is thus reasonable to enhance the classical hard particle model when analysing electrophoretic experiments. One of the simplest options is the soft particle model of Ohshima, in which the charges are uniformly distributed in a polyelectrolyte layer. However, this model is unable to explain the experimental results of the PUDs adequately. The lack of a homogeneous charge distribution as evidenced by the titration results is most likely the reason for its failure. Instead, the electrokinetic properties can be explained quite well with basic hard particle theories. Nevertheless, the comparison of the determined surface potential and the determined surface charge densities leads to differences. Therefore, it can be concluded that the electrophoretic behaviour of PUDs of this study is currently best described with the hard particle model with the calculated surface potential ψ_0 to be considered as an effective potential for an ion-impenetrable particle with the same electrophoretic mobility, whose charges are completely arranged on the particle surface.

7.4 Determination of interaction forces

To gain deeper insights in the origins of the experimentally determined dispersion stabilities, an evaluation based on DLVO and XDLVO theory is required. Based on the determined dispersion stabilities in terms of the ccc as well as the effective surface potential evaluation of the attractive forces working in the system are now possible. The attractive interaction potential can be calculated with respect to the repulsive potentials and the ccc according to DLVO theory and based on contact angle data according to the vOGC theory. Chapter 7.4.1 compares both approaches. The theoretical evaluation of all generated results in terms of XDLVO theory is presented in chapter 7.4.2.

7.4.1 Attractive interaction energy

The evaluation of the attractive interaction energies is necessary to obtain a full picture of particle interactions. As outlined in chapter 2.3.4 it is assessed by the Hamaker constant, which serve as a measure for the attractive interaction energies of the system. Two approaches are investigated. First, according to DLVO theory and secondly according to the van Oss-Chaudhury-Good theory based on contact angle data within the framework of XDLVO theory. According to DLVO theory the apparent Hamaker constant A_{131}^{app} is calculated, as described in chapter 5.2 and 6.2.3. It accounts for all additional interaction energies present in the system that are not electrostatic in nature, regardless if they are repulsive or attractive. Therefore, its magnitude also serves as an indicator for the presence of any additional forces. If the value is too high, an additional attractive interaction energy is likely to be present. On the other hand, if it is too low, an additional repulsive interaction energy is considered. By this distinction it also allows to determine whether the DLVO theory can adequately describe the experimental findings. The results for all series are illustrated in Figure 7-8.

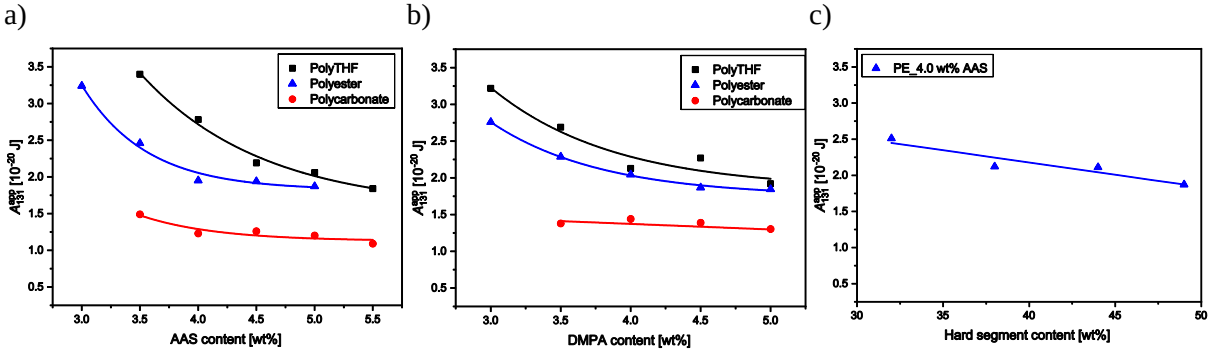

Figure 7-8: Apparent Hamaker constant A_{131}^{app} of all PUD series for a) varying AAS content, b) different DMPA mass fractions and c) PE based PUDs at constant AAS content of 4.0 wt% and different hard segment content..

The apparent Hamaker constants show pronounced differences between the polyol components for both AAS- and DMPA-stabilized PUDs, while values at comparable stabilizer contents remain similar. Comparing the obtained Hamaker constant to literature values for water-based polymer dispersion ($0.3 \cdot 10^{-20}$ J to $1.4 \cdot 10^{-20}$ J[152,153,205–207]) reveals that most values are remarkably high. In this regard, only the PC based PUDs can be considered as reasonable($1.1 \cdot 10^{-20}$ J to $1.5 \cdot 10^{-20}$ J). Additionally, the inconsistent Hamaker constants for different AAS or DMPA contents are unexpected, as the fundamental polymer composition and characteristic synthesis parameter are kept constant. Hence, only minor fluctuations in the Hamaker constant are expected within a given polyol series. For the variation of the hard segment content, the Hamaker constants decrease with increasing hard segment content. This is consistent with the expected changes in the polymer composition. In this case, variations in the hard segment content lead to variations in the hydrophilicity of the polymer structure, which can influence

the attractive interaction energies as well. However, the values for A_{131}^{app} remain unrealistically high for water-based polymer dispersions, ranging from $2.0 \cdot 10^{-20}$ J to $2.5 \cdot 10^{-20}$ J.

An alternative approach to determine the Hamaker constant A_{131}^{vOCG} according to the van Oss-Chaudhury-Good theory is employed in this study. This approach is based on the relationship of the contact angle θ of an apolar test liquid and the apolar surface tension component of the material $\gamma_{\mathrm{S}}^{\mathrm{LW}}$ and is outlined in more detail in chapter 2.3.4. The results of A_{131}^{vOCG} for the variation of the AAS as well as DMPA content are shown in Figure 7-9. PUDs with varying hard segment content are not analysed by contact angle measurements.

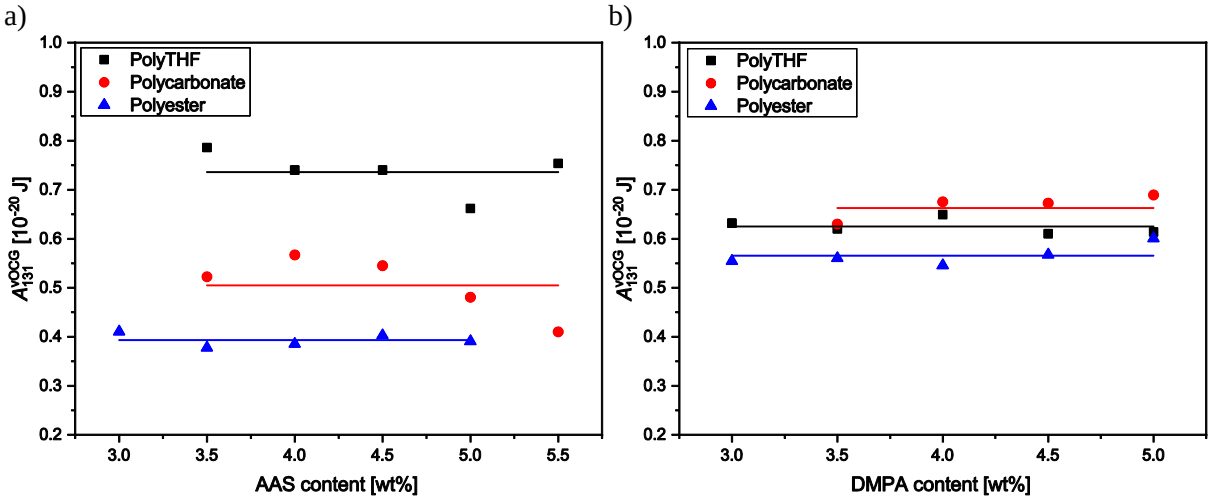

Figure 7-9: Hamaker constant A_{131}^{vOCG} of PTHF (black), PE (blue) and PC (red) based PUDs as a function of a) the AAS concentration and b) the DMPA concentration. The solid lines refer to the average value for each PUD series.

The values of A_{131}^{vOCG} for AAS- as well as DMPA-stabilized PUDs are found to be in the range of $0.4 \cdot 10^{-20}$ J and $0.7 \cdot 10^{-20}$ J. These values are in good accordance with the mentioned characteristic range for polymer dispersions. Furthermore, they show only minor variations within the individual series, meeting expectations arising from the minor differences in the polymer composition. However, trends between the polyol types are not observed. This is likely due to the sensitivity of the contact angle measurement, which can be influenced by the measuring technique, liquid droplet volume, drop spreading time or surface roughness of the investigated solid.[208,209] Additionally, the coalescence of the particles might be affected by the different acidity of DMPA and AAS, respectively. In this regard, recent AFM studies reveal a spherical particle shape of PUD particles based on polyether polyols of different molecular weight stabilized by DMPA after film formation by spin coating.[210] To account for these uncertainties it is decided to use an average value $\overline{A_{131}^{\mathrm{vOCG}}}$ of $(0.6 \pm 0.1) \cdot 10^{-20}$ J for the Hamaker constant of all PUDs.

In view of the too high and inconsistent values of A_{131}^{app} for each polyol series it is likely that additional attractive interaction forces are present. Therefore, it is concluded that the determination of the Hamaker constant according to DLVO theory leads to erroneous results for the PUDs analysed in this study, as it sums up additional interaction energies of the system. On the other hand, the values obtained based on the van Oss-Chaudhury-Good theory A_{131}^{vOCG} lead to reasonable results of the Hamaker constant in the context of water-based polymer dispersions. Therefore, they can be considered as reasonable and are used in XDLVO analysis to assess the total interaction energy profiles.

7.4.2 Assessment of the total interaction energy

The Hamaker constants determined by means of DLVO suggest the presence of additional attractive interaction energies. Therefore, XDLVO approaches are used for further analysis. A source for additional attractive interactions often referred to is the so-called hydrophobic attraction, which is investigated in this study using the approach suggested by Israelachvili.[55] Detailed information regarding the theory and calculation procedure can be found in chapter 2.3.4 and 5.4.3. A more detailed discussion of PUDs stabilized by AAS can be found in chapter 5.4.3and by DMPA in chapter 6.4.5. The results, shown in Figure 7-10. The pre-exponential factor C serves as a measure of the hydrophobic effect and strongly suggest that an additional attractive interaction parameter is necessary to adequately describe the dispersion stability of the synthesized PUDs. For AAS- and DMPA-stabilized systems, PolyTHF based PUDs show the strongest hydrophobic interactions, followed by PE-based systems, while PC-based PUDs demonstrate the lowest hydrophobic contribution. Increasing both AAS and DMPA content results in a reduction in hydrophobic interactions in all series. However, the intrinsic stabilizer concentrations employed are not sufficient to induce hydrophilic repulsion, as reflected in the consistently negative values of the pre-exponential factor C. In the hard segment series, the hydrophobic interaction decreases with increasing hard segment content. Both observations for the different stabilizer- and hard segment content reflect the increasing hydrophilicity of the system.

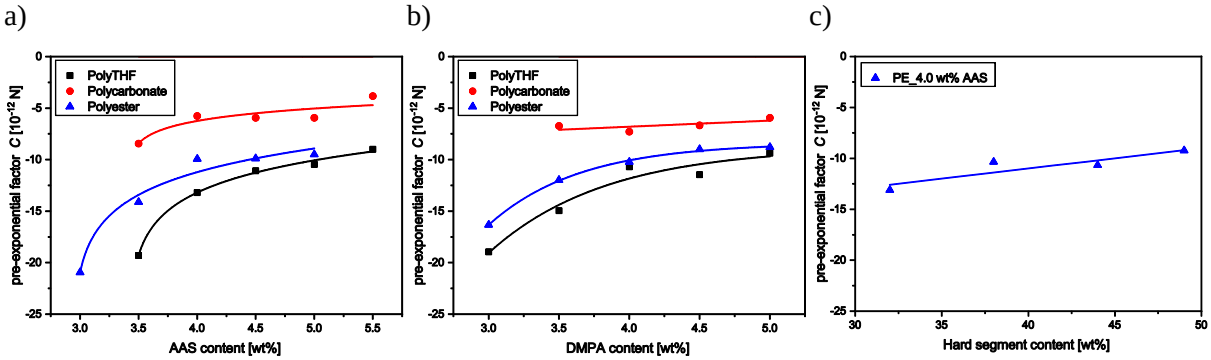

Figure 7-10: Pre-exponential factor C for PTHF (black), PE (blue) and PC (red) based PUDs a) as a function of the AAA content and b) as a function of the DMPA content. c) shows the PUD series based on PE at a constant AAS concentration of 4.0 wt% as a function of the hard segment content. Values are calculated according to XDLVO theory. Solid lines are a guide to the eye.

The determined dispersion stabilities of the aqueous PUDs of this study can be adequately explained by considering additional hydrophobic attraction. This effect likely arises from energetically unfavourable arrangements of water molecules near the particle interface. The presence of functional groups capable of forming hydrogen bonds and charged sites on the substrate's surface are known to enhance the interaction of water with the surface. Consequently, a potential correlation between the properties of the surface and a structural variation of the boundary layers can be anticipated. Hydrophilic surfaces are predicted to yield a distinct boundary layer structure compared to hydrophobic substrates, owing to the lack of hydrogen bonds between water and the surface.[185] In light of this, the impact of the polyol component as well as the influence of the stabiliser content and the hard segment content on the dispersion stability of the PUDs can be properly understood.

However, the XDLVO calculations of this thesis are constrained by the requirement to assume a value for the decay length λ of the hydrophobic attraction, as it cannot be determined from ccc values. Donaldson et al. suggest that λ typically falls within the range of 0.3 nm to 1 nm, noting that discrepancies in reported values likely arise from difficulties in preparing uniform hydrophobic surfaces.[51] For instance, anionic mica surfaces modified with cationic surfactants or lipids exhibit long-range attractions, which have been determined to be based on electrostatic interactions between

oppositely charged domains formed by heterogeneous surface coverage.[211–214] Additional studies have also linked the observed long-range attraction to the bridging of nanobubbles.[215–217] In contrast, more homogeneous systems have yielded shorter decay lengths. Tabor et al. and Moazzami-Gudarzi et al. investigated hydrophobic interactions in systems involving oil droplets and polystyrene particles. Both groups reported decay lengths of approximately 0.3 nm.[53,218] Tabor et al. further concluded that this value is very reasonable for hydrophobic interactions, which are solely due to the orientation of water molecules at hydrophobic surfaces.[56] Therefore, the value of 0.3 nm used in this study seems plausible.

For this reason, the utilisation of alternative investigation methods would be of great interest. For example, force-distance measurements using atomic force microscopy provide detailed information about the decay behaviour of the total interaction energy between two approaching interfaces. Analysis of these force profiles could offer more accurate insights into the range and magnitude of the additional attractive interaction influencing PUD dispersion stability.

8 Summary

Electrostatic stabilization of water-based PUDs is commonly achieved by the incorporation of ionisable functional groups, such as carboxylic or sulfonic acids, which lead to repulsive forces between the particles. Alongside, polyurethanes offer a wide versatility of monomers, including various polyols, short-chain diols, diamines, and isocyanates. This diversity raises the question of the role of polymer architecture for the dispersion stability, in particular the backbone chemistry and the distribution of functional groups in PUDs. Understanding of these relationships is not only of fundamental scientific interest but also of high practical relevance, as PUDs represent an environmentally friendly alternative to solvent-based systems and their stability directly impacts manufacturing as well as end-use performance. The central aim of this thesis is therefore to identify the contributions of polymer structure to dispersion stability and to provide structure–property relationships that offer important insights for the design of water-based PUDs.

A set of systematically designed PUDs is synthesized according to the acetone process, under variation of the polyol component, the type and concentration of hydrophilizing agents, and the hard segment content. The dispersion stability of the PUDs is evaluated through the determination of the critical coagulation concentration. Two complementary techniques are used to investigate the electrostatic interactions. Potentiometric titration is employed to characterize the total amount of ionisable groups, and electrophoretic mobility measurements assess the effective particle potentials. Attractive van der Waals interactions are estimated on the basis of Hamaker constants derived from the classical DLVO approach as well as the contact angle-based van Oss–Chaudhury–Good (vOCG) approach. The interplay between the determined dispersion stability, repulsive interactions, and attractive interactions is analysed using DLVO and XDLVO theory. This combination of complementary methods allows for a detailed investigation of the relationships between polymer architecture and particle interactions.

The results reveal several key findings. All dispersions show a monomodal particle size distribution, with particle size decreasing as stabilizer content increases and asymptotically approaching a lower limit of around 40 nm. A minimum concentration of 3.0–3.5 wt% is required to ensure dispersion stability. Differences in polyol type, hydrophilizer chemistry or hard segment content show only minor effects on particle size, confirming that stabilizer concentration is the dominant factor in particle formation.

In contrast, dispersion stability is significantly affected by structural variations. A higher concentration of both AAS and DMPA improves dispersion stability, although DMPA-stabilized dispersions are generally less stable than the analogous AAS systems. The chemical nature of the polyol has a pronounced effect, with polycarbonate-based PUDs exhibiting substantially higher stability than those derived from polyester or polyTHF diols. Increasing the hard segment content also enhances stability, although to a lesser extent. These results indicate that a certain influence of the hydrophilizer type and incorporation step, but the polyol chemistry and overall polymer polarity are the dominant structural factors determining dispersion stability. To examine the observed differences in more detail, a comprehensive analysis of the repulsive as well as attractive interaction energies proves to be successful.

The repulsive interactions are analysed with respect to the distribution, accessibility and dissociation behaviour of the functional groups as well as the electrokinetic properties of the particles. Potentiometric titration reveals that functional groups introduced via AAS and DMPA are not uniformly distributed at the particle surface, with many buried within the particle core or shielded by the polymer matrix. The determined recovery rates (70 %–85 % for AAS; 50 %–75 % for DMPA) indicate that many groups remain inaccessible, potentially trapped within the particle core. The different chemical environment of the ionizable groups throughout the particle also affects their effective dissociation. Despite the strong acidity of the sulfonate groups, AAS functional groups show one additional weaker ($pK_{a1} \approx 6$), whereas DMPA systems exhibits two weak sites with effective dissociation constants below that of the monomer.

The limited dissociation most likely arises from electrostatic interactions between neighbouring functional groups. AAS incorporated during chain extension is localised in flexible polymer domains, making approximately 85 % of charges surface-accessible, whereas DMPA incorporated into rigid hard segments retains roughly 75 % of charges within the particle interior. Conclusively, the analysis of the potentiometric titration curve indicates that the particle charges are not only located on the particle surface but also distributed in a peripheral ion-penetrable layer with differences between AAS and DMPA potentially arising from the synthesis protocol. Importantly, neither the polyol component nor the hard segment content shows a measurable effect on the titration results, indicating that these structural parameters do not substantially influence the distribution or accessibility of charges.

Electrophoretic mobility measurements show a non-zero limiting mobility. This suggests a soft particle structure, which is consistent with the heterogeneous charge distribution indicated by titration. However, the soft particle model of Ohshima does not adequately describe the experimental data. Besides its failure at low ionic strength, the determined volume charge densities ZN and the corresponding specific particle charges show an implausible trend, likely due to the assumption of a homogeneous charge distribution. In contrast, the electrophoretic behaviour of the PUDs is best described using a hard particle model that accounts for the relaxation effect. In this framework, the zeta potentials as a function of the electrolyte concentration is best to be represented by assuming a constant surface potential ψ_0 and a defined shear-plane position x_s. The surface potentials ψ_0 decreases with increasing stabilizer content, reflecting the increasing specific surface area. The shear-plane positions x_s ranging from 0.2 to 0.4 nm are consistent with a tightly bound layer of water molecules or minor surface structures. The resulting electrokinetic surface-charge density is significantly lower expected from titration, which again indicates that a substantial fraction of ionic groups resides within the polymer shell rather than at the particle surface. Nevertheless, these findings confirm that the hard particle model provides an effective framework for describing the electrokinetic properties of PUDs, with the calculated surface potential ψ_0 representing an effective potential for an equivalent, ion-impenetrable particle with the same electrophoretic mobility, whose charges are completely arranged on the particle surface.

The attractive van der Waals interactions between the PUD particles are initially estimated based on Hamaker constants derived from classical DLVO theory. Despite being a material constant, these values varied inconsistently for different AAS as well as DMPA mass fractions. A more reliable estimation was achieved using the vOCG approach, yielding an average Hamaker constant $\overline{A_{131}^{\mathrm{vOCG}}}$ of $0.6 \pm 0.1 \cdot 10^{-20}$ J, which is typical for aqueous polymer dispersions and thereby suggesting that additional attractive forces contribute to the total interaction potential. To account for the additional attractive interaction energies, the XDLVO framework is applied. The resulting negative pre-exponential factor *C* is interpreted as a measure of hydrophobic interaction. The analysis reveals that hydrophobic forces vary significantly with polyol type and decrease with increasing ionic group content as well as hard segment content, reflecting the influence of polymer hydrophilicity. Together, these findings demonstrate that dispersion stability of water-based PUDs is not determined solely by electrostatic and van der Waals forces, but also critically depends on hydrophobic interactions.

Nonetheless, certain limitations of the XDLVO analysis remain. The indirect methods used to probe the charge distribution cannot adequately resolve the spatial arrangement of ionic sites. In addition, the XDLVO approach relies on several simplifying assumptions. Future studies should therefore employ direct force measurements, for instance by atomic force microscopy, to quantify electrostatic, van der Waals, and hydrophobic contributions more exactly. Such data would allow direct comparison with model predictions and clarify the magnitude and decay length of hydrophobic forces. Extending the synthetic design to a wider range of monomers, particularly by tuning the hydrophilicity of the polyurethane backbone through PEO segments of different molecular weight, could further test these

concepts. This might even enable a transition from attractive hydrophobic to repulsive hydrophilic interactions.

In conclusion, this work demonstrates that the stability of water-based PUDs can fully be explained by the combined effects of electrostatic, van der Waals, and hydrophobic or potentially hydrophilic interactions, governed by the accessibility of ionic groups and the polarity of the polymer matrix. Unlike the classical DLVO theory, which proves to be insufficient to describe these systems, the XDLVO analysis provides a more accurate framework by explicitly accounting for hydrophobic contributions. These insights deepen the theoretical understanding of colloidal stabilization by highlighting that the key to robust, sustainable dispersions lies in linking molecular structure to particle interactions, and provide a base for the design of water-based PUDs with improved stability.

9 Experimental section

9.1 Chemicals

The used chemicals as well as the corresponding supplier and purity are shown in Table 9-1. If not stated differently in the corresponding sections, ultrapure water was used for every purpose.

Table 9-1: List of used chemicals.

Name	Supplier	Purity [%]
Polyester polyol PE90B (1000 g mol^{-1})	Covestro	n.a.
Desmophen C2102 (Polycarbonat, 1000 g mol^{-1})	Covestro	n.a.
Polytetrahydrofurane (PolyTHF, 1000 g mol^{-1})	Merck KGaA	n.a.
AAS-solution aq.(45.5 wt%)	Covestro	45.5
1,4-Butanediol (BDO)	Merck KGaA	≥99.0
Dimethylolpropionicacid	Covestro	n.a.
Isophoronediisocyante (IPDI)	Merck KGaA	≥99.0
Isophornediamine (IPDA)	Merck KGaA	≥99.0
Dibutylamine	Merck KGaA	≥99.0
Dibutyltin dilaurate (DBTDL)	Merck KGaA	≥99.0
Amberlite IRA-900	Sigma Aldrich	n.a.
Amberlite IRN-77	Alfa Aesar	n.a.
Ethanol	Fisher Scientific	≥99.8
Acetone	Fisher Scientific	≥99.8
Magnesiumnitrate	VWR	≥99.6
Methanol	Fisher Scientific	≥99.0
Sodium carbonate	Carl Roth	≥99.5
Sodium chloride	VWR	≥99.5
Sodium bicarbonate	VWR	≥99.7
Sodium hydroxide 1M aq.	Fisher Scientific	1 M reference solution
p-Toluenesulfonyl isocyanate-	Sigma Aldrich	≥96.0
Hydrochloric acid 1 M aq.	VWR	1 M reference solution
Triton X-165	Sigma Aldrich	Solution 70 wt%
Poly-DADMAC	BTG	n.a.
Potassium hydrogenphthalate	Merck KGaA	≥99.5

Acetonitrile	Merck KGaA	≥99.0
Triethylamine	Sigma Aldrich	≥99.5
Potassium nitrate	Merck KGaA	≥99.0
Hydrochloric acid aq.	VWR	Concentrated solution 37%
Sodium hydroxide pellets	Carl Roth	≥98.0
Diiodmethane	Sigma Aldrich	≥99.0
Hydrochloric acid 0.1 M aq	VWR	0.1 M solution

9.2 Experimental methods

9.2.1 Hydroxyl number

The hydroxyl number is determined according to the TSI method described in DIN EN 15168:2006. The titration is done using the *Titroline 7800* of the company *SI Analytics*.

The measurement is done using each polyol component as received as well as dried. For this purpose, each polyol component is dried at 100°C und 200 mbar for 1 hour. Each sample is dissolved in 10 mL acetonitrile. 10 mL p-Toluenesulfonyl isocyanate is added to the solution and stirred for 5 min. Afterwards, 0.5 mL water is added to the solution. 60 mL acetonitrile is added after one minute and the solution is titrated with 0.1 M Tetrabutylammoniumhydroxyd standard solution. Each component is measured three times.

The hydroxyl number of the polyol components is monitored frequently due to the possibility of increasing water content.

9.2.2 Isocyanate content

The determination of the isocyanate (NCO) content is done using the *TitroLine 7800* from *SiAnalytics* according to DIN EN ISO 14896:2009-07. Approximately 0.4 g of the NCO terminated prepolymer is dissolved in 10 mL 0.2 M dibutylamine solution in acetone and 40 mL of acetone. The solution is titrated with 0.1 M hydrochloric acid afterwards to determine the excess of dibutylamine and thus the NCO content in % by the following equation.

$$NCO\ content = \frac{4.2 \cdot c(\mathrm{HCl}) \cdot T(\mathrm{HCl}) \cdot (B_{\mathrm{DBA}} - V_{\mathrm{HCl}})}{m_{\mathrm{Sample}}} \tag{9-1}$$

Here, T is the titer and $c(\mathrm{HCl})$ the concentration of HCl, B_{DBA} the consumed volume of the blank titration of the dibutylamine solution, V_{HCl} the consumed volume of hydrochloric acid for the sample titration and m_{Sample} the mass of the NCO containing sample.

The dibutylamine solution is prepared every week to avoid influences due to aging effects.

9.2.3 pH value

The determination of the pH value is done using the device *SevenCompact Duo* from *Mettler Toledo*. The electrode is calibrated using three different standard buffer solution of pH 4.01, pH 7.00 and pH 9.21 prior to each measurement.

9.2.4 Particle size

The particle size distribution is determined by dynamic light scattering using the *Zetasizer Nano ZS* of *Malvern Instruments.* Each sample is measured at 25 °C using a 632.8 nm He-Laser and detecting the signal at 173° backscatter detection. The standard operating procedure includes the following set up.

The refractive index of the dispersed polyurethane is set to 1.496 and the absorption at the given wavelength to 0.01. Ultrapure water is used as dispersion medium with a dynamic viscosity of 0.8872 mPa s and a refractive index of 1.3340. For each sample three measurements in poly (methyl methacrylate) (PMMA)-macro cuvettes are carried out, with each single measurement resulting from 15 measurement sub runs. The samples are diluted to 0.0001 wt % with ultrapure water in order to avoid multiple light scattering while maintaining an appropriate signal-to-noise ratio using the automatically adjusted attenuation factor as well as the intensity of the detected light intensity as indications. The mean particle size is given by the z-average value (intensity mean).

9.2.5 Electrophoretic mobility

The electrophoretic mobility in dependence of the electrolyte concentration are done at 25 °C using the *Zetasizer Nano ZS* from *Malvern Instruments*. The measurement settings are the same as those for particle size determination, although the signal is detected at 17° front scatter detection. The following adjustments in the standard operating procedure are done. Relative permittivity of water is set to 78.5. The samples are measured at 0.1 vol % in order to obtain an appropriate signal-to-noise ratio. The concentration is higher compared to the determination of the particle size distribution because the scattering intensity in front direction is less intense. Each measurement is performed in a folded capillary cell DTS 1070 as a single measurement consisting out of 15 individual measurement sub runs. KNO_3 is used as electrolyte and the electrolyte concentration is varied in the range of 5mM-300 mM. It must be noted, that increasing electrolyte concentration leads to a degradation of the electrodes of the folded capillary cells due to electrolysis. At concentrations greater than 300 mM KNO_3, higher measurement errors and insufficient results are found. For this reason, 300 mM KNO_3 is used as maximum concentration. To compensate the different degradation status of each cell, each sample is measured four times using different cells. Nevertheless, the cells need to be exchanged frequently.

In case of PUDs stabilized by DMPA the pH is adjusted to pH 10.4 using a sodium carbonate/bicarbonate buffer with a concentration of 2 mM to ensure complete dissociation. All samples were left for 12 hours at room temperature for equilibration purpose.

9.2.6 Polyelectrolyte titration

Polyelectrolyte titration experiments are done using the particle charge detector *PCD-04* as well as the titrator *PCD-T3* of *Mütek*. 0.001 M Poly-DADMAC solution is used as a titrant. Each PUD is diluted to approximately 0.1 wt% with water. NaCl is used as electrolyte and the electrolyte concentration is varied in the range of 5-200 mM. In case of DMPA, the pH is adjusted to pH 10.4 using a sodium carbonate/bicarbonate buffer with a concentration of 2 mM to ensure complete dissociation. Prior to each measurement a blank titration of 10 mL ultrapure water is done to account for the surface charges of the measurement cell. Sample titration is done using 10 mL of the 0.1 wt% PUD solution. Each sample is analysed three times.

Greatest care must be taken to assure cleanliness of the measurement device. For this reason, the measurement equipment is cleaned prior to each measurement using a cleaning solution consisting out of 125 g water, 50 g NaBr and 50 g acetone.

9.2.7 Potentiometric titration

Potentiometric acid-base titration experiments of PUDs stabilized by AAS were performed with titrator *Ti-Touch 916* from *Metrohm* using a linear step width of 0.05 mL. The measuring cell is blanketed with nitrogen to avoid absorption of carbon dioxide. Samples are diluted to a concentration of 5 wt % and treated with a strongly acidic ion-exchange resin Amberlite IRN-77 for 1 h for purification and protonation purpose before titration.

The ion-exchange resin is purified and activated according to a procedure described by McCann. It is first washed with preheated water (>80 °C) and then three times with methanol. For activation purpose, the pH value is shifted several times by alternately using 3 M HCl and 3 M NaOH. After each activation cycle, the pH value is set to neutral by washing several times with ultrapure water. The ion exchange resin activated in this way is used for the treatment of the PUD samples and subsequently removed by filtration. Afterwards, the solids content of the protonated polymer is determined for further evaluation purposes. Finally, the potentiometric titration experiment involves two measurements. At first, a blank titration consisting of 5 mL 0.02 M HCl and 70 mL ultrapure water being titrated with 0.02 M NaOH. Second, sample titration consisting of 10 mL 5 wt % sample, 5 mL 0.02 M HCl and 60 mL ultrapure water.

Potentiometric titrations of PUDs stabilized by DMPA are done using the same device and measurement set up. However, the samples are prepared at a concentration of 5 wt % using a 3 wt% solution of the non-ionic surfactant Triton X-165 to prevent coagulation at an acidic pH level. The samples are treated with a strongly basic ion exchange resin Amberlite IRA900 followed by a strongly acidic ion exchange resin Amberlite IRN-77 for 1 h each for purification and protonation purposes prior to titration. The activation of Amberlite IRA900 is similar to that for Amberlite IRN-77. The titration procedure is also similar.

The difference in volume equivalence between the blank as well as the sample measurements corresponds to the content of acidic groups of the polymer. The titration curves are further evaluated using the procedure of Alves et al.[219] to get insights about the dissociation behaviour of the surface functional groups.

9.2.8 Critical coagulation concentration

The critical coagulation concentration is determined using a UV/VisSpectrophotometer *Evolution 220* from *ThermoScientific* following the procedure of Reerink and Overbeek.[47] The change in absorbance A is measured for 30 s at 0.1 s intervals in PMMA cuvettes at a wavelength of 500 nm. Blank measurements are done with ultrapure water. Each sample is measured at 0.075 wt% and sodium chloride (NaCl) is used as electrolyte in a concentration range of 0.5 – 4.5 mol L^{-1} in the final dispersion. The pH value of DMPA stabilized PUDS is adjusted to pH 10.4 using a sodium carbonate/bicarbonate buffer with a concentration of 2 mM to ensure complete dissociation. Sample and electrolyte solution are mixed immediately prior to measurement within the cuvette already placed in the measurement cell. By measuring at different electrolyte concentrations, a series of curves is obtained for each sample. The initial slope $\mathrm{d}A/\mathrm{d}t$ of each curve is determined and the logarithmic reciprocal $\log(\mathrm{d}t/\mathrm{d}A)$ is plotted against $\log(c)$. The values obtained decrease with increasing electrolyte concentration in the slow coagulation regime, while they remain constant in the fast coagulation regime. The intercept of the two sections gives the critical coagulation concentration.

9.2.9 Contact angle

Static contact angles are measured using the *Contact Angle System OCA* from *Dataphysics* according to DIN 55660-2. Diiodomethane (γ_L: 50.8 mN m^{-1}, γ_L^{AB}: 0 mN m^{-1}, γ_L^{LW}: 50.8 mN m^{-1}) is used as test liquid. At least six contact angles are measured 15 s after dispensing the droplet with a volume of 3 µL on different positions of the polyurethane film. The contact angles are evaluated using Young-Laplace equation.

Polyurethane films are prepared on glass substrate with a wet film thickness of 200 µm, dried at 80°C and stored at a relative humidity of approximately 50 % over a saturated $Mg(NO_3)_2$ solution at room temperature for at least 16 h prior to measurement.

9.3 Synthesis of PUDs

A general description of the synthesis procedure according to the acetone process[8] is provided in the following section. However, detailed tables containing the synthesis recipe for PUDs containing AAS and DMPA as well as different kind of polyol components are already given in the corresponding sections (Table 4-1 and Table 6-1). Therefore, they will not be shown here again. Only the synthesis recipe of PUDs with varying hard segment content is shown in Table 9-2.

Prior to each synthesis, the polyol components are dehydrated to avoid side reactions by water. This is done in a 500 mL round-bottom four-necked flask equipped with thermometer and mechanical stirrer under nitrogen atmosphere at 100 °C and 200 mbar for one hour. Afterwards, the necessary amount of short chain diol components, such as BDO or DMPA, is fed to the polyol component into the four-necked flask, equipped with a mechanical stirrer and condenser. The mixture is preheated up to 70 °C under continuous stirring and nitrogen atmosphere. DBTL is added into the reaction mixture. When a homogenous reaction mixture is obtained, the desired amount of IPDI is added dropwise through a dropping funnel. The reaction temperature is raised to 100 °C after complete addition. The progress of reaction is controlled by determining NCO content using standard dibutylamine back-titration according to DIN EN ISO 14896:2009-07 as described in chapter 9.2.2. Once the theoretical NCO content is reached, the reaction mixture is cooled to 80 °C and acetone is added dropwise through a dropping funnel with approximately 2 mL min^{-1}. After complete addition, the solution is cooled to 40 °C. In case of PUDs stabilized by DMPA, the appropriate amount of TEA to achieve 100% neutralization of the carboxyl groups is added and stirred for 30 minutes. Then chain extension is carried out. For this purpose, the desired amounts of short chain diamine components, such as IPDA and AAS, are dissolved in water and added dropwise to the acetone solution through a dropping funnel. The reaction is carried out for 30 minutes and checked again for completion by monitoring the NCO content. The dispersion process is carried out by adding water constantly with 2.3 mL min^{-1} using *KDS Legato 110* single syringe pumps at 40 °C and 350 rpm. The amount of chain extender and water is adjusted under consideration of the removed mass of prepolymer for the determination of the NCO content. Finally, Acetone is removed by distillation at 40 °C and 200 mbar.

Table 9-2: Synthesis series of waterborne PUD based on PE as polyol component with different hard segment content of 49.8%, 44.1%, 38.5% and 32.8%.NCO/OH=1.7, degree of chain extension=92%, AAS content of 4.0 wt% and solid content of approx. 30 wt-%. All values in g.

Sample	PE	BDO	IPDI	Acetone	IPDA	AAS	Water	Water
PE49.8	24.20	1.91	17.05	76.79	2.90	4.01	7.18	96.48
PE44.1	24.21	1.14	13.83	69.69	2.10	3.48	5.43	84.42
PE38.5	24.20	0.52	11.23	63.99	1.62	3.21	4.38	78.43
PE32.8	24.21	/	9.07	59.24	1.27	3.00	3.63	74.38

10 References

(1) Ates, M., Karadag, S., Eker, A. A., Eker, B. Polyurethane foam materials and their industrial applications. Polymer International **2022**, *71*, 1157–1163, DOI: 10.1002/pi.6441.

(2) Dutta, A. S. Polyurethane Foam Chemistry. In *Recycling of Polyurethane Foams*; Elsevier, 2018, pp. 17–27, ISBN: 9780323511339.

(3) Gama, N. V., Ferreira, A., Barros-Timmons, A. Polyurethane Foams: Past, Present, and Future. Materials (Basel) **2018**, *11*, DOI: 10.3390/ma11101841.

(4) John, J., Bhattacharya, M., Turner, R. B. Characterization of polyurethane foams from soybean oil. J of Applied Polymer Sci **2002**, *86*, 3097–3107, DOI: 10.1002/app.11322.

(5) Wang, J., Zhang, C., Deng, Y., Zhang, P. A Review of Research on the Effect of Temperature on the Properties of Polyurethane Foams. Polymers (Basel) **2022**, *14*, DOI: 10.3390/polym14214586.

(6) Meier-Westhues H.-U., Danielmeier K., Kruppa P., Squiller E. *Polyurethanes: Coatings, Adhesives and Sealants*, 2nd ed.; Vincentz Network: Hannover, 2019, ISBN: 978-3-74860-047-3.

(7) Chattopadhyay, D. K., Raju, K. Structural engineering of polyurethane coatings for high performance applications. Progress in Polymer Science **2007**, *32*, 352–418, DOI: 10.1016/j.progpolymsci.2006.05.003.

(8) Das, A., Mahanwar, P. A brief discussion on advances in polyurethane applications. Advanced Industrial and Engineering Polymer Research **2020**, *3*, 93–101, DOI: 10.1016/j.aiepr.2020.07.002.

(9) Golling, F. E., Pires, R., Hecking, A., Weikard, J., Richter, F., Danielmeier, K., Dijkstra, D. Polyurethanes for coatings and adhesives – chemistry and applications. Polymer International **2019**, *68*, 848–855, DOI: 10.1002/pi.5665.

(10) Llevot, A., Meier, M. Perspective: green polyurethane synthesis for coating applications. Polymer International **2019**, *68*, 826–831, DOI: 10.1002/pi.5655.

(11) Mucci, V. L., Hormaiztegui, M. E. V., Amalvy, J. I., Aranguren, M. I. Formulation, structure and properties of waterborne polyurethane coatings: a brief review. Journal of Adhesion Science and Technology **2024**, *38*, 489–516, DOI: 10.1080/01694243.2023.2240587.

(12) Camadanli, S., Hisir, A., Dural, S. Synthesis and performance of moisture curable solvent free silane terminated polyurethanes for coating and sealant applications. J of Applied Polymer Sci **2022**, *139*, DOI: 10.1002/app.51722.

(13) Cong, P., Liu, C., Zhang, X. Preparation of thermoplastic polyurethane sealant and its adherence properties under various environments. Composites Part B: Engineering **2025**, *293*, 112125, DOI: 10.1016/j.compositesb.2025.112125.

(14) Dang, G., Gu, J., Wan, Q., Niu, L. Polyurethanes for Sealants. In *Polyurethanes: Preparation, properties, and applications Volume 2, Advanced applications*; Gupta, R. K., Ed.; AMERICAN CHEMICAL SOCIETY: Washington, DC, 2023; Vols. 1453, pp. 153–168, ISBN: 9780841296916.

(15) Paulina, K., Adam, O., Nowak, P., Łukasz, P. Polyurethanes for Coating, Adhesives, and Other Applications. In *Polyurethane chemistry: Renewable polyols and isocyanates*; Gupta, R. K., Kahol, P. K., Eds.; AMERICAN CHEMICAL SOCIETY: Washington, DC, 2021; Vols. 1380, pp. 305–326, ISBN: 9780841298408.

(16) Pourahmady, N. Coatings, adhesives, and sealants from polyester polyurethanes. In *Rethinking Polyester Polyurethanes: Algae Based Renewable, Sustainable, Biodegradable and Recyclable Materials*; Pomeroy, R. S., Ed.; Elsevier: Amsterda, 2023, pp. 195–213, ISBN: 9780323999823.

(17) Mittal K. L., Pizzi A., Eds. *Handbook of adhesive technology*; CRC Press: Boca Raton, 2018, ISBN: 9781315120942.

(18) Segura, D. M., Nurse, A. D., McCourt, A., Phelps, R., Segura, A. Chapter 3 Chemistry of polyurethane adhesives and sealants. In *Handbook of adhesives and sealants*; Cognard, P., Ed.; Elsevier: Amsterdam, San Diego, CA, 2006; Vol. 1, pp. 101–162, ISBN: 9780080445540.

(19) Shirmohammadli, Y., Pizzi, A., Raftery, G. M., Hashemi, A. One-component polyurethane adhesives in timber engineering applications: A review. Int. J. Adhes. Adhes. **2023**, *123*, 103358, DOI: 10.1016/j.ijadhadh.2023.103358.

(20) Bayer, O. Das Di-Isocyanat-Polyadditionsverfahren (Polyurethane). Angewandte Chemie **1947**, *59*, 257–272, DOI: 10.1002/ange.19470590901.

(21) *Ullmann's Encyclopedia of Industrial Chemistry*; Wiley, 2003, ISBN: 9783527303854.

(22) Adam, N., Avar, G., Blankenheim, H., Friederichs, W., Giersig, M., Weigand, E., Halfmann, M., Wittbecker, F.-W., Larimer, D.-R., Maier, U., Meyer-Ahrens, S., Noble, K.-L., Wussow, H.-G. Polyurethanes. In *Ullmann's Encyclopedia of Industrial Chemistry*; Wiley, 2003, ISBN: 9783527303854.

(23) Akindoyo, J. O., Beg, M. D. H., Ghazali, S., Islam, M. R., Jeyaratnam, N., Yuvaraj, A. R. Polyurethane types, synthesis and applications – a review. RSC Adv. **2016**, *6*, 114453–114482, DOI: 10.1039/c6ra14525f.

(24) KROL, P. Synthesis methods, chemical structures and phase structures of linear polyurethanes. Properties and applications of linear polyurethanes in polyurethane elastomers, copolymers and ionomers. Progress in Materials Science **2007**, *52*, 915–1015, DOI: 10.1016/j.pmatsci.2006.11.001.

(25) Petrović, Z. S., Ferguson, J. Polyurethane elastomers. Progress in Polymer Science **1991**, *16*, 695–836, DOI: 10.1016/0079-6700(91)90011-9.

(26) Saunders, J. H. The Relations between Polymer Structure and Properties in Urethans. Rubber Chemistry and Technology **1960**, *33*, 1259–1292, DOI: 10.5254/1.3542246.

(27) Abele L., Oertel G. *Polyurethane handbook: Chemistry, raw materials, processing application, properties*, 2nd ed.; Hanser: Munich, 1994, ISBN: 3-446-17198-3.

(28) Hepburn C. *Polyurethane elastomers*; Elsevier Applied Science: London, 1992, ISBN: 1-85166-589-7.

(29) Ionescu M., Bayer O. *Polyols for polyurethanes: Chemistry and technology*, 3rd ed.; De Gruyter: Berlin, Boston, 2019, ISBN: 978-3-11-064033-5.

(30) Meier-Westhues U. *Polyurethane: Lacke, Kleb- und Dichtstoffe*; Vincentz Network: Hannover, 2007, ISBN: 978-3866308961.

(31) Dieterich, D. Aqueous emulsions, dispersions and solutions of polyurethanes; synthesis and properties. Progress in Organic Coatings **1981**, *9*, 281–340, DOI: 10.1016/0033-0655(81)80002-7.

(32) Kim, B. K. Aqueous polyurethane dispersions. Colloid Polym Sci **1996**, *274*, 599–611, DOI: 10.1007/BF00653056.

(33) Noble, K.-L. Waterborne polyurethanes. Progress in Organic Coatings **1997**, *32*, 131–136, DOI: 10.1016/S0300-9440(97)00071-4.

(34) Honarkar, H. Waterborne polyurethanes: A review. Journal of Dispersion Science and Technology **2018**, *39*, 507–516, DOI: 10.1080/01932691.2017.1327818.

(35) Howarth, G. A. Polyurethanes, polyurethane dispersions and polyureas: Past, present and future. Surface Coatings International Part B: Coatings Transactions **2003**, *86*, 111–118, DOI: 10.1007/BF02699621.

(36) Santamaria-Echart, A., Fernandes, I., Barreiro, F., Corcuera, M. A., Eceiza, A. Advances in Waterborne Polyurethane and Polyurethane-Urea Dispersions and Their Eco-friendly Derivatives: A Review. Polymers (Basel) **2021**, *13*, DOI: 10.3390/polym13030409.

(37) Tennebroek, R., van der Hoeven-van Casteren, I., Swaans, R., van der Slot, S., Stals, P. J. M., Tuijtelaars, B., Koning, C. Water-based polyurethane dispersions. Polymer International **2019**, *68*, 832–842, DOI: 10.1002/pi.5627.

(38) Nanda, A. K., Wicks, D. A. The influence of the ionic concentration, concentration of the polymer, degree of neutralization and chain extension on aqueous polyurethane dispersions prepared by the acetone process. Polymer **2006**, *47*, 1805–1811, DOI: 10.1016/j.polymer.2006.01.074.

(39) Lijie, H., Yongtao, D., Zhiliang, Z., Zhongsheng, S., Zhihua, S. Synergistic effect of anionic and nonionic monomers on the synthesis of high solid content waterborne polyurethane. Colloids and Surfaces A: Physicochemical and Engineering Aspects **2015**, *467*, 46–56, DOI: 10.1016/j.colsurfa.2014.11.014.

(40) Nurdin, N. S., Saalah, S., Lim, A. T., Francis, A. Y., Abdullah, L., SaifulAzry, S. Effect of DMPA Content on Colloidal Stability of Jatropha Oil-based waterborne Polyurethane Dispersion. IOP Conference Series: Materials Science and Engineering **2020**, *778*, 12107, DOI: 10.1088/1757-899X/778/1/012107.

(41) Chen, R., Zhang, C., Kessler, M. R. Anionic waterborne polyurethane dispersion from a bio-based ionic segment. RSC Advances **2014**, *4*, 35476–35483, DOI: 10.1039/c4ra07519f.

(42) Cao, X., Ge, X., Chen, H., Li, W. Effects of trimethylol propane and AAS salt on properties of waterborne polyurethane with low gloss. Progress in Organic Coatings **2017**, *107*, 5–13, DOI: 10.1016/j.porgcoat.2017.02.021.

(43) Grau, C., Schmidt, A. M., Wilkens, J. Water-Based Polyurethane Dispersions: A Detailed Analysis of the Particle Charge Using Soft and Hard Particle Model. Langmuir **2024**, *40*, 22123–22135, DOI: 10.1021/acs.langmuir.4c02498.

(44) Verwey E. J. W., Overbeek J. T. G. *Theory of the Stability of Lyophobic Colloids*: New York, 1948, ISBN: 9780486409290.

(45) Derjaguin, B., Landau, L. Theory of the stability of strongly charged lyophobic sols and of the adhesion of strongly charged particles in solutions of electrolytes. Progress in Surface Science **1993**, *43*, 30–59, DOI: 10.1016/0079-6816(93)90013-L.

(46) Overbeek, J. T. G. The Rule of Schulze and Hardy. Pure Appl. Chem. **1980**, *52*, 1151–1161.

(47) Reerink, H., Overbeek, J. T. G. The rate of coagulation as a measure of the stability of silver iodide sols. Discussions of the Faraday Society **1954**, *18*, 74–84, DOI: 10.1039/DF9541800074.

(48) Ohshima, H., Nakamura, M., Kondo, T. Electrophoretic mobility of colloidal particles coated with a layer of adsorbed polymers. Colloid Polym Sci **1992**, *270*, 873–877, DOI: 10.1007/BF00657731.

(49) Ohshima, H. Electrophoretic Mobility of Soft Particles. J Colloid Interface Sci **1994**, *163*, 474–483, DOI: 10.1006/jcis.1994.1126.

(50) Ohshima, H. Theory of electrostatics and electrokinetics of soft particles. Science and Technology of Advanced Materials **2009**, *10*, DOI: 10.1088/1468-6996/10/6/063001.

(51) Donaldson, S. H., Røyne, A., Kristiansen, K., Rapp, M. V., Das, S., Gebbie, M. A., Lee, D. W., Stock, P., Valtiner, M., Israelachvili, J. Developing a general interaction potential for hydrophobic and hydrophilic interactions. Langmuir **2015**, *31*, 2051–2064, DOI: 10.1021/la502115g.

(52) Smith, A. M., Borkovec, M., Trefalt, G. Forces between solid surfaces in aqueous electrolyte solutions. Adv Colloid Interface Sci **2020**, *275*, 102078, DOI: 10.1016/j.cis.2019.102078.

(53) Moazzami-Gudarzi, M., Trefalt, G., Szilagyi, I., Maroni, P., Borkovec, M. Nanometer-ranged attraction induced by multivalent ions between similar and dissimilar surfaces probed using an atomic force microscope (AFM). Phys Chem Chem Phys **2016**, *18*, 8739–8751, DOI: 10.1039/c5cp07830j.

(54) Ducker, W. A., Mastropietro, D. Forces between extended hydrophobic solids: Is there a long-range hydrophobic force? Current Opinion in Colloid & Interface Science **2016**, *22*, 51–58, DOI: 10.1016/j.cocis.2016.02.006.

(55) Israelachvili, J., Pashley, R. The hydrophobic interaction is long range, decaying exponentially with distance. Nature **1982**, *300*, 341–342, DOI: 10.1038/300341a0.

(56) Tabor, R. F., Grieser, F., Dagastine, R. R., Chan, D. Y. C. The hydrophobic force: measurements and methods. Phys Chem Chem Phys **2014**, *16*, 18065–18075, DOI: 10.1039/c4cp01410c.

(57) Butt, H.-J., Cappella, B., Kappl, M. Force measurements with the atomic force microscope: Technique, interpretation and applications. Surface Science Reports **2005**, *59*, 1–152, DOI: 10.1016/j.surfrep.2005.08.003.

(58) Brant, J. A., Childress, A. E. Colloidal adhesion to hydrophilic membrane surfaces. Journal of Membrane Science **2004**, *241*, 235–248, DOI: 10.1016/j.memsci.2004.04.036.

(59) Cao, H., Qi, F., Liu, R., Wang, F., Zhang, C., Zhang, X., Chai, Y., Zhai, L. The influence of hydrogen bonding on N-methyldiethanolamine-extended polyurethane solid–solid phase change materials for energy storage. RSC Adv. **2017**, *7*, 11244–11252, DOI: 10.1039/c7ra00405b.

(60) Chen, Y., Chen, Y.-L. Aqueous dispersions of polyurethane anionomers: Effects of countercation. Journal of Applied Polymer Science **1992**, *46*, 435–443, DOI: 10.1002/app.1992.070460308.

(61) Delpech, M. C., Coutinho, F. M. Waterborne anionic polyurethanes and poly(urethane-urea)s: influence of the chain extender on mechanical and adhesive properties. Polymer Testing **2000**, *19*, 939–952, DOI: 10.1016/S0142-9418(99)00066-5.

(62) Chan, W.-C., Chen, S.-A. Polyurethane ionomers: effects of emulsification on properties of hexamethylene diisocyanate-based polyether polyurethane cationomers. Polymer **1988**, *29*, 1995–2001, DOI: 10.1016/0032-3861(88)90173-5.

(63) Rueda-Larraz, L., d'Arlas, B. F., Tercjak, A., Ribes, A., Mondragon, I., Eceiza, A. Synthesis and microstructure–mechanical property relationships of segmented polyurethanes based on a PCL–PTHF–PCL block copolymer as soft segment. European Polymer Journal **2009**, *45*, 2096–2109, DOI: 10.1016/j.eurpolymj.2009.03.013.

(64) Yoon Jang, J., Kuk Jhon, Y., in Woo Cheong, Hyun Kim, J. Effect of process variables on molecular weight and mechanical properties of water-based polyurethane dispersion. 27th European Colloid and Interface Society conference (27th ECIS 2013) **2002**, *196*, 135–143, DOI: 10.1016/S0927-7757(01)00857-3.

(65) Pérez-Limiñana, M. A., Arán-Aís, F., Torró-Palau, A. M., Orgilés-Barcel, C., Martín-Martínez, J. M. Influence of the hard-to-soft segment ratio on the adhesion of water-borne polyurethane adhesive. Journal of Adhesion Science and Technology **2007**, *21*, 755–773, DOI: 10.1163/156856107781362635.

(66) Bao, H., Zhang, Z., Ying, S. Effect of ionic group on the behaviour of polyurethaneurea emulsion. Polymer **1996**, *37*, 2751–2754, DOI: 10.1016/0032-3861(96)87637-3.

(67) Barikani, M., Valipour Ebrahimi, M., Seyed Mohaghegh, S. M. Preparation and characterization of aqueous polyurethane dispersions containing ionic centers. Journal of Applied Polymer Science **2007**, *104*, 3931–3937, DOI: 10.1002/app.26138.

(68) Cakić, S. M., Ristić, I. S., Krakovský, I., Stojiljković, D. T., Bělský, P., Kollová, L. Crystallization and thermal properties in waterborne polyurethane elastomers: Influence of mixed soft segment block. Materials Chemistry and Physics **2014**, *144*, 31–40, DOI: 10.1016/j.matchemphys.2013.12.008.

(69) Gündüz, G., Kısakürek, R. R. Structure–Property Study of Waterborne Polyurethane Coatings with Different Hydrophilic Contents and Polyols. Journal of Dispersion Science and Technology **2004**, *25*, 217–228, DOI: 10.1081/DIS-120030668.

(70) Hong, J.-L., Lillya, C., Chien, J. C. Degree of phase separation in polyether-polyurethane copolymers with different chemical structures of hard segments. Polymer **1992**, *33*, 4347–4351, DOI: 10.1016/0032-3861(92)90278-5.

(71) Hourston, D. J., Williams, G., Satguru, R., Padget, J. D., Pears, D. Structure-property study of polyurethane anionomers based on various polyols and diisocyanates. Journal of Applied Polymer Science **1997**, *66*, 2035–2044, DOI: 10.1002/(SICI)1097-4628(19971205)66:10<2035: AID-APP21>3.0.CO;2-1.

(72) Hsu, S. L., Xiao, H. X., Szmant, H. H., Frisch, K. C. Polyurethane ionomers. I. Structure–properties relationships of polyurethane ionomers. Journal of Applied Polymer Science **1984**, *29*, 2467–2479, DOI: 10.1002/app.1984.070290804.

(73) Kim, B., Yang, J., Yoo, S., Lee, J. Waterborne polyurethanes containing ionic groups in soft segments. Colloid Polym Sci **2003**, *281*, 461–468, DOI: 10.1007/s00396-002-0799-4.

(74) Lee, S. K., Kim, B. K. High solid and high stability waterborne polyurethanes via ionic groups in soft segments and chain termini. J Colloid Interface Sci **2009**, *336*, 208–214, DOI: 10.1016/j.jcis.2009.03.028.

(75) van BOGART, J. W. C., LILAONITKUL, A., COOPER, S. L. Morphology and Properties of Segmented Copolymers. In *Multiphase Polymers*; Cooper, S. L., Estes, G. M., Eds.; AMERICAN CHEMICAL SOCIETY: WASHINGTON, D. C., 1979; Vols. 176, pp. 3–30, ISBN: 9780841204577.

(76) Wang, H., Shen, Y., Fei, G., Li, X., Liang, Y. Micromorphology and phase behavior of cationic polyurethane segmented copolymer modified with hydroxysilane. J Colloid Interface Sci **2008**, *324*, 36–41, DOI: 10.1016/j.jcis.2008.04.068.

(77) Wang, L., Shen, Y., Lai, X., Li, Z., Liu, M. Synthesis and properties of crosslinked waterborne polyurethane. J Polym Res **2011**, *18*, 469–476, DOI: 10.1007/s10965-010-9438-9.

(78) Xiao, H., Xiao, H. X., Frisch, K. C., Malwitz, N. Polyurethane–urea anionomer dispersions. I. Journal of Applied Polymer Science **1994**, *54*, 1643–1650, DOI: 10.1002/app.1994.070541107.

(79) Xin, H., Shen, Y., Li, X. Novel cationic polyurethane-fluorinated acrylic hybrid latexes: Synthesis, characterization and properties. 27th European Colloid and Interface Society conference (27th ECIS 2013) **2011**, *384*, 205–211, DOI: 10.1016/j.colsurfa.2011.03.056.

(80) Yang, J.-E., Kong, J.-S., Park, S.-W., Lee, D.-J., Kim, H.-D. Preparation and properties of waterborne polyurethane–urea anionomers. I. The influence of the degree of neutralization and counterion. Journal of Applied Polymer Science **2002**, *86*, 2375–2383, DOI: 10.1002/app.11249.

(81) Athawale, V. D., Kulkarni, M. A. Polyester polyols for waterborne polyurethanes and hybrid dispersions. Progress in Organic Coatings **2010**, *67*, 44–54, DOI: 10.1016/j.porgcoat.2009.09.015.

(82) Chinwanitcharoen, C., Kanoh, S., Yamada, T., Tada, K., Hayashi, S., Sugano, S. Preparation and Shelf-Life Stability of Aqueous Polyurethane Dispersion. Macromolecular Symposia **2004**, *216*, 229–240, DOI: 10.1002/masy.200451222.

(83) Kim, B. K., Kim, T. K., Jeong, H. M. Aqueous dispersion of polyurethane anionomers from H 12 MDI/IPDI, PCL, BD, and DMPA. Journal of Applied Polymer Science **1994**, *53*, 371–378, DOI: 10.1002/app.1994.070530315.

(84) Kim, C. K., Kim, B. K. IPDI-based polyurethane ionomer dispersions: Effects of ionic, nonionic hydrophilic segments, and extender on particle size and physical properties of emulsion cast film. Journal of Applied Polymer Science **1991**, *43*, 2295–2301, DOI: 10.1002/app.1991.070431219.

(85) Lei, L., Xia, Z., Ou, C., Zhang, L., Zhong, L. Effects of crosslinking on adhesion behavior of waterborne polyurethane ink binder. Progress in Organic Coatings **2015**, *88*, 155–163, DOI: 10.1016/j.porgcoat.2015.07.002.

(86) Madbouly, S. A., Otaigbe, J. U., Nanda, A. K., Wicks, D. A. Rheological Behavior of Aqueous Polyurethane Dispersions: Effects of Solid Content, Degree of Neutralization, Chain Extension, and Temperature. Macromolecules **2005**, *38*, 4014–4023, DOI: 10.1021/ma050453u.

(87) Santamaria-Echart, A., Arbelaiz, A., Saralegi, A., Fernández-d'Arlas, B., Eceiza, A., Corcuera, M. Relationship between reagents molar ratio and dispersion stability and film properties of waterborne polyurethanes. Colloids and Surfaces A: Physicochemical and Engineering Aspects **2015**, *482*, 554–561, DOI: 10.1016/j.colsurfa.2015.07.012.

(88) Velayutham, T. S., Majid, W. A., Ahmad, A. B., Kang, G. Y., Gan, S. N. Synthesis and characterization of polyurethane coatings derived from polyols synthesized with glycerol, phthalic anhydride and oleic acid. Progress in Organic Coatings **2009**, *66*, 367–371, DOI: 10.1016/j.porgcoat.2009.08.013.

(89) García-Pacios, V., Costa, V., Colera, M., Martín-Martínez, J. M. Waterborne polyurethane dispersions obtained with polycarbonate of hexanediol intended for use as coatings. Progress in Organic Coatings **2011**, *71*, 136–146, DOI: 10.1016/j.porgcoat.2011.01.006.

(90) García-Pacios, V., Iwata, Y., Colera, M., Miguel Martín-Martínez, J. Influence of the solids content on the properties of waterborne polyurethane dispersions obtained with polycarbonate of hexanediol. Int. J. Adhes. Adhes. **2011**, *31*, 787–794, DOI: 10.1016/j.ijadhadh.2011.05.010.

(91) García-Pacios, V., Jofre-Reche, J. A., Costa, V., Colera, M., Martín-Martínez, J. M. Coatings prepared from waterborne polyurethane dispersions obtained with polycarbonates of 1,6-hexanediol of different molecular weights. Progress in Organic Coatings **2013**, *76*, 1484–1493, DOI: 10.1016/j.porgcoat.2013.06.005.

(92) Grau C., Schmidt A. M., Wilkens J. *Waterborne polyurethane dispersions: A detailed analysis of particle charge in terms of soft and hard particle model*. Manuscript in preparation, 2023.

(93) Lee, D.-K., Tsai, H.-B., Wang, H.-H., Tsai, R.-S. Aqueous polyurethane dispersions derived from polycarbonatediols. Journal of Applied Polymer Science **2004**, *94*, 1723–1729, DOI: 10.1002/app.21090.

(94) CHATTOPADHYAY, D. K., PANDA, S. S., RAJU, K. V. S. N. Properties of Diamine Chain Extended Polyurethane Urea Coatings. J. Jpn. Soc. Colour Mater. **2004**, *77*, 540–547, DOI: 10.4011/shikizai1937.77.540.

(95) Jhon, Y.-K., Cheong, I.-W., Kim, J.-H. Chain extension study of aqueous polyurethane dispersions. Colloids and Surfaces A: Physicochemical and Engineering Aspects **2001**, *179*, 71–78, DOI: 10.1016/S0927-7757(00)00714-7.

(96) Javni, I., Hong, D. P., Petrović, Z. S. Polyurethanes from soybean oil, aromatic, and cycloaliphatic diamines by nonisocyanate route. J of Applied Polymer Sci **2013**, *128*, 566–571, DOI: 10.1002/app.38215.

(97) Kim, B. K., Lee, Y. M. Aqueous dispersion of polyurethanes containing ionic and nonionic hydrophilic segments. Journal of Applied Polymer Science **1994**, *54*, 1809–1815, DOI: 10.1002/app.1994.070541204.

(98) Bullermann, J., Friebel, S., Salthammer, T., Spohnholz, R. Novel polyurethane dispersions based on renewable raw materials—Stability studies by variations of DMPA content and degree of neutralisation. Progress in Organic Coatings **2013**, *76*, 609–615, DOI: 10.1016/j.porgcoat.2012.11.011.

(99) Pérez-Limiñana, M. A., Arán-Aís, F., Torró-Palau, A. M., César Orgilés-Barceló, A., Miguel Martín-Martínez, J. Characterization of waterborne polyurethane adhesives containing different amounts of ionic groups. Int. J. Adhes. Adhes. **2005**, *25*, 507–517, DOI: 10.1016/j.ijadhadh.2005.02.002.

(100) Lee, H.-T., Wu, S.-Y., Jeng, R.-J. Effects of sulfonated polyol on the properties of the resultant aqueous polyurethane dispersions. Colloids and Surfaces A: Physicochemical and Engineering Aspects **2006**, *276*, 176–185, DOI: 10.1016/j.colsurfa.2005.10.034.

(101) Zdrahala, R. J., Gerkin, R. M., Hager, S. L., Critchfield, F. E. Polyether-based thermoplastic polyurethanes. I. Effect of the hard-segment content. J of Applied Polymer Sci **1979**, *24*, 2041–2050, DOI: 10.1002/app.1979.070240912.

(102) Lee, H. K., Ko, S. W. Structure and thermal properties of polyether polyurethaneurea elastomers. J of Applied Polymer Sci **1993**, *50*, 1269–1280, DOI: 10.1002/app.1993.070500718.

(103) Spathis, G., Niaounakis, M., Kontou, E., Apekis, L., Pissis, P., Christodoulides, C. Morphological changes in segmented polyurethane elastomers by varying the NCO/OH ratio. J of Applied Polymer Sci **1994**, *54*, 831–842, DOI: 10.1002/app.1994.070540701.

(104) Harris, R. F., Joseph, M. D., Davidson, C., Deporter, C. D., Dais, V. A. Polyurethane elastomers based on molecular weight advanced poly (ethylene ether carbonate) diols. II. Effects of variations in hard segment concentration. J of Applied Polymer Sci **1990**, *41*, 509–525, DOI: 10.1002/app.1990.070410305.

(105) Leung, L. M., Koberstein, J. T. DSC annealing study of microphase separation and multiple endothermic behavior in polyether-based polyurethane block copolymers. Macromolecules **1986**, *19*, 706–713, DOI: 10.1021/ma00157a038.

(106) Hu, W., Koberstein, J. T. The effect of thermal annealing on the thermal properties and molecular weight of a segmented polyurethane copolymer. J Polym Sci B Polym Phys **1994**, *32*, 437–446, DOI: 10.1002/polb.1994.090320304.

(107) Born, L., Hespe, H. On the physical crosslinking of amine-extended polyurethane urea elastomers: A crystallographic analysis of bis-urea from diphenyl methane-4-isocyanate and 1,4-butane diamine. Colloid Polym Sci **1985**, *263*, 335–341, DOI: 10.1007/BF01412250.

(108) Rosthauser, J. W., Nachtkamp, K. Waterborne Polyurethanes. Journal of Coated Fabrics **1986**, *16*, 39–79, DOI: 10.1177/152808378601600103.

(109) R.R. Tirpak and P.H. Markusch. Aqueous Dispersions of Crosslinked Polyurethanes. Journal of Coatings Technology **1986**, 49–54.

(110) Barni, A., Levi, M. Aqueous polyurethane dispersions: A comparative study of polymerization processes. Journal of Applied Polymer Science **2003**, *88*, 716–723, DOI: 10.1002/app.11712.

(111) Szycher M. *Szycher's Handbook of Polyurethanes, Second Edition*, 2nd ed.; Taylor & Francis: Abingdon, 2012, ISBN: 1439839581.

(112) Wicks, Z. W., Wicks, D. A., Rosthauser, J. W. Two package waterborne urethane systems. Progress in Organic Coatings **2002**, *44*, 161–183, DOI: 10.1016/S0300-9440(02)00002-4.

(113) Weiss, K. D. Paint and coatings: A mature industry in transition. Progress in Polymer Science **1997**, *22*, 203–245, DOI: 10.1016/S0079-6700(96)00019-6.

(114) Saw, L. K., Brooks, B. W., Carpenter, K. J., Keight, D. V. Different dispersion regions during the phase inversion of an ionomeric polymer-water system. J Colloid Interface Sci **2003**, *257*, 163–172, DOI: 10.1016/S0021-9797(02)00030-9.

(115) Saw, L. K., Brooks, B. W., Carpenter, K. J., Keight, D. V. Catastrophic phase inversion in region II of an ionomeric polymer-water system. J Colloid Interface Sci **2004**, *279*, 235–243, DOI: 10.1016/j.jcis.2004.06.056.

(116) Wei, Y., Luo, Y., Li, B., Li, B. Phase inversion of UV-curable anionic polyurethane in the presence of acetone solvent. Colloid Polym Sci **2005**, *283*, 1289–1297, DOI: 10.1007/s00396-005-1324-3.

(117) Chang, C.-W., Lu, K.-T. Natural castor oil based 2-package waterborne polyurethane wood coatings. Progress in Organic Coatings **2012**, *75*, 435–443, DOI: 10.1016/j.porgcoat.2012.06.013.

(118) Chinwanitcharoen, C., Kanoh, S., Yamada, T., Hayashi, S., Sugano, S. Preparation of aqueous dispersible polyurethane: Effect of acetone on the particle size and storage stability of polyurethane emulsion. Journal of Applied Polymer Science **2004**, *91*, 3455–3461, DOI: 10.1002/app.13527.

(119) Orgilés-Calpena, E., Arán-Aís, F., Torró-Palau, A. M., Orgilés-Barceló, C. Influence of the Chain Extender Nature on Adhesives Properties of Polyurethane Dispersions. Journal of Dispersion Science and Technology **2012**, *33*, 147–154, DOI: 10.1080/01932691.2010.548250.

(120) Sardon, H., Irusta, L., Fernández-Berridi, M. J., Luna, J., Lansalot, M., Bourgeat-Lami, E. Waterborne polyurethane dispersions obtained by the acetone process: A study of colloidal features. Journal of Applied Polymer Science **2011**, *120*, 2054–2062, DOI: 10.1002/app.33308.

(121) Zhang, Q., Hu, J., Gong, S. Preparation and characterization of aqueous polyurethane dispersions with well-defined soft segments. J of Applied Polymer Sci **2011**, *122*, 3064–3070, DOI: 10.1002/app.34095.

(122) Chapman, D. L. LI. A contribution to the theory of electrocapillarity. The London, Edinburgh, and Dublin Philosophical Magazine and Journal of Science **1913**, *25*, 475–481, DOI: 10.1080/14786440408634187.

(123) Gouy, M. Sur la constitution de la charge électrique à la surface d'un électrolyte. J. Phys. Theor. Appl. **1910**, *9*, 457–468, DOI: 10.1051/jphystap:019100090045700.

(124) Stern, O. ZUR THEORIE DER ELEKTROLYTISCHEN DOPPELSCHICHT. Zeitschrift für Elektrochemie und angewandte physikalische Chemie **1924**, *30*, 508–516, DOI: 10.1002/bbpc.192400182.

(125) Debye P., Hückel E. Zur Theorie der Elektrolyte. Physikalische Zeitschrift **1923**, 185–206.

(126) Overbeek, J. Th. G. Theorie der Elektrophorese: Der Relaxationseffekt. Kolloid-Beihefte **1943**, *54*, 287–364, DOI: 10.1007/BF02556774.

(127) Wiersema, P., Loeb, A., Overbeek, J. Calculation of the electrophoretic mobility of a spherical colloid particle. Journal of Colloid and Interface Science **1966**, *22*, 78–99, DOI: 10.1016/0021-9797(66)90069-5.

(128) Georg Gabriel Stokes. On the effect of the internal friction of fluids on the motion of pendulums. Transactions of the Cambridge Philosophical Society **1851**, 8–106.

(129) Smoluchowski, M. v. Elektrische Endosmose und Strömungsströme. In *Handbuch der Elektrizität und des Magnetismus*; Graetz, L., Ed.; Johann Ambrosius: Barth, Leipzig, 1921; Vols. 2, pp. 366–428.

(130) E. Hückel. Die Kataphorese der Kugel. Physikalische Zeitschrift **1924**, 204–210.

(131) Onsager L. Zur Theorie der Elektrolyte I. Physikalische Zeitschrift **1926**, 388.

(132) Henry, D. C. The Cataphoresis of Suspended Particles. Part I. The Equation of Cataphoresis. Proceedings of the Royal Society A: Mathematical, Physical and Engineering Sciences **1931**, *133*, 106–129, DOI: 10.1098/rspa.1931.0133.

(133) Ohshima, H. A Simple Expression for Henry's Function for the Retardation Effect in Electrophoresis of Spherical Colloidal Particles. J Colloid Interface Sci **1994**, *168*, 269–271, DOI: 10.1006/jcis.1994.1419.

(134) O'Brien, R. W., White, L. R. Electrophoretic mobility of a spherical colloidal particle. Journal of the Chemical Society, Faraday Transactions 2 **1978**, *74*, 1607, DOI: 10.1039/f29787401607.

(135) Ohshima, H., Healy, T. W., White, L. R. Approximate analytic expressions for the electrophoretic mobility of spherical colloidal particles and the conductivity of their dilute suspensions. Journal of the Chemical Society, Faraday Transactions 2 **1983**, *79*, 1613, DOI: 10.1039/f29837901613.

(136) Ohshima, H. Approximate Analytic Expression for the Electrophoretic Mobility of a Spherical Colloidal Particle. J Colloid Interface Sci **2001**, *239*, 587–590, DOI: 10.1006/jcis.2001.7608.

(137) Hermans, J. J., Fujita, H. Electrophoresis of charged polymer molecules with partial free drainage. Koninkl. Ned. Akad. Wetenschap. Proc. **1955**, *B58*, 182–187.

(138) Ohshima H. *Theory of colloid and interfacial electric phenomena*, 1st ed.; Elsevier Academic Press: Amsterdam, Boston, 2006, ISBN: 978-0-12-370642-3.

(139) Ohshima, H., Kondo, T. Electrophoresis of large colloidal particles with surface charge layers. Position of the slipping plane and surface layer thickness. Colloid Polym Sci **1986**, *264*, 1080–1084, DOI: 10.1007/BF01410326.

(140) Ohshima, H., Kondo, T. Approximate analytic expression for the electrophoretic mobility of colloidal particles with surface-charge layers. J Colloid Interface Sci **1989**, *130*, 281–282, DOI: 10.1016/0021-9797(89)90101-X.

(141) Ohshima, H., Makino, K. Electrophoretic mobility of a particle covered with a partially ion-penetrable polyelectrolyte layer. A collection of invited papers by Japanese researchers **1996**, *109*, 71–75, DOI: 10.1016/0927-7757(95)03452-8.

(142) Ohshima, H. Electrophoresis of soft particles: analytic approximations. Electrophoresis **2006**, *27*, 526–533, DOI: 10.1002/elps.200500636.

(143) Ohshima, H. Electrophopretic mobility of soft particles. Electrophoresis **1995**, *16*, 1360–1363, DOI: 10.1002/elps.11501601224.

(144) Ohshima, H. Electrophoretic mobility of soft particles. Colloids and Surfaces A: Physicochemical and Engineering Aspects **1995**, *103*, 249–255, DOI: 10.1016/0927-7757(95)03293-M.

(145) Ohshima, H. On the General Expression for the Electrophoretic Mobility of a Soft Particle. J Colloid Interface Sci **2000**, *228*, 190–193, DOI: 10.1006/jcis.2000.6942.

(146) Ohshima, H. Electrophoretic mobility of a highly charged soft particle: Relaxation effect. Colloids and Surfaces A: Physicochemical and Engineering Aspects **2011**, *376*, 72–75, DOI: 10.1016/j.colsurfa.2010.09.012.

(147) Ohshima, H. Electrokinetics of soft particles. Colloid Polym Sci **2007**, *285*, 1411–1421, DOI: 10.1007/s00396-007-1740-7.

(148) Lagaly G., Schulz O., Zimehl R. *Dispersionen und Emulsionen: Eine Einführung in die Kolloidik feinverteilter Stoffe einschließlich der Tonminerale*; Steinkopff: Heidelberg, 1997, ISBN: 9783798510876.

(149) van Oss C. J. *Interfacial forces in aqueous media*, 2nd ed.; CRC Taylor & Francis: Boca Raton, Fla., 2006, ISBN: 9781574444827.

(150) Sader, J. E., Carnie, S. L., Chan, D. Y. Accurate Analytic Formulas for the Double-Layer Interaction between Spheres. J Colloid Interface Sci **1995**, *171*, 46–54, DOI: 10.1006/jcis.1995.1149.

(151) Hamaker, H. C. The London—van der Waals attraction between spherical particles. Physica **1937**, *4*, 1058–1072, DOI: 10.1016/S0031-8914(37)80203-7.

(152) Prieve, D. C., Russel, W. B. Simplified predictions of Hamaker constants from Lifshitz theory. J Colloid Interface Sci **1988**, *125*, 1–13, DOI: 10.1016/0021-9797(88)90048-3.

(153) Hough, D. B., White, L. R. The calculation of hamaker constants from liftshitz theory with applications to wetting phenomena. Adv Colloid Interface Sci **1980**, *14*, 3–41, DOI: 10.1016/0001-8686(80)80006-6.

(154) Gotoh, K., Kohsaka, R., Abe, K., Tagawa, M. Estimation of the Hamaker constant from flocculation in the secondary minimum and its experimental verification in particle adhesion. Journal of Adhesion Science and Technology **1996**, *10*, 1359–1370, DOI: 10.1163/156856196X00292.

(155) Lyklema, J. Electrokinetics after Smoluchowski. Colloids and Surfaces A: Physicochemical and Engineering Aspects **2003**, *222*, 5–14, DOI: 10.1016/S0927-7757(03)00217-6.

(156) Mathai, K. G., Ottewill, R. H. Stability of hydrophobic sols in the presence of non-ionic surface-active agents. Part 2.? Stability of silver iodide sols in the presence of non-ionic surface-active agents. Trans. Faraday Soc. **1966**, *62*, 759, DOI: 10.1039/tf9666200759.

(157) Ottewill, R. H., Watanabe, A. Studies on the mechanism of coagulation. Kolloid-Zeitschrift **1960**, *171*, 33–42, DOI: 10.1007/BF01520322.

(158) Oster, G. Light scattering from polymerizing and coagulating systems. Journal of Colloid Science **1947**, *2*, 291–299, DOI: 10.1016/0095-8522(47)90031-7.

(159) Ottewill, R. H., Watanabe, A. Studies on the mechanism of coagulation. Kolloid-Zeitschrift **1960**, *170*, 132–139, DOI: 10.1007/BF01525172.

(160) Ottewill, R. H., Shaw, J. N. Stability of monodisperse polystyrene latex dispersions of various sizes. Discussions of the Faraday Society **1966**, *42*, 154, DOI: 10.1039/DF9664200154.

(161) van Oss, C. J., Chaudhury, M. K., Good, R. J. Interfacial Lifshitz-van der Waals and polar interactions in macroscopic systems. Chem Rev **1988**, *88*, 927–941, DOI: 10.1021/cr00088a006.

(162) van Oss, C. J. The Extended DLVO Theory. In; Vols. 16, pp. 31–48.

(163) Fowkes, F. M. Additivity of intermolecular forces at interfaces. I. Determination of the contribution to surface and interfacial tensions of dispersion forces in various liquids. The Journal of Physical Chemistry **1963**, *67*, 2538–2541, DOI: 10.1021/j100806a008.

(164) Good, R. J., Girifalco, L. A. A theory for estimation of surface and interfacial energies. III. Estimation of surface energies of solids from contact angle data. The Journal of Physical Chemistry **1960**, *64*, 561–565, DOI: 10.1021/j100834a012.

(165) Girifalco, L. A., Good, R. J. A Theory for the Estimation of Surface and Interfacial Energies. I. Derivation and Application to Interfacial Tension. The Journal of Physical Chemistry **1957**, *61*, 904–909, DOI: 10.1021/j150553a013.

(166) van Oss, C. J. Acid—base interfacial interactions in aqueous media. Colloids and Surfaces A: Physicochemical and Engineering Aspects **1993**, *78*, 1–49, DOI: 10.1016/0927-7757(93)80308-2.

(167) van Oss C. J. *The properties of water and their role in colloidal and biological systems*, 1st ed.; Elsevier/Acad. Press: Amsterdam, 2008, ISBN: 9780123743039.

(168) Israelachvili J. N. *Intermolecular and surface forces*, 3rd ed.; Academic Press is an imprint of Elsevier: Amsterdam, 2012, ISBN: 978-0-12-391927-4.

(169) Derjaguin, B., Churaev, N. Structural component of disjoining pressure. Journal of Colloid and Interface Science **1974**, *49*, 249–255, DOI: 10.1016/0021-9797(74)90358-0.

(170) Delgado-Calvo-Flores, J. M., Peula-García, J. M., Martínez-García, R., Callejas-Fernández, J. Experimental Evidence of Hydration Forces between Polymer Colloids Obtained by Photon Correlation Spectroscopy Measurements. Journal of Colloid and Interface Science **1997**, *189*, 58–65, DOI: 10.1006/jcis.1997.4815.

(171) Paunov, V. N., Dimova, R. I., Kralchevsky, P. A., Broze, G., Mehreteab, A. The Hydration Repulsion between Charged Surfaces as an Interplay of Volume Exclusion and Dielectric Saturation Effects. Journal of Colloid and Interface Science **1996**, *182*, 239–248, DOI: 10.1006/jcis.1996.0456.

(172) Ducker, W. A., Pashley, R. M. Forces between mica surfaces in the presence of rod-shaped divalent counterions. Langmuir **1992**, *8*, 109–112, DOI: 10.1021/la00037a021.

(173) Xu, Z., Yoon, R.-H. The role of hydrophobia interactions in coagulation. Journal of Colloid and Interface Science **1989**, *132*, 532–541, DOI: 10.1016/0021-9797(89)90267-1.

(174) Pashley, R. M., McGuiggan, P. M., Ninham, B. W., Evans, D. F. Attractive forces between uncharged hydrophobic surfaces: direct measurements in aqueous solution. Science **1985**, *229*, 1088–1089, DOI: 10.1126/science.4035349.

(175) Claesson, P. M., Herder, P. C., Blom, C. E., Ninham, B. W. Interactions between a positively charged hydrophobic surface and a negatively charged bare mica surface. Journal of Colloid and Interface Science **1987**, *118*, 68–79, DOI: 10.1016/0021-9797(87)90435-8.

(176) Tsao, Y. H., Yang, S. X., Evans, D. F., Wennerstroem, H. Interactions between hydrophobic surfaces. Dependence on temperature and alkyl chain length. Langmuir **1991**, *7*, 3154–3159, DOI: 10.1021/la00060a039.

(177) Yoon, R.-H., Ravishankar, S. A. Long-Range Hydrophobic Forces between Mica Surfaces in Dodecylammonium Chloride Solutions in the Presence of Dodecanol. Journal of Colloid and Interface Science **1996**, *179*, 391–402, DOI: 10.1006/jcis.1996.0230.

(178) van Oss, C. J., Chaudhury, M. K., Good, R. J. The Mechanism of Phase Separation of Polymers in Organic Media—Apolar and Polar Systems. Separation Science and Technology **1989**, *24*, 15–30, DOI: 10.1080/01496398908049748.

(179) van Oss, C. J., Good, R. J., Chaudhury, M. K. Additive and nonadditive surface tension components and the interpretation of contact angles. Langmuir **1988**, *4*, 884–891, DOI: 10.1021/la00082a018.

(180) van Oss, C., Ju, L., Chaudhury, M., Good, R. Estimation of the polar parameters of the surface tension of liquids by contact angle measurements on gels. Elkin 06, International Electrokinetics Conference, June 25-29, Nancy, France **1989**, *128*, 313–319, DOI: 10.1016/0021-9797(89)90345-7.

(181) van Oss, C. J. Long-range and short-range mechanisms of hydrophobic attraction and hydrophilic repulsion in specific and aspecific interactions. J Mol Recognit **2003**, *16*, 177–190, DOI: 10.1002/jmr.618.

(182) Derjaguin, B. V., Greene-Kelly, R. Birefringence of thin liquid films. Trans. Faraday Soc. **1964**, *60*, 449, DOI: 10.1039/tf9646000449.

(183) Derjaguin B., Zachavaeva N. *Research in surface forces*, 1st ed.; Consultants Bureau: New York, 1963.

(184) Deryagin, B. V., Churaev, N. V. Structure of water in thin layers. Langmuir **1987**, *3*, 607–612, DOI: 10.1021/la00077a002.

(185) Deryagin, B. V., Churaev, N. V., Zorin, Z. M. Structure and properties of boundary layers of water. Russ Chem Bull **1982**, *31*, 1507–1518, DOI: 10.1007/BF00956884.

(186) Nanda, A. K., Wicks, D. A., Madbouly, S. A., Otaigbe, J. U. Effect of ionic content, solid content, degree of neutralization, and chain extension on aqueous polyurethane dispersions prepared by prepolymer method. Journal of Applied Polymer Science **2005**, *98*, 2514–2520, DOI: 10.1002/app.22141.

(187) Stone-Masui, J., Watillon, A. Characterization of surface charge on polystyrene latices. J Colloid Interface Sci **1975**, *52*, 479–503, DOI: 10.1016/0021-9797(75)90273-8.

(188) Gaboriaud, F., Gee, M. L., Strugnell, R., Duval, J. F. L. Coupled electrostatic, hydrodynamic, and mechanical properties of bacterial interfaces in aqueous media. Langmuir **2008**, *24*, 10988–10995, DOI: 10.1021/la800258n.

(189) Hakim, A., Nishiya, M., Kobayashi, M. Charge reversal of sulfate latex induced by hydrophobic counterion: Effects of surface charge density. Colloid Polym Sci **2016**, *294*, 1671–1678, DOI: 10.1007/s00396-016-3931-6.

(190) Borkovec, M., Behrens, S. H., Semmler, M. Observation of the Mobility Maximum Predicted by the Standard Electrokinetic Model for Highly Charged Amidine Latex Particles. Langmuir **2000**, *16*, 5209–5212, DOI: 10.1021/la9916373.

(191) Gomes, P. A., d'Espinose de Lacaillerie, J.-B., Lartiges, B., Maliet, M., Molinier, V., Passade-Boupat, N., Sanson, N. Microalgae as Soft Permeable Particles. Langmuir **2022**, *38*, 14044–14052, DOI: 10.1021/acs.langmuir.2c01735.

(192) Ohshima, H. On the maximum of the magnitude of the electrophoretic mobility of a spherical colloidal particle in an electrolyte solution. Colloid Polym Sci **2016**, *294*, 13–17, DOI: 10.1007/s00396-015-3756-8.

(193) Kerchove, A. J. de, Elimelech, M. Relevance of electrokinetic theory for "soft" particles to bacterial cells: implications for bacterial adhesion. Langmuir **2005**, *21*, 6462–6472, DOI: 10.1021/la047049t.

(194) Sonohara, R., Muramatsu, N., Ohshima, H., Kondo, T. Difference in surface properties between Escherichia coli and Staphylococcus aureus as revealed by electrophoretic mobility measurements. Biophysical Chemistry **1995**, *55*, 273–277, DOI: 10.1016/0301-4622(95)00004-H.

(195) Wolf, T., Grau, C., Rosengarten, J. F., Stitz, J., Wilkens, J., Barbe, S. Investigation of the Electrokinetic Properties of HIV-Based Virus-Like Particles. Langmuir **2024**, *40*, 4762–4771, DOI: 10.1021/acs.langmuir.3c03535.

(196) Ohshima, H. Limiting electrophoretic mobility of a highly charged soft particle in an electrolyte solution: Solidification effect. Journal of Colloid and Interface Science **2010**, *349*, 641–644.

(197) Ohshima, H., Healy, T. W., White, L. R. Accurate analytic expressions for the surface charge density/surface potential relationship and double-layer potential distribution for a spherical colloidal particle. J Colloid Interface Sci **1982**, *90*, 17–26, DOI: 10.1016/0021-9797(82)90393-9.

(198) Kobayashi, M. Electrophoretic mobility of latex spheres in the presence of divalent ions: experiments and modeling. Colloid Polym Sci **2008**, *286*, 935–940, DOI: 10.1007/s00396-008-1851-9.

(199) Kobayashi, M., Nitanai, M., Satta, N., Adachi, Y. Coagulation and charging of latex particles in the presence of imogolite. Colloids and Surfaces A: Physicochemical and Engineering Aspects **2013**, *435*, 139–146.

(200) Behrens, S. H., Christl, D. I., Emmerzael, R., Schurtenberger, P., Borkovec, M. Charging and Aggregation Properties of Carboxyl Latex Particles: Experiments versus DLVO Theory. Langmuir **2000**, *16*, 2566–2575, DOI: 10.1021/la991154z.

(201) Antonietti, M., Vorwerg, L. Examination of the atypical electrophoretic mobility behavior of charged colloids in the low salt region using the O'Brian-White theory. Colloid Polym Sci **1997**, *275*, 883–887, DOI: 10.1007/s003960050161.

(202) Kobayashi, M., Sasaki, A. Electrophoretic mobility of latex spheres in mixture solutions containing mono and divalent counter ions. 27th European Colloid and Interface Society conference (27th ECIS 2013) **2014**, *440*, 74–78, DOI: 10.1016/j.colsurfa.2012.10.036.

(203) Peula-García, J. M., Hidalgo-Alvarez, R., las Nieves, F. J. de. Colloid stability and electrokinetic characterization of polymer colloids prepared by different methods. 27th European Colloid and Interface Society conference (27th ECIS 2013) **1997**, *127*, 19–24, DOI: 10.1016/s0927-7757(96)03890-3.

(204) Tamai, H., Niino, K., Suzawa, T. Surface characterization of styrene/sodium styrenesulfonate copolymer latex particles. J Colloid Interface Sci **1989**, *131*, 1–7, DOI: 10.1016/0021-9797(89)90138-0.

(205) Lyklema J. *Fundamentals of interface and colloid science: Vol. 1: Fundamentals*; Academic Press: London, 1991, ISBN: 9780124605251.

(206) Lyklema J. *Fundamentals of Interface and Colloid Science: Volume V Soft Colloids*; Elsevier Academic Press: Amsterdam, 2005, ISBN: 9780080457406.

(207) Israelachvili J. N. *Intermolecular and Surface Forces*; Elsevier Science: Burlington, 2010, ISBN: 978-0-12-375182-9.

(208) Rudawska, A., Jacniacka, E. Evaluating uncertainty of surface free energy measurement by the van Oss-Chaudhury-Good method. Int. J. Adhes. Adhes. **2018**, *82*, 139–145, DOI: 10.1016/j.ijadhadh.2018.01.006.

(209) Siboni, S., Della Volpe, C. Acid-Base Theory of Adhesion: A Critical Review. Rev. Adhes. Adhes. **2015**, *3*, 253–310, DOI: 10.7569/RAA.2015.097307.

(210) Quane, E. J., Elders, N., Newman, A. S., van Mourik, S., Williams, N. S. J., van den Berg, K. J., Ryan, A. J., Mykhaylyk, O. O. Synthesis, Morphology, and Particle Size Control of Acidic Aqueous Polyurethane Dispersions. Macromolecules **2024**, *57*, 10623–10634, DOI: 10.1021/acs.macromol.4c02046.

(211) Meyer, E. E., Lin, Q., Hassenkam, T., Oroudjev, E., Israelachvili, J. N. Origin of the long-range attraction between surfactant-coated surfaces. Proc. Natl. Acad. Sci. U S A **2005**, *102*, 6839–6842, DOI: 10.1073/pnas.0502110102.

(212) Perkin, S., Kampf, N., Klein, J. Long-range attraction between charge-mosaic surfaces across water. Phys. Rev. Lett. **2006**, *96*, 38301, DOI: 10.1103/PhysRevLett.96.038301.

(213) Silbert, G., Ben-Yaakov, D., Dror, Y., Perkin, S., Kampf, N., Klein, J. Long-ranged attraction between disordered heterogeneous surfaces. Phys. Rev. Lett. **2012**, *109*, 168305, DOI: 10.1103/PhysRevLett.109.168305.

(214) Jho, Y. S., Brewster, R., Safran, S. A., Pincus, P. A. Long-range interaction between heterogeneously charged membranes. Langmuir **2011**, *27*, 4439–4446, DOI: 10.1021/la1050282.

(215) Attard, P. Nanobubbles and the hydrophobic attraction. Adv Colloid Interface Sci **2003**, *104*, 75–91, DOI: 10.1016/s0001-8686(03)00037-x.

(216) Parker, J. L., Claesson, P. M., Attard, P. Bubbles, cavities, and the long-ranged attraction between hydrophobic surfaces. J. Phys. Chem. **1994**, *98*, 8468–8480, DOI: 10.1021/j100085a029.

(217) Stevens, H., Considine, R. F., Drummond, C. J., Hayes, R. A., Attard, P. Effects of degassing on the long-range attractive force between hydrophobic surfaces in water. Langmuir **2005**, *21*, 6399–6405, DOI: 10.1021/la0507535.

(218) Tabor, R. F., Wu, C., Grieser, F., Dagastine, R. R., Chan, D. Y. C. Measurement of the Hydrophobic Force in a Soft Matter System. J. Phys. Chem. Lett. **2013**, *4*, 3872–3877, DOI: 10.1021/jz402068k.

(219) Alves, L. A., Castro, A. H. de, Mendonça, F. G. de, Mesquita, J. P. de. Characterization of acid functional groups of carbon dots by nonlinear regression data fitting of potentiometric titration curves. Applied Surface Science **2016**, *370*, 486–495, DOI: 10.1016/j.apsusc.2016.02.128.

(220) Szilagyi, I., Trefalt, G., Tiraferri, A., Maroni, P., Borkovec, M. Polyelectrolyte adsorption, interparticle forces, and colloidal aggregation. Soft Matter **2014**, *10*, 2479–2502, DOI: 10.1039/C3SM52132J.

(221) Bonekamp, B. C., van der Schee, H. A., Lyklema, J. Adsorption of oligo-and polypeptides as model polyelectrolytes. Croatica Chemica Acta **1983**, *Nr.4*, 695–704.

(222) Stuart, M. A., Fleer, G. J., Lyklema, J., Norde, W., Scheutjens, J. M. Adsorption of ions, polyelectrolytes and proteins. Adv Colloid Interface Sci **1991**, *34*, 477–535, DOI: 10.1016/0001-8686(91)80056-P.

(223) Ueda, T., Harada, S. Adsorption of cationic polysulfone on bentonite. J of Applied Polymer Sci **1968**, *12*, 2395–2401, DOI: 10.1002/app.1968.070121102.

(224) Degiorgio V., Ed. *Trends in Colloid and Interface Science II*; Steinkopff: Darmstadt, 1988, ISBN: 978-3-7985-0777-7.

(225) Durand, G., Lafuma, F., Audebert, R. Adsorption of cationic polyelectrolytes at clay-colloid interface in dilute aqueous suspensions — effect of the ionic strength of the medium. In *Trends in Colloid and Interface Science II*; Degiorgio, V., Ed.; Steinkopff: Darmstadt, 1988; Vols. 76, pp. 278–282, ISBN: 978-3-7985-0777-7.

(226) Durand-Piana, G., Lafuma, F., Audebert, R. Flocculation and adsorption properties of cationic polyelectrolytes toward Na-montmorillonite dilute suspensions. Elkin 06, International Electrokinetics Conference, June 25-29, Nancy, France **1987**, *119*, 474–480, DOI: 10.1016/0021-9797(87)90293-1.

(227) Froehling, P. E., Bantjes, A., Kolar, Z. Adsorption of a synthetic heparinoid polyelectrolyte on an ion-exchanging surface. Elkin 06, International Electrokinetics Conference, June 25-29, Nancy, France **1977**, *62*, 35–39, DOI: 10.1016/0021-9797(77)90062-5.

(228) Wang, T. K., Audebert, R. Adsorption of cationic copolymers of acrylamide at the silica—water interface: Hydrodynamic layer thickness measurements. Elkin 06, International Electrokinetics Conference, June 25-29, Nancy, France **1988**, *121*, 32–41, DOI: 10.1016/0021-9797(88)90405-5.

(229) Davies, R., Dix, L., Toprakcioglu, C. Adsorption of poly-l-lysine to mica powder. Elkin 06, International Electrokinetics Conference, June 25-29, Nancy, France **1989**, *129*, 145–152, DOI: 10.1016/0021-9797(89)90424-4.

(230) van de Steeg, H. G. M., Cohen Stuart, M. A., Keizer, A. de, Bijsterbosch, B. H. Polyelectrolyte adsorption: a subtle balance of forces. Langmuir **1992**, *8*, 2538–2546, DOI: 10.1021/la00046a030.

11 Appendix

11.1 Particle charge determination by polyelectrolyte titration

This chapter is shown in the appendix, as it does not contribute to the overall results of this work. However, the polyelectrolyte titration is a frequently used method within the industry. Therefore, these findings might be relevant for the interested reader.

An alternative method to determine the particle charge content of the system is the so called polyelectrolyte titration. It uses oppositely charged polyelectrolytes as a titrant to quantitatively compensate the particle charges of the dispersed particles. More specifically, the diluted PUD is titrated with a cationic polyelectrolyte, namely PolyDADMAC, until the isoelectric point is reached. Here charge neutrality is present and all surface charges are compensated by the charges of the polyelectrolyte. Thus, this method can be used as an alternative titration to validate the results of the potentiometric titration experiments. For this purpose, the specific charge as well as the recovery rate are evaluated. The methodology as well as the results are discussed for the PUDs based on polycarbonate polyol using AAS as well as DMPA, as representative example.

Table 11-1: Specific particle charge Q_{Pol} as well as the recovery rate RR_{Pol} obtained by polyelectrolyte titration of the synthesis series PC-x%AAS.

Sample	AAS		DMPA	
	Q_{Pol} [C/g]	RR_{Pol} [%]	Q_{Pol} [C/g]	RR_{Pol} [%]
PC3.5	-17.6	98.9	-17.9	71.3
PC4.0	-22.2	109.3	-24.6	86.0
PC4.5	-25.5	111.7	-30.3	93.4
PC5.0	-30.3	118.9	-33.1	92.3
PC5.5	-34.1	122.4	/	/

Obviously a similar trend of both values compared to the results obtained by potentiometric titration can be observed. As be expected, the specific particle charge Q_{Pol} increases with increasing AAS and DMPA content, respectively. However, the absolute values are higher compared to those obtained by potentiometric titration. This observation is furthermore represented by the high recovery rates, exceeding 100% in the case of AAS. It is evident that the specific charges of the system are attributable to the incorporation of the anionic AAS groups and the manner in which these are arranged on the particle surface. The synthesis procedure did not involve the incorporation of any additional ion-carrying group to AAS. This suggests that the observed values may be considered implausible.

Erroneous results have been eliminated through the utilisation of reproducible outcomes derived from repeated measurements as well as measurements of standard substances. However, as the total charge of the system is calculated on basis of IEP determination, the measurement result may be influenced by adsorbed anions. Two possible factors are examined. First, the adsorption of hydroxyl ions as they are present in every aqueous solution. Second the adsorption of any other anion at the particle surface.

To evaluate the adsorption of hydroxyl ions at the particle surface, measurements at different pH values were done, ranging from acidic to basic region. However, no significant changes in the determined values can be observed. Especially in basic environments, the adsorption of hydroxyl ions should be more likely. To evaluate the adsorption of any other anion at the particle surface, electrolyte dependent

measurements are done using NaCl as an electrolyte. If the adsorption of Cl^- occurs, the determined particle charges should even increase. However, the opposite is the case, as shown in Figure 11-1.

The detected amount of charges and thus the recovery rate decreases for AAS as well as DMPA PUDs based on PC diol at low electrolyte concentrations until a minimum was reached. Towards higher electrolyte concentrations the recovery rate increased again. However, the necessary electrolyte concentration to reach the minimum is different for most of the samples. The AAS series might suggest that the minimum shifts to higher electrolyte concentrations with increasing AAS concentration, but this trend was not found in the case of DMPA. Based on these findings, adsorption of anions at the particle surface causing a higher amount of charges to be detected by polyelectrolyte titration can be excluded, as the determined amount of charges even decreased with increasing electrolyte concentration. However, the value found in the minimum is closer to the determined recovery rates found by potentiometric acid-base titration. Nevertheless, the values are still too high. For this reason, it needs to be pointed out, that charge neutralisation in the case of polyelectrolyte titrations of water based PUDs seems to be rather qualitative than quantitative.

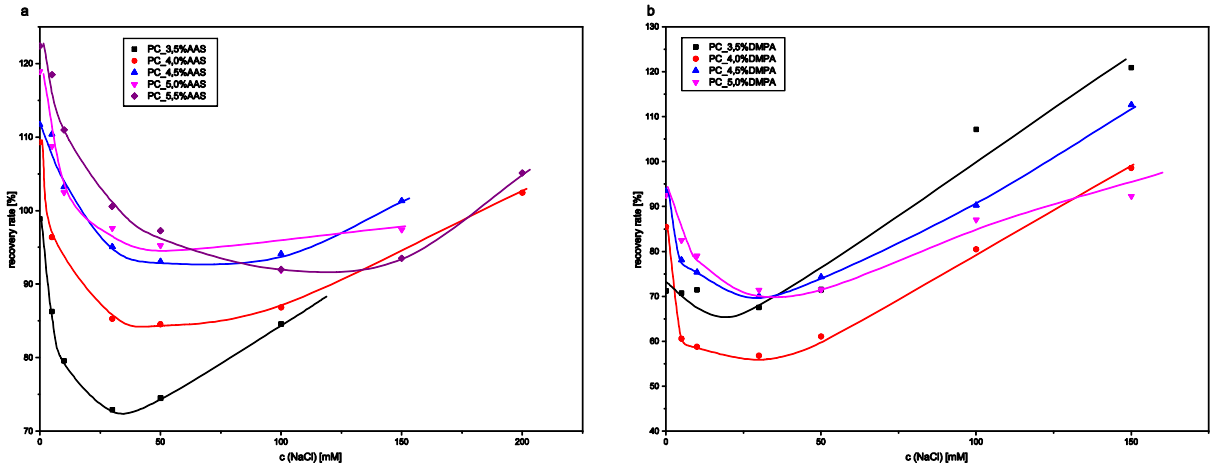

Figure 11-1: Polyelectrolyte titration experiment with varying electrolyte concentration for a) Polycarbonate based PUDs stabilized by AAS and b) Polycarbonate polyol based PUDs stabilized by DMPA. Solid lines are a guide to the eye.

In principle, the adsorption of polyelectrolytes is based on a balance between attractive electrostatic forces, van der Waals forces as well as possible hydration forces.[220] Especially in the case of polyelectrolytes bearing a high charge density (strong polyelectrolytes), like PolyDADMAC employed in this study, the adsorption is mostly governed by attractive electrostatic forces with the oppositely charged interface. The influence of electrolytes has also been analysed in the literature, showing some controversial aspects. At the one hand it was found by several authors, that the adsorbed amount increases with increasing electrolyte concentration.[221–223] This behaviour was explained by the fact, that increasing electrolyte concentrations led to screening of the polyelectrolyte charges and thus conformational changes. At low electrolyte concentrations, the adsorbed layers are rather thin due to a stretched conformation based on the repulsion between each monomer unit. With increasing electrolyte concentrations, the charges will be screened and the polyelectrolyte tends to a conformation of loops and tails as the repulsive interaction between the charged groups decrease.

However, in other studies the opposite observation was made, namely that the adsorbed amount of strong polyelectrolytes decreases with increasing electrolyte concentrations.[224–229] Increasing the salt concentration alters the segment-segment repulsion as well as the segment surface attraction and has thus two distinct effects. According to van de Steeg the adsorption might be altered by the addition of salt based on the balance between electrostatic and non-electrostatic attraction.[230] They proposed two mechanisms for the adsorption of polyelectrolytes in the presence of electrolytes, namely the *screening*

enhanced and the *screening reduced* adsorption regime. In the case of the observed phenomena in this study, the adsorption is enhanced with increasing electrolyte concentration up to a specific point where it decreases again. According to these authors, the screening enhanced adsorption takes place if the interaction between the polyelectrolyte and the surface are not purely electrostatic. They expressed it by variations of the Flory-Huggins interaction parameter and found that the screening enhanced adsorption takes place especially in the case of higher interaction parameters. They found a maximum intermediate interaction parameter like we observed in this study. The adsorption decreases again, once a critical electrolyte concentration is reached, leading to complete screening of the charges. For this reason, it is very likely, that the adsorption of polyelectrolytes on polyurethane interfaces is not solely governed by electrostatic attraction. Nevertheless, further research is necessary to evaluate the contribution of different interactions forces between polyelectrolytes and polyurethane particles in more detail. Since the addition of electrolytes lead to a screening of the surface charges as well as the charges of the polyelectrolyte, the underlying mechanism of the altered adsorption is still questionable. However, it has been not investigated in more detail in this study.

It needs to be pointed out, that the polyelectrolyte titration is not useful as an alternative method for the characterization of the particle charges of the studies samples without a more detailed analysis. The charge amounts detected are too high and do even change by the addition of electrolytes, leading to at least questionable results. Therefore, the results is not used for comparative purposes and the method is not used for further investigations.

11.2 Calculation procedures

Several programs are used to analyse and evaluate the generated data. Electrophoretic mobilities are converted into zeta potentials using Maple applying the discussed approximate analytical expression by Ohshima for two limiting cases of $\kappa a \geq 10$ (equation 4-5) as well as $\kappa a \leq 10$ (equation 4-12). DLVO and XDLVO calculations are also done using Maple. The analysis of the potentiometric acid base titration was done using a Matlab code, kindly provided by Alves et al..

Evaluation procedure of the electrophoretic mobility

Once the raw data has been generated the corresponding zeta potentials were calculated for each electrolyte concentration independently. The script show here is used for the case of $\kappa a \geq 10$ and starts with the definition of the relevant boundary conditions, as shown in Figure 11-2.

Input of functions and boundary conditions

Input of boundary conditions

Temperature in °C resp.. K

```
> θ := 23;
  T := θ + 273.15;
```

$$\theta := 23$$
$$T := 296.15 \quad (1.1.1)$$

Particle radius in m

```
> a := 21.84E−9;
```

$$a := 2.184\,10^{-8} \quad (1.1.2)$$

Limitting conductance of the ions in (S*m^2)/mol (according to CRC-Handbook 5-77)

```
> Λ0K := 73.48·10^−4 ;#Potassium
  #Λ0K := 50.08·10^−4 ;#Sodium
  #Λ0K := 59.47·10^−4 ;#1/2 Calcium
  #Λ0K := 53.0·10^−4 ;#1/2 Magnesium
  #Λ0A := 76.31·10^−4 ;#Chloride
  Λ0A := 71.42·10^−4 ;#Nitrate
  #Λ0A := 80.0·10^−4 ;#1/2 Sulfate
```

$$\Lambda 0K := 0.007348000000$$
$$\Lambda 0A := 0.007142000000 \quad (1.1.3)$$

Valenceof the symmetrical electrolyte

```
> ν := 1;
```

$$\nu := 1 \quad (1.1.4)$$

Figure 11-2: Input of boundary conditions.

Here, the temperature of the measurement, the particle radius, the valence as well as the limiting conductance of the used electrolyte are defined. The limiting conductance already provides a set of literature values. The ones not used during a calculation procedure need to be set inactive by typing # in front. Afterwards, the co and counter ions need to be manually defined. In case of negatively charged particles the counter ions m_{geg} are the cation *mK* and the co ions m_{co} are the anions *mA*.

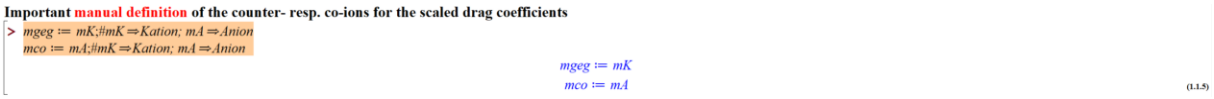

Figure 11-3: Definition of co and counter ions.

Then, relevant constants for the calculation are defined.

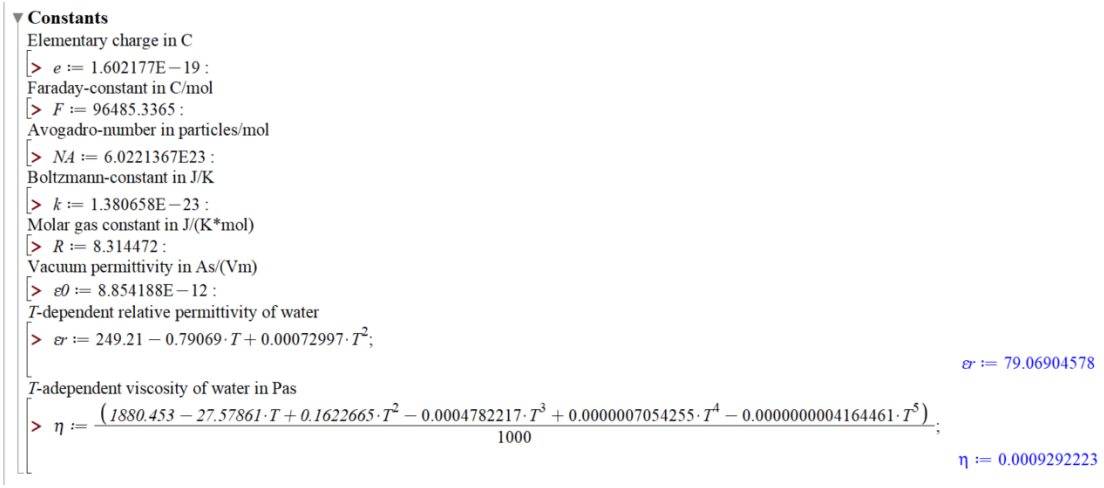

Figure 11-4: Definition of constants used for the calculation.

Afterwards, the relevant expressions are defined, as illustrated in the following figure.

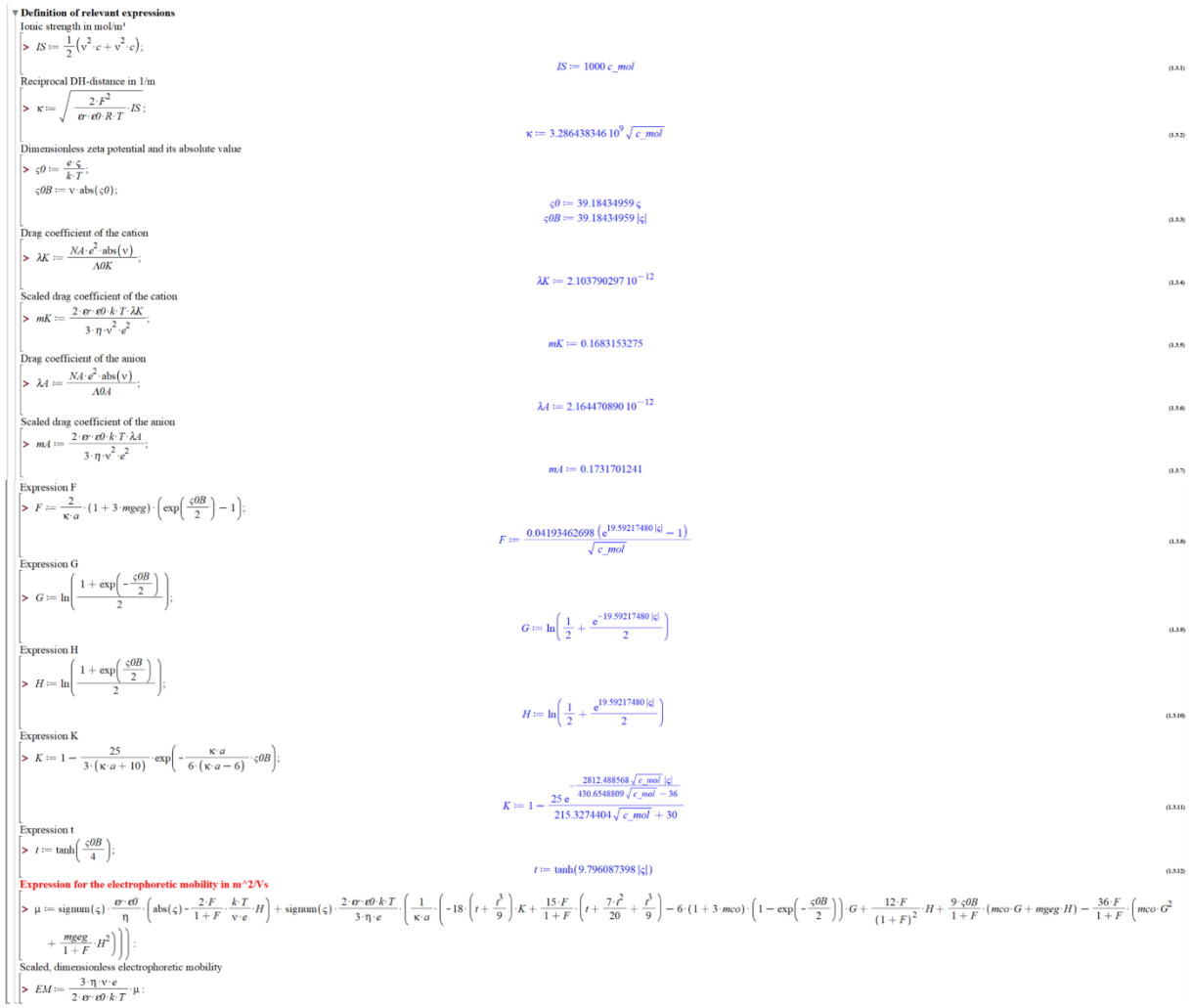

Figure 11-5: Definition of the relevant formulas.

Once the aforementioned data are put in, the zeta potentials can be calculated using the *fsolve* command, which numerically computes the zeroes of one or a set of equations. Here, firstly the experimental electrolyte concentration as well as the measured electrophoretic mobility needs to be set. The zeta potential is calculated within the boundaries of -500 mV and 500 mV. However, depending on the electrophoretic mobility and the zeta potential, two results for the zeta potential are generated. Nevertheless, the first one is unrealistically high and is thus excluded from further evaluation procedures.

Calculation of the zeta potential from the electrophoretic mobility using numerical root analysis

Calculation of individual values for the zeta potential from the electrophoretic mobility

Electrolyte concentration in mol/l

```
> ς :='ς':#Removal of the initial value allocation
  c_mol := 0.02;
```

$$c\_mol := 0.02 \quad (2.1.1)$$

Dimensionless radius κa and validtiy check

```
> κa := κ·a;
  if κa ≥ 10 then"κa'-Valid"else"κa'-Not valid"end if
```

$$\kappa a := 10.15063289$$

$$'\kappa a' - Gültigkeitsbereich\ erfüllt \quad (2.1.2)$$

Experimental determined electrophoretic mobility in m^2/Vs

```
> μMes := -3.492·10^-8;
```

$$\mu Mes := -3.492000000\,10^{-8} \quad (2.1.3)$$

Scaled, dimensionless electrophoretic mobility

```
> EM_Mes := 3·η·ν·e / (2·εr·ε0·k·T)·μMes;
```

$$EM\_Mes := -2.724222174 \quad (2.1.4)$$

Calculation of the corresponding ς-potentials in V based on the experimental determined electrophoretic mobility (valid for κa≥10)

```
> ς1 := fsolve(μMes = μ, ς, -0.5..0.5);
  ς2 := fsolve(μMes = μ, ς, -0.5..0.5, avoid = {ς = ς1});
```

$$\varsigma 1 := -0.2871607667$$

$$\varsigma 2 := -0.06367280781 \quad (2.1.5)$$

Calculation of the dimensionless ς-potentials (valid for κa≥10)

```
> ς01 := eval(ς0, ς = ς1);
  ς02 := eval(ς0, ς = ς2);
```

$$\varsigma 01 := -11.25220787$$

$$\varsigma 02 := -2.494977561 \quad (2.1.6)$$

Figure 11-6: Calculation of the zeta potential .

The script used for the case of $\kappa a \leq 10$ is basically similar. The only difference is the used equation for "Expression for the electrophoretic mobility". Therefore, it will be not shown in detail.

DLVO calculations

To evaluate the DLVO interaction energies, the program maple is used. In the following section the script is explained. Firstly, relevant parameters are defined.

Input of interaction energy expressions

Input of relevant parameter

Surface- or ζ-Potential in V

```
> ΨO := -106.48E-3;
```

$$\Psi O := -0.10648 \quad (1.1.1)$$

Particle radius in m

```
> a := 55.3E-9;
```

$$a := 5.53\,10^{-8} \quad (1.1.2)$$

Valence of the symmetrical electrolyte

```
> ν := 1;
```

$$\nu := 1 \quad (1.1.3)$$

Temperature in °C /. K

```
> θ := 23;
  T := θ + 273.15;
```

$$\theta := 23$$

$$T := 296.15 \quad (1.1.4)$$

Figure 11-7: Input of relevant parameter for DLVO calculations.

Furthermore, the used constants are defined in the subsequent section.

Constants

```
> e := 1.602177E-19 :#Elementary charge in C
  F := 96485.3365 :#Faraday-constant in C/mol
  NA := 6.0221367E23 :#Avogadro-number in particles/mol
  k := 1.380658E-23 :#Boltzmann-constant in J/K
  R := 8.314472 :#Ideal gas constant in J/(K*mol)
  ε0 := 8.854188E-12 :#Elektrische permittivity in vacuum in As/(Vm)
  εr := 249.21 - 0.79069·T + 0.00072997·T^2:#T-dependent relativv permittivity of water
  η := (1880.453 - 27.57861·T + 0.1622665·T^2 - 0.0004782217·T^3 + 0.0000007054255·T^4 - 0.0000000004164461·T^5)/1000:#T-dependent viscosity of water in Pas
  A33 := 3.7E-20 :#Hamaker-Konstante von Wasser im of water in vacuum
```

$$\varepsilon r := 79.06904578$$

$$\eta := 0.0009292223 \quad (1.2.1)$$

Figure 11-8: Definition of used constants for the calculation procedure.

Some of the given and determined parameter are not SI conform and are therefore recalculated.

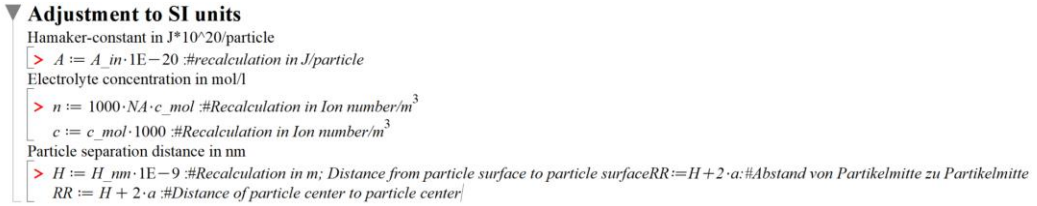

Figure 11-9: Adjustment to SI units of the Hamaker constant, electrolyte concentration and particle separation distance.

In the following, the used expressions for the calculation of the repulsive interaction energies are defined. Following the Maple syntax, the expressions, which are not used are deactivated by writing # in front of each expression. In this study, calculations are solely done by using equation 6 because the boundary conditions are met.

Figure 11-10: Definition of the used expressions to evaluate the repulsive interaction energy.

Similarly, the expressions for the attractive interaction energies are defined in the following section.

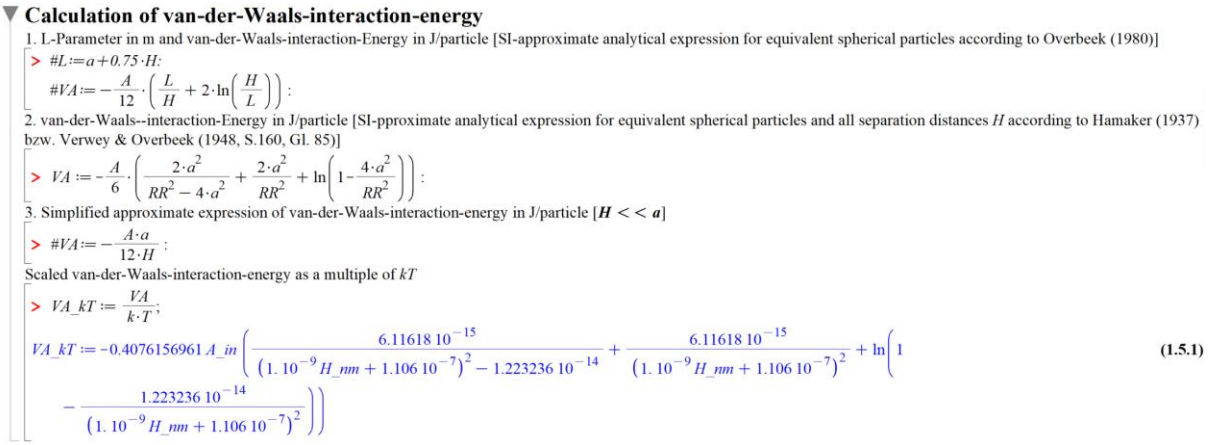

Figure 11-11: Definition of the used expressions to evaluate the attractive interaction energy.

In this study, expression 2 according to Hamaker has been used. Once the relevant parameter, constant and expression are defined the total interaction energy and its corresponding derivations are defined. Therefore, the Hamaker constant can be calculated.

Calculation of total interaction-energy

```
> VT := simplify(VR + VA) :
  VT_kT := simplify(VR_kT + VA_kT) :
> dVT_kT := -simplify(diff(VT_kT, H_nm)) :#interparticle force
  d2VT_kT := -simplify(diff(VT_kT, H_nm$2)) :
```

Calculation of Hamaker-constant

```
> c_mol := 1.50; #critical coagultion concentration
```

$$c\_mol := 1.50 \qquad (1.7.1)$$

Calculation of Hamaker − constant A based on critical coagulation concentrationc_mol (criterium : total interaction−energy)

```
> A_in :='A_in':#Revocation of the initial value assignment
  erg2 := fsolve({VT_kT = 0, dVT_kT = 0}, {H_nm, A_in}, {H_nm = 0..10, A_in = 0..10});
     #H_nm und A_in H_nm and A_in must be deactivated in the boundary conditions
  A_in := subs(erg2[1], A_in);#Effective Hamaker constant of dispersion
  A11 := (sqrt(A) + sqrt(A33))^2;#Hamaker constant of·(swollen) particles in a vacuum
```

$$erg2 := \{A\_in = 3.204911666,\ H\_nm = 0.2462458419\}$$

$$A\_in := 3.204911666$$

$$A11 := 1.379205132\ 10^{-19} \qquad (1.7.1.1)$$

```
> A_DLVO := evalf(sqrt((49.63·(4·π·εr·ε0)^3·(R·T)^5)/F^6 · ga^4/(c_mol·1000·v^6)));#DLVO-approximation (in J/particle)
```

$$A\_DLVO := 3.051756277\ 10^{-20} \qquad (1.7.1.2)$$

Figure 11-12: Definition of the used expressions to evaluate the total interaction energy as well as the calculation of the Hamaker constant.

The calculation of the Hamaker constant at the ccc meeting the conditions of $V_T = 0$ and $dV_T/dH = 0$ is thereby done by using the numerical solution as well as the DLVO-approximation to check for plausibility of the values. For further plausibility checks, the done calculations are graphically evaluated.

Graphical illustration and evaluation

Graphical illustration

Critical coagulation concentration in mol/l

```
> c_mol := 1.5;
  #plot([VT_kT, VR_kT, VA_kT], H_nm = 0..30, labels = [particle distance 'H' [nm], Overall − interaction − energy ['V[T]'/kT]], labeldirections = [horizontal, vertical],
     size = [1000, 600], titlefont = [Arial, bold, 14], title = typeset("Overall-Interaction-Energy"), color = [blue, red, green], view = [0..8, -500.0..500.0], gridlines);
  plot([VT_kT, VR_kT, VA_kT], H_nm = 0..30, labels = [particle distance 'H', Overall − interaction − energy ['V[T]'/kT]], labeldirections = [horizontal, vertical], size
     = [1000, 600], titlefont = [Arial, bold, 14], title = typeset("Overall−Interaction−Energy"), color = [blue, red, green, black], view = [0..10, -40.0..40.0], gridlines);
```

$$c\_mol := 1.5$$

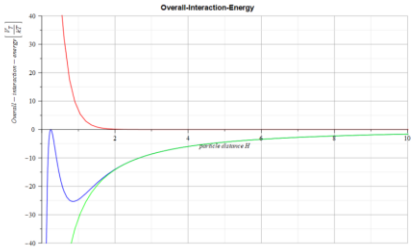

Figure 11-13: Graphical evaluation of DLVO calculations.

XDLVO calculations

The performed XDLVO calculations are also done using maple. In practice, they are done within the same script of the DLVO calculations, because they involve similar parameter. For this reason, the DLVO script is extended. And only the different position is examined below. If not stated differently, the script uses the equivalent expression as stated in the previous chapter.

To calculate the Hamaker constant according to the vOCG approach, the contact angle of Diiodmethane is added.

Input of interaction energy expressions

Input of relevant parameter

Kontaktwinkel Diiodmethan

```
> σ_D := 48.0;
```

$$\sigma\_D := 48.0 \quad (1.1.1)$$

Surface- or ζ-Potential in V

```
> ΨO := -106.48E-3;
```

$$\Psi O := -0.10648 \quad (1.1.2)$$

Particle radius in m

```
> a := 55.3E-9;
```

$$a := 5.53\,10^{-8} \quad (1.1.3)$$

Valence of the symmetrical electrolyte

```
> ν := 1;
```

$$\nu := 1 \quad (1.1.4)$$

Temperature in °C bzw. K

```
> θ := 23;
  T := θ + 273.15;
```

$$\theta := 23$$

$$T := 296.15 \quad (1.1.5)$$

Figure 11-14: Input of relevant parameter for XDLVO calculations.

Besides that, the surface tension, apolar surface tension component and minimum equilibration distance are defined among the constants.

Constants

```
> γl_D := 50.8 :#Surface tension Diiodmethan mN/m
  γLW_D := 50.8 :#unpolar part of surface tension Diiodmethan
  d0 := 0.157E-9 :# closest separation distance in m
  e := 1.602177E-19 :#Elementary charge in C
  F := 96485.3365 :#Faraday-constant in C/mol
  NA := 6.0221367E23 :#Avogadro-number in particles/mol
  k := 1.380658E-23 :#Boltzmann-constant in J/K
  R := 8.314472 :#Ideal gas constant in J/(K*mol)
  ε0 := 8.854188E-12 :#Elektrische permittivity in vacuum in As/(Vm)
  εr := 249.21 - 0.79069·T + 0.00072997·T^2;#T-dependent relativv permittivity of water
  η := (1880.453 - 27.57861·T + 0.1622665·T^2 - 0.0004782217·T^3 + 0.0000007054255·T^4 - 0.0000000004164461·T^5)/1000 ;#T-dependent viscosity of water in Pas
  A33 := 3.7E-20 :#Hamaker-Konstante von Wasser im of water in vacuum
```

$$\varepsilon r := 79.06904578$$

$$\eta := 0.0009292223 \quad (1.2.1)$$

Figure 11-15: Input of relevant constants for XDLVO calculations.

The additional parameters are also converted to SI units.

Adjustment to SI units

Hamaker-constant in J*10^20/particle

```
> A := A_in·1E-20 :#recalculation in J/particle
```

Pre exponential factor C in N

```
> K := K_in·1E-12 :
```

Decay length λw in m

```
> λw := λw_in·1E-9 :
```

Electrolyte concentration in mol/l

```
> n := 1000·NA·c_mol :#Recalculation in Ion number/m^3
  c := c_mol·1000 :#Recalculation in Ion number/m^3
```

Particle separation distance in nm

```
> H := H_nm·1E-9 :#Recalculation in m; Distance from particle surface to particle surfaceRR:=H+2·a:#Abstand von Partikelmitte zu Partikelmitte
  RR := H + 2·a :#Distance of particle center to particle center
```

Figure 11-16: Adjustment to SI units XDLVO calculations.

The expression for the calculation of the hydrophobic interaction parameter are defined.

Calculation of hydrophobic-interaction-energy

```
> Vh := a·K·exp(-H/λw) :
```

Dimensionslose Lewis Säure Base Energie in Vielfachen von kT

```
> Vh_kT := Vh/(k·T);
```

$$Vh\_kT := 13.52468879\, K\_in\, e^{-\frac{1.000000000\, H\_nm}{\lambda w\_in}} \quad (1.6.1)$$

Figure 11-17: Additional interaction energy term accounting for hydrophobic attraction in terms of XDLVO theory.

As the XDLVO theory is used, the calculation of the total interaction energy is adjusted.

Calculation of total interaction-energy XDLVO

Total interaction energy in J/particle and as a multiple *kT*

```
> VT := simplify(VR + VA + Vh) :
  VT_kT := simplify(VR_kT + VA_kT + Vh_kT) :
```

calculation of 1. und 2. derivation

```
> dVT_kT := -simplify(diff(VT_kT, H_nm)) :#interparticle force
  d2VT_kT := -simplify(diff(VT_kT, H_nm$2)) :
```

Figure 11-18: Definition of the used expressions to evaluate the total interaction energy.

The calculation of the vOCG Hamaker constant is implemented as shown in the following figure.

Calculation of vOGC Hamaker constant

```
> γLW_S_1 := ((1 + cos(π·σ_D/180))/2)^2 ·γLW_D;#Calculation of unpolar surface tension component of the solid
```

Hamaker-Konstante aus Kontaktwinkel (XDLVO)

```
> A_in := ((sqrt(γLW_S_1·24·π·d0^2·0.001) - sqrt(3.7·10^-20))^2)·10^20;#Calculation of the vOCG Hamaker constant
```

$$A\_in := 0.4106023469 \quad (1.8.1)$$

Figure 11-19: Calculation of the Hamaker constant according to vOCG theory.

Finally, the corresponding pre-exponential factor is calculated and the interaction energy curves are plotted to check for plausibility.

Graphical illustration and evaluation

Calculation of VT_kT=0 for ccc and A (vOCG) as well as factor K and graphical illustration

```
> c_mol := 1.50 : #critical coagulation cocentration
  A_in := 0.6 : #Average Polyole
  λw_in := 0.3 :
> erg1 := fsolve({VT_kT = 0, dVT_kT = 0}, {H_nm, K_in}, {H_nm = 0..1, K_in = -100..0});
  K_in := subs(erg1[2], K_in) :
  plot([VT_kT, VR_kT, VA_kT, Vh_kT], H_nm = 0..30, labels = [particle distance 'H' [nm], Total - interaction - energy ['V[T]'/kT]], labeldirections = [horizontal,
      vertical], size = [1000, 600], titlefont = [Arial, bold, 14], title = typeset("Total-Interaction-Energy"), color = [blue, red, green, black], view = [0..2.5, -100..100.0],
      gridlines);
```

$$erg1 := \{H\_nm = 0.1068616834, K\_in = -20.95447981\}$$

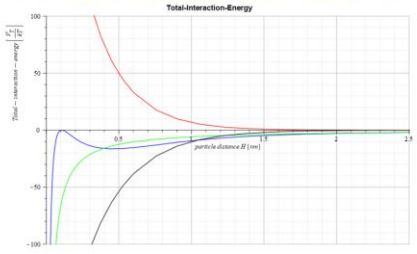

Figure 11-20: Graphical evaluation of XDLVO calculations and determination of the pre-exponential factor.

Evaluation procedure of the potentiometric titration

The matlab code for analysis of the potentiometric acid base titration is kindly provided by Alves et al.. However small adjustments are made to meet the desired purpose. For this study, the constant variables

are defined within the procedure to reduce the number of variables. Therefore, a constant concentration of the used base, the initial volume of the titration and dissociation constant of water are set to the mentioned values. In case of the analysis of DMPA stabilized systems, the volume of the strong acid is also set constant.

The matlab code in Spanish is available upon request by the stated authors.

11.3 Used Software and Tools

Software/Tool	Usage
Maple	Calculation of zeta potentials DLVO/XDLVO calculations
Matlab	Evaluation of potentiometric titration
Origin	Data plotting and fitting
Inkscape	Graphical design and editing
Deepl/Deepl Write	Language editing, text editing
ChatGPT	Language editing, text editing

11.4 List of Abbreviations

AAS	2-[(2- aminoethyl)amino]ethanesulfonic acid
AFM	atomic force microscopy
BDO	1,4-butanediol
ccc	critical coagulation concentration
DABCO	triethylenediamine
DBTL	dibutyltin dilaurate
DLVO	Derjaguin-Landau-Verwey-Overbeek Theory
DMPA	dimethylolpropionic acid
EDA	ethylene diamine
EG	ethylene glycol
HDI	hexamethylene diisocyanate
HDO	1,6-Hexamethylene diol
IPDA	isophorone diamine
IPDI	isophorone diisocyanate
MDI	methylene diphenyl diisocyanate
PC	polycarbonate polyol
PE	polyester polyol
PEO	poly(ethylene glycol) diol
PMMA	polymethylmethacrylate
Poly-DADMAC	poly(diallyldimethylammoniumchloride)
PolyTHF	poly(tetrahydrofurane) diol
PPO	poly(propylene glycol) diol
PUD	polyurethane dispersion
PUR	polyurethanes

TDI	toluene diisocyanate
TMP	trimethylolpropane
VOC	volatile organic compound
vOCG	Van Oss, Chaudhurry, Good theory
XDLVO	extended DLVO theory

11.5 List of Symbols

$\mathrm{p}K_{\mathrm{a},0}$	effective dissociation constant of the strong acid
$\mathrm{p}K_{\mathrm{a},1}$	effective dissociation constant for the first additional weak acidic group
A_{11}	Hamaker constant between two particle in vacuum
A_{131}	Hamaker constant between particle, dispersion medium and particle
A_{131}^{app}	apparent Hamaker constant
A_{131}^{vOCG}	Hamaker constant derived by van Oss, Chaudhury and Good theory
A_{33}	Hamaker constant of molecules of the dispersant in vacuum
A_{oc}	optical constant
F_1	electrostatic force
F_1, H, G, K, t	individual function of hard particle theory
F_2	frictional force
F_3	force of retardation effect
F_4	electrical force of relaxation effect
$K_{\mathrm{HA_n}}.$	dissociation constant of additional weak acidic groups
K_{w}	ionization constant of water
N_{A}	Avogadro constant
$N_{\mathrm{p,m}}$	specific Particle number
Q_{ek}	specific particle charge determined by electrokinetic data on the basis of the soft particle model
Q_{fix}	volume charge density Hermans and Fujita model
Q_{max}	maximum amount of specific particle charge calculated from the synthesis recipe
$Q_{\mathrm{tit,0}}$	specific particle charge for the equivalence point of the strong acid
$Q_{\mathrm{tit,1}}$	specific particle charge for the equivalence point of the first additional weak acid
$Q_{\mathrm{tit,2}}$	specific particle charge for the equivalence point of the second additional weak acid
Q_{tit}	specific charge content determined by titration
$V_{\mathrm{HA_0}}$	volume of the strong acid
V_0	initial volume of the solution to be titrated

V_0	volume of the particle
V_A	attractive interaction energy
V_B	Born repulsion
$V_{\mathrm{HA_n}}$	equivalence volume of additional weak acidic groups
V_h	additional interaction term by XDLVO theory
V_R	repulsive interaction energy
$V_{\mathrm{T,max}}$	magnitude of the energy barrier
V_T	total interaction energy
$c_{\mathrm{H^+}}$	proton concentration
c_B	concentration of the titrant
c^C	concentration of counter ions
c^CO	concentration of co-ions
c_i	concentration of the i-th ionic species
k_0	maximum rate constant of the coagulation process
k_B	Boltzmann constant
m_C	scaled drag coefficient of counter ions
m_CO	scaled drag coefficient co ions
m_i	scaled drag coefficient
n_0	initial particle number
x_s	position of the shear plane
y_0	scaled surface potential
z_i	valence of the i-th ionic species
Λ_i^0	limiting molar conductance
γ_L	surface tension of test liquid
$\gamma_\mathrm{L}^\mathrm{LW}$	apolar surface tension component of the test liquid
$\gamma_\mathrm{S}^\mathrm{LW}$	apolar surface tension component of the substrate
ε_0	vacuum permittivity
ε_r	relative permittivity
$\bar{\zeta}$	dimensionless zeta potential
κ_m	Debye-Hückel parameter of the polyelectrolyte layer
λ^{-1}	electrophoretic softness parameter
λ_HF	softness parameter Herman and Fujita model

λ_{i}	ionic drag coefficient of the i-th ionic species
μ^{∞}	non-zero limiting electrophoretic mobility
ρ_{p}	density of the polymer
σ_0^{ek}	electrokinetic surface charge density
σ_0^{tit}	surface charge density determined by titration
ψ_0	surface potential
ψ_0	surface potential of soft particle theory
ψ_{DON}	donnan potential
ψ_{S}	stern potential
μ	electrophoretic mobility
e	elementary charge
F	faraday constant
n	number density of the electrolyte
$\mathrm{p}K_{\mathrm{a2}}$	effective dissociation constant for the second additional weak acidic group
R	ideal gas constant
T	temperature
A	absorbance
C	pre-exponential factor
E	field strength
H	particle separation distance
N	number density of charged groups inside the polyelectrolyte layer
Q	particle charge
RR	overall recovery rate of particle charges determined by acid-base titration and the synthesis recipe
V	added titrant volume
W	stability factor
Z	valence of charged groups inside the polyelectrolyte layer
ZN	volume charge density according to the soft particle model
a	particle radius
b	total radius of a soft particle
d	thickness of polyelectrolyte layer
k	rate constant of coagulation process

t	time
v	particle velocity
y	reduced surface potential
ζ	zeta potential
η	viscosity
θ	contact angle
κ	Debye-Hückel Parameter
λ	decay length
ρ	density of the particles
τ	turbidity

11.6 List of Figures

11.7 List of Tables